UNIVERSITÉ DU LUXEMBOURG

PhD-FSTM-2025-05
The Faculty of Science, Technology and Medicine

DISSERTATION

Defence held on 05/05/2025 in Luxembourg

to obtain the degree of

DOCTEUR DE L'UNIVERSITÉ DU LUXEMBOURG

EN *CHIMIE*

by

Oussema KACHOURI
Born on 8 March 1997 in Tunisia

DEBOND ON DEMAND ADHESIVES USING THE FLAME- RETARDANCY CONCEPT

Dissertation defence committee

Dr Abdelghani LAACHACHI, dissertation supervisor
Senior Research Scientist, Polymeric & Composite Materials Unit, Luxembourg Institute of Science and Technology (LIST)

Dr Slawomir KEDZIORA, Chairman
Professor, Department of Mechanical Engineering and Design, Université du Luxembourg

Dr Lucas Filipe Martins DA SILVA, Vice Chairman
Professor, Department of Mechanical Engineering, Faculty of Engineering, University of Porto (FEUP)

Dr Fouad LAOUTID
Scientific Leader of the Polymeric & Composite Materials Unit, Materia Nova

Dr Jorge IÑÍGUEZ
Professor, Department of Physics, Faculty of Engineering, Université du Luxembourg

Dedication

This PhD dedicated to my family: my parents, my little brother, friends, siblings, and those who left us during this journey: ***Mohamed Ghorbel****,* ***Aziza Makni****, and* ***Bilel Makni****. You live in my heart.*

To my younger self and future self, do not worry we're not abandoning the dream. We're just building the bridge to reach it.

WHO KNEW THE THINGS WE ENJOYED AS TODDLERS COULD BECOME THE CAREERS OF OUR FUTURE.

Oussema KACHOURI

Acknowledgements

First and foremost, I would like to express my deepest gratitude to God, whose infinite wisdom and boundless mercy have guided me through this journey. It is by His will and grace that I have been given the strength, perseverance, and opportunity to undertake and complete this PhD. Every challenge I faced and every milestone I achieved were only possible through His divine support and blessings.

I would also like to extend my sincere gratitude to Luxembourg, a generous country that has made this achievement possible. A heartfelt thank you to LIST , University of Luxembourg and FNR for concretely giving me this opportunity and supporting my academic journey.

My LIST journey has been nothing short of extraordinary, and I am deeply thankful for the family I found along the way. I have not only been lucky, but I truly feel like I hit jackpot after jackpot. My journey at LIST started with two amazing people who gave me the opportunity to do my end-of- studies internship with them. Out of nowhere, two people decided to give me a shot Dr. Reiner Dieden and Dr. Nathalie Valle. They took a chance on a student from Tunisia with minimal knowledge, allowing me to learn and be trained under their supervision. I am profoundly grateful. A special thank you also to Nacéra Meniri, who ensured I always had a place to stay and that everything went smoothly throughout the journey.

My second jackpot was my supervisor, Dr. Abdelghani Laachachi. At a critical point, he decided to believe in me and trust me with his ideas. Throughout this journey, he has always been there to provide his guidance and training in the ways of a scientist. Thank you I am lucky to be your student, and I am forever grateful. To Julien Bardon and Dr. David Ruch, thank you for your constant support, supervision, and insights, and for always pushing me to explore new ideas. A significant portion of my intellectual growth is thanks to you.

A huge thank you as well to Benoit Marcolini and Doriane Delfrari for all the help you provided throughout this PhD. This work would not have been possible without you.

I also cannot go without naming the people who, over these years, became more than just colleagues they became real friends. Dr. Daniil Nosov, Andrea Iannota, Vladislav Shevstov, Ayman El Bouhali you geniuses are my brothers and with each of you I cherish amazing memories. Dr. Arpan and Dr. Huy, thank you for your help, advice, and our fascinating conversations. To the incredible women Ive had the pleasure of working with: Dr. Margot Bonamtin, Dr. Carla Schnell, Harshada Chothe, and Dr. Iouliana Chrysafi ladies, you have been amazing friends. Over the last few years, you have cared for and supported me in both work and personal matters, and I deeply appreciate it.

In the past few months, I had the privilege of meeting a very special friend, Dr. Sofia Tachtalidou. You are really an amazing friend. Thank you for all your help and support, especially during the last stressful days, giving your time and effort to motivate me, correct and edit this manuscript, and try to make it better than I even wanted it to be. You added the final touch to the cookie now the work is done, so go away!

I would also like to extend my heartfelt gratitude to my family, the small circle of people I love most in this world. To my beloved parents, Basma Ghorbel and Jamel Kachouri, who have been by my side since the very first day of my life, supporting me unconditionally. Though at times they steered my ship against my wind, they were always there for me, standing behind me as my unwavering pillars of strength. Mom, Dad, I love you, and this doctorate is the fruit of your sacrifices and efforts this is for you.

To my little brother, Mohamed Kachouri, the person I love most in this world, every achievement of mine is a reflection of your presence in my life. My relentless pursuit of success has always been fueled by my desire to be your hero, even though, in reality, you have always been mine.

I have always considered myself a lucky person, and while my immediate family has been my foundation, my extended family has played an equally crucial role in shaping the person I am today. To my older brothers, Khaled Kachouri, Tarek Kachouri, Amin Ghorbel, Bilel Makni may his soul rest in peace Houssem Laroussi, thank you for being my guidance and inspiration throughout this journey. I truly look up to you, and at times, I feel humbled and even intimidated by your incredible achievements.

To my older sisters, Ghada Makni, Rym Kachouri, Rahma Wannes, Perrine Malheurty, Khouloud Kachouri, and Fatma Kachouri, you are the sisters I never had. Each of you has imparted invaluable lessons about life and what it means to be an extraordinary woman. Your wisdom, kindness, and strength have left an indelible mark on me, and I am deeply grateful for your presence in my life.

To my brothers from other mothers, Mohamed Amin Mnif, Ahmed Ghorbel, and Karim Hachicha, each of you has touched my life in a unique way, and for that, I am profoundly grateful. Thank you for always being there, for never

judging me despite my missteps, and for standing by my side through thick and thin. I love our dynamic you let me be the crazy one, the one who messes up, while you are always there for the save. I could not ask for better friends and brothers.

I have always been blessed with the presence of incredible uncles and aunts who have been like guardian angels in my life. To Aziza Makni and Ghorbel Mohamed, I am sorry you never got to see this moment, but I hope it brings you pride and joy wherever you are in the skies. To my uncle Mohamed Kachouri, the funniest person I know, and my uncle Salah Makni, the most generous person I have ever met, thank you for your unwavering support. To my aunt Ahlem, for always being there for my mother, your kindness and strength mean the world to me. A special and heartfelt thanks to my aunt Najiba Ghorbel I believe I have as many cherished memories in your home as I do in my own. I even have to admit, sometimes I love your cooking more than my moms! You are truly a superhero in my life.

To the friendships that are as old as family bonds and that I carry with me always, I cannot go without mentioning you here. Arij Ben Jmeaa, the most prideful person I know, I hope that after this PhD, youll see that I am coming closer to your intellect. Yosr Chaaben, the most emotional decision-maker I have ever met, I hope to see you live up to your true potential. Wafa Maalej, the most rational person I know, keep doing what you do you are doing good.To my dear friend Abir Elbeji, you are incredibly smart and artistic. I hope you soon realize that you deserve every bit of success you have achieved. To Farah Jmal, I know you sometimes feel that I have such an impact on you that it scares you, but in many ways, it is the other way around. I have learned so much from you. You know I can see through the bling-bling shell to the sensitive person within, and I see amazing potential. Just a little more belief in yourself and by the way, Im still waiting for my social media coaching! To my friend Lobna Sellami, theres no need to talk about your intelligence you are the only person I know who can work for three different companies in a single day. You are also one of the kindest, most caring people, and you can always count on me to be your big brother. To my friends Oussema Fendri and Dhia Boukhirs, I honestly dont know how you walk such a straight line without mistakes wow! I wish you both all the happiness and stability in your lives. And finally, to my friend Walid Slama, in the last few years, you have truly become like a brother. You are insanely talented keep pushing forward, but know that I am becoming a bigger artist than you or Ill start a rap beef just to catch up!

I would like to express my deepest gratitude to my mathematics teachers, Mr. Mohamed Boukhirs and Mr. Sofiene Smaoui, for their invaluable guidance and dedication throughout my academic journey. Their patience and clarity made even the most complex concepts accessible. To the only teacher who made appreciate and understand the laws of physics and the teacher who always looked after me till today, Mr..Alaeddine Ben Amira. I am also sincerely thankful to my English teacher, Mr. Hassen Ben Aribia, whose passion and

encouragement sparked my own love for the English language a passion that continues to inspire me today. A special thank you goes to Madame Taycir, my university professor, whose unwavering consistency, high standards, and sincere commitment to my growth pushed me to exceed my limits. Her tough love and relentless support played a significant role in shaping the person I am becoming.

I obviously cannot name everyone and every story, and for those I mentioned, trust me, I know I didn't do enough. And for those I forgot to mention, you are in my heart and soul, and I am deeply thankful for everything.

Contents

List of Figures

List of Tables

Abbreviations

1-C One-component reactive adhesive systems

2-C Two-component reactive adhesive systems

2-MI 2-methylimidazole

Δq Heat flow differential

ADC Azodicarbonamide

AFM Atomic force microscopy

AHEW Amine hydrogen equivalent weight

APP Ammonium polyphosphate

APP I Short-chain ammonium polyphosphate

APP II Ammonium polyphosphate phase II

ATH Aluminium trihydroxide

ATSP Aromatic thermosetting copolyesters

BADGE Diglycidyl ether of Bisphenol A

BFRs Brominated flame retardants

BHT Butylated hydroxytoluene

CFRP Carbon fiber reinforced polymer

CP/MAS Cross-polarization/magic angle spinning

DA Diels-Alder

DCB Double cantilever beam

DDS 4,4-Diaminodiphenyl sulfone

D.E.R.332 Diglycidyl ether of Bisphenol A

DETA Diethylenetriamine

DGEBA Diglycidyl ether of Bisphenol A

DLJ Double-lap joints

DMA Dynamic mechanical analysis

DSC Differential scanning calorimetry

EDX / EDS Energy-dispersive X-ray spectroscopy analysis

EEW Epoxide equivalent weight

EG Expandable graphite

ELV End of life vehicle

EMR Electromagnetic radiation

ESEM Environmental scanning electron microscope

EVA Ethylene-vinyl acetate

FRP Fiber-reinforced polymer

FT-IR Fourier transformation-Infrared spectroscopy

GFRP Glass fiber-reinforced plastic

GHG Global greenhouse gas

GICs Graphite intercalation compounds

HMAs Hot Melt Adhesives

IPA Isopropyl alcohol

ITR Interchain transesterification reactions

IUPAC International Union of Pure and Applied Chemistry

LBL Layer-by-layer

MEK Methyl ethyl ketone

Micro-CT Micro-computed tomography

MOP Melamine orthophosphate

MPP Melamine polyphosphates

NMR Nuclear magnetic resonance spectroscopy

PCO 900 Pentaerythritol spirobis (methylphosphonate)

PE Polyethylene

PEEK Polyetheretherketone

PENTA Pentaerythritol

PP Polypropylene

PPS Polyphenylene sulfide

PSAs Pressure-sensitive adhesives

PVA Polyvinyl acetate

Ra Arithmetic average roughness

rDA Retro-Diels-Alder

RF Radio frequency

RMS Recommended surface roughness

Rt Total height of the roughness profile

RT Room temperature

Rz Average maximum height

SBR Styrene-butadiene rubber

SEM Scanning electron microscopy

SLJ Single-lap joints

SMAs Shape memory additives

SMPs Shape memory polymers

SSB Spinning sideband

T°_{deb} Debonding temperature

Tan δ Damping factor

TEG Thermally expanded graphite

TEPs Thermally expandable particles

Tg Glass transition temperature

TGA Thermogravimetric analysis

TPU Thermoplastic polyurethane

UV Ultraviolet

wt.% Weight percentage

XRD X-Ray Diffraction

Introduction

Figure 1: Schematic representation of the recycling concept as nature's invention.

If we carefully observe nature, we find that many modern scientific advancements are, at their core, imitations of natural processes. Nature has long served as a canvas from which we draw inspiration. A striking example is the development of composite materials. In nature, composites are everywhere. Consider a bird's wing, which is composed of feathers and bones. Feathers, made up of keratin, provide the necessary aerodynamic qualities, while bones offer structural support [1, 2]. This natural composite harnesses the distinct properties of each component to achieve a functional whole, a concept that modern material science has adopted to create advanced engineered composites.

This observation extends beyond material composition and encompasses the concept of recycling as well. In nature as illustrated in Figure 1, nothing is wasted; every element, after serving its purpose, is recycled and reused, contributing to the ecosystem's balance. The concept of waste, as we know it today, is a human creation that emerged with the advent of synthetic products. In disrupting natures closed-loop system, we created the need for recycling. In a way, recycling is not our invention, but rather our attempt to mimic nature, striving to restore balance and emulate the natural processes that have always ensured sustainability. Through recycling, we aim to reintegrate synthetic materials into a sustainable cycle.

As we continue to draw inspiration from nature, our focus has increasingly shifted toward mitigating the damage caused by human activity. This shift is particularly evident in the energy, construction, and transportation sectors three pillars of modern civilization that are now embracing composite materials for their superior properties, particularly their low density. This transition marks a crucial step in reducing the environmental

footprint of these sectors, which are major contributors to global greenhouse gas (GHG) emissions and the ongoing threat of global warming, one of the most pressing challenges of our time. As a result, the composite materials market is expected to grow more than 8% annually between 2019 and 2027, reaching approximately 140 billion euros [3].

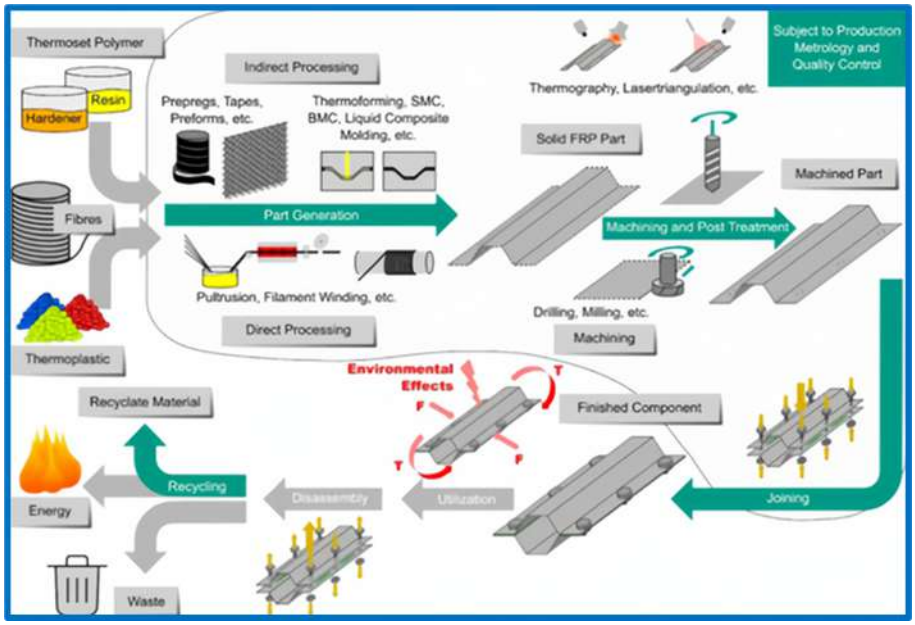

Figure 2: Ideal circular life cycle of composites.
[4]

The growing use of composite materials holds great promise not only in improving quality of life but also in unlocking numerous economic opportunities, fueling further technical and scientific progress. However, despite their role in the promotion of lightweight construction, composites pose a significant challenge: their recyclability. Unlike seamless cycles in nature, where nothing goes waste, our current use of composites fails to achieve a circular economy [5]. Ideally, the life-cycle of composite materials as illustrated in Figure 2 should mirror natures efficiency, yet in Europe, only 20% of the 2.8 million tons of composite structures produced annually are recycled [6].

In the automotive sector, the EU End-of-Life Vehicle (ELV) Directive (2000/53/EC), which mandates that 85% of materials in new vehicles be reusable and recyclable, has driven progress, but the need for more effective solutions is evident. Enhancing the recovery and reuse of composites presents a significant opportunity. Various methods have been explored for recycling composite waste, allowing partial material recovery for future use [5].

Mechanical recycling, in use since the 1970 s, involves grinding fiber-reinforced plastic

(FRP) waste into low-value compounds while preserving the material's basic structure [7]. This method is commonly applied to thermoset composites, which are difficult to recycle due to their rigid, cross-linked networks. Glass fiber-reinforced plastic (GFRP) is frequently recycled this way, though the resulting products often have limited applications [8].

Thermal recycling deconstructs composites by applying heat to separate the matrix from the reinforcing fibers, converting them into usable products like polymers and fibers. This method, typically using pyrolysis, aims to retrieve intact fibers but requires high temperatures (450°C to 700°C), making it energy-intensive [5]. Chemical recycling breaks down polymers into monomers or oligomers through chemical reactions, using either low temperature solvolysis (below 200°C) or sub- and supercritical solvolysis [9]. Of the three methods, chemical and thermal recycling are the only ones that allow for the reuse of composite constituents with properties similar to their original state. However, chemical recycling poses environmental risks, while thermal recycling demands significant energy input.

Balancing material integrity and environmental impact, sub- and supercritical solvolysis stands out as the most promising technique for recycling glass fiber-reinforced (GFRP) or carbon fiber-reinforced polymers (CFRP). It is relatively energy-efficient and allows the fibers to be reused in new composites with performance levels comparable to the original materials [7].

Over the past decade, there has been a significant increase in demand for debonding technologies, as evidenced by the surge in new product introductions, publications, and patent applications. This growing interest stems from the fundamental challenge faced by adhesive technologies: the permanence of the bond, which hinders the reuse and recycling of materials, leading to increased waste and material downgrading. Traditional methods for debonding structural adhesive joints [10], such as mechanical destruction through thermal degradation or cutting, often result in damage or even destruction of the substrates. While acids and solvents are sometimes used, they raise health and safety concerns. Despite the publication of numerous patents on methods for separating bonded joints, only a few techniques have reached commercial availability.

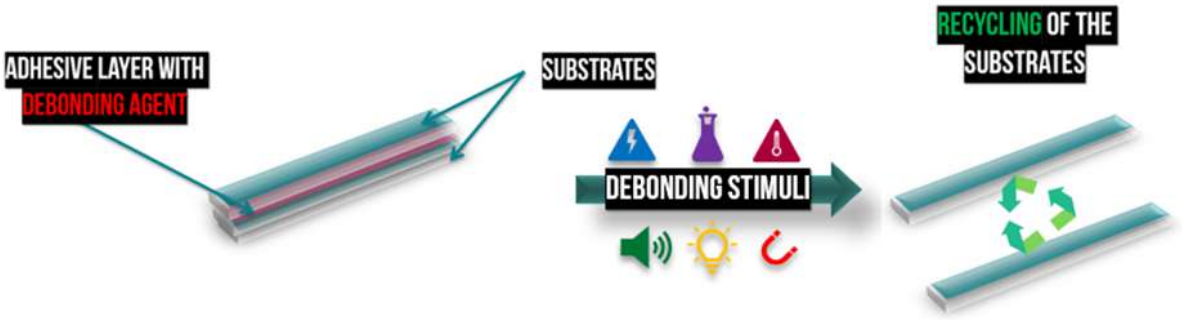

Figure 3: Schematic representation of the debonding on demand concept.

In response to these limitations, reversible or debondable adhesives have been developed as illustrated in Figure 3, allowing for the disassembly of components and the reuse of materials at their original value [10]. Various debonding technologies, ranging from those based on van der Waals forces [11] to those responsive to electrical currents [12], and others, have been explored. However, no universal solution has yet emerged, particularly for structural bonding that balances ease of implementation with the mechanical integrity of the bonded joints.

In this thesis, we present an innovative approach to this problem by leveraging principles from flame retardancy. Our research repurposes flame retardants, utilizing their unique ability to swell when exposed to heat as a trigger for debonding. This method introduces a new dimension to debondable adhesive technology, where the application of thermal stimuli induces a controlled and reversible separation of bonded joints. The study explores the effects of several flame-retardant systems on the mechanical properties of bonded structures, both before and after the debonding process. The systems investigated include two forms of Ammonium Polyphosphate (APP), Melamine Polyphosphate (MPP), Organophosphorus Flame Retardants (PCO 900), and Expandable Graphite (EG). By examining these systems, the research aims to identify the most effective strategies for achieving reliable debonding while maintaining the structural integrity of the materials involved, ultimately contributing to the development of more sustainable and versatile adhesive technologies. The thesis is structured as follows: It opens with a comprehensive literature review that establishes the scientific background for the research. This review covers the key principles of flame retardancy, the design of adhesive joints, an overview of other debonding technologies and an introduction to the characterization methods employed throughout the study. Following this foundational review, the thesis presents a series of papers, each contributing to different aspects of the project.

The first paper examines Melamine Polyphosphate (MPP) and Ammonium Polyphosphate (APP) flame retardants, providing initial validation of the projects proof of concept. This is followed by a paper exploring PCO 900, an organophosphorus flame retardant, and another focusing on Expandable Graphite (EG) as a spin-off technology. The final paper delves into the use of short-chain APP, aimed at further reinforcing the proof of concept and achieving debonding at lower temperatures. Each study is paired with an in-depth analysis of the mechanical and physicochemical impacts of these fillers on epoxy matrices, enriching the existing literature and contributing new insights. To ensure a thorough understanding, advanced technologies such as Micro-Computed Tomography (Micro-CT), Nuclear Magnetic Resonance (NMR), Thermogravimetric Analysis (TGA), Dynamic Mechanical Analysis (DMA), Fourier Transform Infrared Spectroscopy (FTIR), Scanning Electron Microscopy (SEM), and optical microscopy have been employed throughout the research.

The final section of the thesis discusses the collective findings, showcasing the practical application of the debonding technologies in composites like sandwich composites and Carbon Fiber Reinforced Polymer (CFRP) composites. The thesis concludes with a summary and outlook, highlighting the limitations of the current work and proposing future research directions.

1

Literature Review

1 Introduction to adhesive bonding and adhesives

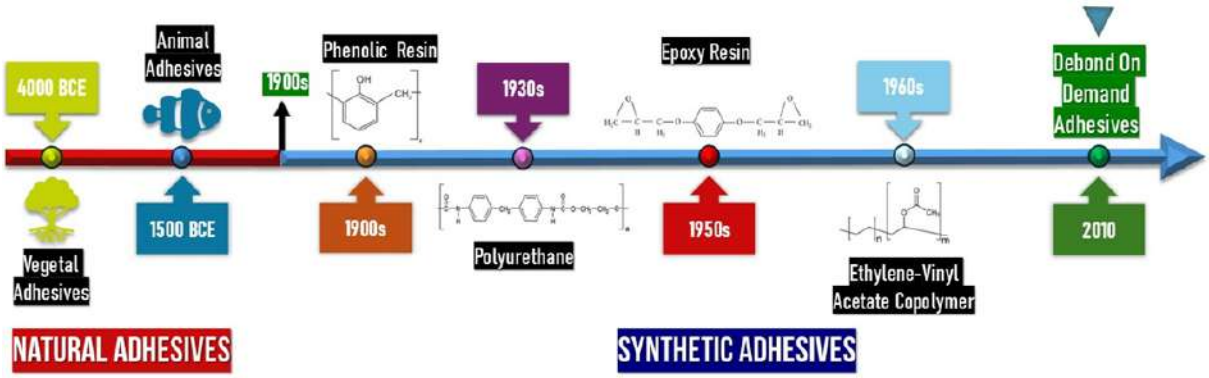

Figure 1.1: Development of adhesives from natural to synthetic across history.

Since the dawn of time, humans figured that the only way to control the harsh environment was by joining different materials. This method allowed them to harness various properties of these materials, leading to the creation of the first tools. Ancient tools, such as stones attached to sticks or horns bound to handles, represent humanity's earliest use of joining techniques or adhesive bonding. Such techniques, as illustrated in Figure 1.1, predate even scripting and counting . Adhesive substances have always been abundant in nature ranging from plant-based glues derived from tree bark or gum Arabic from acacia trees [13], for example to animal-based adhesives like egg whites and casein glue made from milk proteins which were used in woodworking and bookkeeping [14].

Only in the last few centuries have science and industry turned their attention to adhesives, recognizing the significance of their performance and the advantages they offer [15]. This interest sparked the development of modern synthetic adhesives, such as polyurethanes, phenolic resins, epoxies, and acrylates, which began to be produced on an industrial scale [16]. There has been a heavier focus on adhesion as a phenomenon, exploring the aging of these substances on different materials, and classifying them based on their properties and applications [17]. Simultaneously, these products have become increasingly diversified and widely produced. Fast forward to today, adhesives are ubiquitous, found in everything from kindergarten tool kits to high-end technologies like smartphones, modern vehicles, and aircraft [18].

What, then, constitutes adhesion bonding? How is an adhesive defined? Furthermore, what are the various phenomena (Adhesion theories) that occur between adhesive

substances and the surfaces they bond, which govern and delineate adhesion?

1.1 Definition of an adhesive and adhesion

An adhesive any material or substance that is applied in low quantities to the surface of two dissimilar materials to form an adhesive joint that becomes permanently bonded structure [19, 20]. Adhesion can be defined in multiple ways, and it is challenging to find a single definition that englobes all aspects. For instance, the International Union of Pure and Applied Chemistry (IUPAC) defines adhesion as the "process of attachment of a substance to the surface of another substance." Alternatively, Wu suggests that "Adhesion refers to the state in which two dissimilar bodies are held together by intimate interfacial contact such that mechanical force or work can be transferred across the interface." [21,22] However, theres an agreement that adhesion is primarily driven by multiple interfacial forces operating at the nanometer scale [23], which are also referred to as adhesion theories.

In this context, before exploring these theories in detail, it is necessary to distinguish between adhesion and cohesion represented in Figure 1.2. While adhesion refers to the cumulative interfacial forces that result in the bonding of surfaces, cohesion represents the sum forces that maintain the integrity of the polymer, essentially the internal strength of a material. It is important to note that although cohesion is not adhesion, strong cohesion is crucial for effective adhesion [24, 25].

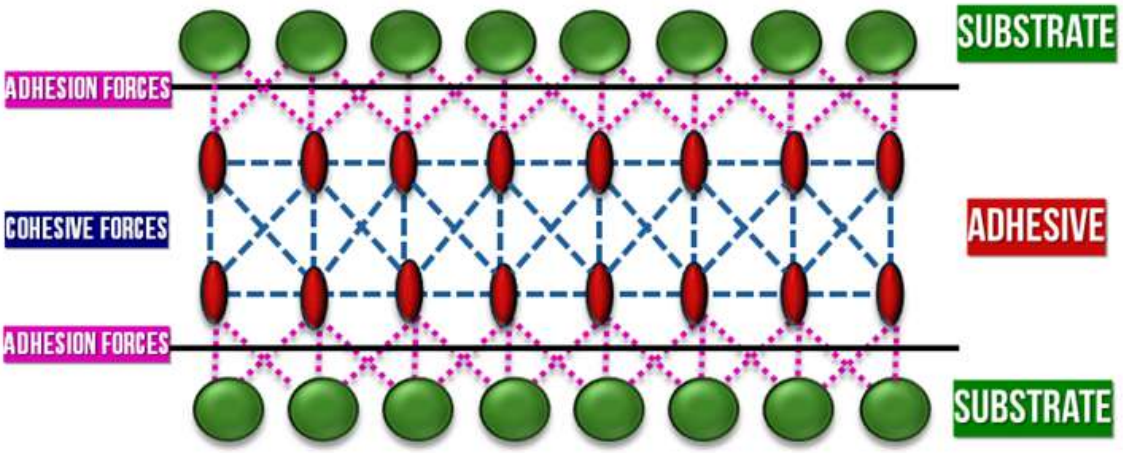

Figure 1.2: Schematic representation of adhesion and cohesion forces.

1.2 Adhesion theories

1.2.1 Diffusion theory

Diffusion theory, illustrated in Figure 1.3, stipulates that adhesion occurs when molecules from the adhesive and the substrate inter-diffuse. This mechanism is particularly relevant when the adhesive and substrate consist of long-chain polymer molecules that are capable of mobility. The binding conditions and the specific properties of the materials involved influence the thickness of the resultant diffusion layer, which generally varies between 10 Å and 1,000 Å [26, 27]. For instance, when two different polymers are involved, the bond strength significantly increases if the adhesion process is conducted at a temperature above the melting points of both polymers [28].

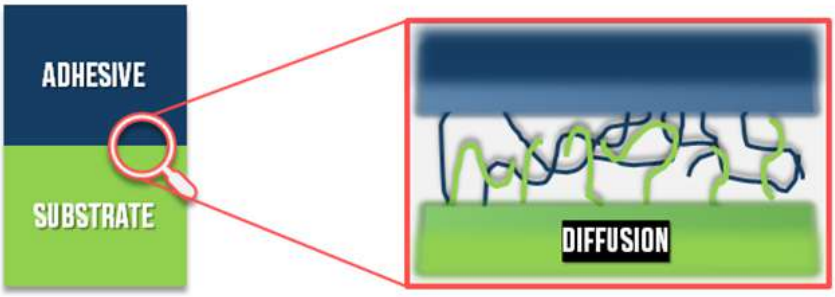

Figure 1.3: Schematic representation of diffusion adhesion theory.

1.2.2 Mechanical interlocking

Mechanical interlocking theory, illustrated in Figure 1.4, suggests that adhesion occurs when the adhesive fills and penetrates the surface roughness of the substrate, which consists of micro-pores and cavities, by displacing the air and occupying its space. Generally, bonding tends to be stronger on rough surfaces compared to smooth ones [29, 30]. Adhesion is primarily enhanced by abrasion of the surface for mechanical interlocking, but it may also benefit from the increased cleanliness and contact surface area that result from this process [31].

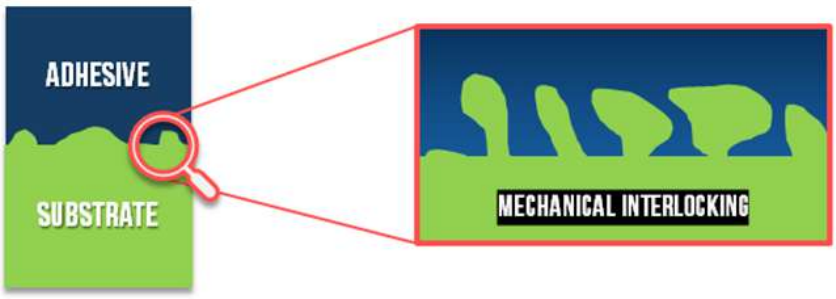

Figure 1.4: Schematic representation of mechanical interlocking.

1.2.3 Electrostatic theory

Electrostatic theory, illustrated in Figure 1.5, emerges from observing the electrical discharge that occurs when an adhesive is peeled off a substrate [32]. Infact, at the adhesive-adherend interface, an electric double layer is formed due to electrostatic forces resulting from electron transfer, which is attributed to differing electronic band structures [33, 34]. This theory is particularly relevant when the adhesive joint under study consists of metal and polymer components [35].

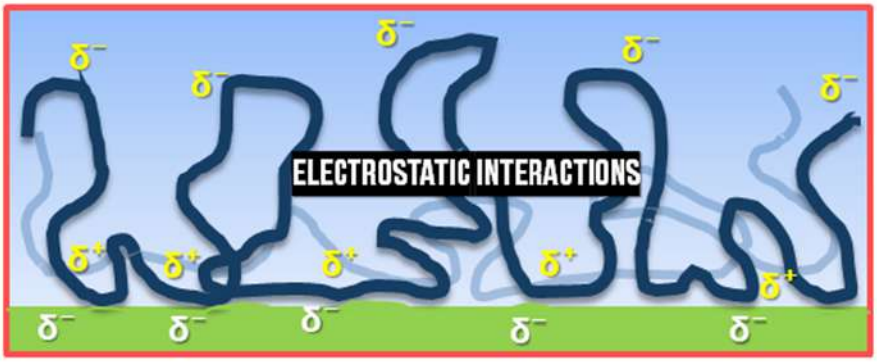

Figure 1.5: Schematic Representation of electrostatic adhesion theory.

1.2.4 Chemical bonding

At the interface between the adhesive and the substrate, several types of chemical interactions can contribute to forming a strong bond. These include covalent bonds, hydrogen bonds, acid-base interactions, and Lifshitz van der Waals forces. Among them, covalent bonds are the strongest and most stable , with bond energies typically between 150 and 1100 kJ/mol, often leading to permanent adhesion. Hydrogen bonds are less strong but

still significant, usually falling in the 10 to 40 kJ/mol range, and are especially relevant when polar groups like OH or NH are involved. Acid-base interactions, though more complex, generally share similar strengths to hydrogen bonding, depending on the nature of the donor and acceptor groups. Finally, Lifshitz van der Waals forces though the weakest individually, with energies ranging from 0.05 to 40 kJ/mol can collectively play a key role in adhesion, particularly over large contact areas. [36, 37].

1.2.5 Acid-Base theory

Acid-Base theory draws on Lewis's definition of acids and bases An acid is a substance which can accept an electron pair from a base; a base is a substance which can donate an electron pair., this theory suggests that adhesion results from an electron exchange between positively and negatively charged molecules. This exchange results in a polar attraction, highlighting molecular-level forces that enable materials to adhere to one another [38, 39].

1.2.6 Weak boundary theory

Weak boundary theory, illustrated in Figure 1.6, was Proposed by Bikerman, this theory contends that failures in adhesive bonds result from either cohesive failure or a weak boundary layer [40]. These weak boundary layers can originate from the adherend, the adhesive, environmental factors, or a combination of these elements. When impurities accumulate on the bonding surface of either the adhesive or the adherend, they form a weak layer that ultimately leads to the failure of the bond [41, 42].

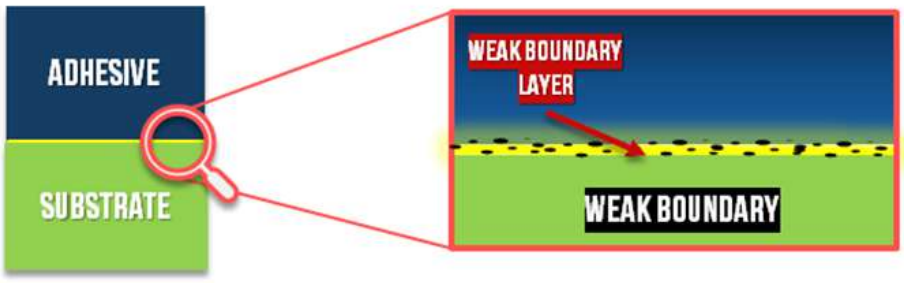

Figure 1.6: Schematic representation of weak boundary theory.

1.2.7 Wetting theory

The wetting theory, illustrated in Figure 1.7, is one of the most well-established and widely recognized theories of adhesion. It describes how interfacial forces develop when two materials come into contact, a process referred to as the wetting of the surface [32]. For adhesion to be effective, the adhesive must exhibit a lower surface tension than that of the substrate. A high surface tension of the substrate is typically achieved through surface treatments. Complete wetting maximizes bond strength by allowing the adhesive to fully penetrate surface imperfections, whereas incomplete wetting results in weaker bonds due to limited contact and the formation of interfacial defects [43,44]. Organic adhesives such as epoxies are effective at bonding with metal surfaces due to good wetting properties, but they often struggle to adhere to untreated polymeric substrates like polyethylene and polypropylene, whose surface tensions are lower than those of the adhesives. To enhance adhesion, the surface energy of these plastic materials is frequently elevated through a variety of treatment methods, there by improving their receptiveness to the adhesive [45].

Figure 1.7: Schematic representation of the wetting theory.

1.3 Adhesives and adhesive materials

Adhesive materials, despite their distinct applications and categorizations as different products, fundamentally consist of polymers characterized by large molecular chains form intricate networks at both the substrate-adhesive and adhesive-adhesive interfaces. These polymeric structures are crucial, as they largely dictate the final properties of the cured adhesive, including its mechanical strength, flexibility, and resistance to various environmental factors, such as moisture, temperature, and chemical exposure [46,47].

Adhesives can be systematically classified according to several criteria, illustrated in Figure 1.8, each aligning with specific application needs and performance requirements. A

critical aspect of adhesive materials is the curing process, which involves transforming the adhesive from a liquid or semi-liquid state to a solid state, essential for achieving effective bonding. This curing step is pivotal, as it converts the adhesive into a durable, functional material. Consequently, one primary classification of adhesives is based on their reactivity and behavior during the curing process [48, 49].

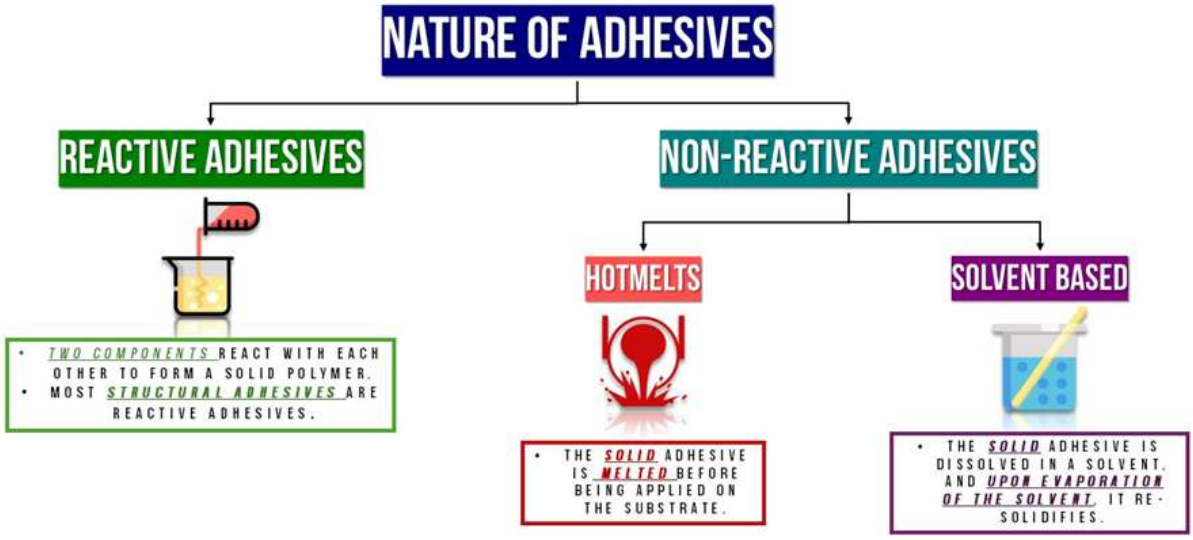

Figure 1.8: Different natures of adhesives: reactive / non-Reactive.

1.3.1 Reactive/ non-reactive adhesives

Reactive adhesives

Reactive adhesives necessitate a chemical reaction during the curing stage, where the polymer network is formed through polymerization. They exist as either one-component (1-C) reactive adhesives or two-component (2-C) systems, typically consisting of a resin and a hardener that initiate cross-linking. An example of such adhesives includes thermosets, like epoxy resins [50].

Non-reactive adhesives

Non-reactive adhesives are those in which the polymer is pre-formed, and the curing process does not involve a chemical reaction but rather a physical process, such as the application of pressure or heat [50]. This category includes:

- Solvent-based adhesives, which solidify as the solvent evaporates.
- Hot melts and high-performance thermoplastics, which require heating to specific temperatures to melt, then solidify upon cooling back to room temperature [51, 52].

1.3.2 Origin of adhesives

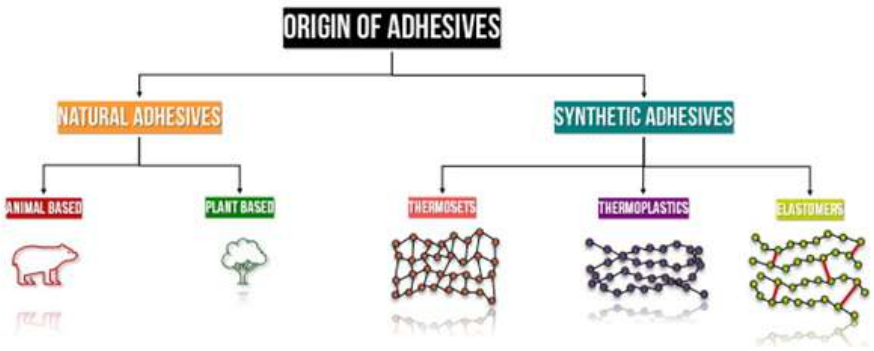

Figure 1.9: Origin of adhesives.

1.3.2.1 Natural adhesives

Natural adhesives are extracted from natural sources, illustrated in Figure 1.9, including both animal and plant-based origins. Animal-based adhesives encompass products such as collagen, casein glue, and blood albumen glue [53], while plant-based alternatives include dextrin, starch, and natural gums derived from agar and acacia [54]. The emergence of synthetic adhesives significantly reduced the demand for these natural options due to differences in mechanical properties and the broader range of applications available with synthetic materials [55]. Nonetheless, these natural adhesives have recently garnered renewed interest due to their potential for sustainability and environmentally friendly attributes. However, their use remains largely restricted to packaging, woodworking, and, in certain instances, medical applications [56].

1.3.2.2 Synthetic adhesives

Synthetic adhesives, illustrated in Figure 1.9, offer the advantage of consistent supply and uniform properties. Moreover, their characteristics can be precisely tailored to suit specific applications, such as reducing viscosity for improved wetting on difficult surfaces. Synthetic adhesives are generally classified into three main categories: thermoplastics, thermosets, and elastomers [53].

1.3.2.3 Thermoset adhesives

Thermoset adhesives form permanent, heat-resistant, and insoluble bonds that cannot be altered without degradation once crosslinking occurs. These adhesives are extensively used in the aerospace industry due to their durability. Examples of thermosetting poly-

mers include phenolic resins such as phenol-formaldehyde, urea-formaldehyde, as well as unsaturated polyesters, epoxies, and polyurethanes [48].

1.3.2.4 Thermoplastic adhesives

Thermoplastics are less heat-resistant but provide strong adhesion at room temperature. They can be softened at elevated temperatures before eventually degrading. Common thermoplastic resins used in adhesives include polyvinyl acetate (PVA), vinyl acetate-ethylene copolymers, polyethylene (PE), polypropylene (PP), polyamides, polyesters, acrylics, and cyanoacrylates [50, 51].

1.3.2.5 Elastomer adhesives

Elastomers can behave as either thermoplastics or thermosets, depending on whether crosslinking is present. Their defining features are flexibility and versatility. Elastomers commonly used in adhesives include various rubbers (e.g., butadiene rubber, butyl rubber, nitrile rubber), silicones, and, in some cases, polyurethanes, which can also be categorized as elastomers [57].

1.3.3 Forms of adhesives

Various forms of adhesive materials, illustrated in Figure 1.10, have been developed in response to modern applications, each tailored for specific uses:

- **Liquid:** Liquid adhesives are straightforward to apply and are well-suited for large surfaces or detailed tasks. Examples include polyvinyl acetate (PVA) and cyanoacrylate [58].
- **Paste:** Paste adhesives, which are thicker than liquids, are ideal for gap filling. High-viscosity epoxy resins are commonly used in this form [58].
- **Tape:** Adhesive tapes, which are pressure-sensitive, consist of an adhesive layer on a backing material. They are typically used for light-duty tasks such as sealing and temporary bonding [59].
- **Film:** Film adhesives offer precise thickness control and are commonly used in laminating processes [58].
- **Pellets:** Pellet adhesives, often thermoplastics or hot melts, are melted for application. Hot melt guns are used for hot melts, while thermoplastics may require equipment like

hot presses or ovens [58].

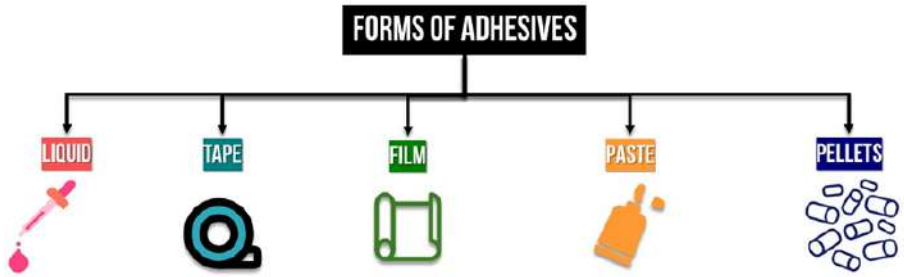

Figure 1.10: Forms of adhesives.

1.3.4 Applications of adhesives

1.3.4.1 Structural adhesives

Structural adhesives, also known as high-performance adhesives, are designed to form strong, durable bonds that can bear significant loads and resist environmental factors such as solvents, heat, vibration, and fatigue [58, 60]. Based on their chemical composition, these adhesives can be categorized into five main families:

- **Epoxy adhesives**

  Epoxy adhesives are thermosetting adhesives known for their mechanical strength, durability, and versatility, making them one of the most commonly used types of structural adhesives in industries such as aerospace, automotive, construction, and electronics. These adhesives are formed by polymerizing epoxy resins, illustrated in Figure 1.11, typically the most used one is diglycidyl ether of bisphenol A (DGEBA) accounting for over 90% of global production. DGEBA is synthesized by O-alkylation of epichlorohydrin with bisphenol A, and its properties vary with chain length: it is crystalline when $n = 0$, liquid for $n < 0.5$, and amorphous for higher values. The oxirane rings in DGEBA facilitate curing, while its aromatic rings provide thermal and chemical resistance, alkyl chains contribute flexibility, and hydroxyl groups enhance adhesion and reactivity. Epoxies can be cured using a variety of hardeners, with amines being the most common. Amines are categorized into aliphatic, cycloaliphatic, and aromatic types, each affecting the curing conditions and final properties of the epoxy. Two key parameters for evaluating epoxy systems are pot life (time to double viscosity) and glass transition temperature (Tg), the latter indicating the polymer's transition from a

glassy to a rubbery state. Aliphatic amines offer short pot lives and are suited for low-temperature applications, while aromatic amines provide superior thermal resistance but require elevated curing temperatures [61].

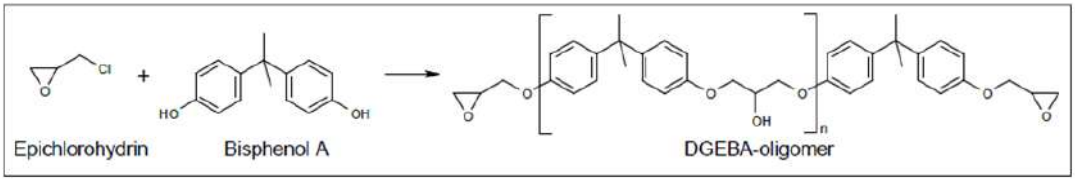

Figure 1.11: Synthesis of Diglycidyl Ether of Bisphenol A (DGEBA) from Epichlorohydrin and Bisphenol A.

- **Polyurethane adhesives**

  Polyurethane adhesives are versatile and are known for their ability to form strong, durable bonds across a wide range of substrates, including metals, plastics, and composites. These adhesives are formed through a reaction between polyols and isocyanates, illustrated in Figure 1.12, resulting in a polymer structure that can be tailored to meet specific application requirements. The unique advantage of polyurethane adhesives lies in their flexibility, which allows them to absorb stress and resist impacts, making them ideal for dynamic environments such as automotive and construction applications. The curing process of polyurethane adhesives can be influenced by the choice of harden-ers, which can include aliphatic or aromatic Poly- isocyanates, each offering different properties such as cure speed, mechanical strength, and environmental resistance [62].

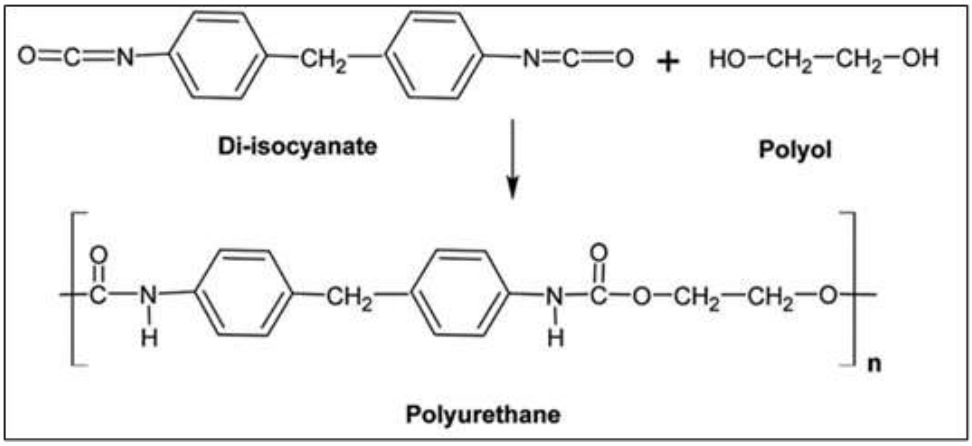

Figure 1.12: Schematic representation of polyurethane (PU) and its monomers. [62]

- **Acrylic adhesives**

Acrylic adhesives, illustrated in Figure 1.13, provide robust bonding strength and rapid curing, making them essential in sectors such as automotive, construction, and electronics. Composed mainly of acrylate and methacrylate monomers, these adhesives undergo polymerization through a free-radical mechanism, resulting in highly durable bonds. Available in both one-part and two-part systems, they are particularly effective in structural applications, with two-part systems offering increased mechanical strength and resistance to harsh environmental conditions. The curing process, typically initiated by peroxides, can be precisely controlled by modifying the adhesive's formulation and the specific substrates involved [63, 64].

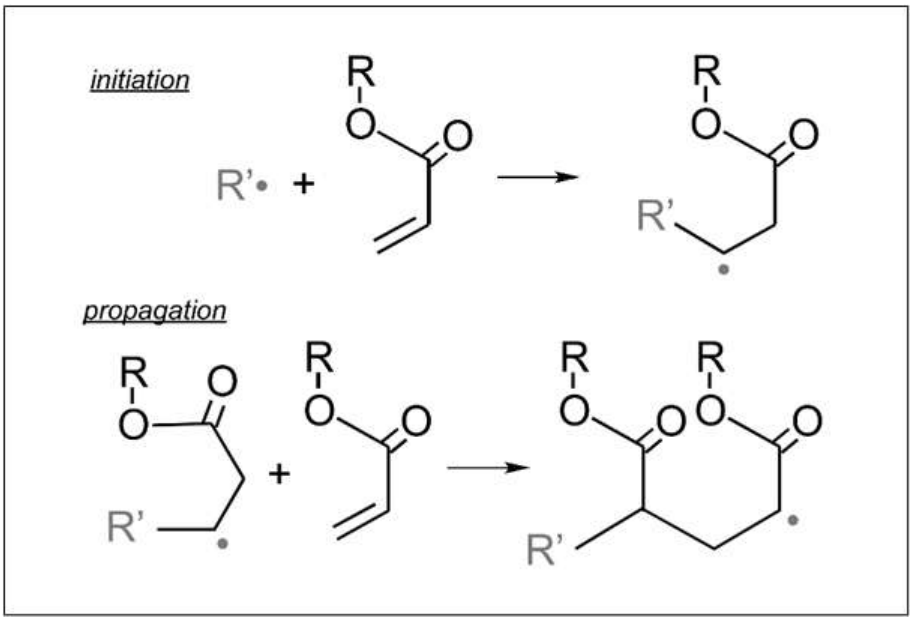

Figure 1.13: Acrylic adhesives polymerization reaction.
[63, 64]

- **Phenolic adhesives**

  Phenolic adhesives, illustrated in Figure 1.14, are a class of thermosetting adhesives that are particularly valued for their high thermal stability, water resistance, and mechanical strength. These adhesives are derived from the polycondensation of phenol with formaldehyde, producing a robust polymer network that is well-suited for applications in harsh environments, such as aerospace, automotive, and construction. Phenolic adhesives can be modified with different fillers or co-polymers to enhance specific properties like flexibility or adhesion to various substrates. The curing process of phenolic adhesives generally requires heat, which promotes the cross-linking of the polymer chains, resulting in a rigid and durable bond [65].

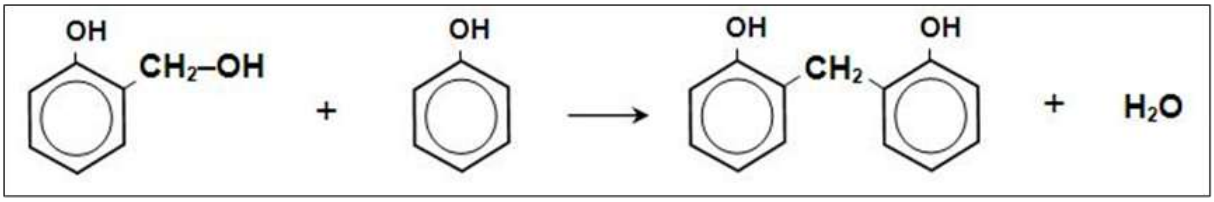

Figure 1.14: Phenolic adhesives polymerization reaction.
[65]

- **Structural thermoplastics**

  Structural thermoplastics are a class of high-performance materials recognized for their durability, flexibility, and resistance to impact and environmental stress. Unlike thermosetting polymers, these materials can be repeatedly melted and reshaped, offering significant advantages in both processing and recyclability. Key examples of structural thermoplastics include polyamide (nylon), polycarbonate, polyetheretherketone (PEEK), illustrated in Figure 1.15,and polyphenylene sulfide (PPS). The molecular structure of these thermoplastics often features a high degree of crystallinity, which enhances their strength and rigidity.Thanks to their mechanical properties and resistance to chemicals and high temperatures, these thermoplastics find applications in industries such as automotive, aerospace, and medical devices such as the use of PEEK for medical implants [66, 67].

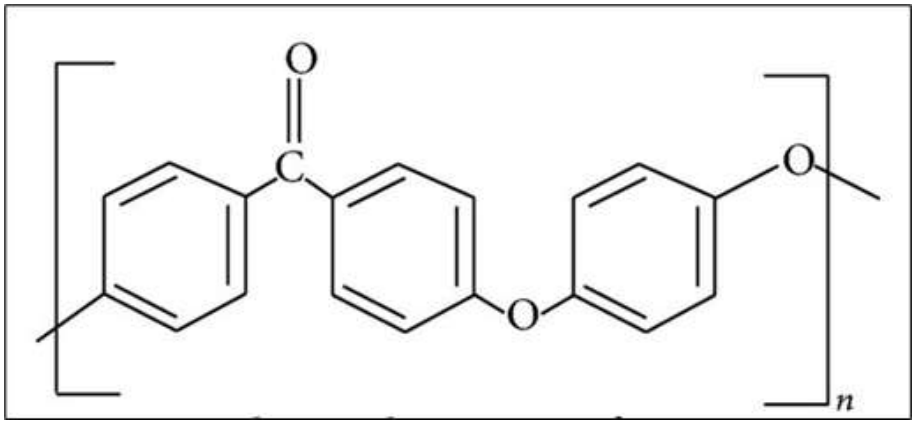

Figure 1.15: Chemical structure of PEEK.

1.3.4.2 Non-structural adhesives

Non-structural adhesives are used in applications that do not require high load-bearing capacity. These adhesives are typically chosen for their ease of use, flexibility, and ability to adhere to a variety of surfaces. They can be categorized as well under 5 different families:

- **Elastomeric adhesives**

  Elastomeric adhesives are a subset of non-structural adhesives, characterized by their flexibility and resistance to environmental stressors, such as moisture and temperature variations. These adhesives are broadly classified into two primary types: rubber-based and silicone-based. Rubber-based elastomeric adhesives, which encompass both natural rubber and synthetic forms like styrene-butadiene rubber (SBR), are usually utilized in applications such as footwear, upholstery, and general-purpose sealing, where both durability and flexibility are essential. In contrast, silicone-based elastomeric adhesives are distinguished by their superior resistance to extreme thermal conditions and weathering, making them particularly suitable for applications in sealing, gasketing, and caulking within the construction and electronics sectors [68, 69].

- **Pressure-sensitive adhesives (PSAs)**

  Pressure-sensitive adhesives (PSAs) are a class of nonstructural adhesives designed to adhere to surfaces with light pressure without the need for additional activation, such as heat or solvents. The performance of PSAs is critically dependent on their rheological properties, which influence their tack, peel strength, and shear resistance. These adhesives are primarily based on viscoelastic polymers, which allow them to form strong bonds that are flexible and durable. PSAs are commonly categorized into different types, including rubber-based and acrylic-based formulations, each offering specific properties tailored to various applications. Rubber-based PSAs are known for their flexibility, good initial tack, and resilience, making them ideal for use in tapes, labels, and packaging. Acrylic-based PSAs, on the other hand, provide excellent aging resistance, UV stability, and clarity, which are particularly valuable in medical, automotive, and electronic applications [59, 70].

- **Hot melt adhesives**

  Hot melt adhesives, illustrated in Figure 1.16, are thermoplastic materials that provide instant bonding through rapid solidification as they cool, making them ideal for high-speed production processes. These adhesives are composed of polymers that provide structural integrity, tackifiers that enhance adhesion by lowering the glass transition temperature and viscosity, and sometimes waxes to speed up the setting process. A common example of HMAs is EVA-based (ethylene-vinyl acetate) hot melt adhesives. The performance of HMAs is heavily influenced by their rheological properties, which govern the adhesive's flow behavior in its molten state, as well as its tack, peel strength, and shear resistance once solidified. Common applications of HMAs include packaging,

bookbinding, automotive assembly, and woodworking, where it is possible to benefit from their ability to bond a variety of substrates with minimal environmental impact [69, 71].

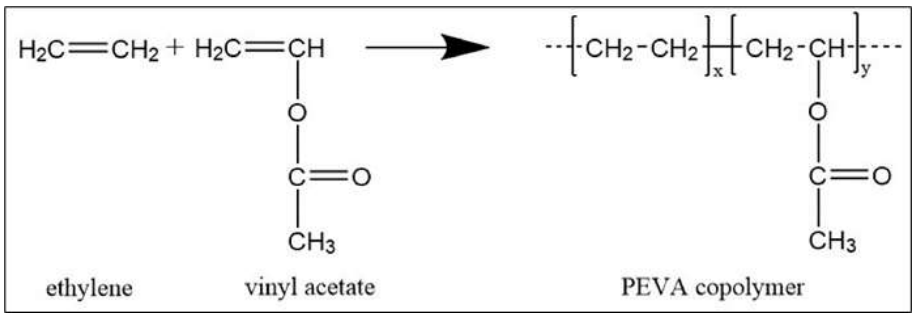

Figure 1.16: Ethylene-vinyl acetate hot-melt adhesive.

- **Polyvinyl acetate (PVA) adhesives**

  Polyvinyl acetate (PVA) , illustrated in Figure 1.17,adhesives are non-structural adhesives, particularly valued for their strong bonding capabilities with porous materials such as wood, paper, and fabrics. As water-based adhesives, PVA adhesives are easy to use, non-toxic, and clean up easily with water, making them ideal for applications in woodworking, bookbinding, and various crafts. These adhesives function by forming a flexible film upon drying, which provides good adhesion and durability under dry conditions [72]. Meanwhile traditional PVA adhesives suffer from limitations such as low water resistance and poor performance in humid environments. As a solution to these various modifications have been proposed. For example, adding nano-clay or cellulose nanofibrils to PVA adhesives has been shown to improve their thermal stability, water resistance, and mechanical strength [73].

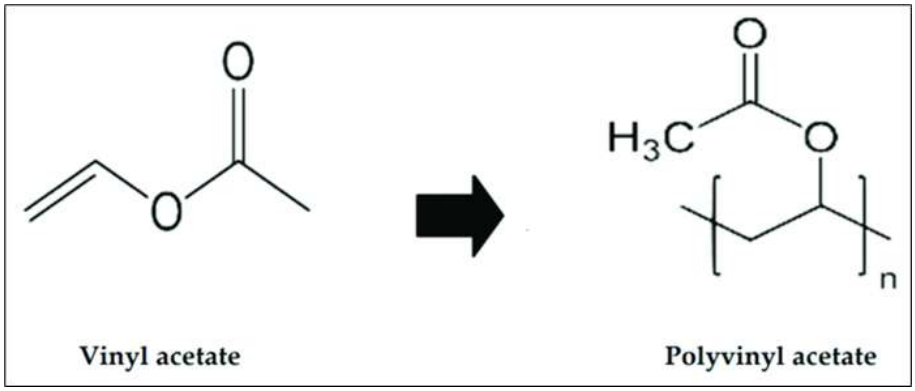

Figure 1.17: Polyvinyle acetate adhesives polymerisation.

1.3.5 Composition of adhesives

An adhesive formulation is not solely composed of a resin; rather, it typically consists of a carefully blended mixture, illustrated in Figure 1.18, tailored to meet specific application needs and desired final properties. While the primary components in synthetic adhesives are the polymer backbone (resin) and hardeners various other constituents are often incorporated into the formulation to modify the adhesive's properties both before and after curing. These additional components can significantly impact the adhesive's behavior, including its mechanical strength, flexibility, and environmental resistance [61, 69]. Among these components we find:

- **Solvents:** Used to control viscosity and facilitate the application and spread of the adhesive across the substrate surface. However, the use of solvents often necessitates an additional evaporation step [69].
- **Fillers and additives:** Widely employed in industrial applications, fillers and additives serve multiple purposes. Primarily, they reduce the cost of the adhesive but can also enhance its mechanical and thermal properties. They are used in substantial amounts, sometimes comprising 60-70% of the total weight. For instance, tackifiers improve adhesion, while metallic fillers create conductive layers [69].
- **Catalysts:** Catalysts are added to initiate and accelerate the curing reaction, thereby reducing the curing temperature and time [69]. An example is 2-methylimidazole (2-MI), which significantly speeds up the epoxy-amine curing process [74].
- **Plasticizers:** Introduced at low concentrations, plasticizers reduce viscosity and enhance flexibility without compromising the adhesive's mechanical properties [69, 75].
- **Antioxidants:** Added to protect the polymer matrix from oxygen, heat, and UV light, antioxidants prevent the formation of free radicals that can degrade the polymer. They also improve shelf life and durability [69]. For example, butylated hydroxytoluene (BHT) is effective in stabilizing polymers by scavenging free radicals and interrupting oxidative chain reactions [76].
- **Pigments and dyes:** These are incorporated to modify the color of the cured adhesive [61].

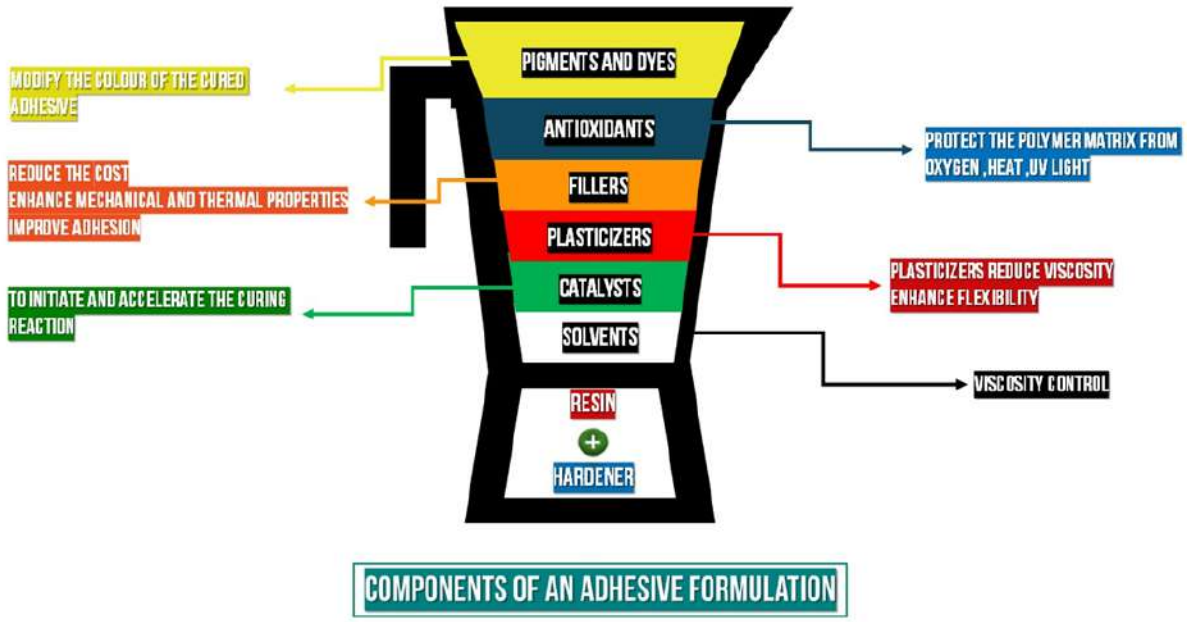

Figure 1.18: Different components of an adhesive formulation.

1.4 Adhesive joints design

An adhesive joint is a complex system composed of multiple components, , illustrated in Figure 1.19,each contributing various factors that must be carefully optimized to achieve strong bonding and ensure that the joint can withstand mechanical loads and environmental conditions throughout the component's lifespan. Designing an adhesive joint requires a multifaceted approach that considers both internal and external factors. Internal factors include surface treatment, adhesive composition, joint geometry, and processing parameters, all of which directly influence the performance of the adhesive bond. External factors, such as environmental conditions and application parameters, also play a critical role in determining the durability and effectiveness of the adhesive joint over time [77, 78].

1.4.1 Surface treatment

In theory, any type of material can be bonded using an adhesive layer. However, the distinct surface properties of different materials require specific pretreatments to achieve effective bonding [77].

Moreover, the chosen surface preparation method must be compatible with the adhesive system in use. For example, high-temperature treatments intended to activate a sur-

face are not suitable for low Tg thermosets, as they may lead to premature crosslinking [79] . Generally, all surfaces undergo an initial cleaning step before further treatment [80].

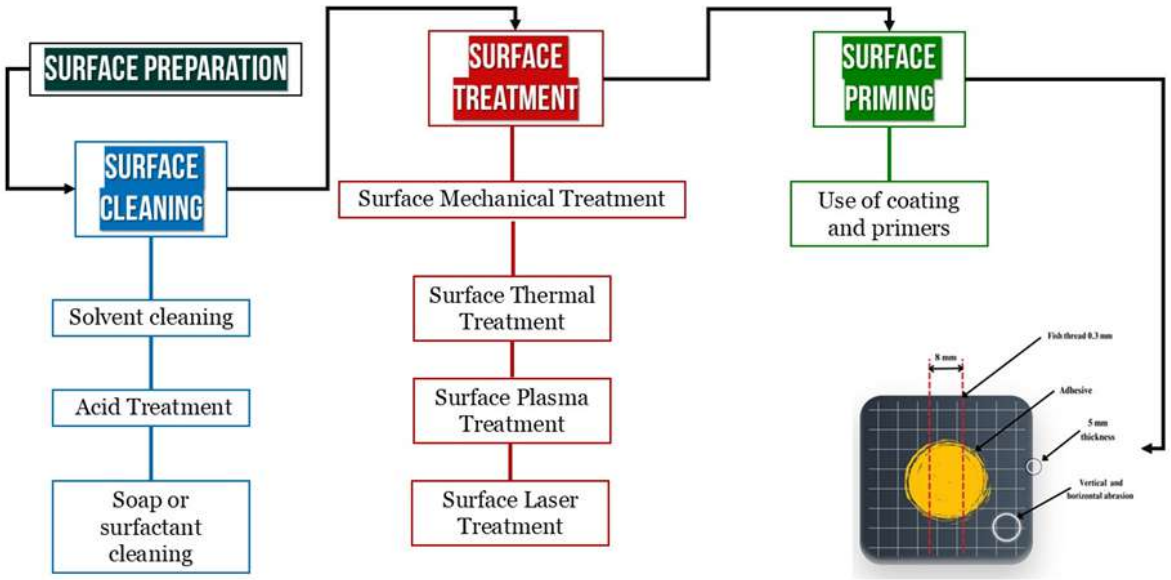

Figure 1.19: Steps of substrate surface treatment.

1.4.1.1 Surface cleaning

An adhesive joint surface treatment almost invariably begins with the cleaning of the surface. This step is essential because it ensures that contaminants such as oils, greases, dirt, and oxidation are removed, thereby ensuring optimal adhesion [77]. Different kinds of treatment can be employed for this purpose, these methods englobe:

- **Solvent cleaning**

  Solvent cleaning also known as degreasing is a common method to remove, dust, oils (fats) and grease from surfaces, utilizing various solvents with specific properties. Common solvents include isopropyl alcohol (IPA), which is effective for general cleaning and a green solvent. Ethanol and acetone are a strong solvent for heavy grease and oil but potentially too aggressive for some plastics. methyl ethyl ketone (MEK), toluene and trichloroethylene are used for heavy-duty cleaning but with significant health and safety concerns. Solvent cleaning is preferably done with lint free cloths or micro-fiber cloths, since they can effectively trap and remove particles and retaining oil and dust [69, 81].

- **Acid treatment**

Acid treatments can be employed to clean and etch surfaces, enhancing adhesion by increasing surface roughness and removing oxide layers. This process temporarily alters the surface chemistry and pH. The choice of acid depends on the substrate [69]. Chromic acid is commonly used on metals like aluminum, where it creates an oxide layer that improves adhesion [82]. Sulfuric acid is effective for treating rubber and certain plastics, both cleaning and roughening the surface [83]. For carbon fibers, nitric acid is often used, as it is a milder acid that cleans the fibers and slightly etches the surface without damaging the fiber structure, thereby promoting better bonding [84]. Hydrochloric acid, often used in combination with other chemicals, is suitable for specific substrates like rubber but is typically avoided on metals due to its highly corrosive nature [85].

- **Soap or surfactant cleaning**

  Soap cleaning method uses of detergents and surfactants, which are highly effective at breaking down and removing organic contaminants such as oils, greases, and dirt from the substrate surface [69]. The surfactants work by reducing the surface tension, allowing the contaminants to be lifted away from the surface more easily [86]. After the cleaning agents have been applied, a thorough rinsing step is essential to remove any remaining residues and to prevent any interference with subsequent adhesive bonding.

1.4.1.2 Surface mechanical treatment

Mechanical treatment of adhesive substrates is a fundamental technique used to enhance adhesion strength by physically modifying the substrate surface. This modification increases surface roughness and, consequently, the effective surface area, which can grow by up to two orders of magnitude compared to the nominal area [86]. The enhanced roughness promotes better surface wettability and facilitates mechanical interlocking between the adhesive and the substrate. Surface roughness is a complex, multi-parameter characteristic that cannot be fully described by a single value. It is typically quantified using various parameters classified into four main categories: amplitude (e.g., Ra, Rz, Rt), which describe the vertical deviations; spacing (e.g., Sm), indicating the distance between surface features; hybrid parameters (e.g., q), reflecting slope and curvature; and symmetry or functional parameters (e.g., Rsk for skewness, Rku for kurtosis), which provide insight into the shape and distribution of peaks and valleys [85, 87]. Measurement techniques include contact profilometers (stylus tracing), non-contact optical profilometers (light scanning), atomic force microscopy (AFM), and scanning electron microscopy

(SEM), each offering unique advantages and limitations. While increasing surface roughness generally enhances adhesion, there is a practical limit; excessively deep cavities and sharp surface asperities can hinder the adhesive's ability to penetrate effectively [88].

Different mechanical treatment methods vary in effectiveness based on the substrate material and specific application requirements. For instance, sandblasting and grit blasting are often preferred for their speed, efficiency, and precise control, typically achieving a recommended surface roughness (RMS) of about 150 to 250 microinches for metals. In contrast, abrasion with sandpaper, though more labor-intensive and operator-dependent, is well-suited for smaller or more delicate components. Wire brushing is another viable option, effectively removing surface deposits and creating a texture conducive to bonding [69, 89].

In addition to altering the surface topography, mechanical treatments also impact the surface chemistry by removing contaminants and weak boundary layers. These treatments can expose fresh, reactive metal surfaces, further enhancing chemical bonding with the adhesive [69].

1.4.1.3 Surface thermal treatment

Surface thermal treatment involves applying heat to the surface of substrates, with temperatures reaching as high as 300°C. Pre-heating the substrates can enhance the wetting and spreading of the adhesive, eliminate adsorbed moisture and contaminants, and promote a more uniform bond line, resulting in better adhesion. However, a potential drawback is that the high temperatures can cause thermal degradation, leading to color changes in some substrates, and in certain cases, may induce premature cross-linking [90].

1.4.1.4 Surface plasma treatment

Plasma is the fourth state of matter, consisting of a gas of freely moving electrons and positively charged ions, which together form an electrically neutral system that reacts strongly to electric and magnetic fields. [90] It is generated by applying an electrical field to a gas, which ionizes the gas atoms, turning the gas into an electrical conductor. his process, typically achieved using radio frequency (RF) or microwave energy, ionizes gases like oxygen, argon, or nitrogen [91]. The resulting energetic ions, electrons, and neutral particles interact with the substrate surface, breaking molecular bonds and creating new reactive sites. This interaction introduces polar functional groups, such as hydroxyl and carboxyl groups, onto the surface, increasing its surface energy and improving wettability

[92,93]. Additionally, plasma treatment effectively cleans the surface by removing organic contaminants and weak boundary layers, making the substrate more chemically active and ready for bonding [93]. Plasma treatment is used, in a controlled environment to "activate" the substrate surface, enhancing its adhesive properties. Plasma treatment can also lead to other effects, such as photoexcitation and coating deposition, and can create surface roughness through chemical etching [94]. While plasma treatment is precise and can create a uniformly activated surface, the duration of its effects varies depending on the substrate material. For instance, on plastics, the activated state may last only a few minutes, while on metals, it can persist for several hours .This rapid loss of activation on polymers is primarily due to hydrophobic recovery a phenomenon in which the surface reverts to its original low-energy state as polar groups reorient or migrate whereas metals retain their surface energy longer, with re-contamination by airborne species being the main factor in the gradual loss of activation [95].

1.4.1.5 Surface laser treatment

Laser treatment is an emerging technology that involves exposing a substrate surface to laser radiation, which is absorbed by the surface, generating intense heat capable of vaporizing various materials. This non-contact technique can be employed for cleaning, texturing, increasing surface roughness, or even incorporating new elements into the surface [96]. The advantages of laser treatment are significant: it eliminates direct contact with the surface, reducing the risk of contamination, allows for precise, localized treatment, and offers a rapid processing speed. Parameters such as laser power, wavelength, pulse duration, and scanning speed can be optimized to suit different materials and achieve specific surface modifications [96,97].

1.4.1.6 Use of coating and primers

Primers are thin coatings applied to substrate surfaces before the adhesive layer, serving as an intermediate layer to enhance the substrate's receptivity to the adhesive [69, 98]. Primers fulfill several critical roles: they increase surface energy and improve the wettability of the surface, ensuring better adhesion [99]. Additionally, primers provide a uniform base layer, which is particularly beneficial for surfaces with deep porosities [61]. Primers can also act as cross-linking agents and serve as barriers against oils, plasticizers, and corrosion, particularly in metal substrates [100]. Typically, primers are diluted epoxy-based or polyurethane-based formulations. Beyond improving adhesion, primers are especially useful for bonding surfaces with inherently low surface energies, such as plastics, and are

commonly used when painting over non-stick surfaces like polyethylene [101, 102].

1.4.2 Adhesive joint geometry

The geometry of an adhesive joint is the factor that will influence how the joint will distribute the stress across the bonded area, thus influencing the joint strength and performance. Various geometries, illustrated in Figure 1.20, are employed depending on the application requirements, with common types including single-lap joints (SLJ), double-lap joints (DLJ), stepped-lap joints, and scarf joints [103]. Single-lap joints are among the most straightforward and cost-effective to produce, making them popular in many applications. However, their simplicity comes with a drawback: the stress distribution across the joint is often uneven, leading to concentrated peel and shear stresses at the edges of the overlap. Double-lap joints, by contrast, offer a more balanced stress distribution compared to single-lap joints. The additional bonded surface area in double-lap joints helps to reduce peel and shear stresses, improving the overall durability of the joint [104]. Stepped-lap joints and scarf joints further optimize stress distribution by providing more gradual transitions across the bonded area, which can significantly enhance the joints load-bearing capacity and resistance to peeling forces [105, 106]. Additionally, improving joint strength can be achieved by incorporating a strapping layer, which reinforces the joint and helps distribute stress more evenly. Increasing the length of the bond line is another effective strategy, as it provides a larger surface area for the adhesive to bond, thereby reducing the stress per unit area and enhancing the overall strength of the joint. This approach is particularly beneficial in applications where high loads are anticipated, or where the joint must withstand harsh environmental conditions [103, 106].

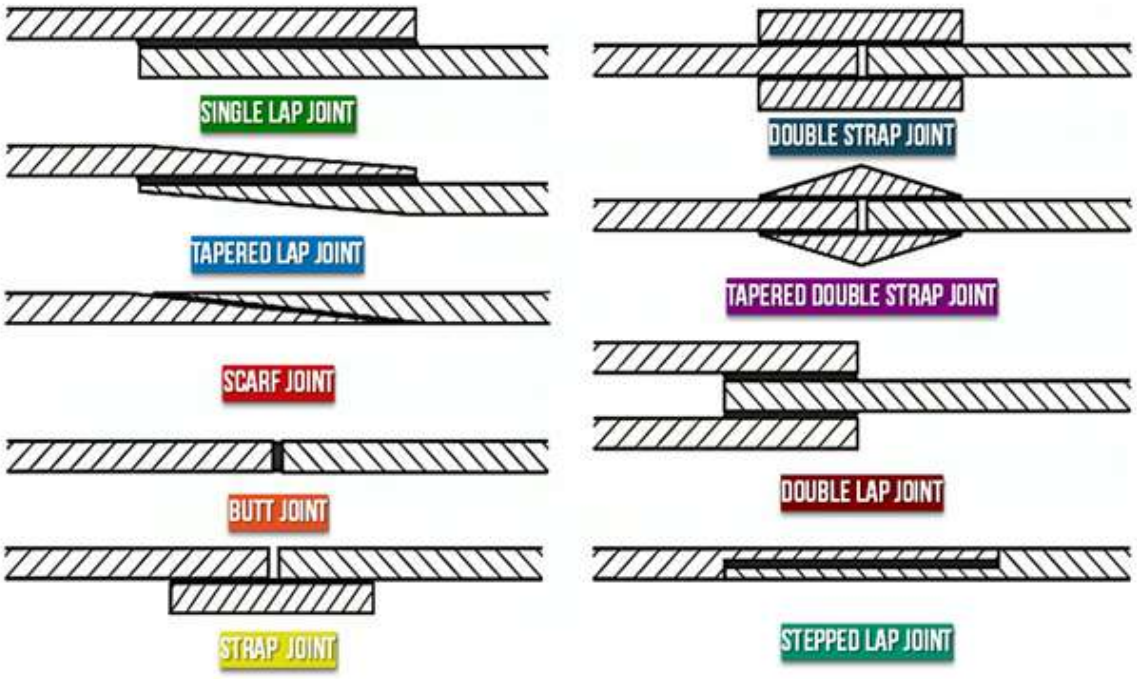

Figure 1.20: Different adhesive joint geometry.
[105, 106]

1.4.3 Application and processing of the adhesives

1.4.3.1 Processing of the adhesives

The processing step involves preparing the adhesive before application is important for ensuring the joints strength. As illustrated in Figure 1.21, The processing step includes degassing to remove air bubbles that could weaken the bond [107]. For two-component adhesives, proper mixing is necessary to achieve a uniform distribution of the components and consistent curing. Various mixing techniques are used depending on the scale and precision required [108]. Manual mixing with a spatula is simple but can introduce air bubbles if not done carefully. Static mixing, often with cartridge systems, provides a consistent mix during dispensing. Mechanical mixers, such as magnetic stirrers or ultrasound probes, offer thorough mixing for larger volumes, but they might introduce air bubbles, which is why the degassing is preferably done after the mixing [109]. Speed mixers, which use centrifugal force to quickly create a homogeneous mixture, are effective in minimizing air bubbles and are preferred in high-performance applications [110]. In-line mixing systems, used in automated production, continuously mix the adhesive as it moves toward the application point. The adhesive formulation and the application needs will define

which technique is selected [111].

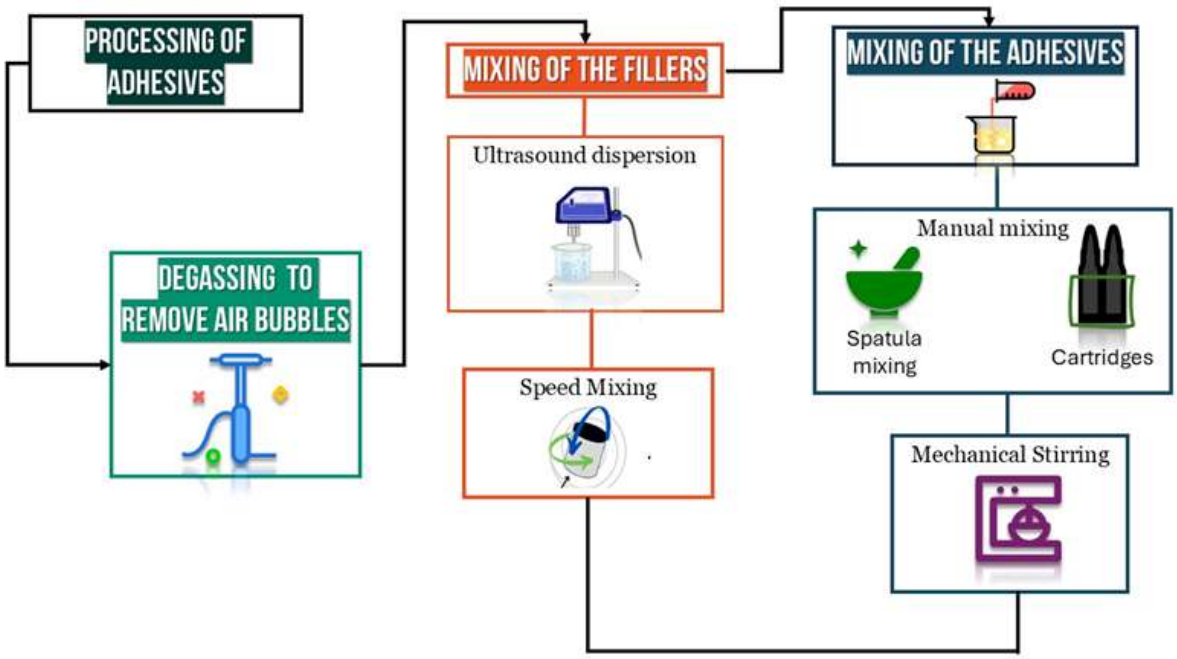

Figure 1.21: Different steps of adhesive processing before application.

1.4.3.2 Application mode

The selection of an appropriate adhesive application method depends on the substrate surface characteristics, the scale of the application, and the specific requirements of the end-use.

- **Manual application**

  Manual application involves the deposition of adhesive materials using handheld tools such as brushes, rollers, glue guns, or trowels. This method is primarily employed in situations requiring fine control and precision, often in small-scale or prototype applications. Manual application is an effective and straightforward approach, making it particularly suitable for processes involving limited surface areas, such as small-sized adhesive joints (e.g., SLJ samples) or lab-scale composites prepared using hand lay-up methods [112].

- **Glue applicators**

  Glue applicators are mechanized devices designed to dispense adhesives with uniformity and precision. These tools are used to large-scale industrial operations where consistency in adhesive application is essential. Glue applicators are commonly used

in sectors such as aerospace, electronics, and automotive manufacturing, where the speed of application and the quality of adhesive distribution directly impact the performance and reliability of the assembled components [113].

- **Spray application**

  Spray application utilizes atomization techniques to disperse adhesives in the form of a fine mist, which facilitates uniform coverage over large surface areas. This method is particularly advantageous in high-volume production environments such as automotive and furniture manufacturing [114].

- **Beads and dots application**

  Adhesive beads and dots are applied using precision dispensing nozzles, enabling targeted deposition in specific areas. This method is utilized in detailed assembly processes, especially within the electronics industry, where accurate adhesive placement is crucial for the functionality and longevity of the final product. The controlled application provided by this technique helps form localized bonds thereby enhancing the overall structural integrity [115].

- **Dipping application**

  Dipping involves immersing components entirely in an adhesive solution to ensure complete coverage, making it particularly useful for complex geometries or surfaces that are difficult to coat by other means. This technique is especially advantageous for parts with intricate designs, ensuring uniform coverage across all surfaces, including recessed or hard-to-reach areas. However, while dipping is effective for achieving thorough coverage, it presents several challenges. A primary concern is the potential for excessive adhesive buildup, which can result in uneven coating thickness and may necessitate additional processing steps, such as draining or wiping, to achieve uniformity. Additionally, the technique can be inefficient in terms of adhesive usage, as significant amounts of adhesive may be wasted during the immersion process [116].

- **Vacuum infusion for composites**

  Vacuum infusion represents an advanced adhesive application technique primarily used in the fabrication of composite materials. In this process, dry reinforcement materials are placed within a mold, and a vacuum is applied to draw in a low-viscosity resin, which acts as the adhesive. The resin permeates the reinforcement fibers under vacuum pressure, ensuring thorough impregnation. This method allows for precise control of the resin-to-fiber ratio, which is critical for optimizing the mechanical properties of

the composite. Specialized adhesives designed for compatibility with vacuum infusion are often employed to enhance interlaminar shear strength and improve the overall bonding quality within the composite structure [117].

1.4.3.3 Application patterns

The application pattern of the adhesive is important for two key reasons. First, it helps reduce costs by preventing excess adhesive from being used, thereby minimizing waste. Second, it ensures effective removal of air bubbles when the adhesive layer is pressed between substrates, which is essential for achieving a strong and uniform bond. Figure 1.22 shows a simplified simulation diagram comparing different application patterns [118].

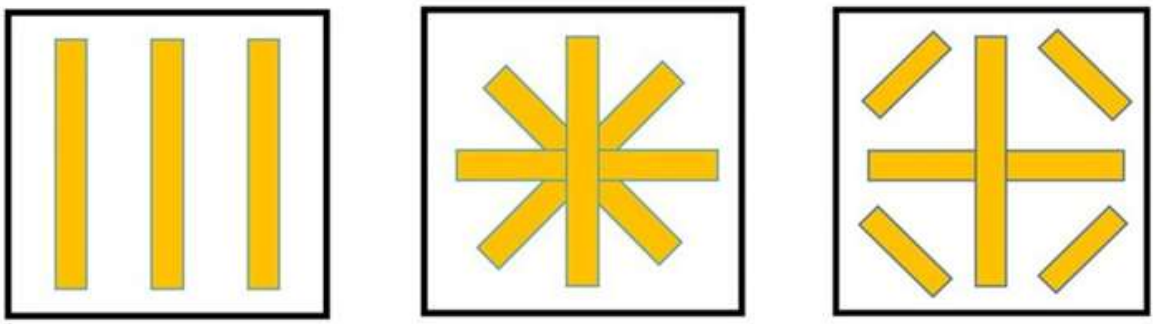

Figure 1.22: Adhesive application patterns: rectangular surfaces, left- conventional application pattern, middle and right - "exotic".
[118]

1.4.4 Adhesive bonding gap (Adhesive layer thickness)

The thickness of the adhesive layer, known as bond line thickness, is an important factor that affects the strength and performance of adhesive joints. Figure 1.23 illustrates the correlation between Bond-line Thickness (mm) and failure stress (MPa). Optimal thickness allows for effective stress distribution across the bonded interface, improving the joint's mechanical properties [119]. Generally, a thinner adhesive layer provides higher shear strength due to reduced stress concentrations and better load transfer between substrates. However, if the layer is too thin, it can lead to adhesive starvation, where there isnt enough adhesive to fill surface irregularities, resulting in weaker bonds [120]. A thicker adhesive layer can accommodate surface roughness and manufacturing tolerances, but it may cause issues like increased peel stresses and a greater chance of cohesive failure within the adhesive [121]. For rigid adhesives like epoxy, the optimal thickness range is typically between 0.1 mm and 0.5 mm, where the balance between flexibility and strength

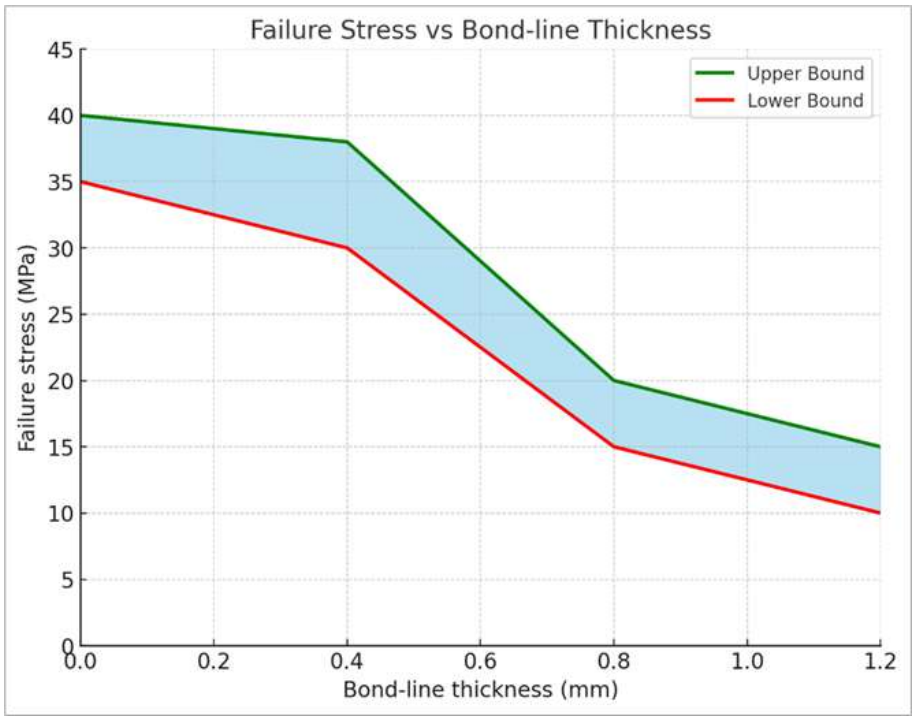

Figure 1.23: Effect of adhesive thickness.
[119, 120]

is most effective. Thicknesses below 0.1 mm usually led to poor performance. Flexible adhesives, such as polyurethanes, can handle thicker bonding layers, with up to 1 mm being common [122]. Bond line thickness can be controlled using shims, glass beads, or wires, especially with rigid thermosetting adhesives. These materials help maintain the desired thickness without negatively impacting the joint's strength [123].

1.4.5 Adhesive joint characterization

The end goal of using adhesive joints is to be incorporated within more complex engineered structures. Which is why adhesive joints are typically tested, or simulated prototypes are evaluated, to predict how they will perform in their intended applications. The characterization process focuses on two main aspects. The first is mechanical testing, where the whole adhesive joint is tested. The second aspect involves the physico-chemical properties, where the adhesive layer is primarily tested.

1.4.5.1 Mechanical characterization

Mechanical characterization of adhesive joints is essential for studying their performance, durability, and applicability. However, at present, no non-destructive technique exists that can assess the integrity of an adhesive joint without subjecting it to stress until

failure [124]. Adhesive joints may fail under various loading conditions, classified into three fundamental fracture modes illustrated in Figure 1.24: Mode I (opening mode), Mode II (sliding mode), and Mode III (tearing or scissoring mode). Mode I involves tensile stresses perpendicular to the crack plane, causing joint opening; Mode II entails in-plane shear stresses parallel to the crack front, leading to sliding between adhesive and adherend; and Mode III involves out-of-plane shear stresses causing tearing along the crack front [125].

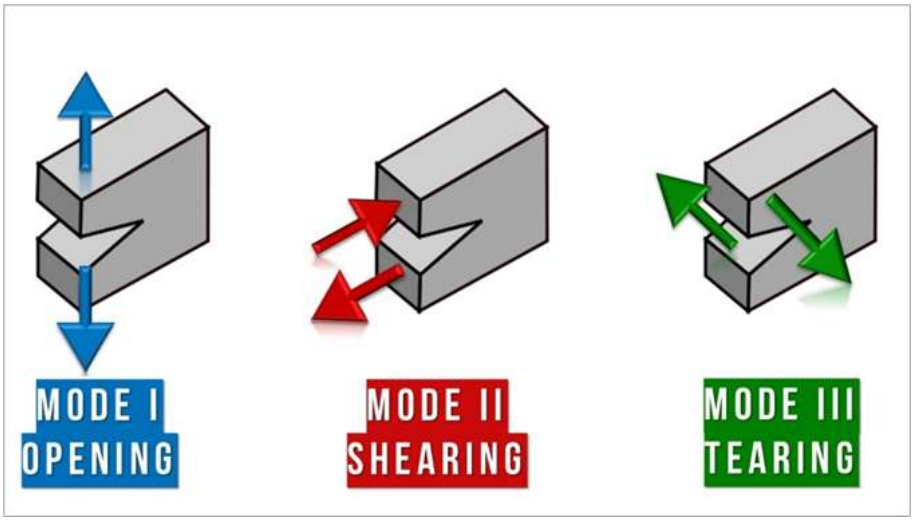

Figure 1.24: Opening modes for mechanical characterization.

Mechanical testing methods for adhesive joints can be classified into quantitative, qualitative, and semi-quantitative techniques. Quantitative methods provide numerical data on mechanical properties. For instance, the Single Lap Joint (SLJ) test, following ASTM D1002 and ISO 4587 standards, measures the shear strength of adhesives by applying tensile load to lap-jointed specimens, inducing shear stress in the adhesive layer. This test is widely used for structural adhesives to assess performance under shear loading [126]. Another example is the Double Cantilever Beam (DCB) test, conforming to ASTM D3433 and ISO 25217 standards, which evaluates Mode I fracture toughness by measuring the energy required to propagate a crack under tensile opening forces. This test provides data on the adhesive's resistance to crack initiation and growth [127]. Flexural tests, as per ASTM D7905, assess Mode II fracture toughness by applying a three-point bending load to a notched specimen, inducing shear loading conditions, and determining the adhesive's ability to resist shear-driven crack propagation.

Semi-quantitative methods offer comparative data that rank adhesives but may not provide absolute values. The scratch test, for example, assesses adhesion by measuring

the force required to scratch through the adhesive layer. Although it does not provide exact adhesion values, it allows for comparative evaluation between different adhesives or surface treatments [126]. Peel tests, such as the T-Peel Test (ASTM D1876) and the 90-Degree Peel Test (ASTM D6862), measure peel strength by separating adherends through peeling action. These tests are considered semi-quantitative because they can be influenced by factors like adherend flexibility and may not always reflect pure adhesive properties [127].

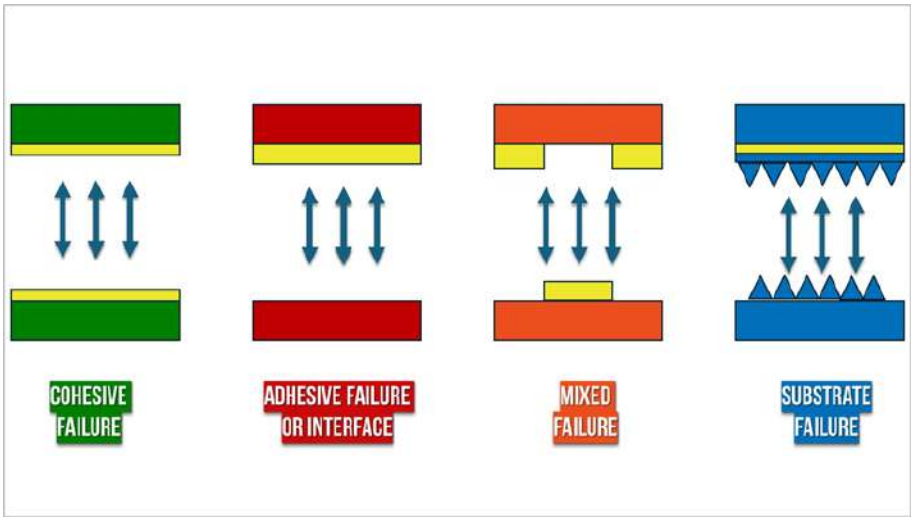

Figure 1.25: Main failure patterns in an adhesive Joint.

Lastly, qualitative methods involve assessments of failure modes, adhesion quality, and surface characteristics. Analyzing failure surfaces after mechanical testing allows for the identification of failure types schematically represented in Figure 1.25: adhesive (at the interface), cohesive (within the adhesive), or mixed, which aids in evaluating the effectiveness of surface preparation and adhesive selection [128, 129]. Visual inspection and microscopic examinations, such as optical microscopy, complement mechanical test data by revealing morphological features of the fracture surface, thereby enhancing the understanding of interfacial bonding quality and failure mechanisms.

1.4.5.2 Physico-chemical characterization

Physico-chemical characterization of adhesive joints focuses on investigating the adhesive layer by examining its thermal behavior, chemical stability, and long-term performance under various environmental conditions. This is achieved primarily through analytical techniques that provide insights into the adhesives properties at both molecular and macroscopic levels. Parameters like the glass transition temperature (Tg) or degrada-

tion behavior of an adhesive formulation are highly sensitive to variation. Using the same epoxy resin for multiple formulations, these properties can be significantly influenced by the choice of hardener, the type of filler incorporated, and the filler loading rate .

In general, to provide a holistic understanding of the physico-chemical properties, a combination of these techniques is used. First, Differential Scanning Calorimetry (DSC) is employed to determine the glass transition temperature (Tg) and other thermal transitions of the adhesive material. DSC provides insights into the thermal properties that influence the mechanical performance and service life of the adhesive joint. The Tg as illustrated in Figure 1.26, marks the temperature range over which the adhesive transitions from a rigid, glassy state to a more flexible, rubbery state, affecting its load-bearing capacity [128]. Second, Thermogravimetric Analysis (TGA) assesses the thermal stability and decomposition behavior by monitoring the mass change of the adhesive as a function of temperature. TGA identifies degradation temperatures and quantifies the amount of volatile compounds released during thermal decomposition, making it possible to predict the adhesive's performance in high-temperature applications and for understanding its thermal degradation mechanisms [129]. In addition, Dynamic Mechanical Analysis (DMA) evaluates the viscoelastic properties of the adhesive, such as storage modulus, loss modulus, and damping factor, over a range of temperatures or frequencies. DMA provides valuable data on the material's stiffness and energy dissipation characteristics under dynamic loading conditions. This analysis is essential for applications where the adhesive joint is subjected to vibrations, cyclic stresses, or varying thermal environments [130].

Finally, the aging of adhesive samples is essential for evaluating their long-term durability under various environmental conditions. Common aging methods include heat cycling, where adhesives are repeatedly subjected to alternating high and low temperatures, simulating thermal stress encountered in real applications. Water aging, which involves immersion in water or exposure to high humidity, is used to assess the adhesives resistance to moisture-related degradation, such as hydrolysis or swelling. Additionally, ultraviolet (UV) aging exposes the adhesive to UV light to replicate prolonged sunlight exposure, which can lead to photodegradation of the polymer matrix [131].

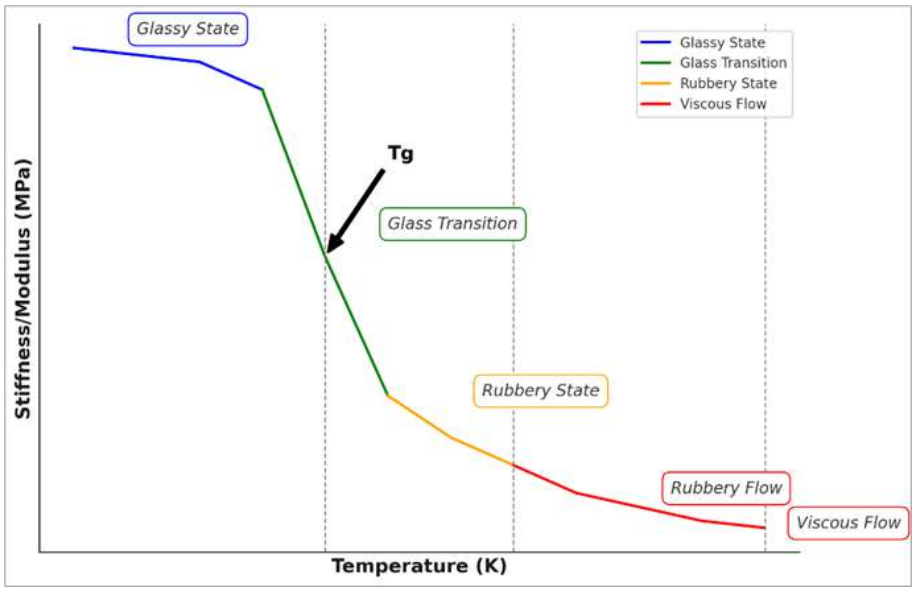

Figure 1.26: Graph of glass transition temperature plotting the temperature and stiffness of a material.

[130, 131]

2 Debond-On-demand technologies

A debond-on-demand technology is an adhesive system that allows bonded joints to be intentionally weakened or separated so that the substrates can be recycled, or the component can be updated when triggered by a specific external stimulus. To qualify as a debonding technology, the adhesive system must maintain all the mechanical properties of the adhesive joint, whether the technology involves the use of fillers within the adhesive material or relies on reactive modifications to the adhesive polymer. In either case, the mechanical properties of the adhesive must be comparable to those of conventional adhesives used in similar applications within the respective field [132, 133]. Throughout its operational lifespan, the adhesive should resist aging and environmental degradation, ensuring that its bonding strength remains intact until debonding is intentionally initiated [134]. The technology must respond precisely to the designated stimulus, whether thermal, electrical, chemical, or otherwise, causing the bond to weaken and enabling easy separation of the substrates [135, 136]. After debonding, the activated adhesive leaves minimal residue, allowing the substrates to be reused without significant reprocessing [137, 138]. These technologies can be categorized into two major types: filler-based technologies and reactive adhesive-based technologies [139, 140].

2.1 Filler based technologies

2.1.1 Thermally expandable fillers

Thermally expandable fillers are debonding technologies that operate by expanding in size when exposed to heat, thereby causing a mechanical compromise in the structure of adhesive joints. These technologies can be broadly segmented into two types: physical foaming agents and chemical foaming agents. Physical foaming agents, such as Thermally Expandable Particles (TEPs), function by increasing in volume upon heating. TEPs consist of polymeric shell materials encapsulating an active agent that, when triggered by heat, causes the entire particle to expand, as shown in Figure 1.27, creating larger voids within the adhesive structure, leading to a reduction in bond strength. Banea et al. [141, 142]. have shown that TEP-modified adhesives, particularly in the automotive industry, can successfully reduce bonding strength when exposed to controlled temperatures, enabling easier debonding. Furthermore, their research demonstrates that the debonding temperature can be adjusted by altering the concentration of TEPs in the adhesive, making it a highly tunable technology [141, 142]. In contrast, chemical foaming agents serve as a debonding mechanism by thermally decomposing within the adhesive matrix, releasing gases like nitrogen and carbon dioxide. This gas generation expands the adhesive material, creating internal pressures that weaken the bond and facilitate separation [143]. Azodicarbonamide (ADC) is the most relevant example of a chemical foaming agent in this context. However, these agents are effective as a debonding technology only with low-temperature curing adhesives; at higher temperatures, the decomposition process initiates prematurely, which can compromise the adhesive's integrity before it fully cures [144].

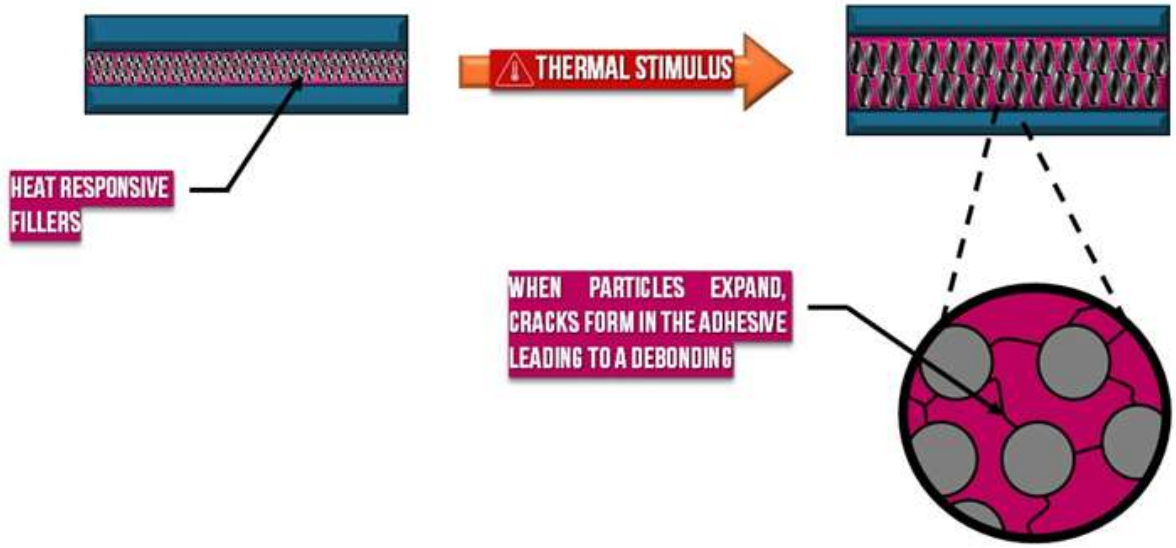

Figure 1.27: Schematic representation showing thermal debonding, via cohesive failure, due to the expansion of additive microparticles.

2.1.2 Magnetically inductive fillers

Magnetically inductive fillers offer a controlled method for debonding adhesives by incorporating magnetic nanoparticles, typically iron oxide, within the adhesive matrix. When subjected to an alternating magnetic field in the 10 kHz to 1 MHz range, these nanoparticles generate localized heat, raising the adhesive temperature between 100°C and 200°C. This controlled heating causes the adhesive to soften or degrade, allowing for separation without the need for mechanical force. Key to the process is the precise regulation of the magnetic field and the uniform distribution of the fillers, ensuring effective debonding while avoiding damage to the substrates. Salimi et al. demonstrated that polyurethane adhesives incorporating iron oxide particles debond successfully with controlled heating when exposed to an oscillating magnetic field, decreasing debonding times significantly [145]. Other studies have confirmed the utility of magnetic nanoparticles in thermoplastic composites for induced healing and debonding applications [146]. This technique is particularly advantageous in complex or hard-to-access structures, enabling remote, non-invasive separation, and holds significant potential in fields like aerospace, automotive, and electronics, where precision and substrate integrity are crucial during disassembly [147].

2.1.3 Electrically conductive fillers

Electrically debondable adhesives offer a controlled method for debonding by applying a low voltage, typically between 10 to 50 V as shown in Figure 1.28. These adhesives contain additives like inorganic or organic salts, often in the form of ionic liquids, which migrate by diffusion of ionic species to the electrode interface upon voltage application. This triggers an electrochemical reaction that disrupts the interfacial bonds and allows the adhesive to release [148, 149]. For this process to work, at least one of the bonded substrates must be metal, and both substrates must be conductive enough to serve as electrodes. In cases involving non-conductive surfaces, this limitation can be overcome by using an intermediate conductive layer, such as adhesive-laminated aluminum sheets. The most notable commercial example of this technology is the ElectRelease adhesive line developed by EIC Laboratories, which primarily consists of amine-cured epoxy resins available in various formulations to suit different adhesive strengths and applications [150, 151].

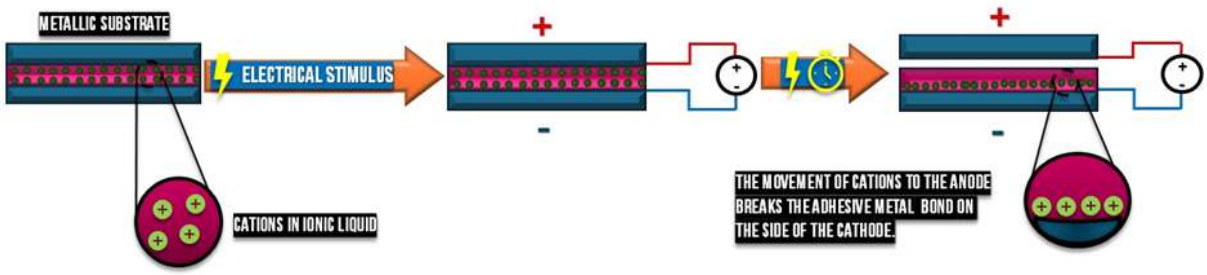

Figure 1.28: Schematic representation of electrically debondable adhesives.

2.2 Reactive based adhesive technologies

2.2.1 Shape memory debonding adhesives

Shape memory alloys (SMAs) and shape memory fillers represent a hybrid debonding technology that combines the properties of shape memory fillers and shape memory adhesives to enable controlled bond separation. These materials, such as shape memory polymers (SMPs) and shape memory alloys (SMAs), are initially deformed into flat geometries and integrated into the adhesive matrix, either as polymer layers, randomly distributed fibers, or embedded fillers. Upon exposure to a thermal stimulus, these additives undergo a shape recovery process, reverting to their original, pre-programmed configuration. This transformation induces mechanical stresses within the adhesive matrix,

leading to microfractures and facilitating the debonding process [152, 153]. An example technology is the combination of is Nitinol alloy as a polymer filler with shape memory epoxy-based polymers, including those based on epoxy systems that are flexible and have shape recovery above their glass transition temperature (Tg). This limits their applications in structural bonding is since this kind of systems have limited mechanical strength and durability, making them less suitable for high-load scenarios [154]. However, they remain particularly valuable in applications requiring multiple bonding and debonding cycles [155].

2.2.2 Photo-induced debonding

Photo-induced debonding technologies enable the controlled separation of bonded structures when exposed to specific wavelengths of light, primarily within the (UV) spectrum. These technologies function through different mechanisms, depending on the polymer type. One mechanism is photoinduced overcuring, as shown in Figure 1.29, where UV exposure increases cross-linking within the adhesive, resulting in a more rigid and less adhesive structure. Another mechanism is photodegradation, where UV-sensitive groups in the adhesive break down polymer chains, weakening the bond [152,156,157]. Additionally, some systems employ photoacid generators, which release acids under UV light, leading to the breakdown of the adhesive matrix and enabling debonding [158]. A second approach involves supramolecular polymers that rely on reversible, non-covalent interactions. When exposed to UV light, these interactions are disrupted, allowing the adhesive to soften and the bonded components to separate [158]. However, these technologies have certain limitations, including the need for substrates that are transparent to UV light, restricting their use to specific applications. There is also a risk of unintentional exposure to UV light causing premature debonding, making controlled UV exposure essential [159]. While these adhesives are well-suited for applications in electronics, packaging, and medical devices due to their flexibility and repeatability, their lower mechanical strength compared to covalent adhesives limits their suitability for high-load or structural applications [130].

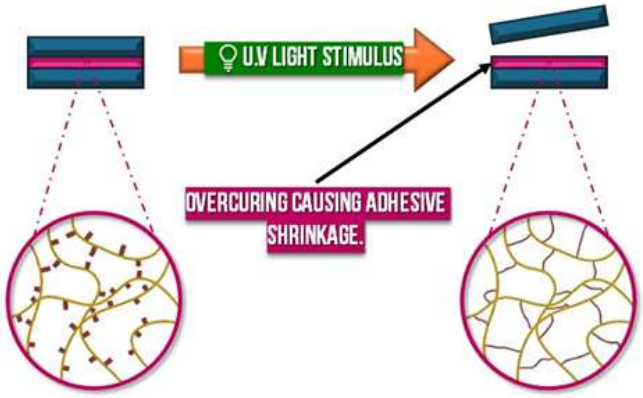

Figure 1.29: Schematic representation of photoinduced overcuring causing adhesive failure.

2.2.3 Thermally responsive reactive adhesives

2.2.3.1 Non-structural suitable technologies

Reversible adhesives based on Diels-Alder (DA) chemistry is a debonding technology based on creating covalent bonds that can be reversed under controlled conditions. The DA reaction involves the formation of a cyclohexene ring by reacting a diene with a dienophile, as shown in Figure 1.30, creating strong covalent bonds at relatively low temperatures. The Tg of such adhesive systems is low (Tg <50°C). This reaction allows adhesives to form and break bonds through thermal cycling. Upon heating, the retro-Diels-Alder (rDA) reaction is triggered, breaking the cyclohexene ring and weakening the adhesive, enabling disassembly of bonded components. This reversible debonding process is advantageous in applications such as electronics, aerospace, and automotive industries, where disassembly and reworkability is nowdays a necessity and in parts where structurally strong bond isnt a priority [160, 161]. DA-based adhesives face certain limitations. Long-term exposure to high temperatures may cause gradual degradation of the DA bonds, limiting their application in environments requiring sustained high-temperature stability [162]. Furthermore, careful selection of the diene and dienophile components is essential to optimizing the adhesive's mechanical properties, such as strength and flexibility, to meet specific application needs [163].

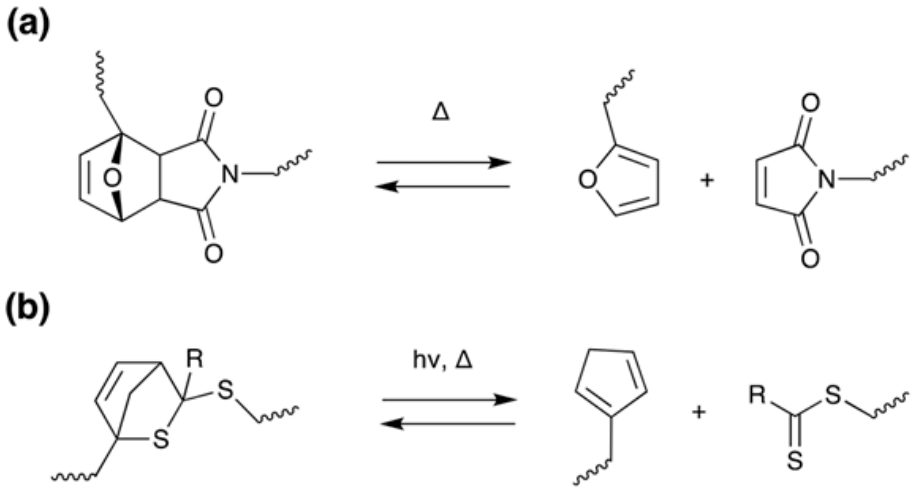

Figure 1.30: Retro (a) DielsAlder (b) hetero DielsAlder [4 + 2] reactions. [160, 161]

2.2.3.2 Structural suitable technologies

Aromatic thermosetting copolyesters (ATSP) are a class of high-performance reactive adhesives designed for structural applications, utilizing dynamic covalent chemistry through interchain transesterification reactions (ITR). When heated above their glass transition temperature (Tg), which ranges from 174°C to 310°C depending on the formulation, ATSP adhesives transition from a viscoelastic solid to a viscoelastic liquid, allowing for reprocessing, repair, and recycling. This behavior provides the reworkability of thermoplastics, shown in Figure 1.31, while retaining the strength of thermosets. Known for their excellent thermal stability, low moisture absorption, and resistance to wear, ATSP adhesives are particularly suited for high-temperature environments, such as in aerospace and automotive applications. Their reversible bond exchange reaction enables disassembly of adhesive joints when heated, preserving substrate integrity, which is crucial in applications requiring reassembly, such as complex composite structures. ATSP adhesives are formed through a polycondensation reaction between carboxylic acid-capped and acetoxy-capped aromatic copolyester oligomers, creating a crosslinked network while releasing acetic acid. Although this provides strong bonding, the high temperatures required for debonding may limit use with heat-sensitive substrates, and repeated reprocessing can degrade mechanical properties over time [163–165].

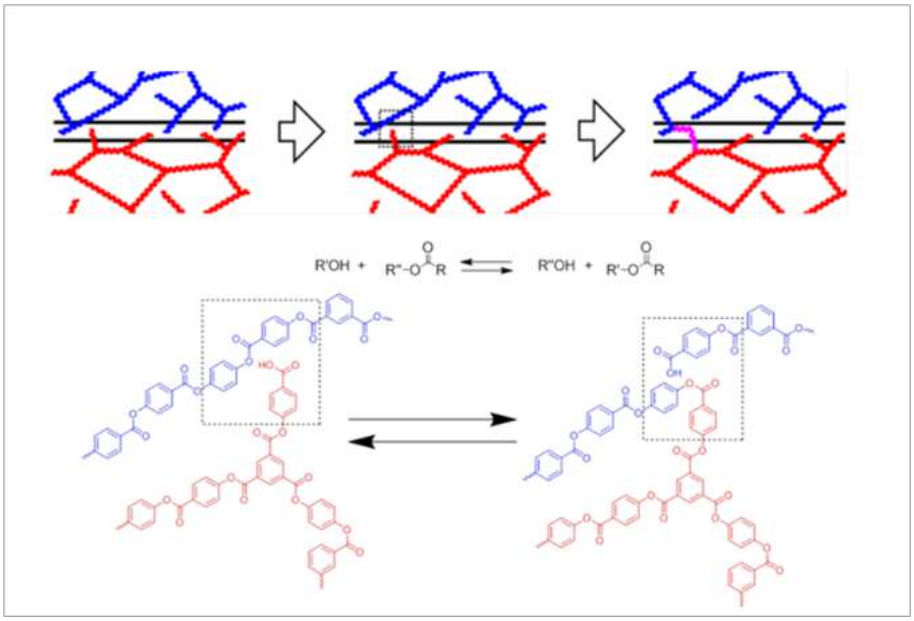

Figure 1.31: Example chemical reaction at surface between carboxylic acid and ester unit via acidolysis. An example reaction for surface-surface bonding of crosslinked aromatic polyesters[163].

2.3 Other technologies

In addition to established debonding technologies, lesser-known approaches utilize ultrasound as a trigger through mechanochemical mechanisms. While ultrasound is typically associated with non-destructive testing, it has been shown to initiate debonding in certain adhesive systems. For example, Tachi and Suyama demonstrated the use of 28 kHz ultrasound to activate acid-generating microcapsules within a polyurethane adhesive, resulting in debonding via acid-catalyzed degradation [166]. Furthermore, Zhang and colleagues reported that ultrasound could cleave Diels-Alder bonds in an epoxy-amine thermoset, suggesting its potential applicability in other epoxy-based adhesives [152]. Ultrasound-induced mechanochemical scission has also been explored in polymers such as perfluorocyclobutane, where pulsed ultrasound triggered degradation, with the material becoming repairable at temperatures above 150°C [167]. In parallel, chemical stimuli such as acids or bases can effectively degrade adhesive networks by promoting hydrolysis of the polymer backbone or cross-linking interactions. Polyurethane adhesives, for instance, have been designed to degrade rapidly in the presence of fluoride ions, where silyl-protected phenol units undergo breakdown, leading to a reduction in molecular weight and cohesive failure [168]. Other studies have employed basic solutions to disrupt hydrogen-bonded structures in adhesives, such as those containing fatty acid and ureido-diethylene-triamine

cross-linkers, where heating to 80°C facilitates debonding through adhesive failure [169]. Additionally, basic species have been used to degrade adhesives by cleaving sterically hindered urea linkages, further demonstrating the effectiveness of chemical hydrolysis for controlled debonding in adhesive applications [152, 170].

3 Introduction to flame retardancy

As with many other modern scientific disciplines, flame retardancy, can be traced back to early civilizations. The earliest use of flame retardants dates back to Ancient Greece around 4000 BC, when asbestos was used to prevent the burning of cremation shrouds [171]. The concept of flame retardancy continued to evolve over the centuries, notably gaining momentum in the 17th century when the burgeoning problem of fires in Parisian theaters necessitated the development of flame-resistant materials [172]. This period saw the emergence of an industry dedicated to enhancing the fire resistance of various substances. The advent of World War II further catalyzed research and innovation in this field, driven primarily by the urgent need for fire-resistant fabrics and coatings for military applications [173]. Today, flame retardants are integral to a wide range of applications, including construction materials, electrical and electronic equipment, wires and cables, transportation vehicles, and furniture. In 2020, global consumption of these materials reached approximately 2.19 million tons [174]. The most commonly used flame retardants include aluminum trihydroxide (ATH), brominated and chlorinated compounds, organophosphorus compounds, and antimony-based compounds [175–177]. The subsequent section will delve into the concept of flame retardancy, outlining its definition, the various methods of incorporating flame retardants, the primary classes of these compounds, and the mechanisms by which they function within different material matrices.

3.1 Flame retardants and flame retardancy

Flame retardants are chemical compounds that, when added to materials, especially polymers, enhance their ability to resist fire [178] or their flame retardancy.

Flame retardancy refers to the characteristic of a material that enables it to resist ignition and slow down the spread of flames [179]. The incorporation of flame retardants into polymers achieves several key objectives: it prolongs the time before ignition, improves

the materials self-extinguishing abilities, decreases the overall heat release, prevents the formation of burning droplets, and significantly reduces the emission of harmful smoke and toxic gases such as carbon monoxide (CO) and hydrogen cyanide (HCN) during combustion [179]. Together, these functions aim to prevent fires from starting or, if they do start, to limit their spread [180].

3.2 Methods of use of flame retardants

Enhancing the flame retardancy of a material can be achieved through different mediums. Two primary methods for incorporating flame retardants into a polymer matrix are surface protection and bulk modification. Surface protection involves applying flame-retardant coatings that shield the material from ignition and combustion. On the other hand, bulk modification integrates flame-retardant additives directly into the polymer matrix, ensuring the material is inherently resistant to fire throughout its structure [181, 182].

3.2.1 Surface modification

Surface modification for flame retardants involves the application of protective layers to the material's surface to enhance its fire resistance. This approach is particularly useful in situations where a material's surface is exposed to thermal stress. Although the protective layer may eventually degrade or lose adhesion over time, leading to a potential reduction in effectiveness [183], it remains a viable strategy for providing temporary or situational flame retardancy. Techniques such as intumescent coatings and the layer-by-layer (LBL) method are commonly used in this context. These methods work by forming a protective barrier when exposed to high temperatures, which helps to insulate the material and slow the spread of fire [184, 185].

3.2.2 Bulk modification

Bulk modification is the most commonly used method for incorporating flame retardants into polymers and involves either simple mixing during processing or chemically reacting with the polymer molecules. These additives must be used in minimal quantities to maintain cost efficiency and to prevent significant alteration of other properties of the polymer, such as its mechanical characteristics. In the reactive approach, the flame re-

tardant chemically reacts with the polymer, becoming an integral part of the polymer matrix. As a result, the material is homogeneous, and the flame retardant no longer exists in its original chemical form [186, 187]. In the additive approach, the flame retardant is physically mixed with the polymer during the processing phase, meaning it is physically embedded within the material, retaining its original chemical structure [188].

Both approaches present their advantages and inconveniences. The reactive approach produces homogeneous materials and preserves mechanical properties well; however, it is expensive and challenging to scale for industrial applications [186]. Conversely, the additive method is more cost-effective and industry-compatible but can negatively impact the mechanical properties of the final product and pose environmental concerns due to possible emissions [189].

3.3 Different classes of flame retardants

Flame retardants as summerized in Figure 1.32, are categorized based on their chemical composition and the mechanisms by which they inhibit combustion:

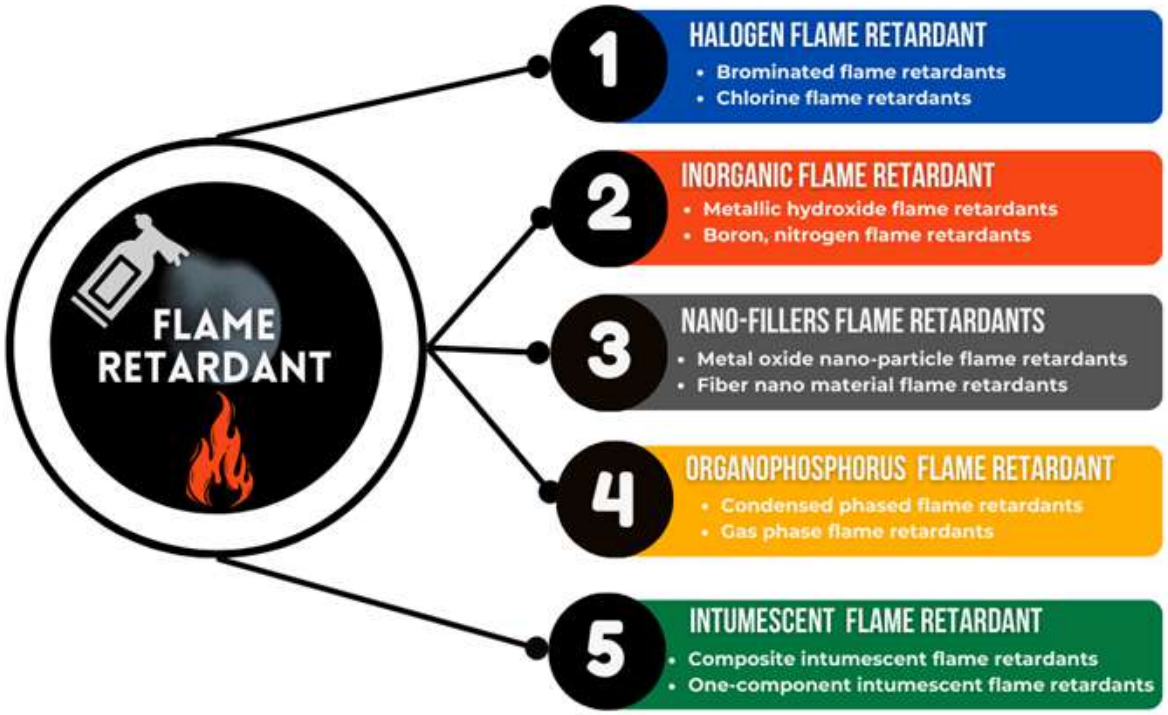

Figure 1.32: Diagram summary of different classes of flame retardants.

3.3.1 Halogenated flame retardants

Halogenated flame retardants contain bromine or chlorine. These compounds are effective because they release halogen radicals that interfere with the combustion process. Brominated flame retardants (BFRs) are widely used in electronics, textiles, and construction materials. Chlorinated flame retardants are used in leathers, paints, coatings, and rubbers. However, due to environmental and health concerns, the use of some halogenated flame retardants is being phased out [190, 191].

3.3.2 Inorganic flame retardants

Inorganic flame retardants encompass a variety of compounds, including aluminum hydroxide, magnesium hydroxide, antimony oxides, and mineral flame retardants such as huntite, hydromagnesite, and various borates. These substances typically function by releasing water vapor or other inert gases when heated, which helps to cool the material and dilute flammable gases. Additionally, they can form a protective char layer on the material's surface. Mineral flame retardants, as a subset of inorganic flame retardants, often act through endothermic decomposition, absorbing heat and further cooling the material. This makes them particularly suitable for use in polyolefins for wire and cable applications due to their relatively low decomposition temperatures. Inorganic flame retardants are frequently combined with other types to enhance their overall effectiveness, offering a balance between fire protection and minimizing health and environmental impacts [192, 193].

3.3.3 Nano-fillers flame retardants

Nano-fillers flame retardants enhance flame retardancy by forming protective barriers that insulate materials from heat and oxygen. Metal oxide nanoparticles, such as TiO_2 and ZnO, reduce peak heat release rates and improve thermal stability [194]. Fiber-based nanomaterials, like carbon nanotubes and nanoclays, promote char formation and reduce flammability by creating a supportive network during combustion [195]. These nano-fillers improve both fire performance and physical properties of composites.

3.3.4 Organophosphorus flame retardants

Organophosphorus flame retardants contain phosphorus and are used in a variety of applications, including textiles, electronics, and industrial materials. They work by promoting char formation and releasing non-combustible gases, which inhibit the combustion process. Organophosphorus compounds can be either reactive or additive and are known for their dual function of flame retardancy and plasticization [191, 196]. There are two main types of organophosphorus flame retardants: those that function in the condensed phase and those that operate in the gas phase. Condensed phase flame retardants enhance char formation, creating a protective barrier on the material's surface that shields it from heat and oxygen. In contrast, gas phase flame retardants release phosphorus-containing

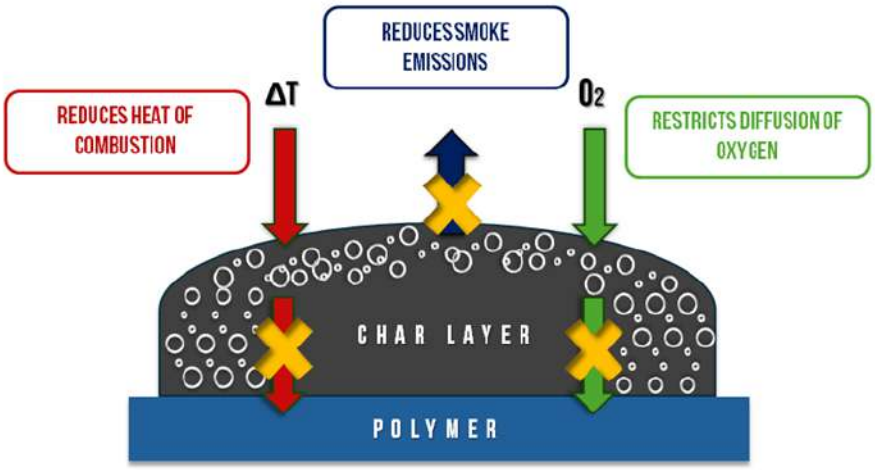

Figure 1.33: Schematic representation of modes of action of flame retardants.

radicals that actively quench the flame and disrupt the combustion process [197].

3.3.5 Intumescent flame retardants

Intumescent flame retardants form a protective, insulating char layer when exposed to heat, effectively creating a barrier that shields the underlying material from high temperatures and slows the spread of fire [198]. These flame retardants often incorporate nitrogen-based and phosphorus-based compounds, which work together to enhance fire resistance. Nitrogen compounds typically aid in the formation of a stable, expanded char layer, while phosphorus compounds facilitate the dehydration of the polymer and contribute to the formation of a carbonaceous residue. Intumescent flame retardants can be designed as single-component systems, where all necessary components are integrated into one material, or as multi-component systems that combine different flame-retardant agents to achieve better performance [199, 200].

3.4 Mode of Action of flame retardant

To interfere with the combustion process, flame retardants react through multiple mechanisms, summerized in Figure 1.33, that can be categorized into physical reactions and chemical reactions.

3.4.1 Physical reactions

3.4.1.1 Endothermic degradation

Endothermic degradation is when flame retardants, such as aluminum hydroxide and magnesium hydroxide, act by undergoing endothermic decomposition when exposed to high temperatures. This process absorbs heat from the surroundings, thereby cooling the material and delaying ignition. The decomposition of these compounds releases water vapor, which further helps to cool the material and dilute flammable gases [201].

3.4.1.2 Thermal shielding

Thermal shielding involves the formation of a protective barrier on the material's surface. Intumescent flame retardants, for example, create a char layer when exposed to heat, which insulates the underlying material from high temperatures and oxygen, effectively slowing the spread of fire. Non-halogenated inorganic and organic phosphate flame retardants often act through this mechanism by generating a polymeric layer of charred phosphoric acid [202, 203].

3.4.1.3 Dilution of gas phase

Dilution of the gas phase occurs when flame retardants release inert gases, such as carbon dioxide and water vapor, during thermal degradation. These gases dilute the concentration of flammable gases and oxygen near the flame, thereby reducing the rate of combustion [201, 202].

3.4.2 Chemical reactions

3.4.2.1 Gas phase: radical quenching

Radical Quenching is when flame retardants release radicals during thermal decomposition, examples for this would be organophosphorus flame retardants and halogenated flame retardants. These radicals are highly effective in quenching the reactive hydrogen ($H\cdot$) and hydroxyl ($OH\cdot$) radicals present in the flame, thereby disrupting the combustion process. This radical quenching mechanism interrupts the chain reactions that sustain the fire [202].

3.4.2.2 Condensed phase: char formation

Char formation is particularly observed when flame retardants promote the development of a carbonaceous char layer on the surface of the material. This char layer acts as a protective barrier, preventing the release of flammable gases and shielding the material from further thermal degradation. This effect is especially prevalent in intumescent flame retardants that incorporate phosphorus compounds as a key component in their formulation [202].

3.4.2.3 Synergistic effects

Synergistic effects are when flame retardants work synergistically with other elements to enhance their effectiveness. For instance, organophosphorus compounds can work in conjunction with nitrogen or boron to improve flame retardancy. The combination of different flame retardants can result in a more effective and comprehensive fire protection system [203].

3.5 Parameters Influencing flame retardant incorporation

3.5.1 Dispersion

For fillers to effectively enhance a polymers fire resistance and mechanical properties, they must be well dispersed within the matrix. Poor dispersion creates weak points in the material, compromising overall integrity. Dispersion is influenced by factors such as particle size, polymer viscosity, processing temperature, mixing duration, and shear rate. In general, dispersion behavior can be examined and predicted using physical and thermodynamic models [204]. On a molecular level, dispersion is governed by both thermodynamic and kinetic principles. The Flory-Huggins interaction parameter (χ) predicts polymer-filler compatibility, where lower values indicate better miscibility and improved dispersion. The DLVO theory further explains how van der Waals attraction and electrostatic repulsion affect particle stability, determining whether fillers remain evenly distributed or tend to agglomerate [205]. Shear forces during processing play a crucial role in dispersion. Shear-induced diffusion helps break apart filler agglomerates and distribute them more uniformly throughout the polymer. Nanometric fillers generally disperse more effectively due to their higher surface area, but their effectiveness depends on interfacial interactions and processing conditions [206]. Finally, coupling agents, such as silanes or functionalized

polymers, can further enhance dispersion by reducing interfacial tension and preventing re-agglomeration, ensuring a more stable and uniform distribution within the matrix [207].

3.5.2 Loading rate

Loading rate significantly impacts the effectiveness of flame retardants. For instance, mineral additives like aluminum hydroxide and magnesium hydroxide are effective only at high loadings, typically above 40% by weight. Ammonium polyphosphate (APP) also requires specific concentrations to be effective in different polymers. In polyamides, APP is effective at loadings above 10-30% by weight; however, excessive loading can lead to poor dispersion, resulting in reduced performance [208].

3.5.3 Synergy

Synergy in flame retardants is achieved by combining different agents to enhance fire resistance through complementary mechanisms. For example, mixing phosphorus-based compounds with nanoclays improves char cohesion, while combining nitrogen and phosphorus additives accelerates char formation and enhances phosphorus retention in the condensed phase. Metal hydroxides paired with zinc borate or montmorillonite also significantly reduce heat release rates and improve fire resistance. The addition of nanoparticles further strengthens barrier layers and promotes robust char formation, enhancing overall fire retardancy [209, 210].

3.6 Intumescent systems

This section will offer a general overview of intumescence, given that intumescent systems are the primary flame retardants utilized in this study as debonding agents, it is crucial to thoroughly understand their underlying mechanisms.

3.6.1 Definition

An intumescent is a substance that swells when exposed to heat, leading to an increase in volume and a decrease in density. This swelling process, known as intumescence, is a key principle in passive fire protection products [211, 212].

3.6.2 Components of a multi-component intumescent system

Intumescent formulations typically contain three key components:

3.6.2.1 Acid source

Provides the acidic environment necessary for the intumescence reaction. Common acid sources include ammonium polyphosphate (APP) having the general formula $(NH_4)(NH_4)_{n+2}P_nO_{3n+1}$, phosphoric acid, and other inorganic acids.

3.6.2.2 Carbon source

Supplies the carbon needed to form the char layer. Typical carbon sources include pentaerythritol, starch, and other polyhydric compounds.

3.6.2.3 Gas source

Generates the gases required for foaming. Common gas sources include melamine, dicyandiamide, and other nitrogen-containing compounds [211, 212].

3.6.3 Intumescence mechanism

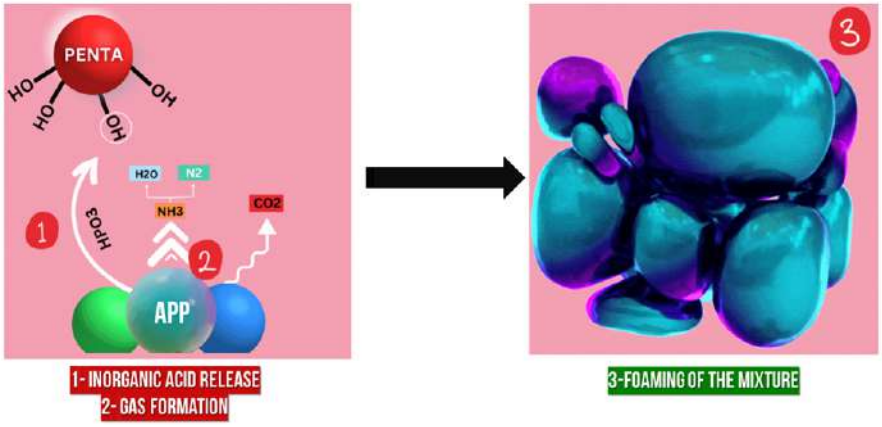

Figure 1.34: Schematic representation of how an intumescent flame retardant is activated.

The intumescence mechanism, summerized in Figure 1.34, involves a series of physical and chemical reactions that occur when the material is exposed to heat. The process can be broken down into several stages:

3.6.3.1 Softening of the binder/polymer

As the binder or polymer matrix heats up, it softens, allowing the intumescent components to react more effectively. **Release of inorganic acid (e.g. Ammonium polyphosphate)** An acid donor, like ammonium polyphosphate (APP), decomposes to release an inorganic acid, catalyzing subsequent reactions.

$$(NH_4PO_3)_n \xrightarrow{>250°C} (HPO_3)_n + nNH_3$$

3.6.3.2 Carbonization

A carbon donor, such as pentaerythritol or starch, undergoes carbonization, forming a crucial insulating char layer.

$$(HPO_3)_n + C_x(H_2O)_m \rightarrow [C']_k + (HPO_3)_n \times mH_2O$$

3.6.3.3 Gas formation (e.g. Melamine)

A foaming agent, like melamine, decomposes to release gases, expanding the softened binder into a foam structure.

$$C_3H_6N_6 \xrightarrow{\Delta} C_3H_3N_3O_3 + NH_3 \xrightarrow{O_2} N_2 + H_2O$$

3.6.3.4 Foaming of the mixture

The released gases expand the mixture, creating a foam that acts as an insulating barrier, reducing heat transfer.

3.6.3.5 Solidification

The expanded foam solidifies through cross-linking, forming a stable char layer that resists heat and fire spread [211, 212].

3.6.4 Nonconventional flame retardants

Expandable graphite, Figure 1.35, is increasingly used as a flame retardant in various applications, including coatings, foams, and construction materials. Its ability to form a protective, thermally insulating layer makes it an effective and environmentally friendly

alternative to traditional flame retardants. Unlike conventional intumescents, which follow a classical mechanism, expandable graphite offers a unique approach to fire protection. Derived from natural graphite flakes treated with intercalation agents like sulfuric acid, expandable graphite expands rapidly when exposed to heat, forming an intumescent layer that acts as a barrier to heat and oxygen. This expansion can increase the material's volume by several hundred times, creating a "worm-like" structure that insulates the underlying substrate and slows the spread of fire [213, 214].

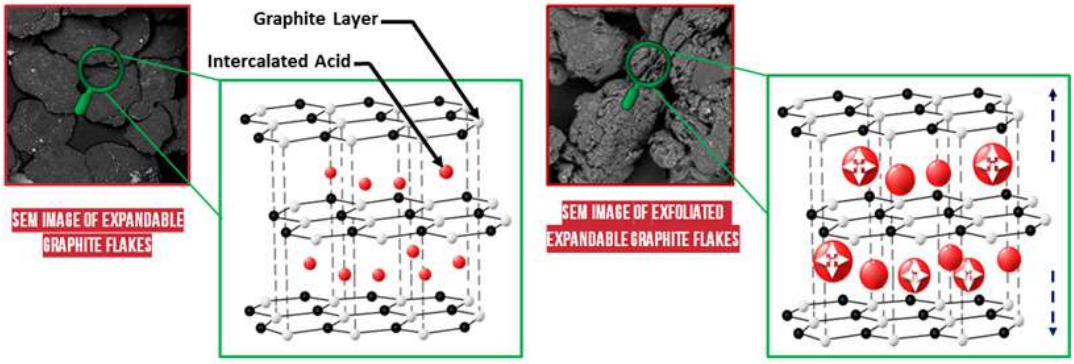

Figure 1.35: Schematic Representation of expandable graphite and its exfoliation.

2

Materials and methods

1 Materials

1.1 Adhesive systems

The primary adhesive systems investigated in this work are epoxy thermosets. As outlined in the literature review, these adhesives belong to the thermosetting polymer family, along with polyurethanes, benzoxazines, and polyesters, and form crosslinked networks through the ring-opening of oxirane groups. The epoxy resin system was selected in line with previous PhD research conducted at LIST by Sébastien Depaifve and Nicolas Burger [215–218]. The chosen epoxy resin is a low-viscosity Bisphenol A diglycidyl ether (D.E.R.332), commonly referred to as BADGE or DGEBA. Two different hardeners were used in this study. Diethylenetriamine (DETA), an aliphatic amine, was employed for curing at room temperature, while 4,4-Diaminodiphenyl sulfone (DDS), an aromatic amine, was utilized for curing at elevated temperatures. All used molecules were illustrated in Figure 2.1. Both DDS and DETA are well-established hardeners in the literature and were selected as models for low and high-temperature curing systems. The DGEBA/DDS system, characterized by a more rigid and complex network with a high glass transition temperature (Tg) of 220°C, was used as a high-temperature structural adhesive suitable for aerospace applications, offering superior mechanical performance. In contrast, the DGEBA/DETA system, with a more flexible network and a lower Tg of 160°C, was employed as a low-temperature structural adhesive. These two systems were chosen to accommodate the different debonding technologies explored in this thesis and their respective characteristics. All chemicals were supplied by Sigma-Aldrich.

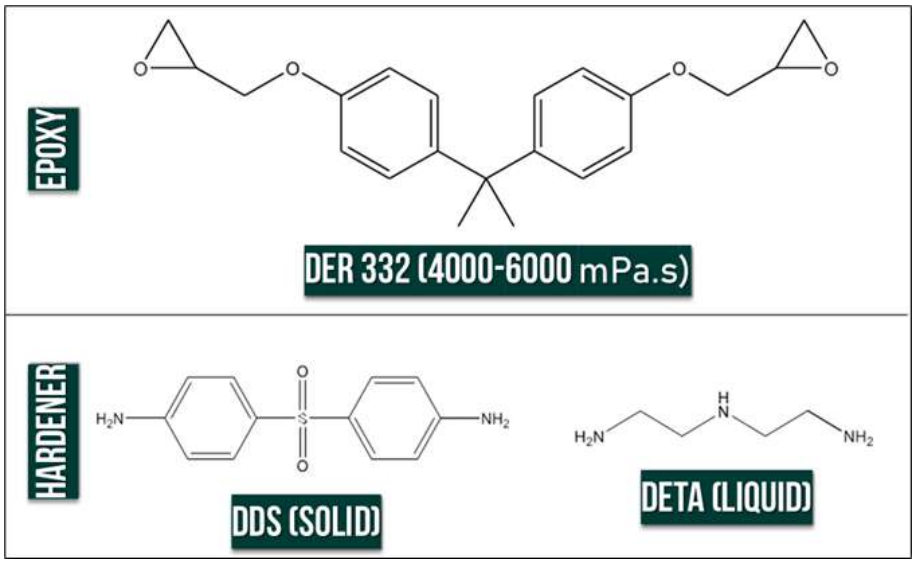

Figure 2.1: Molecular structure of the epoxy resin (DER.332, viscosity in MPa.s) and hardeners (DETA and DDS, and their form at room temperature) used in this thesis.

1.2 Flame retardant fillers

In this thesis, we aimed to explore a comprehensive range of flame retardants, encompassing various mechanisms to provide suitable technologies for a wide spectrum of debonding temperatures. To achieve this, we focused on four distinct studies, each investigating different flame-retardant systems, illustrated in Figure 2.2, including both well-established and novel flame-retardant technologies. The selected systems cover both phosphorus-based and expandable graphite fillers, addressing a diverse set of applications requiring controlled thermal degradation and debonding. The first study focused on ammonium polyphosphate (APP) and melamine polyphosphate (MPP), which are integral to intumescent systems. APP, supplied by Clariant as Exolit AP422, and MPP, supplied by CIBA, Germany as MELAPUR 200 supplied by CIBA,Germany. The second study focuses on pentaerythritol spirobis(methylphosphonate) (PCO 900), an organo-phosphorus-based flame retardant supplied by THOR Gmbh, Germany under the commercial name AFLAMMIT® PCO 900. In the third study, we explore the potential of expandable graphite, a relatively new entrant in flame retardant technology, as a debonding material. Supplied by ACS Materials, USA, the expandable graphite fillers commercially known as CXG5B122, CXG00522, and CXG00622 were selected to investigate their full range by using it to create multiple debonding temperatures. The fourth study focused on evaluating the influence of ammonium polyphosphate (APP) chain length and molecular weight on the debonding temperature of the adhesive system. Two APP variants, supplied by

Shifang (China), were examined: TF-303, a short-chain APP (Phase I), with the general formula $(NH_4)_{n+2}P_nO_{3n+1}$ and a degree of polymerization $n < 20$; and TF-201, a long-chain variant with $n > 1000$. This study aimed to assess the effectiveness of short-chain APP in promoting low-temperature debonding, thereby supporting its suitability for expanding the application range of intumescent flame-retardant systems. In addition, pentaerythritol, supplied by Sigma-Aldrich, was used in this study for its role in forming a char layer during thermal decomposition.

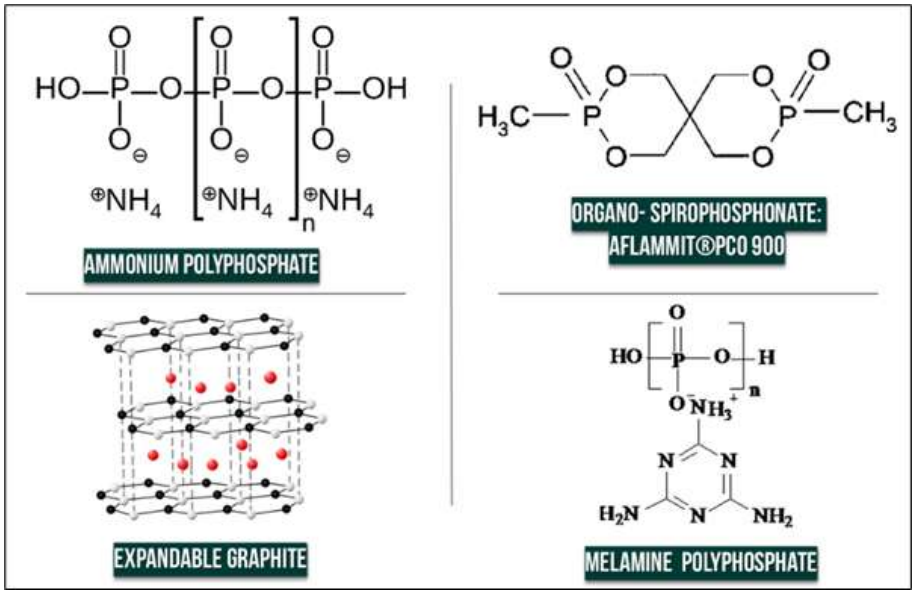

Figure 2.2: Molecular structure of ammonium polyphosphates, melamine polyphosphates, expandable graphite, Melamine Polyphosphates.

No prior chemical treatment was applied to the fillers before their incorporation into the formulations. However, some fillers were dried before use to ensure moisture removal. Additionally, certain fillers were mechanically ground using a coffee grinder to reduce particle size for better dispersion in the formulations. All technical details of the fillers are summarized in the following tables [1,2,3]

Table 2.1: Characteristics of phosphorus flame retardants

Flame Retardant	**Molecule**	**Supplier**	**Nitrogen Content (wt.%)**	**Phosphorus Content (wt.%)**	**Particle Size (D50) (μm)**
MPP (MELAPUR-200)	Melamine Polyphosphate	CIBA, Germany	42–44%	12–14%	70
APP (Exolit AP422)	Ammonium Polyphosphate	Clariant	14–15%	31–32%	170
PCO-900 (AFLAMMIT)	Pentaerythritol-phosphate	THOR GmbH, Germany	N/A	24%	30 (D95)
APP-TF-303a	Ammonium Polyphosphate	Shifang, China	≥17.5%	≥59.5%	200–300
APP-Phase-II (TF-201)	Ammonium Polyphosphate	Clariant	14%	30%	15–25

Table 2.2: Characteristics of expandable graphite flame retardants

Reference	**Supplier**	**Assigned Name**	**Particle Size (μm)**	**Purity (%)**	**Expansion Start Temp. (°C)**	**Expansion Volume (ml/g)**
CXG5B122	ACS Materials, USA	EG225	300	≥95%	180–110	≥250
CXG00522	ACS Materials, USA	EG250	80	≥95%	250	≥180
CXG00622	ACS Materials, USA	EG300	50	≥95%	300	≥170

1.3 Epoxy curing and stoichiometric ratio calculations

1.3.1 Stoichiometric ratio calculations

To determine the required masses of the epoxy resin and curing agents, we use the epoxide equivalent weight (EEW) provided by the supplier and the calculated amine hydrogen equivalent weight (AHEW). The equivalent weight represents the mass containing one mole of reactive sites. EEW of DER 332 is approximately 173.5, indicating that 173.5g of resin contains one mole of epoxy groups.Table 3 summarizes the calculations of the equivalent weights for the epoxy resin specifically DER 332, and the amine hardeners used in this study.

Table 2.3: Equivalent Weight Calculations for Epoxy Resin and Hardeners

Parameter	**Value**	**DGEBA (DER332)**	**DETA**	**DDS**
Molecular Weight (g/mol)	Provided by supplier or literature	-	$M_{\text{W,DETA}} = 103.17$	$M_{\text{W,DDS}} = 248.3$
Number of Active Hydrogens (n_H)	Based on chemical structure	-	$n_{H,\text{DETA}} = 5$	$n_{H,\text{DDS}} = 4$
Equivalent Weight	$\frac{M_W}{n_H}$	EEW = 173.5 (Epoxide Equivalent Weight)	$\text{AHEW}_{\text{DETA}} = \frac{103.17}{5} = 20.634$	$\text{AHEW}_{\text{DDS}} = \frac{248.3}{4} = 62.075$

From the AHEW and EEW, the stoichiometric ratios can be calculated. Table 4 provides the calculations for the mass of curing agent required per given mass of epoxy resin, based on the equivalent weights, and the resulting weight ratios for both DGEBA/DETA and DGEBA/DDS

Table 2.4: Stoichiometric Mass and Weight Ratio Calculations

Parameter	**Equation**	**DGEBA/DETA System**	**DGEBA/DDS System**
Mass of Epoxy Resin (m_{DGEBA})	Chosen mass for calculation	$m_{\text{DGEBA}} = 173.5\,\text{g}$	$m_{\text{DGEBA}} = 173.5\,\text{g}$
Mass of Hardener (m_{Hardener})	$m_{\text{Hardener}} = \frac{\text{AHEW}}{\text{EEW}} \times m_{\text{DGEBA}}$	$m_{\text{DETA}} = \frac{20.634}{173.5} \times 173.5$ $= 20.634\,\text{g}$	$m_{\text{DDS}} = \frac{62.075}{173.5} \times 173.5$ $= 62.075\,\text{g}$
Weight Ratio (Epoxy:Hardener)	Weight Ratio = $\frac{m_{\text{Hardener}}}{m_{\text{DGEBA}}}$	$\frac{20.634}{173.5} = 0.119$ (1:0.119)	$\frac{62.075}{173.5} = 0.358$ (1:0.358)

1.3.2 Fillers mass fraction calculation

The mass fraction (wt.%) of flame-retardant fillers is calculated as follow:

$$\omega_{\text{filler}} = \frac{m_{\text{filler}}}{m_{\text{Total}}} = \frac{m_{\text{filler}}}{m_{\text{DGEBA}} + m_{\text{Hardener}} + m_{\text{filler}}}$$

Table 5 outlines the method to calculate the mass of flame-retardant filler required to achieve a specific mass fraction wfiller in the epoxy system. It shows the relationships between the masses of epoxy resin, hardener, and filler for both systems. Example calcu-

Table 2.5: Mass Fraction Calculations for Flame-Retardant Fillers

Parameter	**Equation**	**DGEBA/DETA System**	**DGEBA/DDS System**
Mass of Hardener (m_{Hardener})	$m_{\text{Hardener}} = \text{Weight Ratio} \times m_{\text{DGEBA}}$	$m_{\text{Hardener}} = 0.119 \times m_{\text{DGEBA}}$	$m_{\text{Hardener}} = 0.358 \times m_{\text{DGEBA}}$
Total Mass Without Filler (m_{Total})	$m_{\text{Total}} = m_{\text{DGEBA}} + m_{\text{Hardener}}$	$m_{\text{Total}} = 1.119 \times m_{\text{DGEBA}}$	$m_{\text{Total}} = 1.358 \times m_{\text{DGEBA}}$
Mass of Filler (m_{Filler})	$m_{\text{Filler}} = \frac{m_{\text{Total}} \times \omega_{\text{Filler}}}{1-\omega_{\text{Filler}}}$	$m_{\text{Filler}} = \frac{1.119\, m_{\text{DGEBA}} \times \omega_{\text{Filler}}}{1-\omega_{\text{Filler}}}$	$m_{\text{Filler}} = \frac{1.358\, m_{\text{DGEBA}} \times \omega_{\text{Filler}}}{1-\omega_{\text{Filler}}}$

lations of for a system of 10 g total with 20 wt.% of filler mass for both DGEBA/DDS and DGEBA/DETA system. I.3.3. Filling rate The loading rates of 10 wt.%, 20 wt.%, 30

Table 2.6: Summary of the Calculated Masses for Both Systems

Component	**DGEBA/DETA System (g)**	**DGEBA/DDS System (g)**
Epoxy Resin (DGEBA)	$m_{\text{DGEBA}} = 7.15$	$m_{\text{DGEBA}} = 5.89$
Hardener	$m_{\text{DETA}} = 0.85$	$m_{\text{DDS}} = 2.11$
Flame-Retardant Filler	$m_{\text{Filler}} = 2$	$m_{\text{Filler}} = 2$
Total Mass	10 g	10 g

wt.%, and 40 wt.% were selected to provide a clear and thorough analysis of the adhesive matrix's performance across a range of conditions. These specific loading levels were chosen to represent both low and high filler contents. The 10 wt.% loading serves as a lower limit, where the influence of the filler on the adhesive matrix properties is expected to be minimal. On the other hand, the 40 wt.% loading represents a higher level, where the filler is likely to have a more pronounced effect on the adhesive matrixs properties. The intermediate loadings of 20 wt.% and 30 wt.% allow for a detailed evaluation of potential trends or changes in performance. This range of loading rates ensures that the study captures the adhesive matrix's behavior at various concentrations, offering insights into its overall performance and potential for different applications.

1.4 Curing of epoxy resins

The DGEBA/DETA system undergoes a 24-hour cure at room temperature, followed by a 2-hour post-cure at 125 °C to ensure complete crosslinking. On the other hand, the DGEBA/DDS system requires an optimized curing process to prevent premature activation of the fillers. To achieve this, a kinetic DSC analysis was performed to determine the time necessary for full crosslinking at various fixed temperatures. Figure 2.3 illustrates the potential curing cycles and the corresponding times to reach complete conversion. Based on this analysis, the optimal curing cycle was determined to be 10 hours at 150 °C.

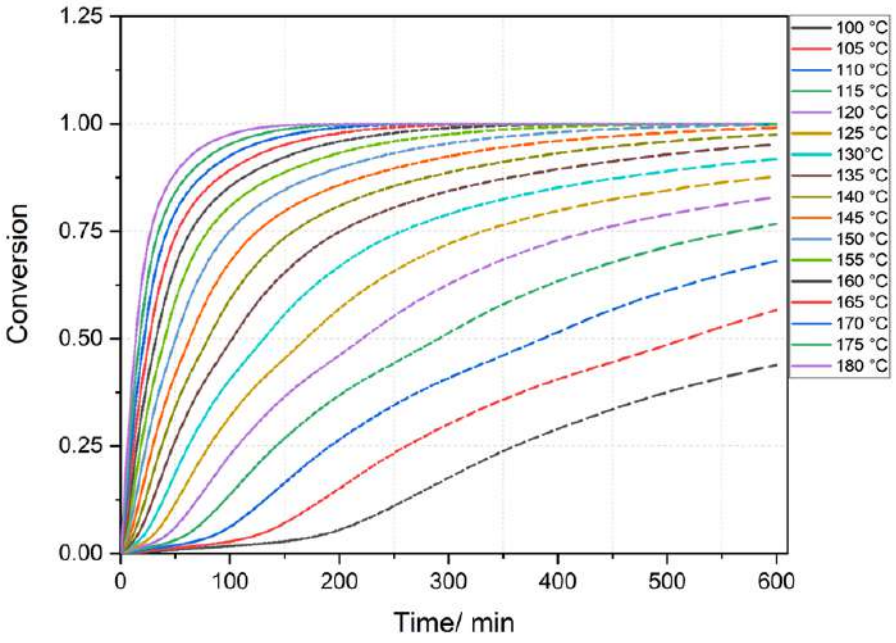

Figure 2.3: Different cross-linking profiles of DGEBA/DDS system.

1.5 Preparation of the formulations

Two distinct experimental methodologies were employed, as illustrated in Figure 2.4. In the first approach, additives were incorporated into the epoxy resin preheated to 130°C to decrease its viscosity and facilitate mixing. The mixture underwent magnetic stirring at 300rpm for approximately 15minutes. To enhance dispersion within the DGEBA matrix, the formulation was subsequently subjected to ultrasonic treatment using an ultrasonic probe (Hielscher Ultrasonic Processor UP400) for an additional 15 minutes. The ultrasonic probe operates by emitting high-frequency ultrasonic waves, inducing cavitation in the liquid medium, which promotes efficient particle dispersion at the microscopic

level [219].

In the alternative method, the mixtures were homogenized using a speed mixer (Hauschild SpeedMixer DAC 400) at 2350 rpm for 10 minutes. A speed mixer is a centrifugal mixing device that utilizes simultaneous rotation and revolution of the mixing vessel to rapidly blend materials, eliminating entrapped air and ensuring bubble-free, homogeneous formulations [220, 221]. For the DGEBA/DDS systems, the hardener was added concurrently with the additives to facilitate curing. In contrast, for the DGEBA/DETA systems, the hardener was omitted at this stage to prevent premature crosslinking prior to the designated curing step.

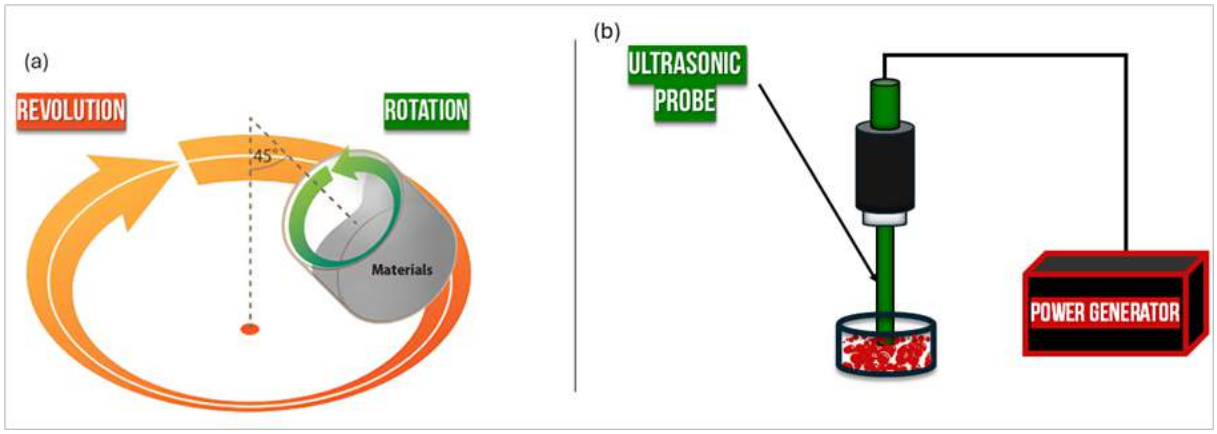

Figure 2.4: Schematic representation of (a) speed mixer (b) ultrasound probe.

1.6 Samples preparation

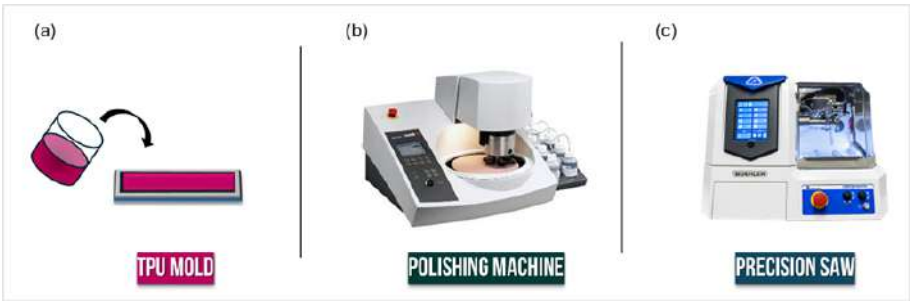

Figure 2.5: (a) schematic presentation of sample preparation (b) Struers Tegramin 25 polishing machine (c) IsoMet High Speed Pro Automatic Precision Sectioning Machine.

1.6.1 Resin molding

To provide a comprehensive characterization of the studied debonding systems, bulk resin samples were prepared using two methods. First, resin plates were fabricated by pressing

the resin into a steel mold during curing to ensure the removal of all air bubbles. Second, in the case of the DGEBA/DETA system, the resin was cast into 3D-printed thermoplastic polyurethane (TPU) molds, shown in Figure 2.5 (a). Prior to casting, a thin layer of release agent was applied to the mold surfaces to facilitate easy removal of the resin plates after curing.

Subsequent processing of the samples was performed based on the requirements of the characterization techniques, involving cutting and polishing procedures. The following instruments were utilized:

1.6.2 Precision saw

Cured epoxy samples were precisely sectioned using an IsoMet High Speed Pro Automatic Precision Sectioning Machine illustrated in Figure 2.5 (c). The machine was equipped with a silicon carbide cut-off wheel (30A15) and operated at a rotation speed of 4500 rpm with an advance speed of 0.55mm/s. A 3% aqueous solution of Corrozip in deionized water served as a lubricant, coolant, and anti-corrosion fluid during the cutting process.

1.6.3 Polishing machine

The samples were polished using a Struers Tegramin 25 (Figure 2.5 (b)). polishing machine to achieve a surface roughness below 1µm, essential for proper contact with the hot disk sensor and reproducible SEM surface topography analysis. Polishing began with grinding at 15N and 150rpm for 60 seconds using #320 grit silicon carbide foil. This was followed by pre-polishing under the same conditions for 90 seconds with #1200 grit paper, then repeated with #2000 grit paper. Final polishing employed a 3μm colloidal diamond suspension (DiaPro Mol R3) for 5 minutes at 150 rpm and 25 N, followed by polishing with colloidal silica (OP-S, <1μm) for 5 minutes at 150 rpm and 10 N.

1.7 Adhesive joints

1.7.1 Surface preparation

To ensure uniform and repeatable surface treatments for the adhesive joints, several preparatory steps were undertaken. This specific surface treatment protocol was selected

after extensive experimentation involving various factors such as solvents, substrate heating, and plasma treatments. All aluminum specimens were initially cleaned with ethanol to remove surface contaminants. The metallic plates were then abraded using SiC FEPA 80 sandpaper (Struers, United Kingdom) through vertical and horizontal grinding to achieve a smooth finish. After abrasion, the plates were cleaned again with ethanol to eliminate any residual particles.

1.7.2 Pull-off joints

For the preparation of pull-off joints, epoxy adhesive was manually applied between two 0.8mm nylon fishing threads and spread by applying pressure with an aluminum dolly. The nylon threads ensured a consistent joint thickness of 0.3mm, regardless of the operator's applied pressure and the viscosity of the modified adhesive. Figure 2.6 illustrates the manufacturing details of the specimens. To maintain the joint geometry during the curing cycle, the joined dolly was secured to the aluminum substrates using tape.

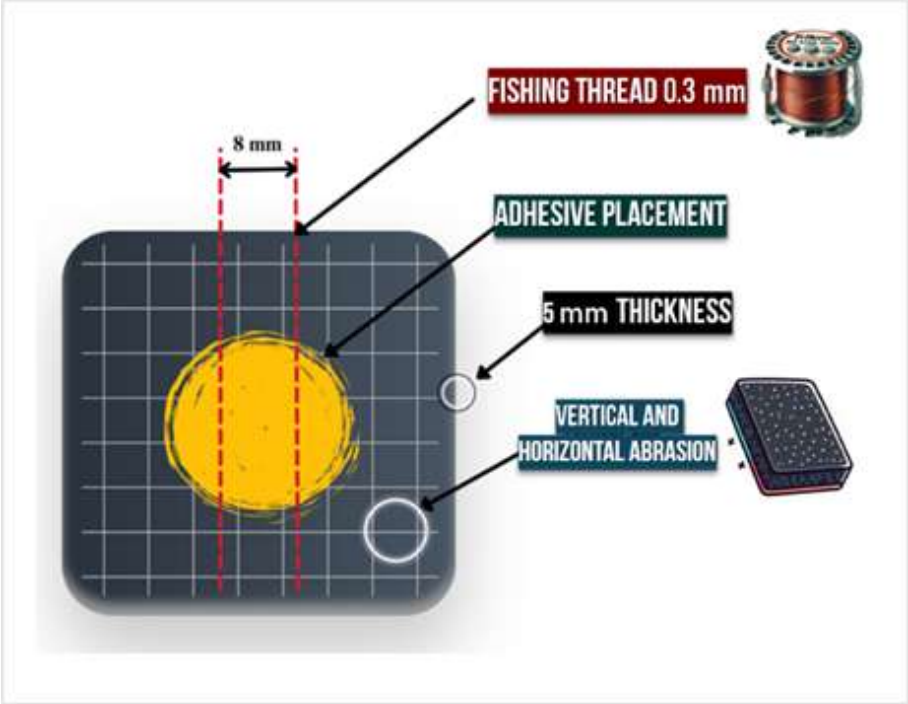

Figure 2.6: Schematic representation of the pull off joint.

1.7.3 Single lap shear (SLJ) adhesive joints

Single lap shear test specimens were prepared following the ISO 4587 and ISO 1465 standards. The sample geometry consisted of aluminum plates measuring 100mm× 25mm,

along the 100mm length. Two plates were overlapped to create a bonded surface area of 12.5mm×25mm. A specific laser-cut mold was employed to control the adhesive thickness and facilitate the preparation of the SLJ samples, as shown in Figure 2.7. Direct clamping of the single lap shear samples in the testing machine was not feasible due to the step formed by the overlapping plates. To address this issue, metallic plates with a width equal to that of the substrate plus the bonding gap were placed on each side of the sample during clamping. This setup leveled the sample, allowing for straight clamping and accurate testing.

Figure 2.7: SLJ laser cut mold.

2 Characterization methods

All characterization methods in this thesis were employed to examine the debonding capabilities and their influence on the mechanical, thermal, and physicochemical properties of both the adhesive joints and the modified resins to assess the impact of filler incorporation on overall performance.

2.1 Thermal analysis

Thermal analysis refers to a number of techniques used to monitor changes in a material's physical properties as its temperature is carefully regulated through a controlled heating or cooling program to assess material's response to different heat variations. Thermogravimetric Analysis Thermogravimetric analysis (TGA) is a method used to measure the mass change of a material as it is heated, providing important information on its thermal stability and decomposition behavior. The technique tracks mass loss events, such as evaporation or degradation, as the temperature increases [222]. The experimental setup is shown in Figure 2.8 , along with an example TGA curve. For this study, samples (515 mg) were placed in alumina crucibles and analyzed using a Mettler Toledo TGA 2 instrument. The samples were heated under an inert nitrogen atmosphere from room

temperature to 800°C at a rate of 10 K/min, unless otherwise noted. In addition, TGA was performed in an air atmosphere to examine residue formation and char development with different concentrations of flame-retardant fillers. A slower heating rate of 1 K/min was also applied in some cases to better distinguish the degradation steps in the modified resins, allowing for more detailed analysis of the decomposition process.

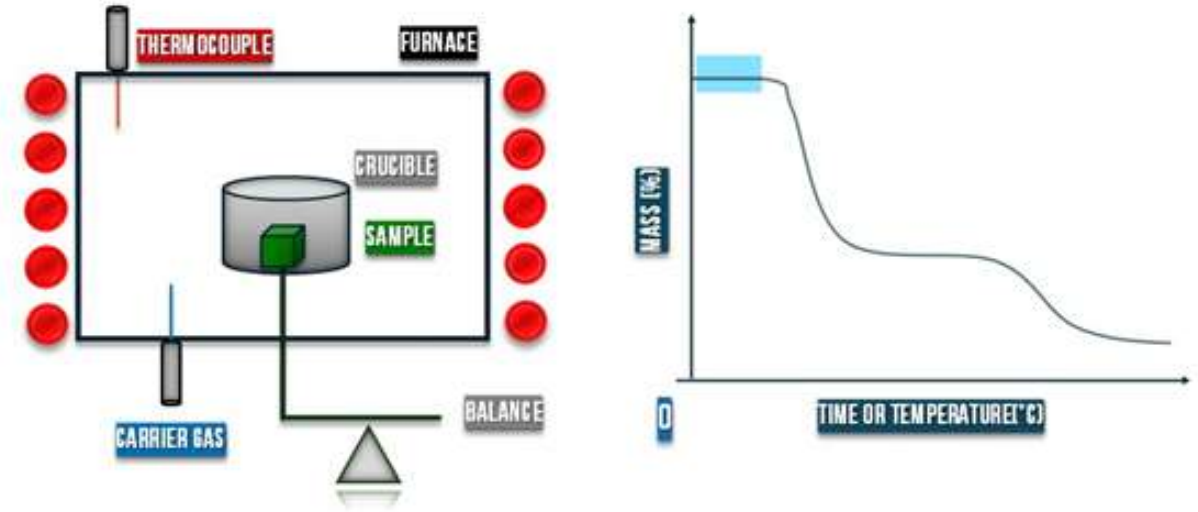

Figure 2.8: Experimental setup (left) and example of a TGA graph (right).

2.1.1 Differential scanning calorimetry (DSC)

Differential Scanning Calorimetry (DSC) is a thermal analysis technique used to quantify the heat flow associated with phase transitions in materials as a function of temperature. The method operates by measuring the differential heat input required to maintain identical temperatures between a sample and a reference, as both are subjected to a controlled temperature program. The resulting DSC thermogram, as seen in Figure 2.9, represents the heat flow differential (q) as a function of temperature, capturing endothermic or exothermic events related to transitions such as melting, crystallization, and the glass transition [223] .

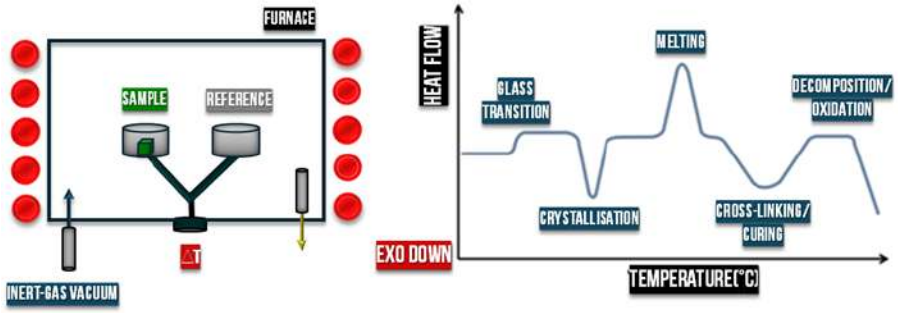

Figure 2.9: Experimental setup of a DSC experiment. A typical DSC thermogram represent the heat flow as a function of temperature.

In this thesis, the glass transition temperature (Tg) of the epoxy resins was determined using a DSC NETZSCH 204F1 PHOENIX instrument. Approximately 10 mg of each sample was sealed in aluminum crucibles and heated from room temperature to 250°C at a rate of 10°C/min under a nitrogen atmosphere. The Tg was extracted from the DSC thermogram by identifying the inflection point during the step change in the heat capacity. This inflection point corresponds to the midpoint of the glass transition region, where the material transitions from a rigid glassy state to a more flexible rubbery state.

2.1.2 Dynamic mechanical analysis

Dynamic Mechanical Analysis (DMA) is a commonly used method to evaluate the mechanical properties of polymer materials as a function of temperature. The technique involves applying a sinusoidal oscillating stress, as shown in Figure 2.10, to the sample at controlled frequencies and measuring the resulting deformation. From this response, key parameters such as the damping factor ($\tan\delta$), complex modulus, and viscosity are obtained, providing insights into the viscoelastic behavior of the material [224]. In this work, DMA was used to measure the glass transition temperature (Tg), $\tan\delta$, and the complex storage and loss moduli of epoxy resins using a Netzsch DMA 242 instrument. Bulk resin samples with dimensions of 60 mm in length and 10 mm in width were tested in dual cantilever mode on a DMA GABO Eplexor 500N instrument (Netzsch-Gerätebau GmbH). The tests were conducted at a frequency of 1 Hz with a heating rate of 3°C/min, over a temperature range from room temperature to 190°C. The data obtained provided information on the stiffness (storage modulus), energy dissipation (loss modulus), and damping behavior of the resins, with particular emphasis on the glass transition region.

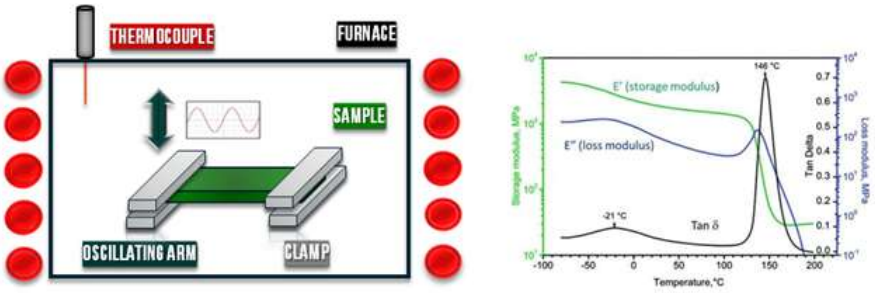

Figure 2.10: DMA set-up experiment. A typical curve obtained from a DMA experiment (right).

2.1.3 Pull off test DeFelsko (PosiTest AT-A)

The pull-off test is a semi-quantitative method for evaluating the adhesion strength of coatings or adhesive bonds to substrates. The test involves bonding a metal dolly to the surface of the coating or adhesive, and then applying a perpendicular force until the dolly detaches. The force required for detachment provides a measure of the adhesion strength. Due to the controlled design of pull-off joints, including precise management of the adhesive gap and adherend thickness, this method offers a more quantitative assessment of bond strength. To evaluate the adhesion performance and debonding behavior of different adhesive systems, pull-off testing was conducted using a DeFelsko PosiTest AT-A automatic adhesion tester with 20 mm diameter dollies. This method ensured controlled and reproducible measurements, allowing for a systematic assessment of joint strength and thermal debonding characteristics. The pull-off test served two primary objectives: (1) to compare the mechanical performance of modified and unmodified adhesive formulations across varying filler concentrations, and (2) to determine the debonding activation temperature by analyzing the thermo-mechanical degradation of adhesive joints under elevated temperatures.

For joint strength evaluation, a comparative approach was applied where each modified adhesive formulation was assessed against its unmodified reference. The impact of filler concentration on adhesion performance was examined, with a total of six joints tested per formulation series to determine the standard deviation. A dedicated reference adhesive was included in each series to establish a comparative baseline.

A modified pull-off test was implemented (Figure 2.11) to investigate the influence of additives on adhesive joint performance at high temperatures. Joints were subjected to a controlled temperature gradient, starting 5°C above the curing temperature and increas-

ing in 25°C increments. The process continued until the reference adhesive experienced severe degradation, enabling the identification of a debonding activation temperature. This temperature was defined as the point at which the joint stress at failure decreased to 10% of the maximum recorded stress for a given formulation. Since data points provided discrete stress values, the corresponding debonding temperature was determined via linear interpolation. Three independent tests were conducted at each temperature increment to assess the reproducibility and standard deviation of the procedure, ensuring the reliability of the results. This methodology allowed for a systematic evaluation of adhesion performance and debonding behavior, contributing to a deeper understanding of the thermal stability of adhesive systems.

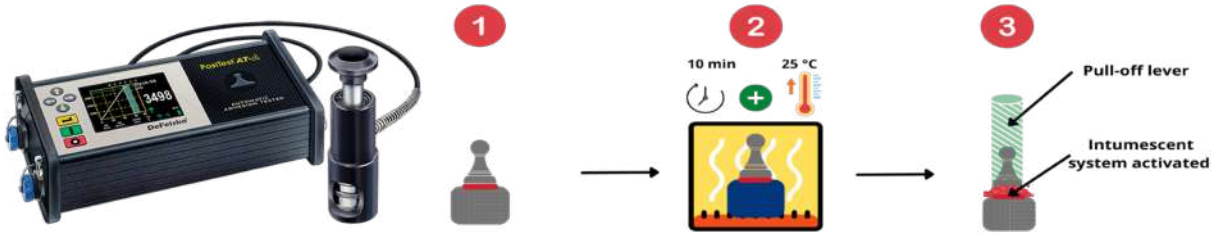

Figure 2.11: Pull off test DeFelsko (PosiTest AT-A) apparatus.

2.1.4 Flexural testing

Flexural testing is a standardized testing method used to evaluate the stiffness, strength, and ductility of polymer-based materials under bending loads. It provides insights into a materials resistance to deformation, failure mechanisms, and overall structural integrity. The deformation of the specimen under the applied load is measured, yielding key mechanical properties such as flexural strength and flexural modulus. The test provides a precise measure of the material's ability to resist bending forces and its load-bearing capacity before the onset of fracture or failure. [225, 226]. In this thesis, flexural tests were conducted on resin samples using an Instron 5967 Universal Testing System, with a crosshead speed of 2 mm/min and a span length of 40 mm. These tests were carried out across all studied formulations to assess the influence of different additive compositions on the flexural behavior of epoxy resins.

2.1.5 Single lap shear testing

Single lap shear (SLS) testing, as in Figure 2.12, is a fundamental method for quantifying the mechanical performance of adhesive joints under shear loading. It provides information about bond strength, load transfer efficiency, and failure mechanisms by subjecting the bonded assembly to controlled shear forces. This method is particularly relevant for evaluating structural adhesives in applications where bonded materials experience in-plane shear stress, simulating real-world service conditions. [227]By analyzing the response of adhesive joints under shear loading, SLS testing aids in assessing the influence of formulation modifications, filler incorporation, and surface treatments on joint durability and adhesion performance. [228, 229]In this thesis, sls tests were conducted on aluminum substrates with a bonded area of 12.5 mm × 25 mm, in accordance with ISO 4587 standards. The tests were performed using an Instron 5967 Universal Testing System with a crosshead speed of 2 mm/min, ensuring precise and reproducible measurements. The results facilitated a comparative evaluation of joint strength, adhesion performance, and failure behavior across different modified adhesive formulations.

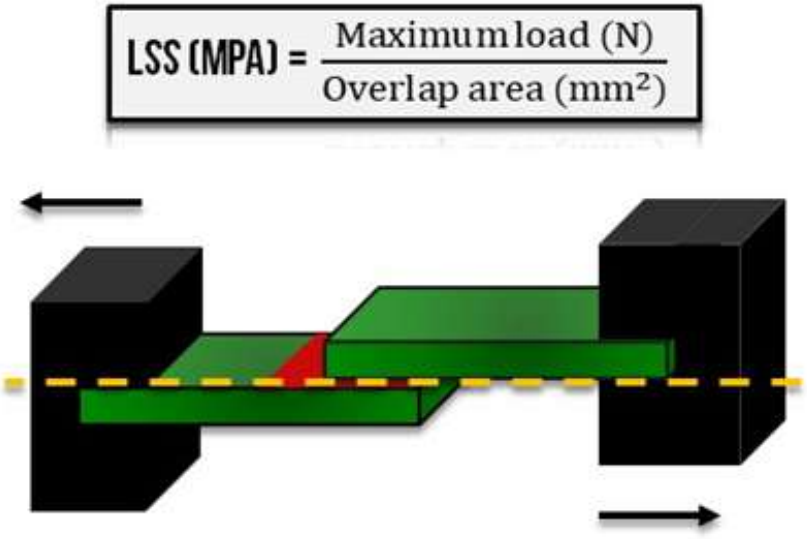

Figure 2.12: Single lap shear testing.

2.2 Spectroscopic analyses

2.2.1 Fourier transform infrared spectroscopy (FT-IR)

Fourier Transform Infrared (FT-IR) spectroscopy examines the interaction of infrared electromagnetic radiation (EMR) with matter, where infrared photons induce specific vibrational modes in molecules, resulting in characteristic absorption or transmission spectra. This provides crucial information on the chemical bonds and overall composition of a material [230]. Figure 2.13 summerizes the experimental setup of FT-IR spectrum. In this thesis, we primarily employed the TGA-FTIR coupled technique. During thermogravimetric analysis (TGA), the gases released were captured and analyzed in real time at different temperatures using a Bruker ALPHA 2 FTIR spectrometer. This coupling allowed for the identification of volatile compounds released from the samples. The TGA provided insights into the thermal stability and degradation steps, while the FT-IR spectra identified characteristic functional groups and chemical interactions. This integrated approach enhanced our understanding of the material behavior during thermal exposure, allowing for detailed analysis of the decomposition mechanisms and chemical changes occurring during heating.

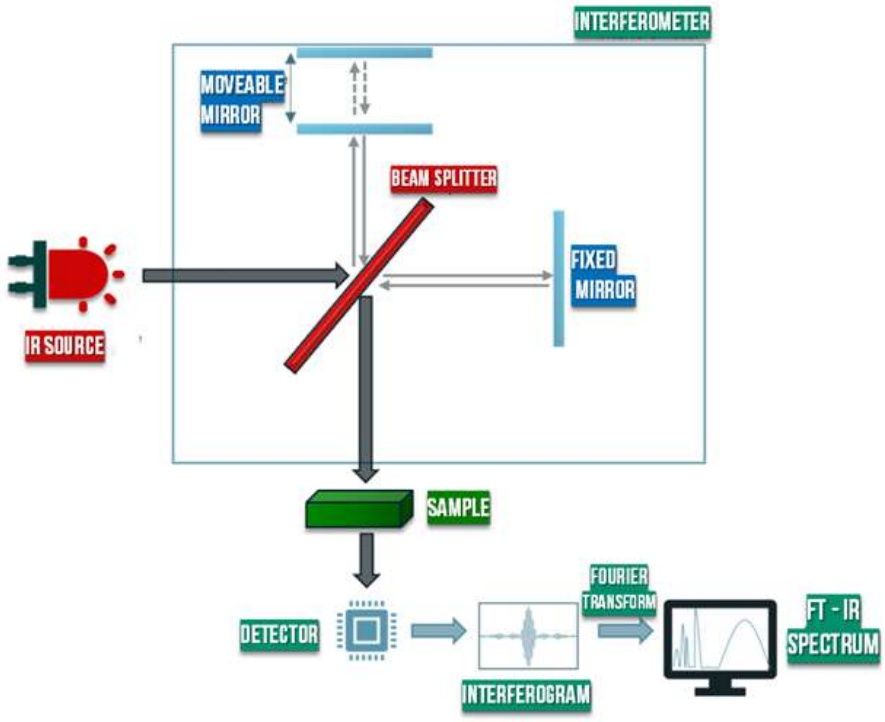

Figure 2.13: Experimental setup of an FT-IR and IR spectrum.

2.2.2 Nuclear magnetic resonance (NMR)

Nuclear Magnetic Resonance (NMR) spectroscopy is a widely utilized analytical technique in both research and industry for the characterization of solid and liquid materials. It allows for the determination of molecular structures, phase composition, and dynamic processes within complex systems, making it particularly useful for studying chemical environments and molecular interactions at the atomic level [231]. NMR operates on the principle that atomic nuclei with an intrinsic nuclear spin possess a magnetic moment [232]. When subjected to an external magnetic field, these nuclei align with the field along the z-axis. By applying an oscillating magnetic field, the nuclei are excited, and as they relax back to their equilibrium state, they generate an electrical signal known as Free Induction Decay (FID). This FID signal is processed through Fourier transformation to produce an NMR spectrum, revealing detailed information about the chemical environment surrounding the nuclei [233] (see Figure 2.14).

In this thesis, solid-state NMR techniques, including Carbon-13 (^{13}C) and Proton (^{1}H) NMR, were employed to analyze the molecular structures and interactions within resin systems modified with flame retardants. NMR was used to study the materials in their solid phase, specifically comparing the structural changes present at room temperature (RT) and after exposure to debonding temperatures. Experiments were conducted using a Bruker Ascend 400 MHz spectrometer. Samples were packed into 4 mm ZrO_2 rotors, and Carbon-13 cross-polarization/magic angle spinning (CP/MAS) spectra were recorded at a spinning rate of 10 kHz, with a cross-polarization contact time of 2 ms at 62.5 kHz, employing a ramp from 50% to 100% centered on the -1 spinning sideband (SSB). A recycle delay of 10 seconds and Spinal64 decoupling were used, with 1,000 transients collected to ensure a high signal-to-noise ratio. Proton (^{1}H) and Phosphorus-31 (^{31}P MAS NMR) spectra were also recorded, with the latter acquired at a spinning rate of 14 kHz using Spinal64 decoupling and 16 transients for optimal spectral clarity.

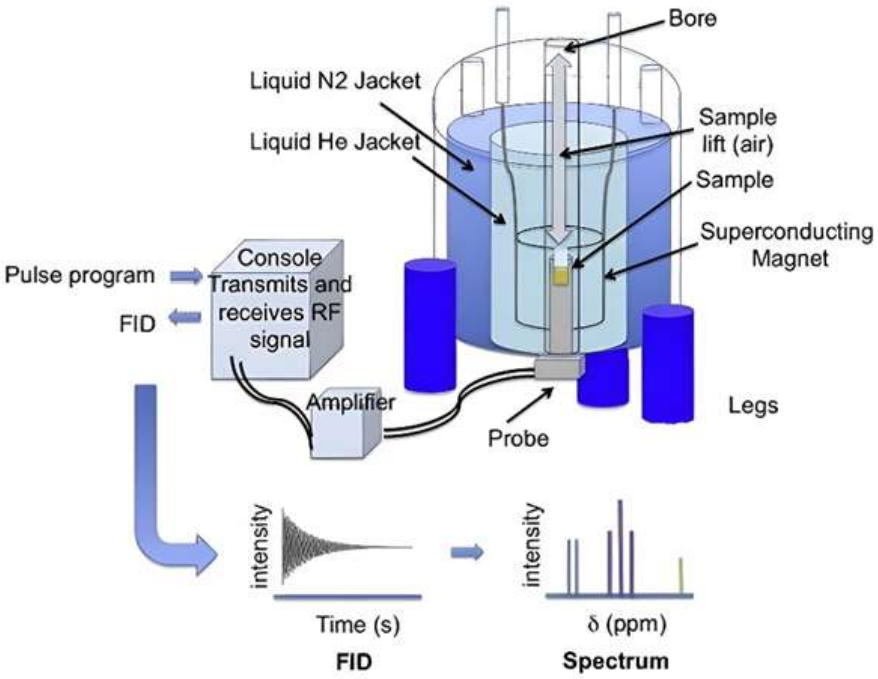

Figure 2.14: schematic setup of an NMR apparatus [1].

2.2.3 Micro computed X-ray tomography (microCT)

Micro-computed X-ray tomography (micro-CT) is a non-destructive imaging technique that provides detailed 3D reconstructions of materials by compiling 2D cross-sectional images. This method leverages the Compton effect, an inelastic scattering of X-rays, where the absorption of radiation energy depends on the density and composition of the material [234]. This enables micro-CT to differentiate between various material compositions based on their absorbance. Similar to medical CT scans, where a detector rotates around a patient, in micro-CT, the sample itself rotates 360°, allowing for detailed internal imaging without physically altering the specimen [235]. In this thesis, micro-CT was employed to investigate bulk resin samples, both modified with flame retardant fillers and non-modified, to assess the dispersion of fillers and the structural changes induced by heat exposure. Scanning was performed at both room temperature and after subjecting the samples to debonding temperatures. The imaging process was conducted using the EasyTom 160 micro-CT apparatus from RX Solutions (see Figure 2.15), with rectangular samples (4 mm×1 mm×1 mm) being scanned at an X-ray source voltage of 40 kV, current of 90 μA, and power of 3.6 W. These parameters allowed for clear phase contrast between the epoxy matrix and the fillers, producing high-resolution images with a voxel

size of 1.75 μm. During scanning, the samples were rotated 360° in angular steps of 0.25°, yielding 1,440 projections to capture a comprehensive view of the internal structure. The 3D reconstruction of the sample volumes was completed using Xact64 software, which included corrections such as spot correction, geometrical offset adjustments, and ring artifact removal. The 3D images were further analyzed and processed using Avizo software, enabling detailed interpretation of the tomographic data.

Figure 2.15: Schematic representation of ţCT experimental set-up and the EasyTom 160 micro-CT instrument.

2.3 Microscopic techniques

2.3.1 Scanning electron microscopy (SEM)

Scanning Electron Microscopy (SEM) is a high-resolution imaging technique that replaces the photons used in optical microscopy with a focused beam of electrons (see Figure 2.16). Unlike traditional light microscopy, SEM leverages the interaction of electrons with the sample's surface to generate detailed information about its topography and composition. As the electron beam scans across the sample, various signals, including secondary electrons and backscattered electrons, are emitted and detected, allowing for the creation of highly magnified, quasi-3D images at the nanoscale [236, 237]. In this thesis, Scanning Electron Microscopy (SEM) was employed to investigate the dispersion of flame retardant fillers in resin matrices and to analyze surface transformations during adhesive bonding and recycling processes. Micrographs were obtained using a FEI QUANTA FEG 200 environmental scanning electron microscope (ESEM), which provided high-resolution imaging for detailed morphological analysis. Various experimental approaches were used depending on the specific objectives of each investigation. First, bulk resin samples with different

filler systems and concentrations were imaged to evaluate filler-matrix interactions and assess the uniformity of filler dispersion within the resin. This analysis provided insights into the distribution of flame retardant additives and their integration into the polymer matrix. Second, to examine filler dispersion within adhesive joints, both modified and unmodified epoxy formulations were assembled between two aluminum substrates using a simple recovery joint configuration. A 300 μm fish thread was used to maintain a consistent bondline thickness. The cross-sections of these assemblies were mirror-polished before SEM analysis to ensure precise visualization of filler distribution and interfacial characteristics. Additionally, SEM coupled with Energy Dispersive Spectroscopy (EDS) was performed to evaluate the aluminum substrate surfaces at three critical stages: before adhesive application, after the debonding process, and following substrate cleaning. This combined approach enabled a detailed assessment of elemental composition changes and surface modifications, offering valuable insights into adhesion mechanisms, material degradation, and the overall efficiency of the recycling process.

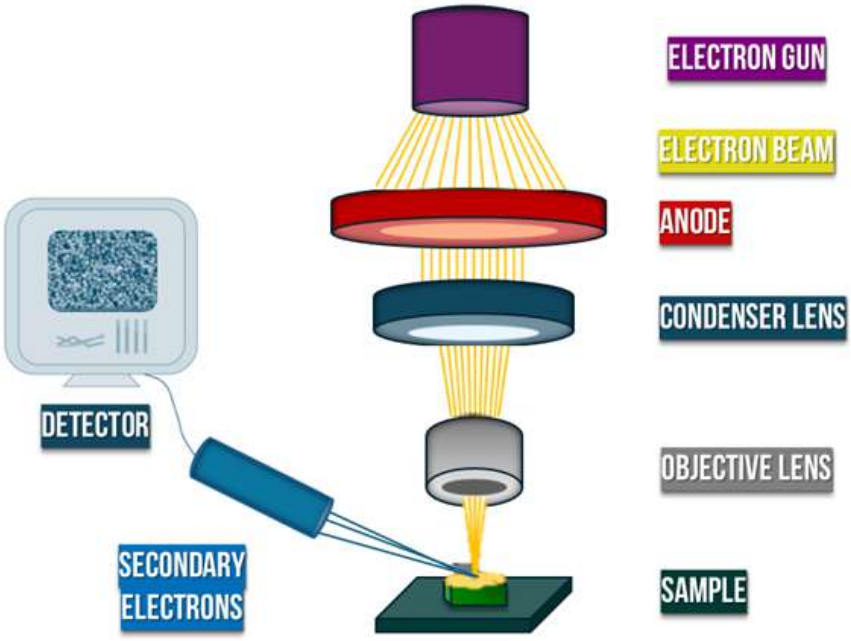

Figure 2.16: Schematic representation of Scanning electron microscopy.

2.3.2 Optical microscope

An optical microscope utilizes visible light to magnify and resolve the fine details of a specimen. Light is either transmitted through or reflected from the sample, passing first through an objective lens and then through an eyepiece lens to produce a magnified image.

The microscope setup includes a light source, a condenser to focus the light onto the sample, and an adjustable stage to hold the specimen in place [238]. The magnification and resolution are determined by the numerical aperture of the objective lens and the wavelength of the light used.

In this study, a Nikon N-STORM super-resolution microscope was employed to capture multiple images of modified resins. This allowed for the examination of filler dispersion within the resin at varying magnifications (x10, x20, x50), providing detailed insights into the distribution and interaction of the fillers across different scales.

2.4 X-Ray diffraction

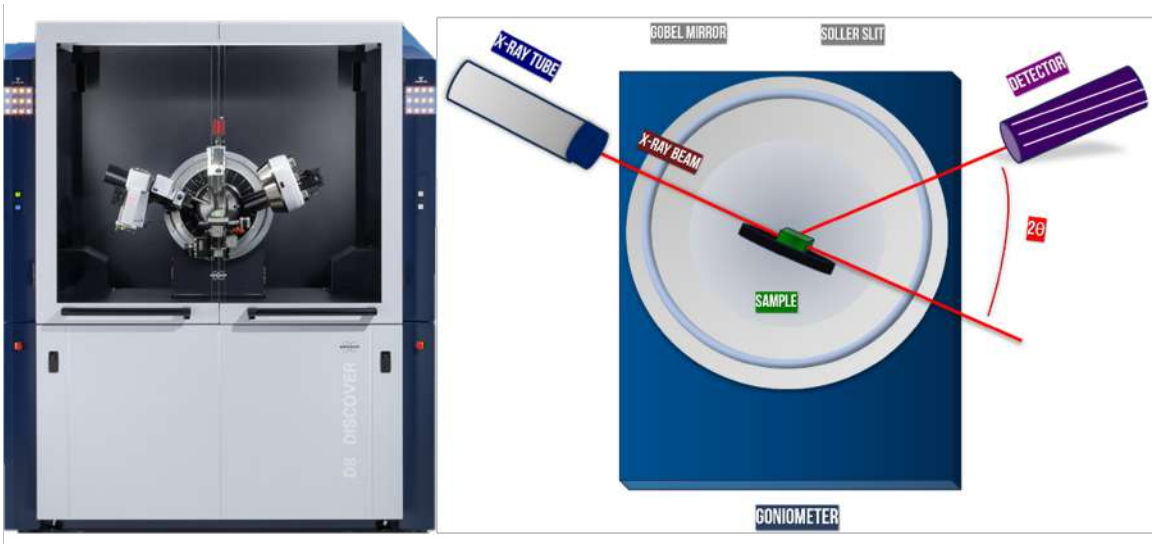

Figure 2.17: Schematic representation of X-Ray diffraction experimental set-up and the a Bruker D8 Advance diffractometer instrument.

X-ray Diffraction (XRD) is a fundamental technique for analyzing the crystallographic structure of materials, providing insights into phase composition, crystallite size, lattice strain, and structural defects. It operates based on Braggs law, which describes the diffraction of X-rays when they interact with atomic planes in a crystalline material. XRD works by directing a monochromatic X-ray beam at a sample, where the X-rays are scattered by the periodic arrangement of atoms in the crystal lattice. When the path difference between scattered waves satisfies Braggs condition ($n\lambda = 2d \sin\theta$), constructive interference occurs, producing a diffraction pattern unique to the material. This pattern is recorded by a detector and analyzed to determine phase composition, structural characteristics, and material properties such as lattice parameters and residual stress [239–241]. In this

thesis, XRD analysis was performed using a Bruker D8 Advance diffractometer in ($\theta/2\theta$) reflection mode, with a 2θ range of 5° to 70° and a step size of 0.026°, using a 10 mm spinner stage to ensure uniform exposure. The analysis was conducted on expandable graphite (EG) powder, EG embedded in resin before exposure to debonding temperatures, and EG powder and resin after debonding. This allowed for the examination of structural changes, interlayer spacing variations, and the effects of resin incorporation and thermal activation on the crystallographic properties of the material.

2.5 Recycling experiment: evaluation of adhesive Joint reusability

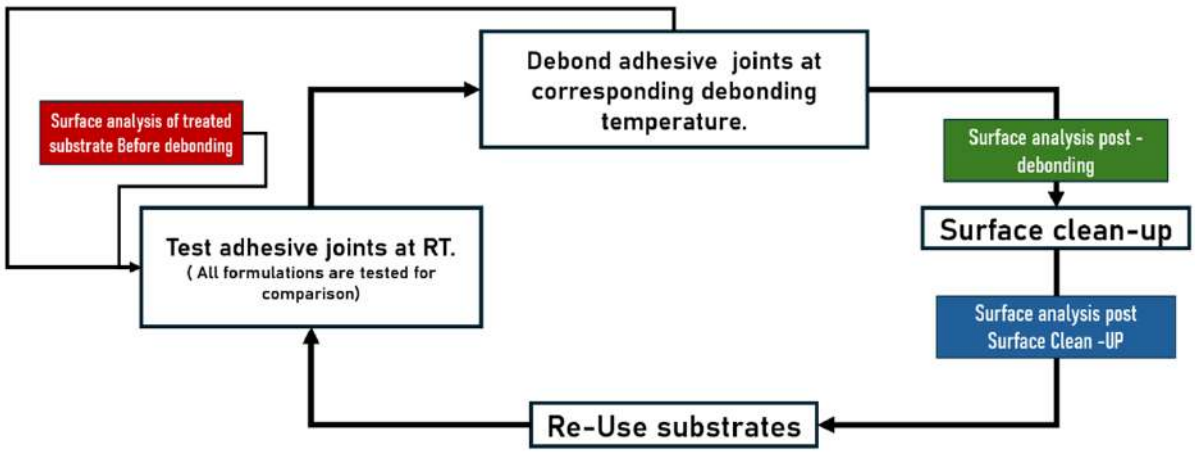

Figure 2.18: Schematic representation of X-Ray diffraction experimental set-up and the a Bruker D8 Advance diffractometer instrument.

A systematic recycling experiment was conducted to assess the reusability of aluminum substrates following adhesive debonding and surface treatment (summerized in the diagram in Figure 2.18). Initially, adhesive joints were fabricated and subjected to adhesion strength testing at RT to establish baseline performance across all formulations. Prior to debonding, a surface analysis was performed to characterize the initial condition of the treated substrates. The adhesive joints were then thermally exposed at their respective debonding temperatures to induce adhesive failure. Immediately after debonding, re-manufactured samples were prepared using the unmodified adhesive system, and ad-

hesion strength tests were conducted to evaluate the adhesive performance before surface treatment. A post-debonding surface analysis was performed to assess thermal degradation and potential surface modifications. The substrates then underwent a laboratory cleaning process involving solvent application and light abrasion to remove residual adhesive. A final surface analysis was conducted to determine the effectiveness of the cleaning process and any morphological changes to the substrate. Following cleaning, the substrates were re-bonded using the unmodified adhesive system to fabricate remanufactured adhesive joints, which were mechanically tested at RT to assess their adhesion strength and overall performance.

3

Use of intumescent flame-retardant systems in epoxy adhesives for debonding purpose

Chapter 3:

Use of intumescent flame-retardant systems in epoxy adhesives for debonding purpose

This paper focuses on validating the proof of concept that intumescent flame retardants can be effectively used to achieve debonding in adhesive joints. The study investigates the incorporation of melamine polyphosphate (MPP) and ammonium polyphosphate (APP) into epoxy adhesives, assessing their ability to enable thermally responsive debonding. By leveraging the intumescent properties of these flame retardants, activated under heat, the research demonstrates that localized swelling and porosity can be induced within the adhesive layer, facilitating the controlled separation of bonded substrates. This mechanism offers a practical alternative to existing debonding methods, which often require complex chemical formulations or are limited in their material compatibility.

A key novelty of this research lies in the dual functionality of MPP and APP. While traditionally used in fire protection applications for their char-forming abilities, this study explores their new role in debonding adhesives through thermal swelling. This approach utilizes the intrinsic properties of the flame retardants without additional chemical modifications, simplifying preparation and broadening their applicability to other adhesive systems.

The experimental results evaluate the impact of different loading rates of MPP and APP on the mechanical properties and debonding behavior of adhesive joints. The inclusion of 20 wt.% of either additive is identified as optimal, enhancing adhesive strength prior to activation while ensuring efficient debonding at elevated temperatures. MPP-based formulations consistently demonstrate superior performance, with lower debonding temperatures and improved dispersion in the epoxy matrix compared to APP. Higher loading rates, such as 40 wt.%, result in increased viscosity and additive aggregation, which can negatively affect joint quality.

Thermal analysis confirms that the inclusion of intumescent additives reduces the thermal stability of the adhesives at controlled temperatures, aiding degradation and debonding. Scanning electron microscopy (SEM) analysis highlights that MPP exhibits better dispersion within the adhesive matrix, while APP shows a tendency to aggregate

at higher concentrations. This improved dispersion of MPP correlates with its more consistent debonding performance and lower activation temperatures.

The study concludes that intumescent flame retardants, particularly MPP, provide an effective method for achieving thermally responsive debonding in adhesive joints. This approach enables substrate separation without compromising mechanical performance during the adhesive's operational lifespan. The findings confirm that these additives can be integrated into epoxy systems to create adhesives capable of on-demand debonding, presenting a practical solution for applications requiring recyclability and disassembly. Future investigations will focus on optimizing additive combinations and extending this approach to other adhesive systems and substrate materials.

Use of Intumescent Flame-Retardant Systems in Epoxy Adhesives for Debonding Purpose

Oussema Kachouri, Julien Bardon, David Ruch, and Abdelghani Laachachi

Luxembourg Institute of Science and Technology (LIST), Department of Materials Research and Technology (MRT),

5, ZAE Robert Steichen, L-4940 Hautcharage, Luxembourg.

Abstract

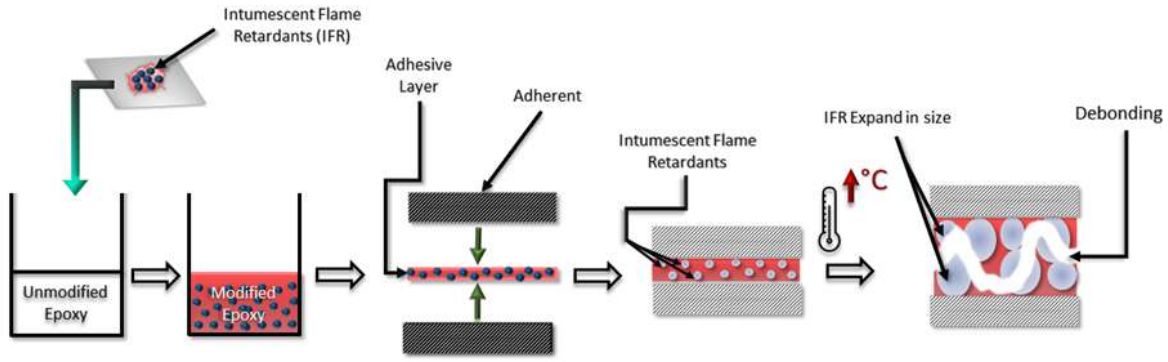

Figure 3.1: Process Flow of Adhesive Debonding Using Intumescent Flame Retardants (IFR)

In this work, we investigated the use of intumescent flame-retardant additives as a new debonding solution to disassemble bonded aluminum substrates. Melamine polyphosphate (MPP) or ammonium polyphosphate (APP) was incorporated into an epoxy adhesive joint as both an acid source and a swelling agent. This stimulus responsive behavior is triggered by heating. The ability of the system containing intumescent additives to swell and foam under heat radiation was efficiently exploited to provide enough local pressure to induce porosities and cracks at the interface, facilitating the disassembling of bonded aluminum substrates. Several of aluminum/intumescent-epoxy/aluminum laminates were assembled and tested to assess the influence of the MPP and APP content on the mechanical strength of the joints. The structural, morphological, mechanical, and thermal

properties of these modified epoxy resins and assemblies with aluminum substrates were studied using Scanning Electron Microscopy (SEM), a pull-off test, Differential Scanning Calorimetry (DSC), and Thermogravimetric Analysis (TGA). The ability of the intumescent-modified joints to support temperature-controlled debonding was evaluated using an oven. The lower debonding temperatures found were comparable to laminates with unmodified epoxy joint systems. Our patented debonding on-demand technology, based on an intumescent flame-retardant system, represents a promising treatment for multi-material structures and will enable products to be recycled at the end of their service life.

1.Introduction

Adhesively bonded joints have profoundly influenced material production methods. The construction of materials has transitioned from mechanical joining methods, such as riveting, screwing, and thermal joining, like welding, to systems that bind multiple materials together by incorporating an adhesive layer into the assembly [242,243]. Owing to its ability to combine and thin dissimilar kinds of materials, adhesive bonding has streamlined the development of innovative, lighter-weight assemblies that boast superior mechanical qualities [244]. This process eliminates the need for the additional components typically used in classical methods, such as screws. Indeed, the adhesive joints exhibit increased resilience to application stresses, thereby conveying superior fatigue resistance and an extended fatigue life [245,246]. The employment of lighter materials in this process addresses a critical environmental concern. The reduction in the overall weight of the finished products corresponds to a significant decrease in carbon footprint, due to lower energy consumption in the manufacturing process and product usage [247]. Nevertheless, the recyclability of these assemblies, for instance in the automotive industry, remains constrained due to the absence of suitable design and debonding technologies [248]. At present, existing recycling processes for reclaiming adherents remain both costly and time-consuming [143].

The imperative for recycling or repair has spurred the evolution of adhesive technologies capable of debonding on demand in response to specific triggers or stimuli such as heat, electrical current, and chemical reactions. Various effective adhesive methods, including reverse Diels-Alder, electrically induced debonding, and the integration of thermally expanding particles, have previously been investigated, and technical solutions are

already accessible [249, 250]. Furthermore, certain debonding technologies, such as those based on Diels-Alder [251] or reversible supramolecular methods [252,253], offer reversibility for the debonding process. However, due to the inferior mechanical strength of the corresponding adhesive materials, these technologies are unsuitable for structural bonding. Moreover, these methods present a significant limitation as they require the specific chemical tuning of the adhesives in advance. Conversely, debonding technology based on electrically induced debonding is initiated by an electrochemical reaction at the interface between the adhesive and anodic adherent [148,149]. While this method is notable for not requiring a heat stimulus, it is only compatible with conductive adherents or requires the addition of metal adherent patches [150, 151, 254]. Moreover, promising technologies exist that employ a heat trigger to induce debonding. These technologies involve the incorporation of special particles or agents into the adhesive to enable debonding. These can be thermally expanding particles [255–258], foaming agents [259], migrating agents [260], or expandable graphite [261].

While these technologies are suitable for structural bonding, their incorporation into the adhesive matrix impairs joint strength and predisposes it to aging [262, 263]. This is well-documented in the case of thermally expanding particles in an epoxy adhesive, where the incorporation of 25% wt. of particles into the epoxy leads to a decrease of 33% in the lap shear strength of the modified adhesive [142]. Moreover, most of these technologies are incompatible with epoxy thermosets, despite epoxy adhesives being the primary choice for structural adhesive bonding. Although many patents have been granted for different methods of separating bonded joints, few technologies are commercially available [143]. This underscores the need to address the challenge of developing a solution that is apt for structural bonding, easy to apply, resistant to aging, applicable to adhesive thermosets, and does not result in the degradation of the joint strength.

The focus of this study is epoxy adhesives, as they are the standard and most effective solution for high-performance structural bonding [264]. Modifications to epoxy resins occur primarily via two methodologies. The first method, known as reactive modification, integrates a component during the polymerization phase. However, this approach is fraught with challenges, requiring substantial developmental exertions in chemical synthesis at both the laboratory and industrial scales to develop a product suitable for use [265]. Conversely, the additive approach has proven to be more versatile and easier to employ, and is highly appealing to both the industrial and academic sectors [264, 265], due to the straightforwardness of mixing additives into the epoxy adhesive prior to the curing

process. Among the functional additives that can be incorporated into an epoxy material, flame retardants are often utilized for specialized applications. Flame retardants are a category of chemical compound that can be applied to a multitude of manufactured materials, including plastics, textiles, and coatings. These compounds are activated in the presence of a flame source and are designed to prevent or delay the spread of fire via various physical and chemical mechanisms [266, 267]. Flame retardants commonly feature halogens, phosphorus, nitrogen-based chemicals, and mineral fillers. Among the various flame-retardant technologies explored, intumescent systems have emerged as the most promising. These systems rely on a polymer's ability to expand or foam upon exposure to heat, thereby creating a porous layer that acts as a barrier against heat or gas transfer. Typically, an intumescent system primarily comprises an acid source like APP that, when heated, discharges polyphosphoric acid. This, in combination with a swelling agent such as melamine, facilitates expansion through the release of inert gases (NH_3, CO_2, H_2O). This sequence culminates with a carbon source, for instance, pentaerythritol, forming a cross-linked char layer. The most frequently documented intumescent system is APP/pentaerythritol, the mechanism of which has been comprehensively elucidated in the work of Schartel and coworkers [268]. Indeed, as noted earlier, intumescent flame retardants have traditionally been used in fire-proofing applications [269].

However, our study aims to innovatively utilize the foaming and swelling effects of these systems, as well as their early thermal degradation. Upon heating, the epoxy layer bridging the two substrates expands, forming a thermally degraded porous layer that diminishes its mechanical properties, thereby facilitating a debonding effect.

Our research team has patented an innovative technology, which this study focuses on, that involves the debonding of an epoxy joint using flame retardant agents activated by heat [270]. More specifically, we will examine the behavior of two well-known epoxy adhesive systems (DGEBA/DDS and DEGBA/DETA), which have been modified by the inclusion of traditional intumescent flame retardants (APP and MPP) at various filling rates. In particular, we will study the degradation of the joint strength as a function of thermal loading and adhesive modification. Furthermore, the thermochemical characteristics of the modified adhesives will be investigated to provide complementary information about their thermal behavior. Ultimately, the objective of the present study is not to utilize intumescent flame retardants in their traditional capacity to improve the flame retardancy of materials. Instead, we aspire to leverage these materials to pioneer an innovative and effective debonding strategy that is specifically tailored to thermosets.

2.Materials and methods

See section materials and methods of the thesis.

2.1.Materials

2.1.1.Adhesives

We employed Bisphenol A diglycidyl ether (D.E.R.332, commonly abbreviated as BADGE or DGEBA), a low common viscosity epoxy resin. We also used two distinct hardeners, an aromatic high-crosslinking agent, 4-Aminophenyl sulfone (abbreviated as DDS), and an aliphatic flexible hardener, Diethylenetriamine (abbreviated as DETA). All products were supplied by Sigma-Aldrich Germany.

2.1.2.Intumescent flame-retardants

The intumescent flame-retardant systems selected for this study were melamine polyphosphate (MPP) and Ammonium polyphosphate (APP), supplied by CIBA Germany. The commercial name of MPP is MELAPUR 200. The following table summarizes the main characteristics of the flame retardants, as supplied by the manufacturer.

Technical characteristics of the flame retardants used in this study

Flame-retardant	**MPP (MELAPUR-200)**	**APP (Exolit AP-422)**
Nitrogen Content (wt.%)	42–44	14–15
Phosphor Content (wt.%)	12–14	31–32
Particle Size (D98) (μm)	70	-
Particle Size (D50) (μm)	-	17
Real Density (g/cm^3)	1.85	1.9

3.Results

The next section elucidates the results of the experiments outlined in the experimental section. We investigated the influence of APP and MPP additives on the joint properties, including joint strength, debonding temperatures, failure modes, physicochemical properties, and thermal properties. In addition, we closely examined the failure modes and dispersion of the fillers in the adhesive.

3.1.Joint strength

The adhesive properties of epoxy formulations were evaluated using "dolly-plate" assemblies. The evolution of the adhesive strength at room temperature for an epoxy with varying amounts of MPP or APP is depicted in the figure 3.2.

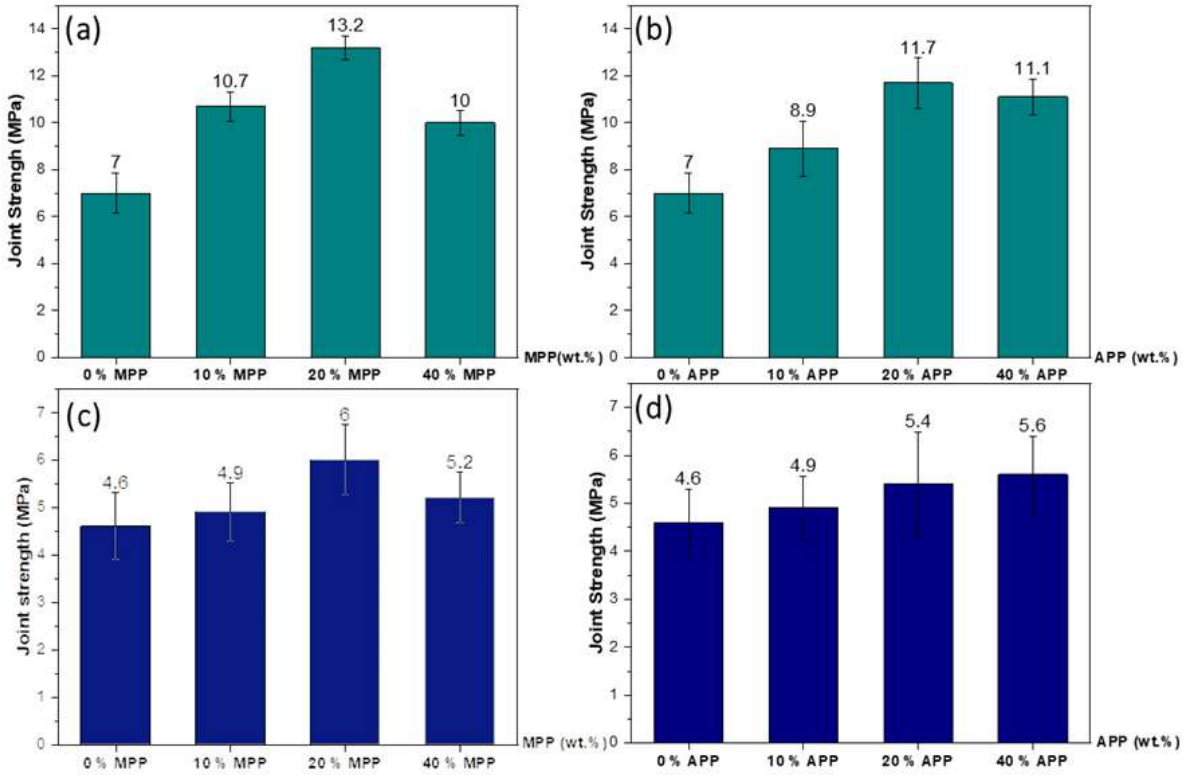

Figure 3.2: Joint strength of unmodified and modified resin epoxy at room temperature: (a) DGEBA/DDS with MPP, (b) DGEBA/DDS with APP, (c) DGEBA/DETA with MPP, (d) DGEBA/DETA with APP.

We observed that the introduction of MPP and APP as additives in epoxy resins substantially enhanced the adhesive joint strength compared to the unmodified epoxy ref-

erence: MPP at 20 wt.% and APP at 20 wt.%, with the MPP strength increasing from 7 to 13.2 MPa, and APP from 7 to 11.7 MPa, respectively. For DGEBA/DETA systems (with incorporated MPP and APP), the increase in joint strength was moderate and potentially insignificant considering the values of standard deviation. For instance, joint strength rose from 4.6 MPa to 6 MPa with the presence of 20 wt.% MPP. Although the findings were more significant in the DGEBA/DDS adhesive matrix than in the DGEBA/DETA matrix, no decline in joint strength was observed in any formulation. Given that all joint failures were adhesive, and that joint strength increased after a modification of the adhesive, these results suggest that the presence of both APP and MPP additives did not adversely impact adhesion at the adhesive/substrate interface, and is therefore a notable outcome. Furthermore, the values of joint strength measured by pull-off testing in the present study are of similar magnitude to those from a previous study in which bio-based epoxy adhesives were bonded to aluminum surfaces [271]. These joint strength values were in the range 4-6.5 MPa.

It is also worth highlighting the positive impact of incorporating APP or MPP. The Figure illustrates that the joint strength at 20 wt.% of additives surpassed that at 10 wt.% in all cases. However, at 40 wt.%, the values dropped below those at 20 wt.%. This decline may be associated with the observations made during the execution of the experimental protocol. When the mass fraction of additives exceeded 20%, the adhesive became excessively viscous, which compromised the joint quality. Another potential explanation for the decrease in joint strength could be the higher presence of aggregates when loading surpasses 20%, which might cause early joint failure. Based on the joint strength assessment (Figure 3.2), it is plausible to conclude that joint strength peaks at 20 wt.% of additive concentration. As observed later, when performing joint testing, there is a failure in the adhesive at the aluminum substrate epoxy joint interface. Furthermore, the addition of stiff microparticles such as MPP or APP to an epoxy matrix generally leads to a significant improvement of the composite elastic modulus, as observed for the epoxy with an APP filler [272]. It is then hypothesized for the present study that the addition of polyphosphate particles to the epoxy joint leads to an increase in the joint elastic modulus, which reduces the elastic modulus mismatch at the epoxy aluminum interface. This in turn delays the failure at the interface for a given normal stress and could lead to an increase in joint strength. When the loading rate exceeds 20%, this reinforcement mechanism is still valid, but the formation of particle agglomerates could reduce the joint elastic modulus by creating an additional porosity and could also trigger the premature

failure of the joint, starting within the agglomerate and possibly propagating to the epoxy aluminum interface.

3.2.Debonding test

To investigate the thermal response of the intumescent compositions within the epoxy adhesive on the disassembly of the aluminum/epoxy/aluminum assembly, a debonding test was conducted using a pull-off method after heat treatment, as detailed in the experimental section.

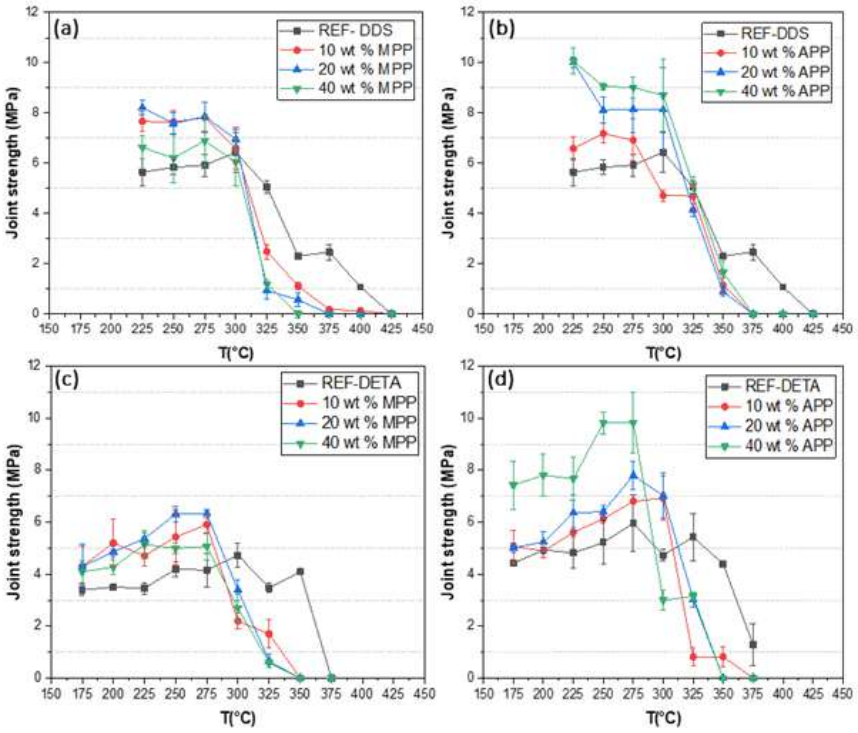

Figure 3.3: The evolution of the adhesive strength as a function of the temperature of aluminum/epoxy/aluminum assemblies: (a) DGEBA/DDS with MPP, (b) DGEBA/DDS with APP, (c) DGEBA/DETA with MPP, (d) DGEBA/DETA with APP.

Figure 3.3 presents the evolution of adhesive strength as a function of temperature for aluminum/epoxy/aluminum assemblies containing different amounts of MPP or APP. The thermal response of every adhesive composition with both hardener systems was analyzed in incremental temperature steps until the reference epoxy in each system was completely thermally degraded. As displayed in Figure 3.3, DGEBA/DDS systems consistently exhibited stronger joint strength than the DGEBA/DETA systems. As anticipated, non-modified DGEBA/DDS formulations proved more resilient to higher temper-

atures, with DGEBA/DDS joints retaining some mechanical resistance beyond 400°C, while DGEBA/DETA joints fully degraded after reaching 375°C. Throughout the application range (beginning at 225°C for DGEBA/DDS and 175°C for DGEBA/DETA and ending at the debonding temperature), modified adhesives with MPP and APP maintained their mechanical properties effectively. Across all loading rates (10%, 20%, 40%) for modified formulations, the mechanical strength exceeded that of the reference adhesive. Additionally, all formulations with APP and MPP exhibited a slight increase in joint strength values when subjected to high temperatures. Two theories have been developed to explain these findings: firstly, the curing and post-curing cycles may not have achieved a full crosslinking of the network, and secondly, the addition of flame-retardant additives may have altered the physicochemical properties of the epoxies. Further investigations of this latter hypothesis were conducted through DSC experiments.

The adhesive formulations containing 20 wt.% and 40 wt.% of additives exhibited the highest strength during heating. As can be seen in Figure 3.3 (a), 20 wt.% MPP outperformed 40 wt.% MPP, with the former peaking at a maximum value of 8.2 MPa while the latter did not exceed 6.4 MPa. However, in Figure 3.3 (b), at 225°C, both 20 wt.% APP and 40 wt.% APP show comparable values, but as the temperature rose, the more concentrated formulations demonstrated superior strength until the debonding temperature was reached. This observation can be rationalized by considering the particle size of our additives and their dispersion within the DGEBA matrix. Given the much smaller particle size of APP powders, better dispersion is expected.

In the presence of the MPP additive, as demonstrated in Figure 3.3 (a) and (c), the mechanical performance of the joints abruptly deteriorated at 325°C, falling from 7 MPa in both DGEBA/DDS and DGEBA/DETA at 300°C to less than 1 MPa for both systems at 325°C. Conversely, for formulations containing APP additive, as shown in Figure 3.3 (b) and (d), debonding occurred after 350°C, as the joint strength decreased from 8.1 MPa in 20 wt.% APP for DGEBA/DDS and 6.4 MPa for the same mass fraction for DGEBA/DETA to less than 0.5 MPa. The debonding temperatures (T°deb) of the formulations under study were extracted from Figure 3.3 and are presented in the following table (Table 3.1).

The inclusion of APP or MPP in the epoxy resin significantly lowered the debonding temperature of the resin, with temperature reductions ranging from 17°C to 86°C. Notably, the greatest decrease was achieved with the inclusion of 20wt.% MPP.

Table 3.1: Debonding temperatures (T_{deb}) of unmodified and modified resin epoxy with APP and MPP additives

	T_{deb} **in DGEBA/DDS (°C)**	T_{deb} **in DGEBA/DETA (°C)**
Ref. (neat resin)	411	372
10% APP	360	355
20% APP	352	344
40% APP	361	336
10% MPP	358	341
20% MPP	325	326
40% MPP	325	329

3.3.Examination of the failure modes

We concentrated our examination of joint failures on samples collected at ambient temperatures and those obtained at the debonding temperature (see Figure 3.4). We evaluated these failure modes visually and identified two primary types: mixed failure and cohesive failure. It was observed that failure modes transitioned from cohesive to mixed failures as the loading of flame retardants in the adhesives increased. Additionally, we noted adhesive failures, particularly in the non-modified adhesive systems, in the post-debonding phase.

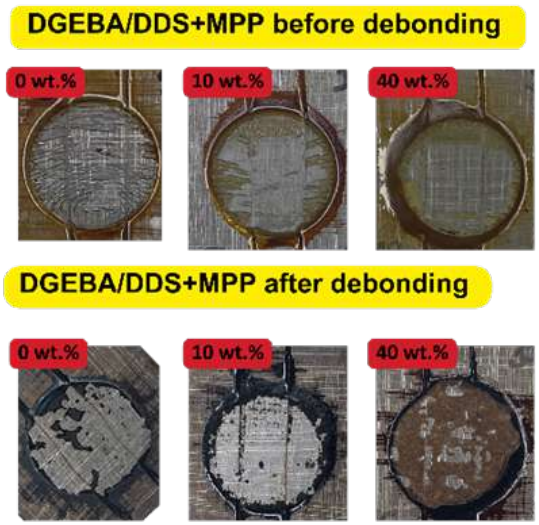

Figure 3.4: Sample observation of failure modes

3.4.Influence of the additives on the physicochemical properties

3.4.1.Influence on the glass transition temperature

To investigate the impact of additives and filling rates on the resin matrix, Differential Scanning Calorimetry (DSC) measurements were taken for all formulations at different loading rates and for both hardeners. The results obtained for glass transition temperature (Tg) are summarized in the table 3.2 below. These results show that the incorporation of MPP and APP additives, at various mass fractions, exerts a negligible influence on the glass transition temperature (Tg) of the epoxy matrices. As illustrated in the previous table, the Tg of the reference DGEBA/DDS system registered at 206°C, whereas when MPP was introduced at a 40% weight ratio, the Tg exhibited a minor deviation of merely 1°C, reaching 207°C. The same behavior was exhibited in all other formulations.

Table 3.2: Temperatures of glass transitions (T_g) of the formulations studied in DGEBA/DDS and DGEBA/DETA

	T_g **in DGEBA/DDS (°C)**	T_g **in DGEBA/DETA (°C)**
Ref.	206	155
10% MPP	206	155
20% MPP	206	155
40% MPP	207	155
10% APP	208	155
20% APP	208	156
40% APP	208	156

3.4.2.Thermogravimetric study

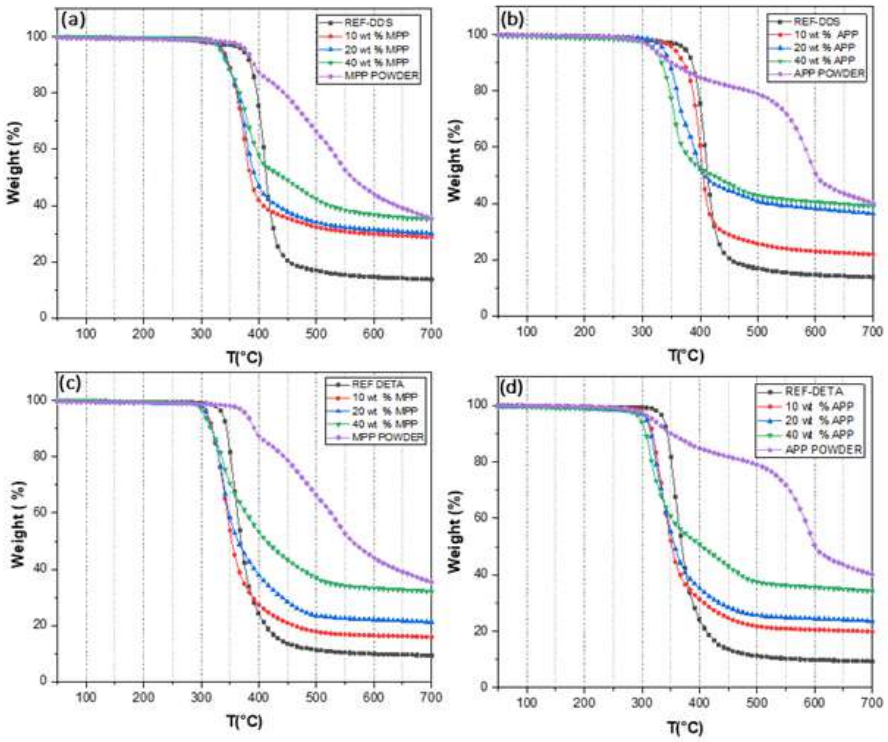

Figure 3.5: TGA curves of all formulations under N2, (a) DGEBA/DDS with MPP, (b) DGEBA/DDS with APP, (c) DGEBA/DETA with MPP, (d) DGEBA/DETA with APP.

The thermal degradation of modified DGEBA epoxies was assessed in comparison to that of unmodified DGEBA epoxies. Figure 3.5 presents the TG curves for DGEBA-DDS and DGEBA-DETA with varying contents of MPP and APP (10, 20, and 40 wt.%). The onset temperatures of degradation at 5% of weight loss ($T_{\text{onset5\%}}$)are reported for each formulation in the following table (Table 3.3).

The TGA results indicate that the inclusion of either MPP or APP in the DGEBA resins reduced their thermal stabilities. In fact, with the APP additive, $T_{\text{onset5\%}}$ decreased as the mass fraction of APP increased. The most significant decrease in $T_{\text{onset5\%}}$ was observed with the incorporation of APP at a 40% loading rate for both resins, DGEBA/DDS and DGEBA/DETA. The lowest onset temperature (297°C) was noted for APP at a 40% loading rate for DGEBA/DETA, while the greatest decrease in onset temperature (53°C) was observed for APP at a 40% loading rate for DGEBA/DDS.

For MPP additives, it was observed that the $T_{\text{onset5\%}}$ remained relatively consistent regardless of the mass fraction. In DGEBA/DDS, $T_{\text{onset5\%}}$ for 10%, 20%, and 40% MPP

Table 3.3: Onset temperatures of degradation at 5% of weight loss ($T_{\text{onset5\%}}$) in DGEBA/DDS and DGEBA/DETA

	$T_{\text{onset5\%}}$ **in DGEBA/DDS (°C)**	$T_{\text{onset5\%}}$ **in DGEBA/DETA (°C)**
Ref. (neat resin)	373	338
10% APP	355	311
20% APP	336	308
40% APP	320	297
10% MPP	336	311
20% MPP	335	310
40% MPP	334	305

was approximately 334 ± 2 °C. Conversely, increasing the mass fraction affected only the residue amount at 700°C.

When compared to DGEBA/DDS systems, degradation always commences earlier in DGEBA/DETA. Thus, the deterioration of thermal properties in adhesives is dependent both on the type of flame retardant used and its properties, as well as the matrix into which the flame retardant is introduced.

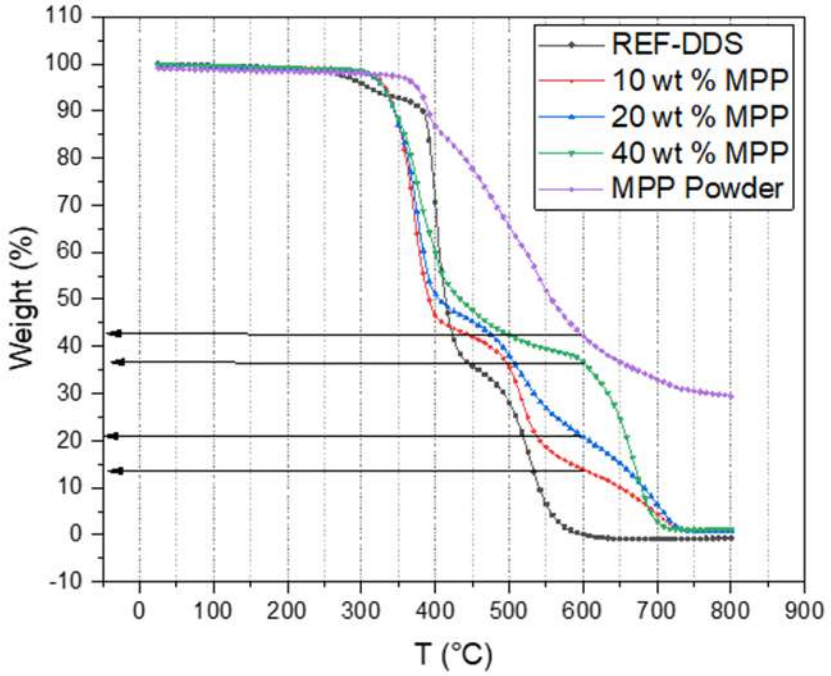

Figure 3.6: TGA curves of different DGEBA-DDS based formulations with MPP under AIR.

Regarding the mechanism or mode of action, it is understood that the phosphoric acid released from MPP or APP is expected to react with the carbon source (the DGEBA matrix in our case), resulting in a higher formation of char. In our study, we utilized the TGA curves under air to verify the quantity of residue and its evolution with the addition of additives as in Figure 3.6. Table 3.4 details the amount of residue from different formulations at 600°C. We compared the residue amount obtained experimentally with the residue calculated from the theoretical curve according to the mixing law. The deviation between the theoretical and experimental data indicates the presence of an interaction, facilitated by the activation of the intumescent systems. For instance, with 40 wt.% of

Table 3.4: Theoretical and experimental mass residue at 600°C of the different flame retardants wt.% within both DGEBA matrixes.

Flame retardants	Theoretical residue (%)	Experimental value (DGEBA/DDS) (%)	Experimental value (DGEBA/DETA) (%)
10 % MPP	4.2	14.015	8.9
20 % MPP	8.41	21.17	17.59
40 % MPP	16.82	37.05	34.15
10 % APP	4.98	20.73	14.61
20 % APP	9.96	38.19	30.47
40 % APP	19.92	43.24	37.36

APP, the residue amounts were 38.19% in DGEBA/DDS and 37.36% in DGEBA/DETA, while the theoretical value was only 19.92%. The mass residue in all DGEBA/DDS systems consistently surpassed the mass residue in DGEBA/DETA systems. This difference could be attributed to the distinct chemical and structural compositions of the hardeners, given that DDS includes more aromatic structures than DETA, which in turn contributes to an increase in the char residue formed during thermal decomposition. Notably, when MPP was used, the residue was less than that when using APP. For example, 20 wt.% MPP in DGEBA/DDS resulted in 21.17% char, whereas 20 wt.% APP generated 38.19%. This is likely due to the presence of melamine molecules in MPP, which contribute to the creation of additional gases that ultimately evaporate as the matrix degrades.

3.5.Influence of the dispersion of the additive

To elucidate the dispersion characteristics of the additives within the epoxy resin matrix, we assembled both modified and unmodified epoxy resins between two aluminum substrates, employing a simplistic recovery joint. Figure 3.7 presents representative SEM micrographs of both adhesive systems, each containing 20 wt.% of MPP and APP.

It can be discerned from the images that the MPP and APP additives do not exhibit the same dispersion behavior in the epoxy resin: while MPP additives show well-distributed particles, there is a tendency towards aggregation in the case of APP. Concurrently, a precipitation phenomenon is particularly noticeable with APP, whereby a higher density of particles is observed near the lower aluminum substrate. This trend is amplified at higher loading rates; the primary distinction lies in the significantly escalated levels of agglomeration and precipitation for APP samples. In contrast, the MPP samples maintain a largely homogeneous dispersion despite the visible increase in agglomerate formation.

We also observed that the specific type of hardener employed does not significantly influence these dispersion states, suggesting the primacy of the additives themselves in shaping the distribution and behavior of the components within the epoxy resin matrix.

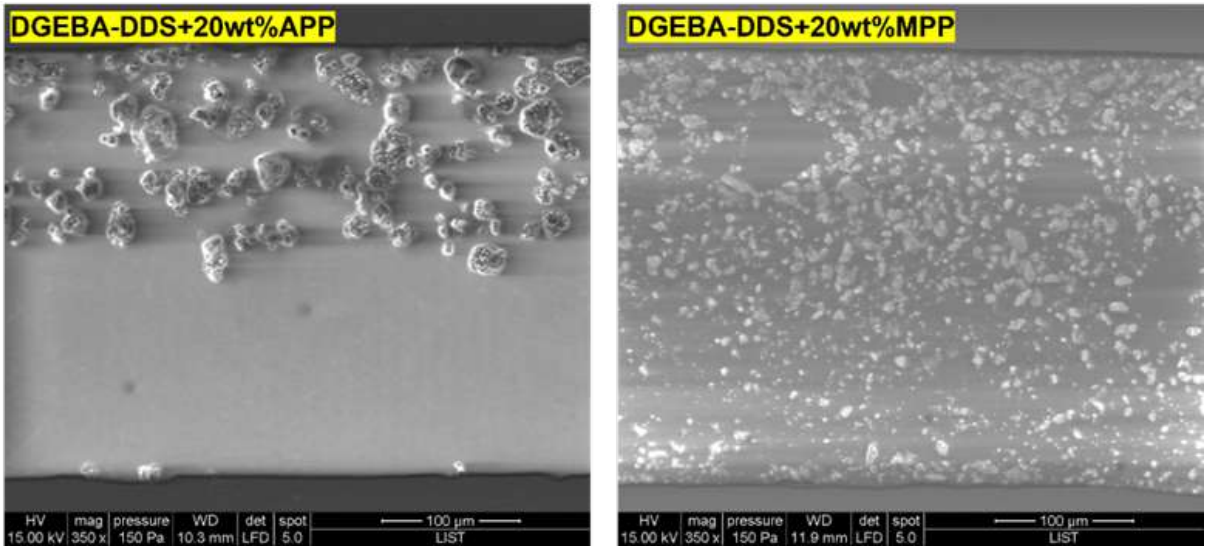

Figure 3.7: SEM images of the different additives at 20 wt.% in DGEBA/DDS, (a) 20 % APP, (b) 20 % MPP, (c) close up on the epoxy adherend interface.

4.Discussion

Previous works on the debonding effect obtained by the incorporation of a dedicated functional additive into a structural adhesive have studied chemical and physical foaming agents [259], thermally expandable particles [255–258], expandable graphite [261], and migrating agents [260]. To the best of our knowledge, this is the first research to investigate the use of intumescent flame retardants as additives to impart a debonding effect on adhesives.

A methodology was developed in order to determine a debonding temperature characteristic of the adhesive modification (see Table 3.5). This allowed a direct comparison of the effects on the debonding temperature obtained with the incorporation of various flame-retardant additives at different loading rates. The criterion to evaluate a debonding temperature was selected as 20% of the maximum load after a statistical evaluation of the correlation between debonding data and thermogravimetry data. More precisely, debonding test data and TGA curves were carefully analyzed, and characteristic figures were extracted from the data. For TGA curves, the following temperatures were evaluated:

- The temperature at which 5% of the initial weight is lost. This temperature is sometimes described as the onset of degradation and is therefore called: $T_{\text{onset5\%}}$
- The temperature at which 10% of the initial weight is lost. This temperature is sometimes described as the onset of degradation and is therefore called:$T_{\text{onset10\%}}$
- The temperature at which 20% of the initial weight is lost, $T_{\text{weight20\%}}$
- The temperature at which 50% of the weight is lost, $T_{\text{weight50\%}}$

As for the debonding test data, the following temperatures were evaluated:

- The temperature at which 50% of the maximum joint strength is obtained, $T_{\text{50\%stress}}$
- The temperature at which 20% of the maximum joint strength is obtained, $T_{\text{20\%stress}}$
- The temperature at which 10% of the maximum joint strength is obtained, $T_{\text{10\%stress}}$
- The temperature at which the joint strength falls to zero, $T_{\text{0\%stress}}$

After acquiring these datasets for all reference and modified resins, we evaluated the correlation between data from TGA and debonding tests by calculating the Pearson correlation coefficient. The calculated coefficients are presented in the table below. The best correlation between TGA data and debonding tests is observed for $T_{\text{onset5\%}}$ and $T_{\text{0\%stress}}$. However, the information contained in $T_{\text{0\%stress}}$, i.e. the temperature at which the joint fails, is not very useful since the testing was undertaken at 25°C, meaning that in the end, many modified resins exhibited the same $T_{\text{0\%stress}}$, which provided little differentiation. Therefore $T_{\text{10\%stress}}$ is preferred as a characteristic debonding value; justifying a posteriori why this particular resin characteristic temperature was selected in the Method section.

Table 3.5: Correlation coefficient values between the datasets (data for all resins)

	$\mathbf{T}_{0\%\ \text{resid}}$	$\mathbf{T}_{20\%\ \text{resid}}$	$\mathbf{T}_{10\%\ \text{resid}}$	$\mathbf{T}_{0\%\ \text{resid}}$
$\mathbf{T}_{\text{onset 5\%}}$	0.71	0.71	0.73	0.74
$\mathbf{T}_{\text{onset 10\%}}$	0.68	0.69	0.71	0.72
$\mathbf{T}_{\text{weight 20\%}}$	0.59	0.59	0.61	0.66
$\mathbf{T}_{\text{weight 50\%}}$	0.11	0.16	0.12	0.13

The value of correlation coefficient between these two datasets, $T_{\text{onset5\%}}$ and $T_{\text{10\%stress}}$, shows a rather good, but not perfect, correlation. It is therefore assumed that the phenomena leading to the joint thermal degradation and weight loss are different to those leading to the thermal degradation and mechanical strength of the joint. Nevertheless, observing the TGA results might give a first insight into the capacity of additives to lead to debonding when increasing temperature.

Furthermore, the comparison between debonding data and TGA data, in particular, as shown in Table 3.4, should be further analyzed. For instance, it is observed that the onset temperature for TGA tests tends to decrease more for APP incorporation, in particular for 40% wt.% of APP, than for MPP incorporation. This is not correlated to the debonding data in which MPP incorporation is more effective than APP, i.e., the debonding temperature is much lower in the case of MPP incorporation.

Observation of SEM pictures for the cases of APP and MPP incorporation shows that APP particles are quite big after being incorporated into the epoxy, and that agglomeration certainly occurs. This reduces the contact area between APP and the epoxy matrix, in contrast to MPP where the particles are much smaller, thus increasing the corresponding area of contact with the matrix. It can therefore be assumed that at a given temperature, the intumescence phenomena are enhanced for MPP compared to APP, which leads to better debonding. Lastly, this might explain a lower debonding temperature for MPP.

In addition, we confirmed that the incorporation of flame retardants had no effect on the physicochemical characteristics of the adhesives, since the Tg remained practically the same after APP or MPP incorporation. This is interesting, since Tg is a critical characteristic of polymers and adhesives, and the addition of these two fillers does not modify this characteristic despite the high loading rate (40 wt.%) tested in this study.

To the best of the authors knowledge, this study is the first to describe how the addition

of intumescent flame-retardant additives to an adhesive can lead to a better debonding of the adhesive joint. For this reason, a patent describing this innovative approach was granted [270]. A complete methodology was developed to characterize the thermal and debonding properties of modified adhesive joints. The current debonding temperatures are in the 325-350°C range after adhesive modification. This is rather high compared to typical debonding temperatures for epoxy adhesives loaded with thermally expandable particles [255–258] or expandable graphite [261] where debonding temperatures are close to 170°C or 235°C, respectively. Although the glass transition temperature of the epoxy adhesives and the debonding methods are different for the other debonding approaches, the current debonding temperatures are quite high and further investigations with other intumescent systems are necessary in order to achieve lower debonding temperatures. For instance, the combination of several flame-retardant additives could be investigated to hopefully obtain a synergistic effect between them [269].

Finally, we also anticipate extending the range of applicability of the current study, which was first developed on aluminum-epoxy-aluminum joints. More generally, the addition of functional additives in epoxy adhesives to obtain a debonding on-demand function could first be employed to trigger the debonding of fiber-reinforced polymer (FRP) composites, in particular, when the polymer matrix is an epoxy thermoset. Furthermore, a more advanced application could separate reinforcement fibers and matrix in FRPs to allow higher-value fibers to be recycled.

5.Conclusion

In this study, we developed a novel methodology to facilitate the easy debonding of adhesive joints employing traditional intumescent flame-retardant systems. We tested ammonium polyphosphate and melamine polyphosphate for this purpose and observed a reduction in debonding temperatures. Our findings showed that these additives did not impact the adhesive joint properties, namely, adhesion and mechanical strength. Furthermore, MPP and APP notably enhanced the adhesive joint strength compared to unmodified epoxy. To investigate the thermal response of intumescent additives within the epoxy adhesive during the disassembly of the aluminum/epoxy/aluminum assembly, we conducted a debonding test using the pull-off method after heat treatment. For the first time, this study shows that the addition of intumescent agents such as APP or MPP in epoxy-based

joint can promote an easier debonding of the joint by an accelerated thermal degradation of the modified epoxy. In the present study, the reduction of debonding temperature after flame-retardant agents incorporation is less than 100°C. Further investigations to introduce other flame-retardants as debonding agents are conducted in order to activate debonding at even lower temperatures in epoxy-based materials, thereby broadening the potential applications of this debonding on-demand technology.

4

Use of non-intumescent organophosphorus flame-retardant systems in epoxy adhesives for debonding purpose

Chapter 4:

Use of non-intumescent organophosphorus flame-retardant systems in epoxy adhesives for debonding purpose

This paper contributes directly to the objectives of this thesis by expanding the investigation of flame retardant-based debonding agents to include non-intumescent organophosphorus compounds. Building on prior studies that validated the potential of intumescent flame retardants for thermally responsive debonding, this work shifts focus to AFLAMMIT®PCO-900 , a phosphorus-based compound, to broaden the scope of the research and explore its performance within adhesive systems.

The study provides a thorough characterization of the modified adhesive system, including its mechanical properties, thermal behavior, and debonding mechanism. By examining AFLAMMIT®PCO-900 at various loading rates, the research identifies optimal conditions where efficient debonding can occur without compromising the adhesives structural integrity during its operational phase. The systematic evaluation includes thermogravimetric analysis (TGA), differential scanning calorimetry (DSC), tomography, and scanning electron microscopy (SEM), which together provide insights into the materials performance and its interaction within the epoxy matrix.

This work also contributes to the thesis by extending the understanding of debonding mechanisms through detailed analyses. The findings reveal that the incorporation of AFLAMMIT®PCO-900 results in a significant reduction in debonding temperatures, with efficient debonding observed around 250°C. Additionally, the study explores the effect of filler dispersion on debonding efficiency and joint performance, highlighting the role of optimized formulations in achieving both high mechanical strength and effective thermal activation.

In the context of this thesis, this paper contribution lies in its systematic exploration of alternative flame retardants, emphasizing their potential as functional additives for adhesive debonding technologies.

Use of non-intumescent organophosphorus flame-retardant systems in epoxy adhesives for debonding purpose

Oussema Kachouri, Julien Bardon, David Ruch, and Abdelghani Laachachi

Luxembourg Institute of Science and Technology (LIST), Department of Materials Research and Technology (MRT),

5, ZAE Robert Steichen, L-4940 Hautcharage, Luxembourg.

Abstract

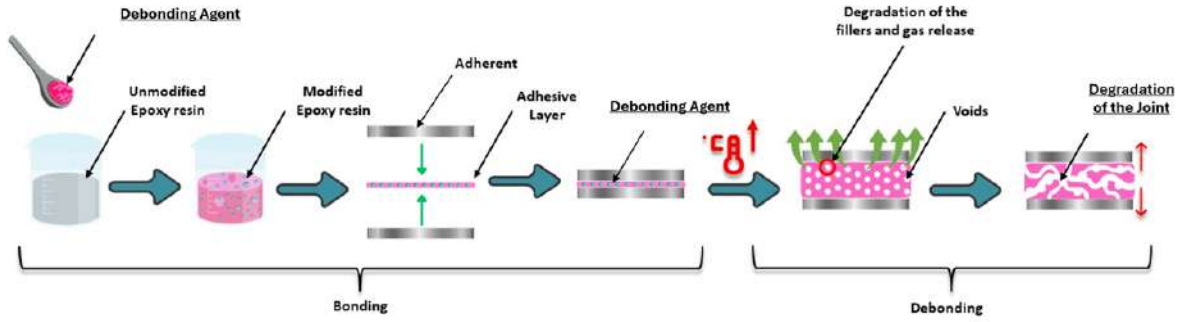

Figure 4.1: Schematic Representation of the Bonding and Debonding Process Using a Debonding Agent in Epoxy Resin Systems

This paper investigates the novel application of an organophosphorus flame retardant AFLAMMIT®PCO-900, referred to as the debonding agent, for inducing debonding in adhesive joints. Building on our previous study, which demonstrated that traditional intumescent flame retardants like Melamine polyphosphate (MPP) and Ammonium polyphosphate (APP) can lower debonding temperatures by weakening joint strength at temperatures significantly below the degradation threshold of unmodified adhesives, we explore the debonding agent's distinct non-intumescent mechanism. This study employs tomography to examine the modified resin both before and after reaching the debonding temperature. Additionally, we investigate the performance of a structural adhesive system modified with the debonding agent at various concentrations (0, 10, 20, 30, 40 wt.%). The mechani-

cal properties and thermal/mechanical degradation of these joints were assessed using a modified pull-off test with specific experimental parameters, including surface preparation, adhesive gap, substrate thickness, and curing temperatures. Thermogravimetric Analysis (TGA) and Differential Scanning Calorimetry (DSC) were conducted to evaluate the physicochemical properties of the resin samples. Scanning Electron Microscopy (SEM) was used to analyze the dispersion of the debonding agent in the epoxy matrix and examine the joint microstructure. The results demonstrate that incorporating the debonding agent into adhesive formulations not only lowers the degradation temperature of structural adhesives but also enhances joint strength within the application range. It offers a debonding solution at a distinct temperature window as low as 250 °C, promoting efficient end-of-life recycling and advancing sustainable manufacturing practices.

1.Introduction

Adhesives have became a preferred alternative to conventional bonding techniques such as riveting and welding in a multitude of structural joining applications [242]. In fact, the introduction of an adhesive layer between two materials offers several advantages including weight reduction, impermeability to water and air, as well as good resistance to vibrations [243,244] while preserving the intrinsic properties of the bonded materials and their optimal characteristics [245]. Moreover, adhesive bonding addresses a range of technical challenges and serves as a key enabler in reducing environmental impact by significantly decreasing the weight of the product and minimizing raw material use [246, 247]. This dual advantage results in a lower carbon footprint both during manufacturing and across the product's lifespan [248], aligning with most recent worldwide guidelines for sustainable constructions like the European Union's emphasis on more sustainable construction practices [273]. However, the permanent nature of adhesive-bonded joints poses a significant drawback, highlighting the need for innovative debonding strategies [143]. The ability to disassemble adhesive joints allows for easy recycling and reworking of valuable and expensive components [248,274], thereby tackling both economic and environmental challenges [9]. Present solutions, such as mechanical destruction and chemical debonding, while already established, potentially harm substrates and drastically reduce their recyclability because of the depreciation of their original value [7, 9]. As a result, there's an escalating demand for the development of innovative techniques and processes that facilitate the easier recycling and recovery of adherends from bonded structures. A variety of

technologies documented in literature promote adhesive reversibility or debonding. These technologies typically fall into two principal categories: the first involves the synthesis or modification of the adhesive structure itself, such as Diels-Alder and supramolecular adhesives [251,252]. The second category comprises techniques that integrate both synthesis and modification of the adhesive structure [10]. Alongside these, a promising approach under exploration revolves around the creation of reworkable adhesives, incorporating elements that facilitate network breakdown [253]. Yet, the scalability to industry remains limited [141]. The second category involves the modification of adhesives by integrating fillers that render the matrix reactive to specific triggers such as heat, electrical current, or chemical stimuli [149]. This category includes, debonding through an electrochemical reaction at the adhesive-adherent interface, making this technology only compatible with conductive adherents [151, 152, 254]. Another set of promising technologies utilizes a heat trigger, leveraging physical volume expansion to induce debonding. Promising examples of such technologies are thermally expanding particles [255–257] and expandable graphite [261]. While some of these methods are apt for structural bonding, their incorporation into the adhesive matrix may compromise joint strength and accelerate the aging process. Despite advancements in debonding technology, there remains a need for a comprehensive solution that presents no compatibility limitations with different materials and meets essential criteria, such as preserving joint strength within the application range, resisting aging, and facilitating debonding at the appropriate temperature windows [275,276]. In response to this challenge, this work proposes an innovative debonding strategy inspired by the concept of flame retardancy. Our previous research demonstrated that integrating flame retardants into thermosets effectively reduces the degradation temperature, thereby triggering a debonding effect. This debonding effect primarily arises from the swelling or foaming that occurs during a specific period of heat exposure, consequently weakening the joint strength [277]. In our examination of various flame retardants, we found that phosphorus flame retardants are increasingly replacing halogenated variants due to their superior performance and environmental compatibility. Notably, organo-phosphorus compounds have demonstrated excellent flame retardancy properties. Protocols for synthesizing these compounds exist in the literature, and they are now commercially available as AFLAMMIT®PCO-900, a product by Thor [278, 279]. PCO 900, also known as PENTAERYTHRITOL SPIROBIS(METHYLPHOSPHONATE), operates through a distinct mechanism. Unlike conventional flame retardants that form a protective char layer to inhibit flame propagation, PCO 900 is non-intumescent and does not induce charring as demonstrated in [280]. Instead, its behavior involves degradation

into specific volatile compounds at elevated temperatures. This process does not involve the creation of a char layer but rather alters the adhesive matrix differently. Its specific impact on adhesive properties under thermal stress is explored and discussed further in the results section. Building on this concept, this study investigates the performance of an epoxy adhesive system (DGEBA/DDS) modified with a phosphorus-based flame retardant, AFLAMMIT®PCO-900, referred to and used as as the debonding agent throughout this work. The assessment focuses on joint strength degradation due to thermal response and filler loading, aiming to identify the optimal heating time and debonding temperature ratio. Additionally, it examines the thermo-mechanical and functional properties of the modified adhesives and elucidates the reaction mechanism of the debonding agent within the epoxy matrix.

2.Materials and methods

See section materials and methods of the thesis.

2.1.Materials

2.1.1.Adhesive System

Low-viscosity epoxy resin Bisphenol A diglycidyl ether (D.E.R.332, commonly abbreviated as BADGE or DGEBA), was selected for this study. The curing agent used is 4-Aminophenyl Sulfone, a high-crosslinking aromatic hardener provided by Sigma-Aldrich (commonly abbreviated DDS). The mixing rule between the epoxy resin and the curing agent follows a stoichiometric ratio, calculated using the epoxide equivalent weight (EEW) of the resin and the amine hydrogen equivalent weight (AHEW) of the hardener. The EEW, provided by the supplier, is approximately 172175 g/eq for DGEBA, meaning 173.5 g of resin contains one mole of epoxy rings. Similarly, the AHEW of DDS is calculated as 248.30/4, resulting in a value of 62.075 g/eq. From these values, the stoichiometric ratio for the DGEBA/DDS system is determined to be 1:0.358 by weight.

2.1.2.Debonding Agent

The debonding agent selected for this study is the flame retardant pentaerythritol spiro-bis(methylphosphonate), commercially known as AFLAMMIT®PCO-900, supplied by THOR GmbH, Germany. The abbreviation "PCO" in the commercial name represents Organo-Phosphorus-based Compounds. It is a white powder and, according to the manufacturer data, the principal characteristics are phosphorus content of 24 wt.% and Particle size D95 = 30 ţm ţm and real density = 1,44 g/cmş.

3.Results

This section presents the outcomes of the experiments on the impact of debonding agent additives on adhesive joints. It explores the enhancement of joint strength, changes in debonding temperatures, and alterations in the physicochemical properties of the adhesive. Detailed tomographic analysis compares the internal structures of resins with and without debonding agent modification, both before and after debonding. Additionally, it examines the microscale dispersion of the debonding agent fillers within the adhesive matrix.

3.1.Mechanical study

The assessment of the influence of varying debonding agent loading rates on joint strength was conducted at room temperature, as depicted in the Figure 4.2. When the debonding agent, an organo-phosphorus flame retardant, was incorporated into epoxy resins, a notable increase in adhesive joint strength was observed compared to unmodified epoxy. This enhancement was particularly evident with a 20 wt.% concentration, where the strength saw an approximate 1.5-fold increase, rising from 7 to 10.7 MPa. When evaluating the quantitative impact of the debonding agent, it was found that REF-DDS formulations with 20 wt.%, 30 wt.%, and 40 wt.% consistently outperformed those with a 10 wt.% concentration and unmodified epoxy. However, 30 wt.% and 40 wt.% led to a slight decrease in joint strength compared to 20 wt.%, declining from 10.7 MPa to 9.2 MPa and 9.7 MPa, respectively.

This observed trend was attributed to several factors identified during the experimental

process. It was noted that as the concentration of flame retardants exceeded 30 %, there was a significant increase in the adhesive's viscosity, which could potentially compromise the quality of the joint.

An alternative explanation for the diminished joint strength could be attributed to the augmented concentration of aggregates when the load exceeds 30%, potentially precipitating early failure of the joint (see SEM observation in Section 3.4). The evaluation of joint strength in Figure 4.2 suggests that the optimum additive concentration for peak joint strength is around 20 wt.%. Furthermore, the addition of the debonding agent, which consists of stiff microparticles, to an epoxy matrix generally leads to a significant improvement in the composite elastic modulus, as observed for epoxy with APP fillers [263, 264]. Therefore, in this study, it is hypothesized that the introduction of the debonding agent into the epoxy joint increases its elastic modulus, which may reduce the modulus mismatch at the epoxy-aluminum interface. This could delay interface failure under normal stress conditions and potentially enhance joint strength. However, when the loading rate exceeds 30%, this reinforcing mechanism remains valid, but the formation of particle agglomerates might either lower the joint's elastic modulus due to porosities or act as defects that initiate joint failure. Both phenomena could lead to premature joint failure and could explain the slight decrease in joint strength.

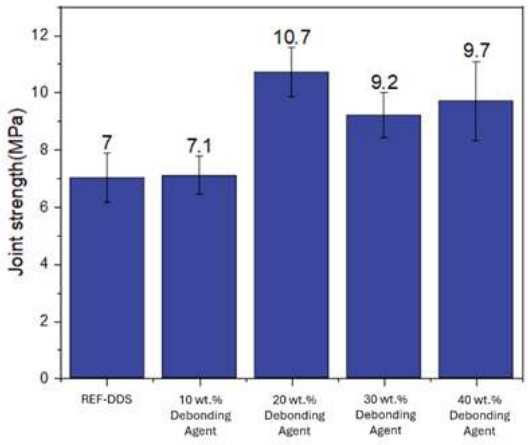

Figure 4.2: Comparison of joint strength in various resin formulations with different debonding agent loadings and REF-DDS

To investigate the thermal response of the debonding agent-modified formulations within the epoxy adhesive on the disassembly of the aluminum/epoxy/aluminum assembly, a debonding test was conducted using a pull-off method after heat treatment, as detailed in the experimental section. The outcomes of the debonding experiment are

graphically represented in Figure 4.3, comparing a reference formulation with the different debonding agent loading rates. The analysis focused on the adhesive composition with DDS hardener, and all formulations were heated progressively until the REF-DDS adhesive joints suffered from complete thermal degradation, leading to loss of joint strength. It was found that these reference joints preserved their mechanical properties until reaching a critical temperature of 400 °C, beyond which they began to drastically degrade.

In the temperature range from ambient to 25 °C above the curing temperature (175 °C), all modified adhesives and the reference exhibited consistent mechanical properties. In the span from 175 °C to 225 °C, the joint strength values for the modified formulations remained mostly unaffected by the rising temperature, albeit marginally lower than the reference. Excluding the reference joint, a significant decline in joint strength starting at 250 °C was observed across all joints. For instance, the joint strength dipped from 8.4 MPa at 225 °C to 4.7 MPa at 250 °C at 40 wt.% of the debonding agent. This downward trajectory persisted until a pronounced plunge was noted in all modified formulations at 300 °C. At this point, the joint strength for the filler fell below 1 MPa for 40 wt.% debonding agent and 1.1 MPa for 20 wt.% for 20, 30, and 40 wt. %, respectively. As such, we have assigned this temperature (300°C) as T°deb, calculated by extrapolating data points from 275 °C to 300 °C. Further observations showed that joint strength values for 10 wt.% of the debonding agent significantly decreased to approximately 3 MPa at 300°C and only plunged below 1 MPa at 325 °C. This strong tendency clearly demonstrates the debonding agent's capacity to undermine joint strength as a function of its loading rate.The inclusion of the debonding agent in the epoxy resin significantly lowered the debonding temperature. We observed that the filling rate affects the debonding temperature in a monotonous trend, with higher filling rates resulting in progressively lower debonding temperatures.

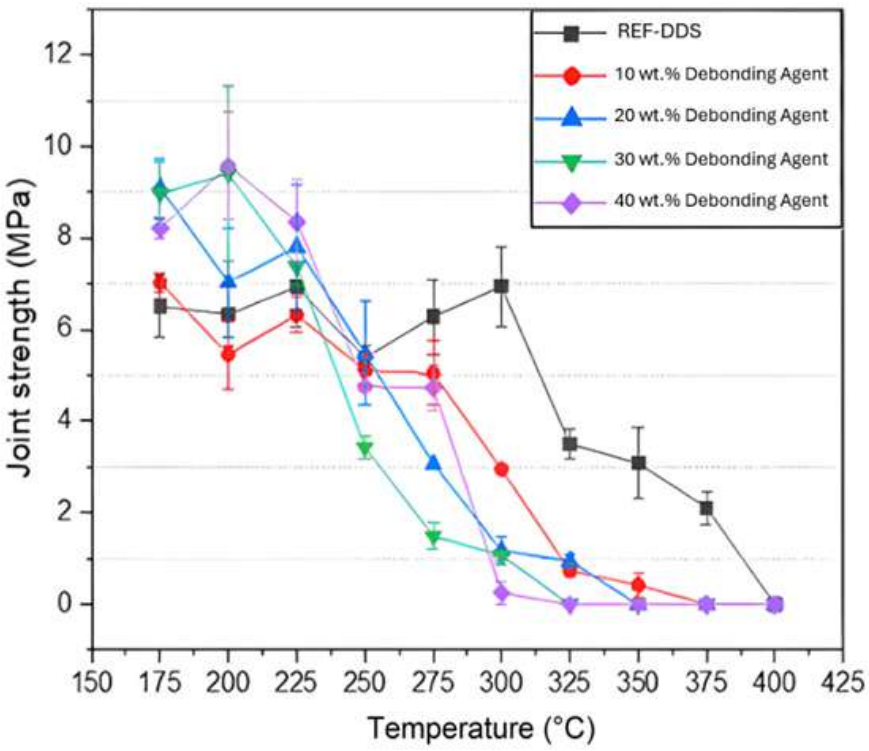

Figure 4.3: Joint strength as a function of temperature for different debonding agent loadings with a fixed heating time of 10 minutes

The following Figure 4.4 presents the outcomes of the debonding experiment conducted over varied time intervals, comparing the reference formulation (REF-DDS) with different debonding agent loading rates. The adhesive composition was subjected to heating durations ranging from 5 to 25 minutes at a constant temperature of 250 °C. This temperature was chosen as it marked the initial point at which a decrease in joint strength was observed for the modified adhesives during the debonding test. Throughout the entire experiment, the reference formulation maintained consistent joint strength. However, a gradual decline in joint strength was observed for the other formulations, intensifying with longer heating durations. At 250 °C and after 5 minutes of heating, the intumescent systems within the joints began partial activation, leading to a degradation of the adhesive joints to values lower than the joint strength observed at room temperature. For longer heating times, 10 minutes and above, strength is progressively and continuously decreasing for loading rates of 20% and above and reaches full debonding after 25 minutes. Strength is decreasing as well for joints with a 10 % loading rate, but it reaches a kind of plateau at 2.5 MPa and does not reach full debonding. For high loading rates, a comparison between 20 %, 30 %, and 40 % can be obtained by considering the time needed to reach a significantly low value of debonding, such as 1 MPa. This characteristic

time is 15 minutes for the 40 % loading rate, 20 minutes for the 30 % loading rate, and between 20 and 25 minutes for the 20 % loading rate. This shows that a higher debonding efficiency is obtained for high loading rates, i.e., 40 % here.

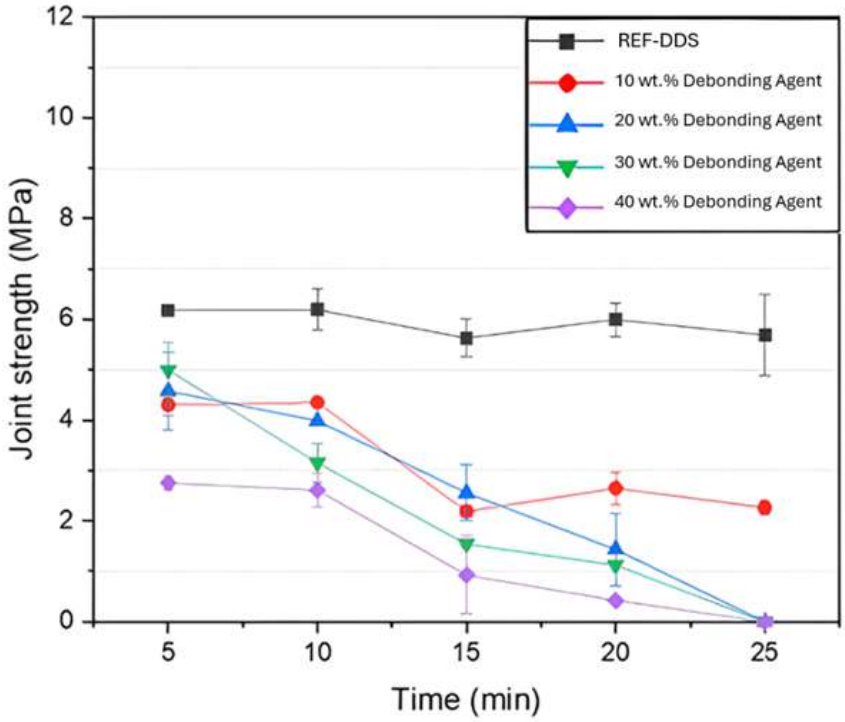

Figure 4.4: Joint strength over time at a fixed temperature of 250°C for different debonding agent loadings

Post the mechanical tests, a thorough examination of the failure modes was conducted, with focus on the effect of loading rate and the temperature exposure and identify the main trends. And while the REF-DDS samples only showed adhesive failures like the previous publication [277]. Two primary failure mechanisms were identified in our analysis of modified samples as shown in Figure 4.5. Prior to reaching the debonding temperature , the observed failure mode was cohesive failure. Beyond the debonding temperatures, two cases were identified. At low to medium loading rates, the primary failure mechanism was cohesive failure within the adhesive itself. However, at high loading rates, the predominant failure mechanism shifted to interface failure. Adhesives with high loading rates showed a tendency to detach from one or both adherend interfaces.

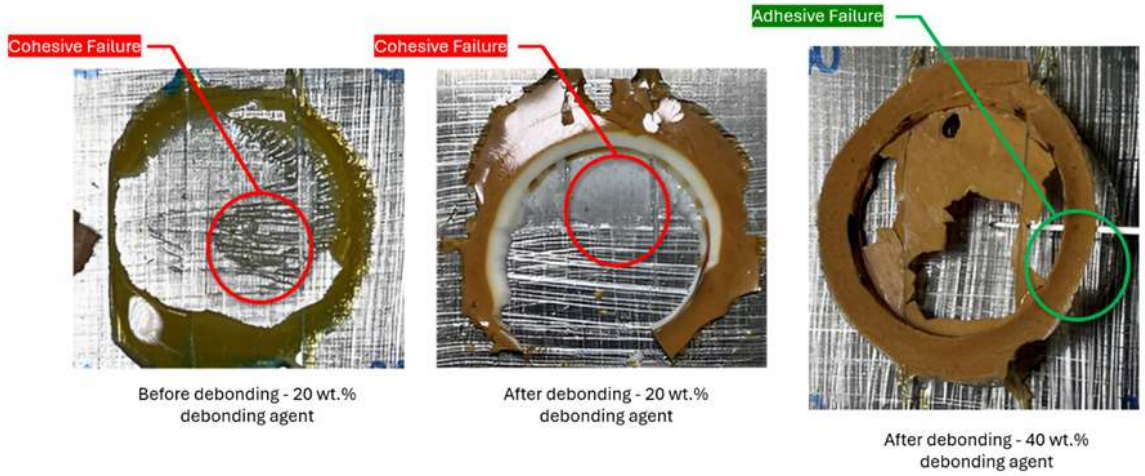

Figure 4.5: Photographic observations and comparison of failure modes in resin samples with debonding agent before and fillers before and after debonding

3.2.Influence of the additives on the physicochemical properties

3.2.1.Glass transition temperature

The glass transition temperature (Tg) for different loading rates is summarized in Figure 4.6. DSC analyses indicated that introducing the debonding agent at various mass fractions reduces the Tg of the epoxy resins. As the loading rate of the debonding agent increases, the Tg decreases, dropping from 206 °C at 0 wt.% to 161 °C at 40 wt.%. These results support the assertion that the debonding agent acts as a plasticizer within the resin matrix, thereby modifying the epoxy's physicochemical characteristics. The significant drop in Tg at high loading rates, 30 % and above, is likely attributed to the agglomeration of the additive particles.

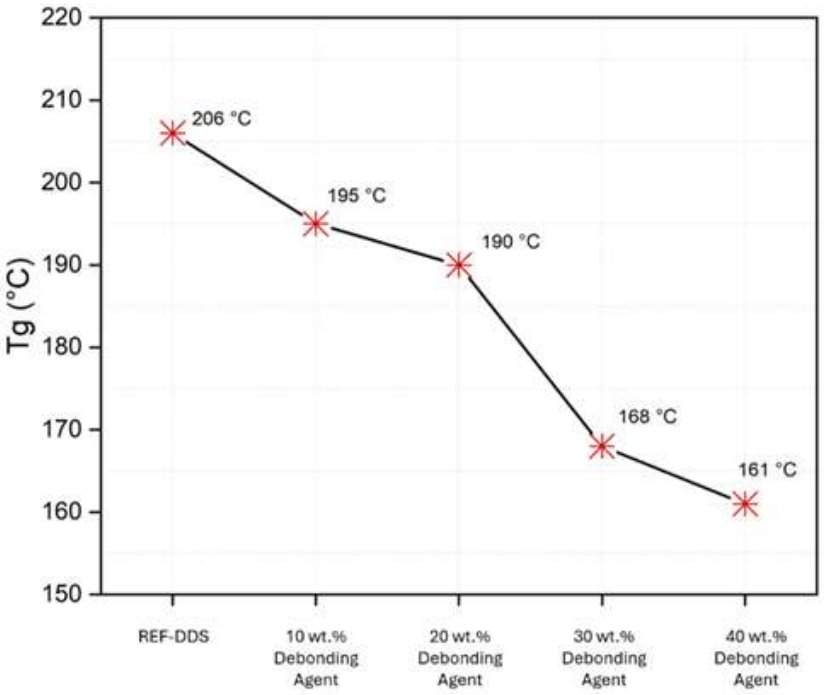

Figure 4.6: Temperatures of glass transitions of the different formulations at different loading rates

3.2.2.Thermal stability

Table 4.1: Characteristic degradation temperatures in TGA

Formulation	$\mathbf{T}_{\text{onset 5\%}}$ (°C)	$\mathbf{T}_{\text{max}}$ (°C)
REF-DDS	368	408
10 wt.% Debonding Agent	323	376
20 wt.% Debonding Agent	321	373
30 wt.% Debonding Agent	297	359
40 wt.% Debonding Agent	292	355

As depicted in the following Figure 4.7 and Table 4.1, the incorporation of the debonding agent into the resin precipitated a premature deterioration of the modified resin's thermal attributes. Notably, the mass loss for the modified resin commenced at a lower temperature relative to the reference resin. For instance, the onset of 5% mass loss ($T_{\text{onset5\%}}$) for the formulation with 30 wt.% occurs around 297 °C, while the reference formulation only registers a 5% mass loss at an elevated temperature of approximately 368 °C. The thermal degradation behaviour of the modified formulations, across different

loading rates, positions them intermediary between the reference and the powder. Specifically, the sequence of degradation commences with the powder, succeeded by modified adhesives in descending order of filler content. To illustrate, the $T_{\text{onset5\%}}$ values are as follows: 292 °C for 40 wt.%, 297 °C for 30 wt.%, 323 °C for 20 wt.%, and 321 °C for 10 wt.%. There is a discernible trend: the degradation rate of the adhesive accelerates with increasing the debonding agent content. Interestingly, this result is correlated with debonding results in which the temperature of debonding decreases when the filling rate increases.

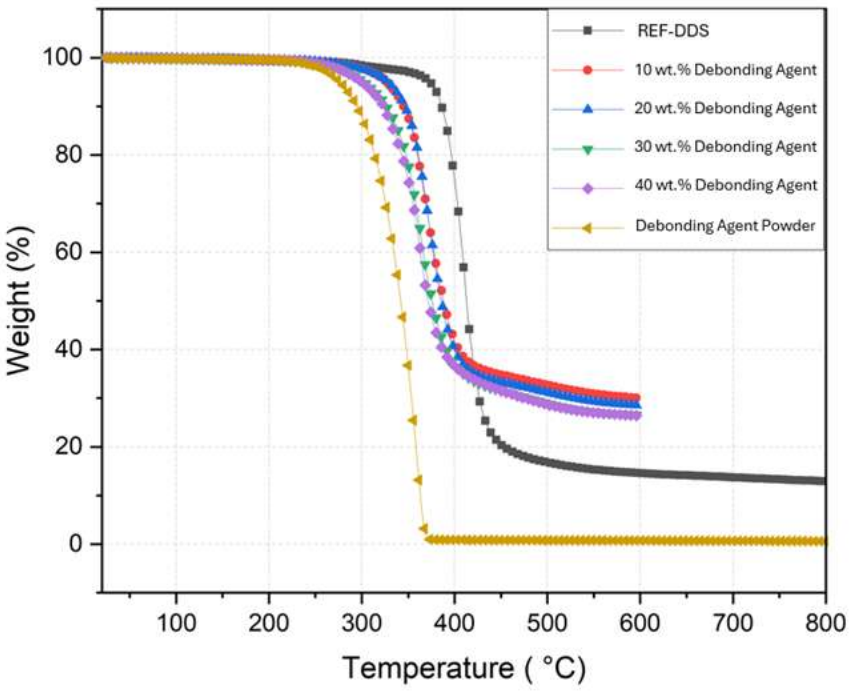

Figure 4.7: Thermal degradation profiles of REF-DDS and epoxy formulations with varying debonding agent loadings, including debonding agent Powder, under N atmosphere at a heating rate of 10 K/min

3.2.3.Dispersion and morphology

To study the dispersion characteristics of the additives in the epoxy resin matrix, resin samples were fabricated and polished as described in the experimental section. The next Figure 4.8 presents representative Scanning Electron Microscope (SEM) micrographs of the DGEBA/DDS adhesive system, incorporating 10 wt.% and 30 wt.% of the debonding agent to enable a comparative assessment of dispersion at low and high loading rates. The micrographs reveal that the debonding agent is homogeneously distributed within

the resin matrix. However, an observable tendency toward aggregation is noted at higher loading rates, which can be attributed to the increased filler content.

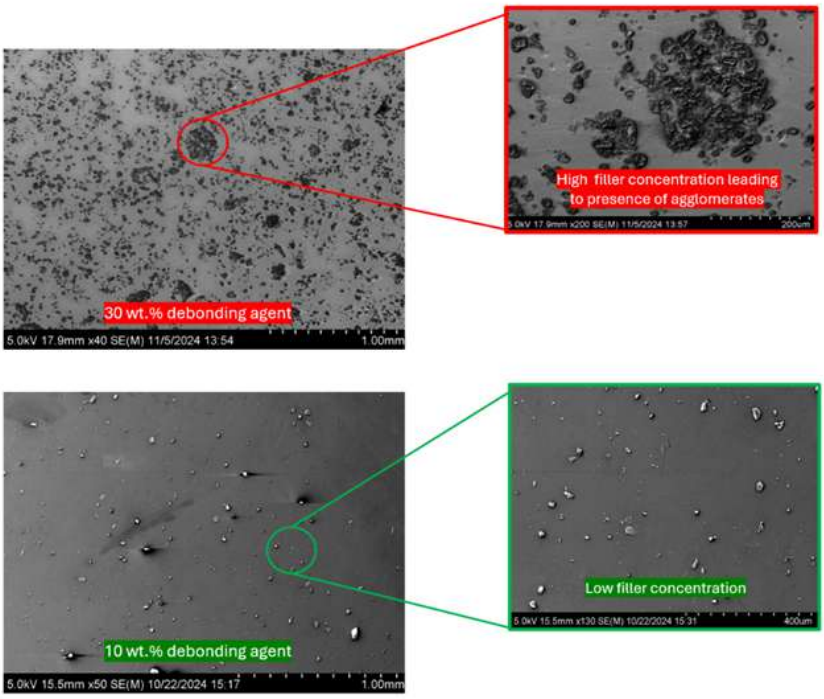

Figure 4.8: SEM micrographs showing dispersion of the debonding agent in epoxy resin at 10 wt.% and 30 wt.% loading rates.

3.3.Mechanism Study

The mechanism study will delve into the debonding process in detail and will be divided into two sections. The first section focuses on the physical mechanism of debonding, observed through micro-CT analysis. The second section examines the chemical mechanism to investigate the specific changes occurring within the adhesive layer or the modified resin containing the debonding agent at T°deb = 250°C. To achieve this, a combination of techniques was employed. First, the gas phase was studied using slow-rate dynamic TGA at 1 K/min in an N environment to better separate the degradation steps of the resin, debonding agent powder, and their combination. Subsequently, the gases extracted at 250 °C were analyzed by FTIR to identify the reaction mode of the debonding agent within the resin in the gas phase. Additionally, solid-state NMR was used to analyze the condensed phase at both room temperature and after the heating step at T °deb.

All the reactions and phenomena identified in this study are summarized in the Figure

4.19.

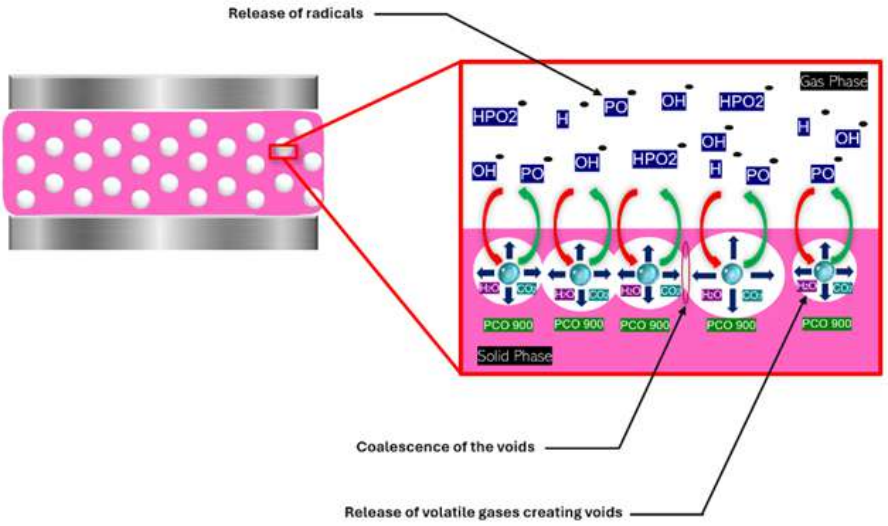

Figure 4.9: Schematic representation of the Debonding Mechanism of the Modified Resin Containing the Debonding Agent, Highlighting Gas and Solid Phase Interactions

3.3.1.Physical debonding Mechanism

In the experimental section, tomographic analysis was conducted on resin samples at room temperature (RT) and after exposure to a debonding temperature (T°deb) of 250 °C for 15 minutes. The analysis compared two different cuts: one at a 20 wt.% filling rate where fillers are homogeneously distributed, and another at a high loading rate (>40 wt.%) where agglomerates formed. This comparison aimed to better visualize and intensify the effect of heat on the adhesives, particularly the formation of voids. The images presented in Figure 4.10 (a) and (b) indicate the presence of initial voids in the resin due to the manufacturing process.

After heating at 250 °C, the emergence of micropores throughout the resin matrix was noted. Comparative analysis of the 2D, 3D renders in Figure 4.10 (c) and (d) revealed that micropores appear predominantly at the locations of the resin's fillers. Both samples from figure 3.17 (a) and (b) exhibited a void formation, of values of 3.16 %, and 0.46 % of the total volume, for 40 % and 20 % loading rates, respectively. In contrast, the regions without fillers, which can be compared to the non-modified resin, exhibit no presence of micropores after heating. This observed micropores are identified as a primary factor contributing to the debonding phenomenon. It is also noteworthy to mention that there were smaller micropores that fall under the detection limit of 4 m of the apparatus, which were not quantified in these respective percentages.

Furthermore, Figure 4.10 (c) illustrates the formation of a small internal crack within the matrix structure through the coalescence of the micropores. It is posited that these cracks consequently impair the mechanical integrity of the resin. In the context of an adhesive joint, the presence of these micropores, and their subsequent coalescence, leads to mechanical degradation and the ensuing debonding phenomenon.

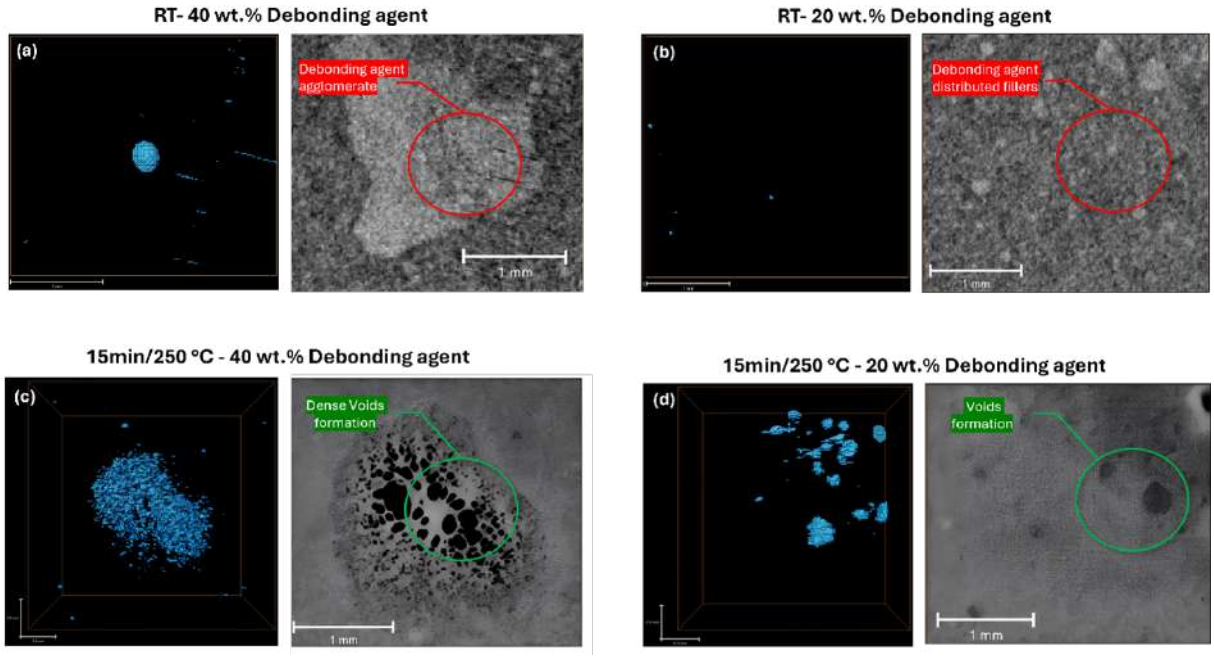

Figure 4.10: Micro-CT analysis of resin sample cuts with 20 wt.% ,40 wt.% of debonding agent at room temperature and after 15 minutes of heating at 250°C.

3.3.2.Chemical debonding mechanism

3.3.2.1 The gas phase

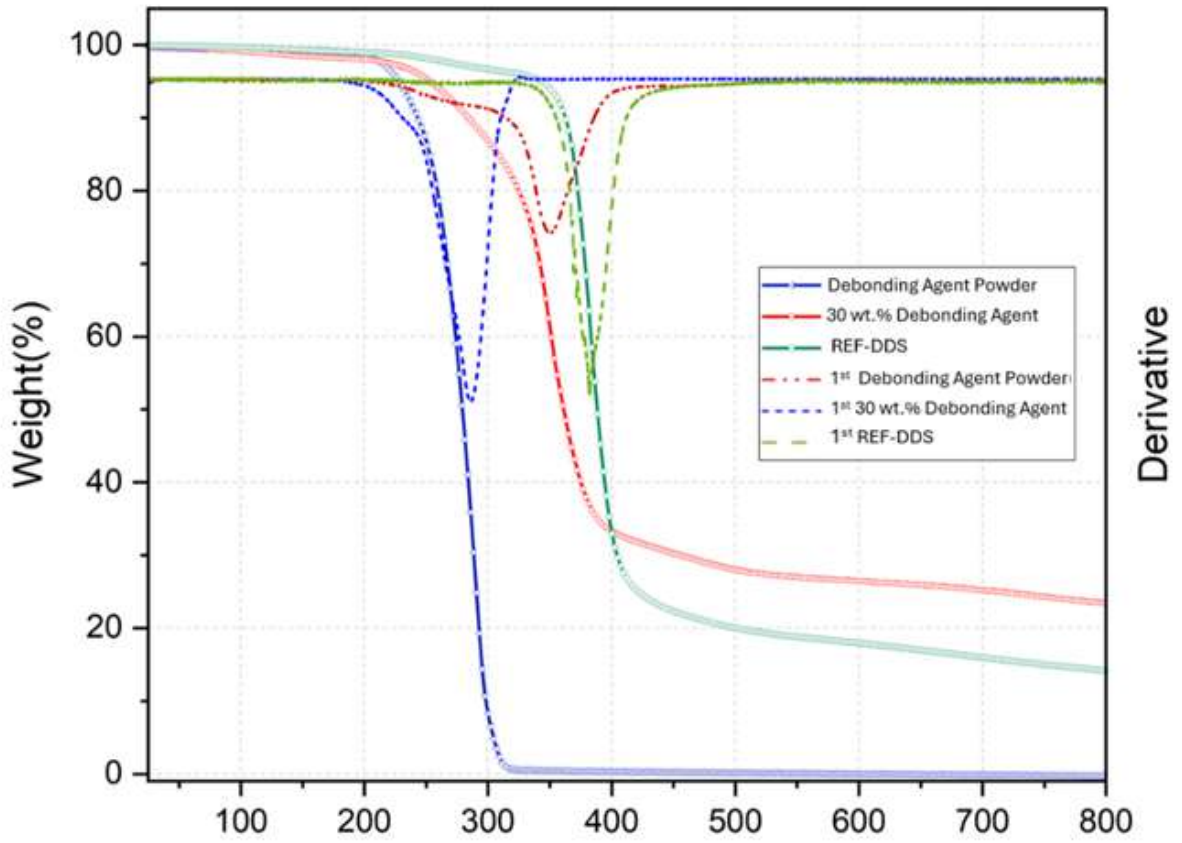

Figure 4.11: TGA and derivative analysis of debonding agent powder, 30 wt.% debonding agents in resin, and REF-DDS under nitrogen atmosphere with a heating rate of 1 K/min.

Figure 4.11 presents the TGA graph, offering insight into the thermal degradation behavior of the debonding agent powder, unmodified resin, and the combination of 30 wt.% debonding agent powder and resin under a heating rate of 1 K/min in a nitrogen (N) atmosphere. The debonding agent powder starts to degrade around 200 °C, with a significant peak in the derivative curve near 300 °C, and completes its decomposition by 400°C. The resin alone begins to degrade around 350 °C, with its main degradation phase peaking at 400 °C and continuing until about 500 °C. For the combination of 30 wt.% debonding agent powder and resin, a two-step degradation process is observed: the first peak in the derivative curve around 300 °C corresponds to the debonding agent degradation, while the second peak around 400 °C aligns with the resin's degradation temperature. This two-step pattern suggests that the debonding agent degrades independently within the resin matrix, with no visible interaction between the two, although the addition of the debonding agent appears to have a catalytic effect on the degradation behavior of the resin.

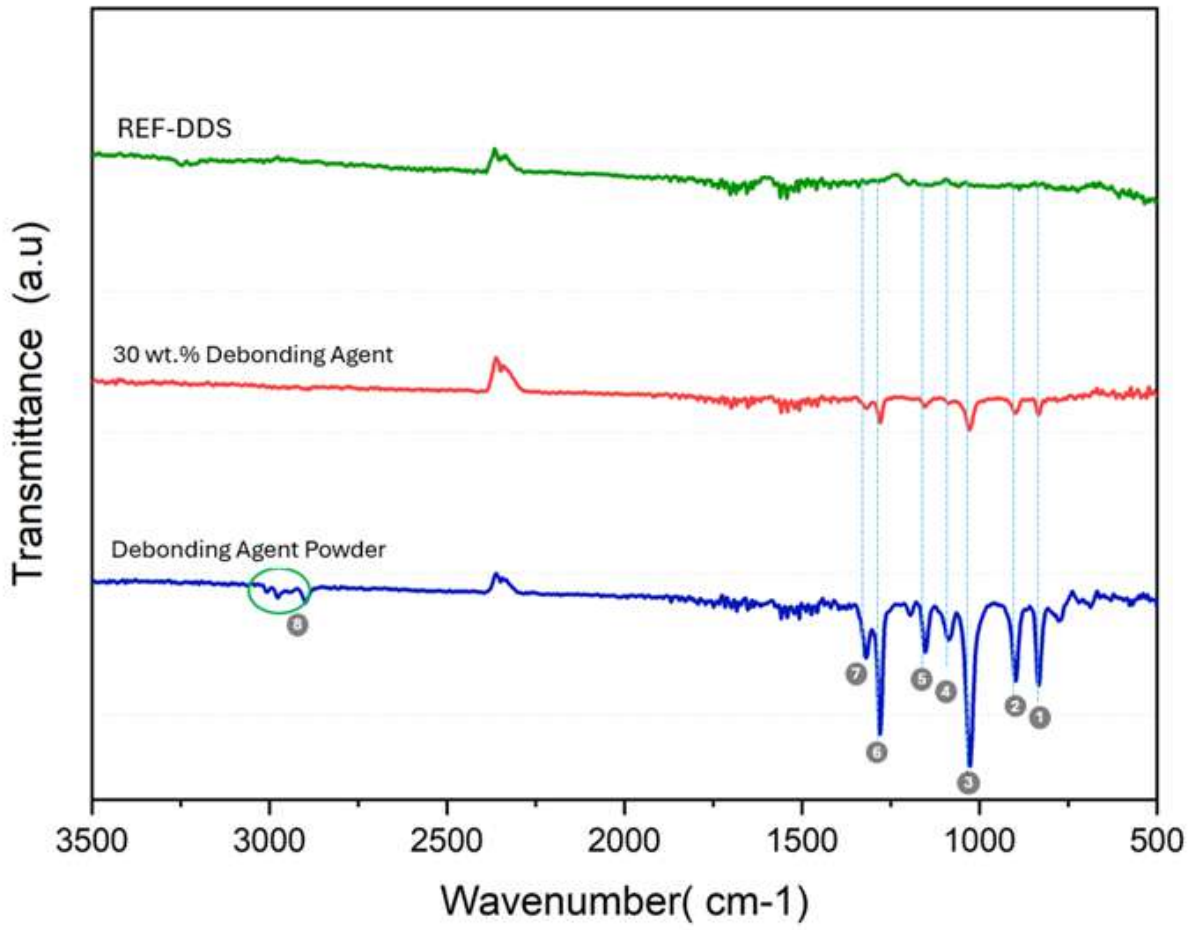

Figure 4.12: FTIR analysis of released gases from REF-DDS, 30 wt.% debonding agent, and debonding agent Powder at T°deb = 250°C.

Figure 4.12 and the Table 4.2 present the results of a TGA-coupled FTIR experiment, showing FTIR spectra extracted at 250°C (T°deb), the debonding temperature of our system, along with a summary of all identified peaks. This provides a detailed comparison of the reference resin REF-DDS, resin combined with 30 wt.% debonding agent, and debonding agent powder. The spectrum of the resin alone shows minimal features, with the only significant peak corresponding to CO absorbance, indicating that the resin remains largely stable and does not release volatile compounds at this temperature.

In contrast, the spectrum of the resin combined with 30 wt.% debonding agent exhibits several peaks that, while less pronounced and broader than those in the debonding agent powder spectrum, clearly indicate the presence and degradation of the debonding agent within the resin matrix. Importantly, the combined spectrum does not show any new peaks, signifying that the interaction between the resin and the debonding agent likely does not result in the formation of new chemical entities, even at T°deb = 250°C. Notably,

these peaks correspond to those in the debonding agent powder spectrum, which serves as a reference with sharp and well-defined peaks.

The identified peaks include P-C stretching at 795 cm^{-1}, multiple P-O-C stretching bands at 1045, 1087, and 1150 cm^{-1}, and P=O stretching bands at 1275 and 1320 cm^{-1} [281, 282] for peaks present in both spectra, and the -CH- stretch at 2983 cm^{-1} [282], observed only in the debonding agent powder spectrum.

Table 4.2: Summary of wavenumbers of different identified peaks

Number	**Wavenumber (cm^{-1})**	**Peak Identification**
1	795	P-C stretching band
2	839	P-O-C symmetrical stretching
3	1045	P-O-C stretching band
4	1087	P-O-C stretching band
5	1150	P-O-C stretching band
6	1275	P=O band stretch
7	1320	P=O stretching band
8	2983	$-CH_2$

3.3.2.2 Solid phase

Figure 4.13 summarizes all the NMR results, providing detailed insights into the thermal stability and molecular dynamics of the studied materials. Figure 4.13 (a) presents the Carbon-13 NMR spectra of REF-DDS (DGEBA-DDS) at room temperature and 250°C. At room temperature, the peaks are sharp and well-defined, indicating distinct chemical environments for the carbon atoms in the DGEBA-DDS structure. The peaks labelled 1 to 10 correspond to specific aromatic and aliphatic carbons, with chemical shifts ranging from approximately 0 to 200 ppm. The peaks in the aromatic region (100-160 ppm) and the aliphatic region (20-80 ppm) show the typical chemical environments of REF-DDS [283]. As the temperature increases to 250°C, the peaks broaden, reflecting increased molecular motion and potential changes in the chemical environment. However, the relative positions of the peaks remain similar, suggesting that the fundamental structure of REF-DDS remains intact. The presence of side bands in both spectra, which are artifacts of the solid-state NMR technique, further supports the stability of the chemical structure under elevated temperatures. This broadening of peaks at higher temperatures

indicates increased molecular mobility.

Figure 4.13 (b) illustrates the 31 Phosphorus NMR spectra, revealing significant insights into the behavior of the debonding agent powder when mixed with resin at room temperature (RT) and at 250°C. The characteristic peaks of the debonding agent, particularly the peak labelled 1, are sharp and well-defined in the debonding agent powder spectrum and in the spectrum of powder + resin at RT. The chemical shift for the phosphorus peak of the debonding agent is around 20 ppm. However, at 250°C, the peaks corresponding to the phosphorus environment in the debonding agent are almost completely absent.

Figure 4.13 (c) shows the Carbon-13 NMR spectra for the debonding agent powder, both alone and when mixed with resin (DGEBA-DDS) at room temperature (RT) and at 250°C, providing critical insights into the chemical environments and interactions. The characteristic peaks of the debonding agent powder are observed at chemical shifts around 19 ppm (peak 1), 21 ppm (peak 2), and 23 ppm (peak 3). When the debonding agent powder is mixed with resin at RT, these peaks are still present at the same chemical shifts. At 250°C, the peaks corresponding to the debonding agent at 19, 21, and 23 ppm disappear almost completely, indicating substantial changes or degradation of the debonding agent within the resin matrix at elevated temperatures. In contrast, the resin's peaks remain prominent and well-defined under both conditions, demonstrating its chemical stability.

In conclusion, the combined NMR analyses (Carbon-13 and 31 Phosphorus) clearly indicate that the debonding agent powder degrades independently within the resin matrix. The chemical shifts of the debonding agent peaks, which are distinct in the pure powder form, diminish or disappear when mixed with the resin, especially at elevated temperatures, indicating significant changes in the chemical environment. Moreover, no new peaks are detected in either the phosphorus or carbon spectra after exposure to heat, demonstrating that no new chemical species are formed during the degradation process.

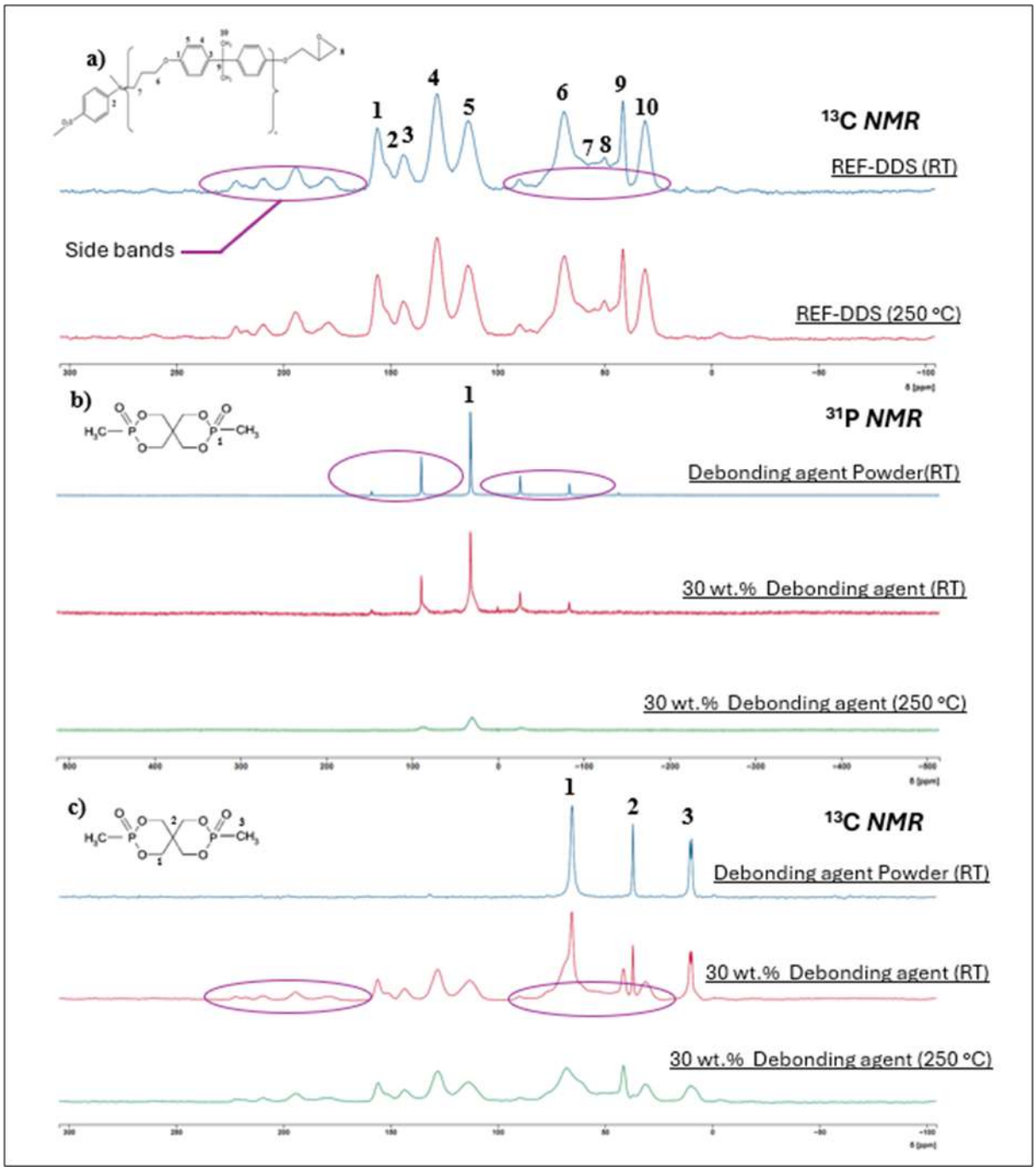

Figure 4.13: Solid-state NMR Analysis: Carbon-13 NMR of PCO powder and 30 wt.% resin at room temperature and 250°C, compared with reference DDS at room temperature and 250°C, and phosphorus-31 NMR of PCO powder and 30 wt.% PCO 900 at room temperature and 250°C

4.Discussion

Previous research conducted by the authors demonstrated that the incorporation of conventional flame retardants into structural adhesives led to a reduction in debonding temperatures, thereby validating their effectiveness as a debonding technology [277]. Building on this foundation, the current study explores a different category of flame retardants, specifically organo-phosphorus flame retardants. The debonding agent, known for its non-intumescent properties, has shown promise as an effective technology. This paper delves into the various parameters involved in the utilization of this flame retardant, aiming to broaden its applicability and, in particular, to further decrease the debonding temperatures.

To the authors best knowledge, this study represents the first comprehensive investigation into how the addition of the debonding agent to an adhesive can enhance the debonding process of the adhesive joint. Consequently, a patent application detailing this novel approach has been filed. The methodology employed for determining the debonding temperature adheres to the same approach as that used in previous studies involving flame retardants as a debonding technology, reflecting the characteristic modification of the adhesive. This consistency facilitates a direct comparison of the impacts on debonding temperature resulting from the incorporation of various flame-retardant additives at differing loading rates. An additional methodology was introduced to assess the activation time required for the flame retardants within the matrix.

Examination of SEM images following the incorporation of the debonding agent reveals that the particles are relatively large post-incorporation into the epoxy, with a notable increase in agglomeration at higher loading rates. This agglomeration diminishes the contact area between the debonding agent and the epoxy matrix. However, the formation of these agglomerates does not impede the debonding process; in fact, a higher loading rate appears to enhance the debonding effectiveness.

Furthermore, it is important to highlight that the incorporation of flame retardants has impacted the physicochemical characteristics of the adhesives. Specifically, the glass transition temperature (Tg) of the modified resins decreases with increasing debonding agent loading rate, reaching values as low as 161 °C compared to the 206 °C of the reference. However, this alteration is considered acceptable as the joint strength remains enhanced, and the fillers, even at high loading rates, do not compromise the processability

of the modified adhesives. Additionally, the curing cycle adapted for these resins remains effective and applicable.

It can be reasonably deduced from the joint strength and debonding tests that the optimal debonding agent loading rate falls within the range of 20-30 wt.%. While this value is specifically applicable to the REF-DDS system and other similar thermoset systems, slight variations may occur depending on factors such as the viscosity of the resin, the type of hardener used, and the rigidity of the crosslinked network post-curing. Furthermore, the debonding test incorporating a time gradient suggests that to achieve debonding at a temperature as low as 250 °C, the samples should be exposed to this temperature for a minimum duration of 15 minutes.

Thermogravimetric analysis conducted on varying loading rates of the debonding agent, ranging from 0 to 40 wt.%, revealed that higher filling rates bring the degradation profile of the resin closer to that of the pure powder. This observation, when coupled with tomographic data showing that micropores appear precisely at the filler locations, supports the conclusion that the debonding agent reacts independently without interacting with the resin matrix. Unlike traditional flame retardants, the debonding agent does not engage with the resin to form a carbonous layer.

The physical reaction mechanism of the debonding agent within the resin is intrinsically linked to the chemical degradation of the filler. Remarkably, the debonding agent does not require an external carbon source to facilitate debonding in the condensed phase. This behavior is elucidated by slow-rate TGA analysis and its derivatives, which reveal a distinct two-step degradation process when the resin is mixed with 30 wt.% of the filler. Each degradation step coincides with the degradation temperatures of the individual components, indicating that the debonding agent powder degrades independently within the resin matrix. Upon activation, the debonding agent begins to chemically degrade, releasing volatile compounds as gases, as detected by TGA-FTIR analysis. This analysis identifies the presence of P=O, P-O-C, and P-C bands, suggesting the formation of reactive radicals such as PO·, OH·, H·, HPO_2· [282–285]. These radicals act as chemical scavengers, interacting with the filler in the solid phase and participating in reactions that release gases, including water vapor, carbon dioxide, and other non-halogenated compounds. NMR analysis further supports this mechanism by confirming that no new compounds form in the solid phase of the debonding agent and that the REF-DDS resin retains its structural integrity at 250°C. This indicates that the radicals

predominantly interact with the fillers, leading to an auto-degradation reaction within the solid phase. The transformation of the debonding agent into reactive species results in the formation of micropores and voids within the resin matrix. The pressure generated by the release of gases causes these micropores and voids to expand and coalesce, leading to crack formation. These cracks weaken the joint strength, ultimately resulting in debonding.

The debonding temperature observed in the current study is 250°C following the modification of the adhesive. While this temperature is somewhat elevated, it remains in a range that is comparable to the typical debonding temperatures of epoxy adhesives loaded with thermally expandable particles [285] or expandable graphite [261], which are around 140°C and 235°C, respectively. A significant advantage of this technology lies in its compatibility with extended curing cycles that involve high temperatures for curing and prolonged exposure to heat, a feature not shared by other technologies. This compatibility is particularly relevant for high-performance systems such as DGEBA/DDS. To further reduce the debonding temperature, exploring the combination of multiple flame-retardant additives might be beneficial. It is hoped that such a combination could lead to a synergistic effect, enhancing the debonding characteristics [285].

Finally, the scope of the current study, initially focused on aluminum-epoxy-aluminum joints, is expected to broaden. Broadly speaking, the integration of functional additives into epoxy adhesives for achieving debonding-on-demand could be initially applied to facilitate the debonding of fiber-reinforced polymer (FRP) composites, particularly those with an epoxy thermoset matrix. Furthermore, this approach holds potential for more advanced applications, such as the separation of reinforcement fibers from the matrix in FRPs, thereby enabling the recycling of high-value fibers.

5.Conclusion

In this study, the innovative application of non-intumescent organophosphorus flame-retardant systems, specifically AFLAMMIT®PCO-900 (the debonding agent), for debonding purposes in epoxy adhesives is thoroughly investigated. Unlike traditional intumescent flame retardants, the debonding agent demonstrates a unique mechanism by forming micropores in the resin matrix, leading to a significant reduction in the debonding temperature, a desirable characteristic in adhesive technology. The research reveals that

the debonding agent fillers do not interact with the resin matrix to form a carbonaceous layer, as is typical with classic flame retardants. Instead, they independently react, causing chemical degradation and gas release that contribute to the debonding process. The study successfully identifies an optimal debonding agent loading rate and highlights the potential of these fillers in enhancing the debonding capability of epoxy adhesives, providing a promising use for sustainable recycling and advanced manufacturing practices. Additionally, we are currently applying this technology to carbon fiber-reinforced composites, showing promising results with similar trends in improving mechanical and debonding properties. This further expands its potential impact in the field of material engineering and sustainable materials.

Acknowledgements

We kindly acknowledge the support of the Luxembourg National Research Fund (FNR C20/MS/14707266).

Data availability statement

The raw/processed data required to reproduce these findings cannot be shared at this time as the data also forms part of an ongoing study.

5

Use of different structures of expandable graphite for controllable debonding temperature

Chapter 5 :

Use of different structures of expandable graphite for controllable debonding temperature

This study investigates the use of thermally responsive additives to enable controlled debonding in adhesive joints, a critical step toward enhancing the sustainability and recyclability of adhesively bonded systems. Previous research demonstrated that the integration of intumescent flame retardants can significantly reduce the debonding temperature by modifying the thermomechanical properties of adhesive joints at temperatures well below the degradation onset of the unmodified adhesive system. Among these additives, expandable graphite (EG) has shown promise as a thermally responsive material. When incorporated into adhesive layers, even in small amounts, EG undergoes significant expansion upon heating, providing an effective mechanism for disassembling adhesively bonded structures.

Building upon these findings, the present work aims to investigate the influence of manufacturing processes on the thermal response of EG. The central hypothesis is that tailoring the production parameters of EG can modulate its behavior, enabling debonding to occur at targeted temperature ranges, thus broadening its potential applications.

To explore this hypothesis, the study employs a systematic experimental approach. The initial mechanical properties and thermomechanical degradation of EG-modified adhesive systems at low loading rates are assessed using a modified pull-off test, designed to ensure repeatability and accuracy. Microstructural changes in the resin, both before and after exposure to the debonding temperature, are analyzed using tomography techniques, while X-ray Diffraction (XRD) provides insights into the structural transformations associated with the thermal activation of EG.

Thermal degradation and thermomechanical properties are further examined using Thermogravimetric Analysis (TGA) and Dynamic Mechanical Analysis (DMA). These analyses are complemented by Scanning Electron Microscopy (SEM), which evaluates the

dispersion of EG particles within the epoxy matrix and their influence on the joint microstructure. Together, these techniques provide a detailed understanding of the interactions between the adhesive and the thermally responsive filler, elucidating the mechanisms underpinning the debonding process.

Finally, the study demonstrates the practical feasibility of the debonding technology through the reuse of substrates after debonding, facilitated by a simple cleaning procedure. This research not only advances the understanding of EG as a thermally responsive additive but also highlights its potential to enable efficient, controlled debonding, contributing to the development of recyclable and sustainable adhesive systems.

Use of different structures of expandable graphite for controllable debonding temperature

Oussema Kachouri, Julien Bardon, David Ruch, and Abdelghani Laachachi

Luxembourg Institute of Science and Technology (LIST), Department of Materials Research and Technology (MRT), Bommelscheuer

5, ZAE Robert Steichen, L-4940 Hautcharage, Luxembourg.

Abstract

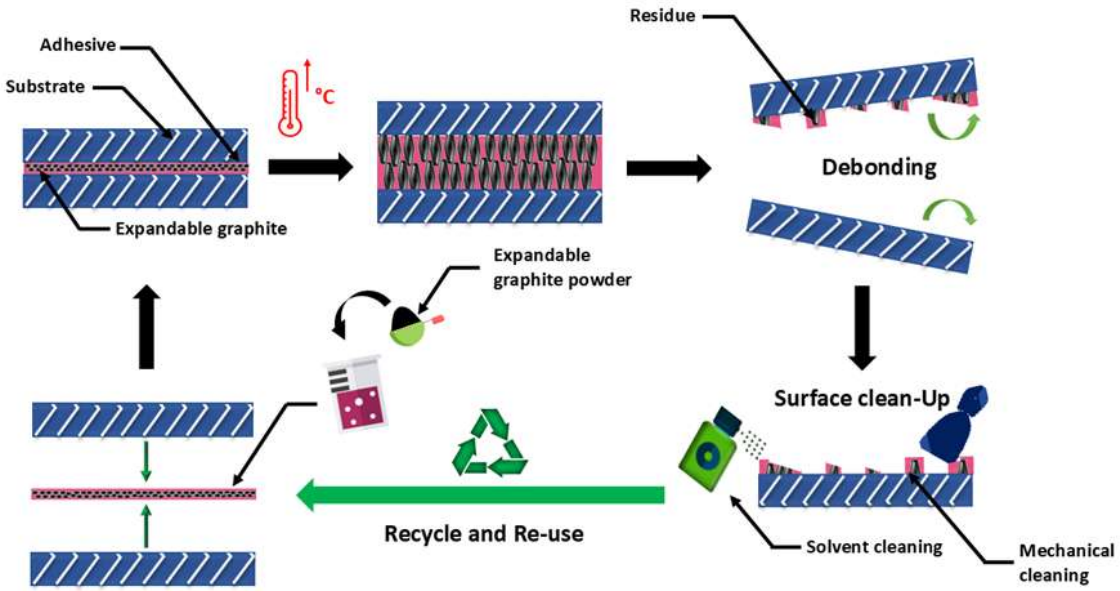

Figure 5.1: Thermally Assisted Debonding and Recycling Process Using Expandable Graphite

The emergence of debonding technologies has enabled adhesive systems to better align with the principles of sustainability and the circular economy by addressing the gap between the end-of-life stage of adhesively bonded products and the potential for component reuse. In this context, the present study explores the application of thermally responsive additives to induce controlled debonding in adhesive joints. In our previous

investigations, it was shown that integrating various types of flame retardants (intumescent and non-intumescent) significantly reduced the debonding temperature, by altering the thermomechanical properties of the joint at temperatures substantially lower than the degradation onset of the unmodified adhesive system. Expandable graphite (EG), a thermally responsive material, has previously been employed with success for similar purposes. Its incorporation into the adhesive layer, even in trace amounts, results in a very significant expansion upon the application of heat, thereby providing an effective mechanism for disassembling adhesively bonded structural assemblies. The present study builds on this prior research and probes deeper into the manufacturing processes underlying EG. The primary hypothesis explored is whether tailoring these processes can result in modulating the thermal response of adhesives modified by EG, thereby achieving debonding at distinct temperature ranges suitable for a wide spectrum of applications. This study investigates EG-modified adhesives, assessing their mechanical properties, thermomechanical degradation, and microstructural changes using characterization techniques such as pull-off tests, microtomography, TGA, and DMA. Finally, the recycling potential is demonstrated through the successful reuse of debonded substrates after a simple cleaning process.

1.Introduction

The development of a universal debonding method, suitable for various types of substrates and adaptable to different variables inherent in the manufacturing process of adhesive joints (such as curing cycles and adhesive degradation temperatures), is highly desirable. This kind of adhesive system addresses the imperative of material recycling in several significant ways. It enables the recycling of valuable materials at the end of the product's lifecycle, as well as facilitates repair and upgrade while the assembly is still in service [152, 286]. In order to qualify as a universal solution, a debond-on-demand adhesive must not interfere with the two critical steps involved in adhesive joint life cycle: the processing and the life in service. Additionally, the debonding step should be quick, reliable, and ensure that no unintended debonding occurs [287]. Given these criteria, the incorporation of functional additives emerges as the most appealing solution, especially for structural bonding applications [143]. In most instances, these additives facilitate the mechanical deterioration of the adhesive layer through expansion and the release of gases when subjected to a heat stimulus [141].

Numerous debonding strategies have been explored thus far, including the addition of foaming agents, thermally expandable particles (TEPs) [288,289] or electrically responsive agents [151,254], which have demonstrated efficacy as debonding solutions. However, they fall short in aspiring to be a universal solution. For example, some commercial TEPs can expand during the curing cycles of high-performance structural adhesives, with expansion occurring at temperatures as low as 60 °C. Additionally, most of these technologies are designed to operate at a single, specified debonding temperature, which limits their versatility. In our previous work, our research team ventured to address this limitation by integrating intumescent flame retardants into the adhesive formulation. Through the modification of the adhesive by incorporation of melamine polyphosphate, ammonium polyphosphate, and organophosphorus flame retardants in an epoxy adhesive, we successfully developed debonding solutions for a broader temperature window, ranging from 325 °C to as low as 250 °C [277].

Recently, a new contender with substantial expansion and charring capacity has emerged in the flame-retardant industry: expandable graphite [290]. Expandable graphite, also known as exfoliated graphite, is derived from the naturally occurring mineral [291], graphite. The unique layered structure of graphite facilitates the intercalation of molecules between its layers [292]. The term "intercalation" denotes the process of inserting an intercalant material between the graphene layers of a graphite crystal or particle, a characteristic feature of expandable graphite. These molecules are intercalated, or inserted, between its layers, often aided using chemicals such as acids, like sulfuric acid. When subjected to heat, the intercalated compounds within the graphite layers start to decompose and to release gas. This gas release generates a significant force that drives the graphite layers apart, resulting in the expansion of the material [293]. Moreover, the thermal energy from heating further boosts the expansion by inducing the exfoliation of the graphite, essentially a rapid separation of the graphite layers. This phenomenon leads to a notable increase in volume, transforming the graphite into a worm-like or vermicular structure [294]. Due to its distinctive properties, notably its chemical inertness, expandable graphite is finding a wide range of applications. It is nowadays utilized as a flame retardant, wherein upon exposure to heat, it forms an insulation layer similar to an intumescent layer that significantly slows down the spread of fire and mitigates the emission of toxic gases and smoke [292]. Moreover, its porous structure proves beneficial in environmental applications, aiding in wastewater purification and the absorption of chemical solvents and oils [294]. Thermally Expanded Graphite (TEG), a derivative of

expandable graphite, is proving to be pivotal in energy storage and sensor technologies. It is employed in crafting composite materials, in conjunction with various conducting polymers and metal chlorides, for a range of applications including hydrogen storage, thermal energy storage, fuel cells, batteries, supercapacitors, and sensors [293]. Also, expandable graphite has been effectively utilized as a debonding solution when incorporated in a thermoset adhesive, achieving a debonding temperature of 235 °C as elucidated in the work N. Pausan et al. Although this investigation presents a noteworthy endeavor, it didnt explore the versatility of expandable graphite as a universal debonding solution [261,290]. In fact, by tuning the preparation methodology of expandable graphite, the onset expanding temperature can be marginally altered. For instance, the employment of strong oxidizing agents such as perchloric acid or potassium permanganate could facilitate superior intercalation, potentially leading to a lower onset temperature. Moreover, adjusting the ratios of chemicals used in the intercalation process can also influence the onset temperature. For instance, a specific ratio of graphite to hydrogen peroxide, perchloric acid, potassium permanganate, and acetic acid was demonstrated to yield an onset temperature of approximately 155 °C [290]. The particle size of expandable graphite also significantly impacts the onset temperature; larger particle sizes can reduce the surface area, consequently impeding the intercalation process and leading to higher onset temperatures for the powders [295–297]. This paper presents the incorporation of various expandable graphite fillers with different onset temperatures in an epoxy adhesive to achieve distinct debonding temperatures of an adhesive joint. The tailored solutions devised are capable of debonding at temperatures as low as 225°C, while also enduring the curing cycles of high-performance adhesives and facilitating debonding at multiple debonding temperatures extending up to 300 °C. Our examination will focus on the degradation of joint strength influenced by thermal response, optimizing various parameters to achieve the best mechanical properties and multiple debonding temperatures. Additionally, we will investigate the thermo-mechanical properties using TGA and DMA for different fillers, loading rates, and functional properties of the modified adhesives, elucidating the reaction mechanism within the epoxy matrix that induces debonding. Furthermore, X-Ray Diffraction (XRD) will be employed to analyse the structural changes in expandable graphite, offering insights into interlayer spacing, crystalline integrity, and the effects of thermal activation both within the resin matrix and in its powder state. An additional experiment has been included to showcase the full potential of the debonding technology in a view of materials recycling. This involves the re-use of the adherends and the examination of the substrate surface after debonding. The re-used adherends were incorporated into new

adhesive joints after a cleaning step, and their joint strength was tested. This comprehensive analysis aims to provide pertinent insights into the applicability of these expandable graphite fillers as a universal debonding solution for structural adhesives, in the field of structural bonding and the recycling of adhesive assemblies.

2.Materials and methods

See section materials and methods of the thesis.

2.1.Materials

2.1.1.Adhesives

Low viscosity epoxy resin Bisphenol A diglycidyl ether (D.E.R.332, commonly abbreviated as BADGE or DGEBA), was selected for this study. The hardener used is an aliphatic flexible hardener, Diethylenetriamine (abbreviated as DETA). All products were supplied by Sigma-Aldrich Germany.

2.1.2.Fillers

The selected flame retardant for this study comprises different forms of expandable graphites with various characteristics, supplied by ACS Materials, USA, and commercially referenced as CXG5B122, CXG00522, and CXG00622. It is a black flaky powder, and according to the manufacturer's data, the principal characteristics of these three forms of expandable graphite will be summarized in the following table. For the sake of ease, we will rename the fillers as EG and a number corresponding to their debonding temperature.

Technical details of the used fillers.

Reference	Assigned Name	Particle Size (ţm)	Purity (%)	Expansion Start Temperature (°C)	Expansion Volume (ml/g)
CXG5B122	EG225	300	≥95.0%	180°C	≥2250 ml/g
CXG00522	EG250	80	≥95%	250°C	≥180 ml/g
CXG00622	EG300	50	≥95%	300°C	≥170 ml/g

3.Results

This section details the experimental results on the effects of various EG filler additives on adhesive joints. It examines the improvements in joint strength, variations in debonding temperatures, and modifications in the adhesive's physicochemical properties.

3.1.Mechanical study

3.1.1.Joint strength

The assessment of joint strength focused on two main factors. The first factor compared different formulations, specifically examining the various forms of expandable graphite used in reference formulations with REF (0 wt.%) filler. The second factor considered the impact of increasing the filler rate on the joint strength of the samples. All results were expressed as joint strength fractions relative to the reference value, which was assigned a fraction of one allowing of comparison gain or loss in percentage of mechanical properties. As shown in the Figure 5.2 (a), all modified formulations containing expandable graphite fillers demonstrated a slight improvement in joint strength. For example, EG225 exhibited an increase of 12%. This increase was more pronounced in EG250, with a value of 33%, but decreased again in EG300 to only 6% increase. These findings confirm that at a 10 wt.% loading rate, expandable graphite positively influences joint strength. It is assumed that smaller EG fillers tend to yield higher joint strength values. For instance, EG250 particles, measuring 80 m, showed higher joint strength than EG225 particles, which were 300 m. The decrease in joint strength fraction for smaller fillers, such as EG300, can be attributed to filler aggregation, which may promote early failure during joint strength testing. The following Figure 5.2 (b) highlights the impact of increasing loading rates on joint strength fractions. Using EG225, the loading rate was increased up to 40 wt.%. A clear trend was observed: higher loading rates corresponded to lower joint strength fractions, decreasing from an optimal value of 112% at 10 wt.% to a low of 74% at 40 wt.%. This suggests that the optimal joint strength is achieved at a 10 wt.% loading rate and that higher rates may lead to weaker joint strength because of aggregation. As 10 wt.% is the minimum effective debonding rate, it is recommended for debonding tests. However, to gain a comprehensive understanding of the use of expandable graphite as a filler in the DEGBA/DETA system and comparable structural adhesive systems, all

loading rates will be further examined.

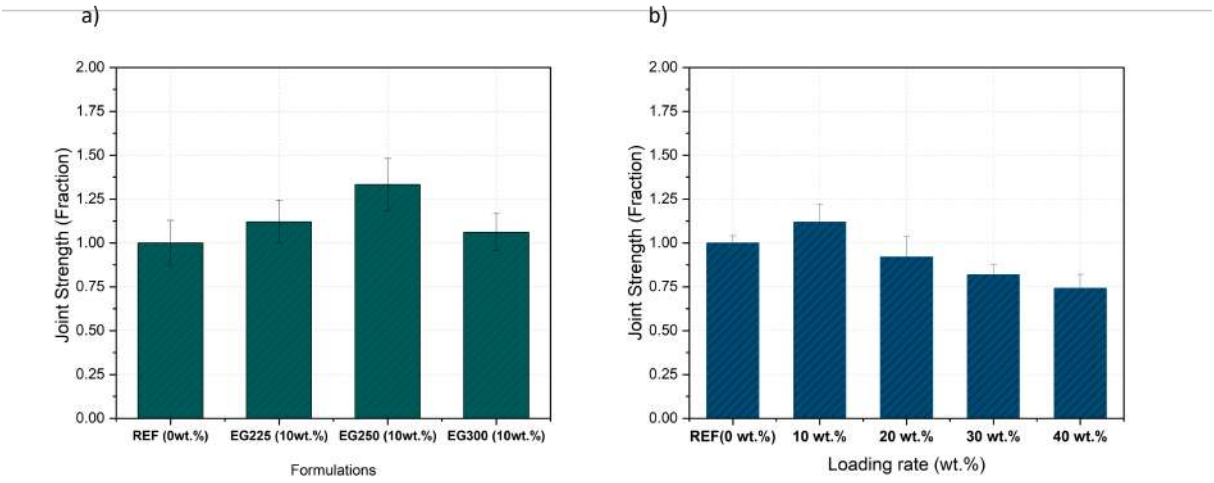

Figure 5.2: Adhesion test at room temperature, (a) joint strength of different formulations (b) joint strength of different loading rates.

3.1.2.Debonding test

The results of the debonding test are shown in Figure 5.3. It compares the reference formulation with various modified formulations, each containing a different type of expandable graphite (EG) at a 10 wt.% loading rate. The focus was on the adhesive composition with the DETA hardener, with all formulations being heated progressively until the non-modified (REF) adhesive joints fully degraded. It was observed that these joints retained their mechanical properties up to a critical temperature of 375 °C, after which they began to degrade rapidly. To make the data better suited for a comparative study, the results are presented as joint strength fractions, meaning all results use the initial joint strength of the DGEBA/DETA formulation as a reference point. Throughout the experiment, the reference formulation exhibited stable joint strength values, with minor fluctuations observed between 200 and 300 °C. The lowest joint strength percentage recorded in this range was 94%, while the highest was 115%. Before reaching their respective debonding temperatures, the EG225, EG250, and EG300 formulations showed joint strength values comparable to the reference formulation. For instance, at 200 °C, the joint strength percentages were 115% for EG225, 110% for EG250, and 105% for EG300, compared to the reference value of 105%. There was no gradual degradation of mechanical properties observed, indicating that the EG fillers not only improve joint strength at room temperature but also do not pose a risk of premature debonding within the operational temperature range of the adhesive joint. This is certainly coming from the chemical inertness of EG.

Debonding occurred only at the respective debonding temperatures for each formulation. Specifically:

- **EG225:** Joint strength percentage decreased from 115% at 200 °C to 5% at 225 °C.
- **EG250:** Joint strength percentage decreased from 123% at 225 °C to 4% at 250 °C.
- **EG300:** Joint strength percentage decreased from 94% at 275 °C to 10% at 300 °C.

When comparing the technical data sheets of the fillers, it is observed that both EG250 and EG300 debond at temperatures corresponding to their onset expansion temperatures specified by the manufacturer, see Table2.2. However, EG225 exhibited debonding at 225 °C, whereas its manufacturer's specified expansion temperature was 180 °C. This delay in activation can be attributed to several factors. At 180 °C, the adhesive system is above its Tg but not yet in the rubbery plateau, see the figure below , making it more rigid and less flexible, thereby hindering the expansion ability of the expandable graphite fillers. In contrast, at higher temperatures, the DGEBA/DETA system becomes flexible enough to allow the fillers to expand and induce debonding.

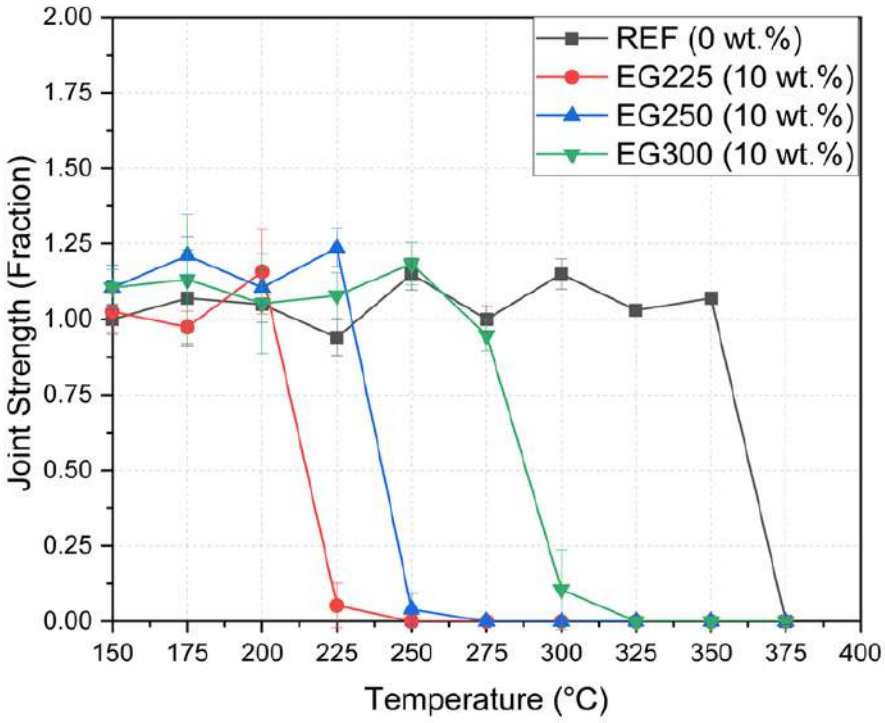

Figure 5.3: Debonding test with temperature gradient for different EG formulations at 10 wt.%

3.1.3.Failure modes

Two main failure modes were observed as seen Figure 5.4. Before debonding, the failure is primarily adhesive failure, occurring at the interface substrate-EG fillers layer. After debonding, due to the expansion of the EG filler and its downward migration, the failure becomes primarily near-interface cohesive or adhesive, occurring at or near the interface between the expanded EG filler and the substrate, with residue on the substrate surface persisting after the debonding. It is therefore assumed that failure is coming from the presence of defects which are located close to the adhesive-aluminum bottom interface. This is certainly related to the expansion of EG which has settled in the bottom part of the joint.

Figure 5.4: Observation of disjointed substrates before and after debonding.

3.2.Influence of the additives on the physicochemical properties

3.2.1.Thermal stability

Figure 5.5(a) presents the thermogravimetric analysis (TGA) curves for three different EG powders: EG225, EG250, and EG300, conducted in a nitrogen (N) environment at a heating rate of 10 K/min. The corresponding characteristic temperatures are summarized in Table 5.1. The degradation profiles of EG225 curve shows an onset of degradation ($T_{\text{onset5\%}}$) at 174°C, with the maximum rate of weight loss ($T_{\text{Max\%}}$) occurring at 256°C. This degradation profile indicates a two-step process: an initial minor weight loss followed

by a more important degradation phase. The EG250 curve, begins its degradation at a higher$T_{\text{onset5\%}}$ of 208°C, with a $T_{\text{Max\%}}$ at 225°C. EG250 also exhibits a two-step degradation process, with a noticeable rapid weight loss initially, followed by a gradual weight loss. The third curve of EG300, demonstrates superior thermal stability with a $T_{\text{onset5\%}}$ of 294°C and a $T_{\text{Max\%}}$ at 331°C. Unlike EG225 and EG250, EG300 shows a single-step degradation process with a gradual and continuous weight loss throughout the temperature range, maintaining a higher weight percentage. Two main hypotheses can be extracted from these findings. Firstly, similar to the debonding test, there is a direct correlation between the size of the fillers and the degradation temperatures, indicating that smaller particles have better thermal stability and thus delay the debonding effect when integrated within a resin. Second, despite the differences in degradation temperatures, the residual weight at temperatures above 700°C is similar for EG225 and EG300, but much lower for EG250, suggesting that the amount of residue is independent of the particle size and pointing to other influencing factors, such as the type of intercalated acids.

Figure 5.5 (b) shows the TGA curves for the reference resin (DGEBA-DETA), EG225 powder, and the resin modified with EG225 at different loading rates (10, 20, 30, and 40 wt.%) under the same conditions as the previous TGA experiment. The degradation profile of the reference resin shows $T_{\text{onset5\%}}$ at 355°C and $T_{\text{Max\%}}$ at 374°C. The EG225 powder alone exhibits a $T_{\text{onset5\%}}$ at 174°C and$T_{\text{Max\%}}$ at 256°C, as previously noted. When the resin is modified with 10 wt.% of EG225, the $T_{\text{onset5\%}}$ is reduced to 299°C, with a $T_{\text{Max\%}}$ at 372°C. Increasing the loading rate to 20 wt.% further lowers the $T_{\text{onset5\%}}$ to 290°C, with a TMax at 371°C. At 30 wt.% loading, the TOnset 5% decreases more significantly to 248°C, with a $T_{\text{Max\%}}$ at 356°C. Finally, at the highest loading of 40 wt.%, the $T_{\text{onset5\%}}$ drops to 228°C, and the $T_{\text{Max\%}}$ is observed at 340°C. These results indicate a clear trend. Increasing the loading rate of EG225 in the resin matrix leads to a decrease in both the onset of degradation temperature and the maximum degradation rate temperature. Another noticeable trend is the multi-step degradation behavior observed when EG225 is incorporated into the resin, especially at higher loading rates. The 10 wt.% and 20 wt.% modified resins show a relatively smooth single-step degradation similar to the reference resin, albeit at lower temperatures. However, at 30 wt.% and 40 wt.% loadings, the degradation profiles display distinct multi-step behavior. This is indicated by initial weight losses at lower temperatures followed by further degradation steps, suggesting interactions between the resin and the EG225 particles, as well as possible phase separation during decomposition. In addition, there are notable observations regarding the residue

amounts at temperatures above 700°C. The reference resin leaves minimal residue, indicating nearly complete decomposition. The EG225 powder, on the other hand, has a significant residue, consistent with its higher initial degradation. When EG225 is incorporated into the resin at different loading rates, the residue amount increases with higher EG225 content. At 10 wt.% loading, the residue is higher than that of the reference resin but significantly lower than the pure EG225 powder. As the loading increases to 20, 30, and 40 wt.%, the residue amounts progressively increase. This can be explained by the high content of thermally stable graphite particles in the composite.

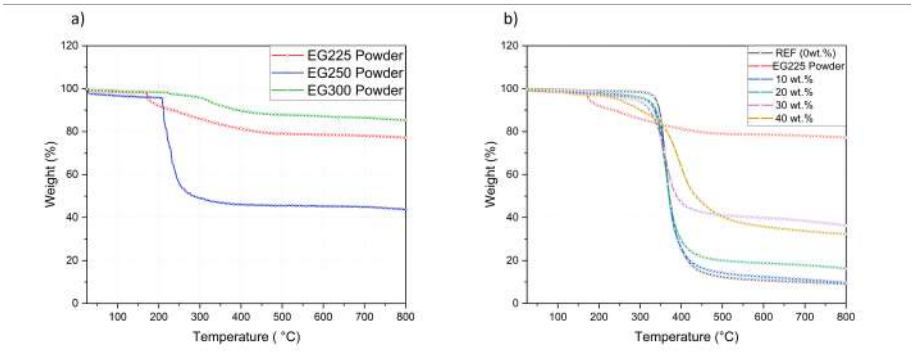

Figure 5.5: TGA Analysis of (a) Expandable Graphite Powders (EG225, EG250, EG300) and (b) Resin Composites with Varying EG225 Loading Rates at 10 K/min in Nitrogen Atmosphere.

Table 5.1: Onset temperatures of degradation at 5% and at $T_{\max}$ of weight loss

Formulation	$T_{\text{Onset,5\%}}$ (°C)	T_{Max} (°C)
REF-(0wt.%)	355	374
EG-225-POWDER	174	256
EG-250-POWDER	208	225
EG-300-POWDER	294	331
EG–225 10-wt.%	299	372
EG–225 20-wt.%	290	371
EG–225 30-wt.%	248	356
EG–225 40-wt.%	228	340

3.2.2.Dispersion and morphology

To study the dispersion characteristics of the additives in the epoxy matrix, different loading rate samples (10 wt.%, and 30 wt.%) with EG fillers were fabricated and polished for detailed examination. Figure 5.6 displays the cross-sectional micrographs of these

two different loading rates. A common observation between the 10 wt.% and 30 wt.% EG loading rates is that the fillers tend to settle towards the lower part of the resin, indicating there is no interaction between the fillers and the matrix. This phenomenon of settlement is more pronounced at the 30 wt.% loading rates, showing the formation of agglomerates and for both there is the formation of a separate EG layer or an interface between the resin and the loaded resin layer in both loading rates 10 wt.% and 30 wt.% loading rates.

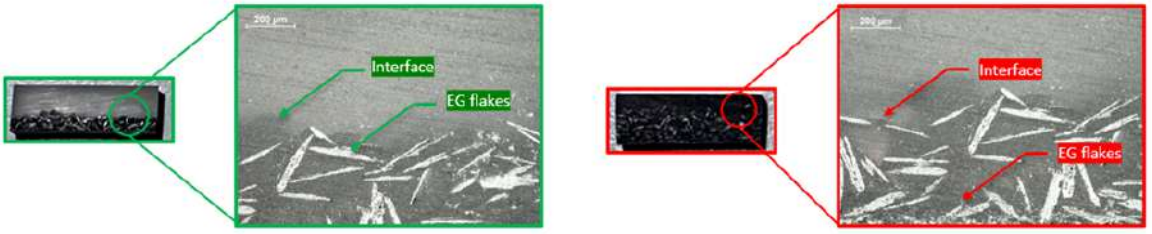

Figure 5.6: Microscopic observation of modified resin with 10 wt.% EG225 and 30 wt.% EG225

3.2.3.Thermomechanical properties

The analysis of storage modulus and tan δ curves provides valuable insights into the reinforcing efficiency of expandable graphite (EG) fillers under varying temperatures and stress conditions. Figure 5.7 (a), (b), and (c) illustrate the changes in storage modulus, loss modulus, and tan δ of epoxy resin with different types and concentrations of EG fillers. The storage modulus increases with the addition of EG fillers, showing a clear correlation with the loading rate of EG225, similar to the trends seen in flexural modulus tests. This enhancement in storage modulus can be attributed to the improved stiffness of the epoxy due to the high-stiffness EG particles. When comparing different types of EG fillers, the resins modified with 10 wt.% of EG250 and EG300 also show an increased storage modulus compared to the reference resin. EG250 exhibits the highest storage modulus among the three types of fillers, followed by EG300 and then EG225. As the concentration of EG225 increases, more particles interact with the epoxy matrix, leading to further improvements in storage modulus. Additionally, the interaction between EG particles and the epoxy matrix restricts the mobility of the epoxys molecular chains near the particles, resulting in increased storage modulus. However, as temperature increases, the storage modulus declines which can be explained by the increased mobility of the epoxy chains. The loss modulus, in Figure 5.7 (b). The reference resin has a peak loss modulus around 150°C.

The resin modified with 10 wt.% EG225 shows a similar peak, while increasing the loading rate to 20, 30, and 40 wt.% shifts the peak to higher temperatures, indicating an increase in Tg. The peaks for 20 wt.% and 30 wt.% loadings of EG225 are around 160°C, while the peak for 40 wt.% is slightly lower. The resins with 10 wt.% of EG250 and EG300 show peaks at higher temperatures than the reference resin, with EG250 showing the highest peak temperature. The increase in loss modulus with higher EG content indicates that the material's ability to dissipate energy as heat improves, which is expected since expandable graphite is mainly made of graphite flake that are used to improve heat conductivity and dissipation when used as a filler in a polymer resin [298, 299]. Figure 57 (c) shows the temperature-dependent changes in tan δ , with the Tg values of the samples extracted in Table 5.2 based on the peak points of the graphs. The reference resin has a Tg of 151°C and adding 10 wt.% EG225 only slightly alters this value to 154 °C. However, adding 10 wt.% of EG250 and EG300 increases the Tg to 157°C and 156°C, respectively. Higher loadings of EG225 (20, 30, and 40 wt.%) further increase the Tg to 163°C for 20 and 30 wt.%, while 40 wt.% slightly reduces it to 160°C. These minor variations in Tg can be attributed to the restriction of the movement of polymer chains near the filler-matrix interface. It is important to note that EG fillers are inert and do not chemically interact with the epoxy, which helps to maintain the stability of the Tg.

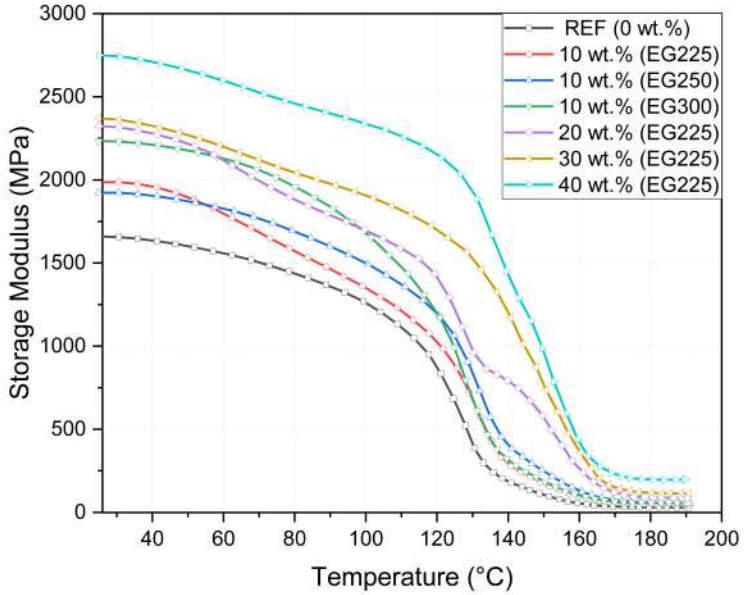

(a) Storage Modulus

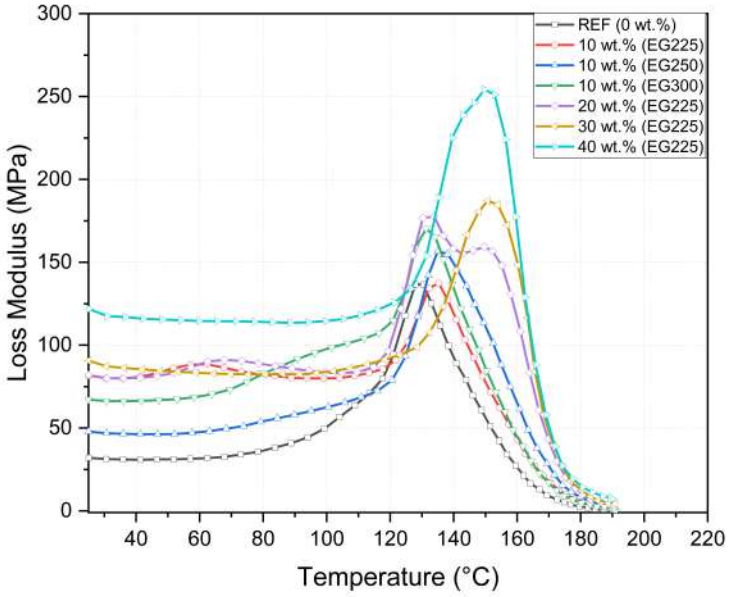

(b) Loss Modulus

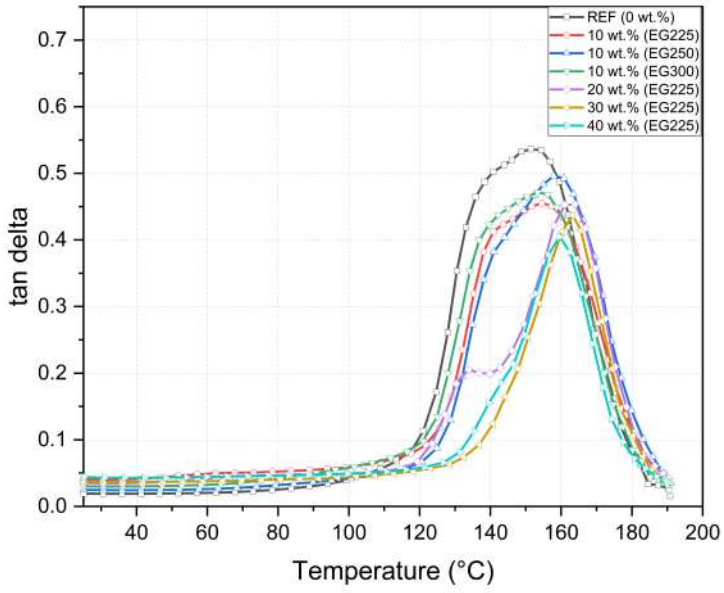

(c) Tan δ

Figure 5.7: Dynamic Mechanical Analysis (DMA) of Resin Composites: (a) Storage Modulus, (b) Loss Modulus, and (c) Tan Delta for Different Expandable Graphite (EG) Fillers and Loading Rates.

Table 5.2: Glass transition temperatures of all modified formulations

Formulation	T_g (°C)
REF-(0-wt.%)	151
10-wt.%-(EG225)	154
10-wt.%-(EG250)	157
10-wt.%-(EG300)	156
20-wt.%-(EG225)	163
30-wt.%-(EG225)	163
40-wt.%-(EG225)	160

3.3.Mechanism study

3.3.1.Micro-CT analysis

Micro-CT analysis was conducted to investigate the structural changes in modified resin samples containing EG225 before and after exposure to the debonding temperature (T°deb). The results, presented in Figure 5.8, illustrate porosity development and filler activation at both the bulk and surface levels. Figures 5.8 (a) and 5.8 (b) focus on observations in the bulk resin. Before debonding, the resin exhibits minimal porosity, measured at 0.46% (Figure 5.8 (a)). After exposure to (T°deb), the porosity significantly increases to 27% (Figure 5.8 (b)), driven by the activation and expansion of EG225. Expandable graphite particles physically expand, creating voids without chemically interacting with the resin, as shown in TGA data and existing literature [293]. These structural changes in the bulk resin confirm that EG225 acts independently, with the expansion phenomenon degrading the integrity of the matrix structure upon heating.

Figure 5.8 (c) presents observations at the surface level, where the activation and exfoliation of EG225 are more pronounced. At the surface, EG flakes undergo extensive expansion and exfoliation, forming characteristic plate-like structures. This localized activation plays a crucial role in weakening the resin-substrate interface, ultimately enabling debonding. The observed surface exfoliation directly correlates with the mechanical failure, demonstrating the efficiency of the debonding mechanism at the resin-substrate interface.

The results from both the bulk and surface-level analyses highlight the dual role of EG225 as a debonding agent. The increase in bulk porosity upon heating and the surface-

level activation and exfoliation are instrumental in ensuring effective debonding. These phenomena also explain the ease of cleaning in the post-debonding process, which will be further explored in Section 3.4.

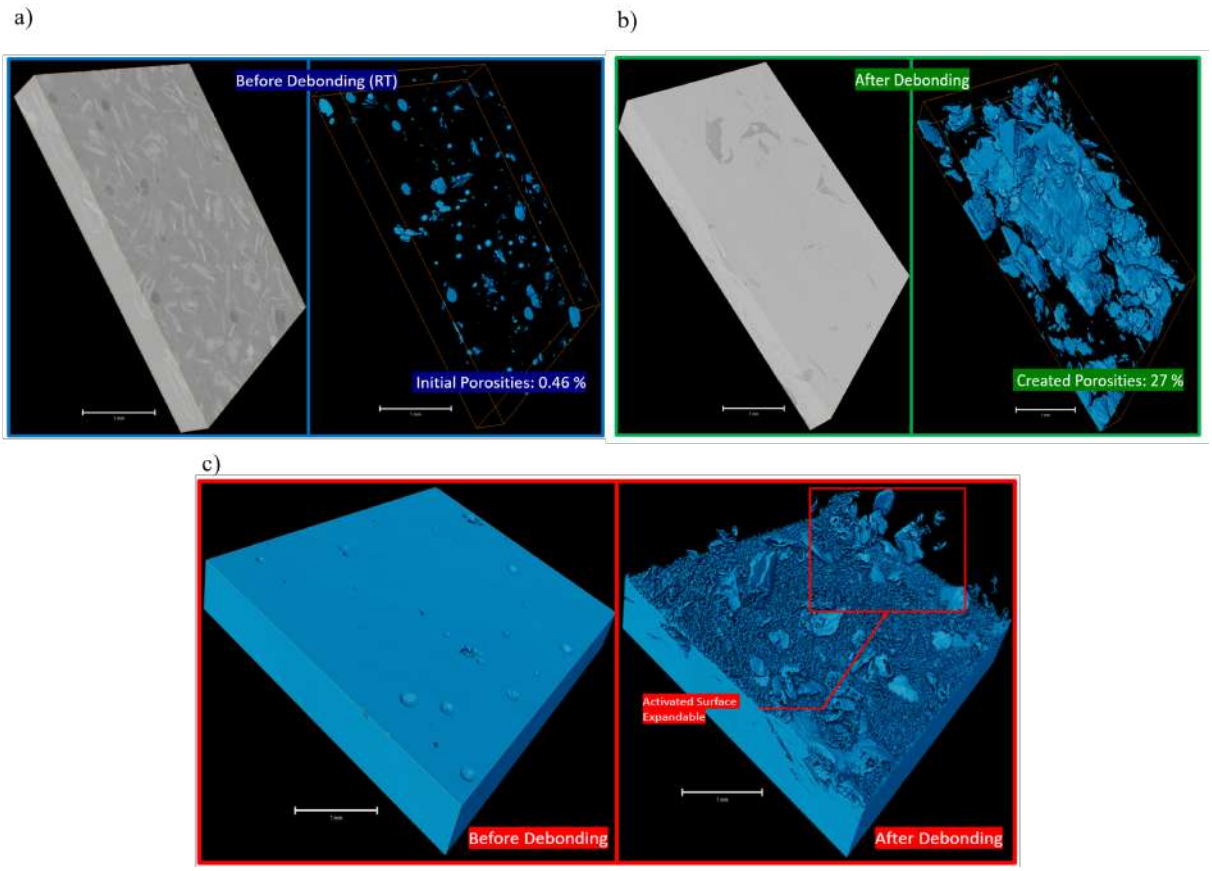

Figure 5.8: Micro-CT Analysis of Porosity Evolution in EG-Modified Resin: (a) Bulk Resin Before Debonding, (b) Bulk Resin After Debonding, and (c) Surface-Level Changes Before and After Debonding.

3.3.2.XRD analysis

The X-ray diffraction (XRD) patterns in Figure 5.9 provide a comparative analysis of EG225 in both powder form and within a resin matrix, before and after exposure to the debonding temperature (T°deb). To enhance clarity, the diffraction signal from the post-debonding samples has been amplified. In both powder (Figure 5.9 (a)) and resin samples (Figure 5.9(b)), the primary peak at 26.5°, corresponding to the (002) reflection plane of graphite, is split into two distinct summits. This phenomenon is indicative of structural heterogeneity in expandable graphite, likely caused by variations in intercalation or staging behavior. Staging in graphite intercalation compounds (GICs) refers to the arrangement of intercalants between the graphene layers, which affects interlayer spacing.

In Stage 1, intercalants are present in every interlayer, expanding the spacing and shifting the peak to a lower 2 value. In Stage 2+, intercalants are present between every second or third layer, resulting in a peak near 26.5°. This heterogeneity produces regions with varying degrees of intercalation, reflected by the two peaks: the first at 26.5°, corresponding to less intercalated regions, and the second at 25.9°, corresponding to expanded regions with greater interlayer spacing.

After exposure to T°deb, the intensity of the primary peak decreases significantly, indicating a partial loss of crystallinity due to thermal expansion. Despite this intensity reduction, there is no noticeable shift in the peak position, confirming that the graphite's hexagonal crystalline structure remains largely stable. The decrease in intensity can be attributed to the exfoliation process, during which intercalated agents or acids are released as vapor or gas. This release disrupts the long-range order of the graphite, thereby reducing the number of coherent diffracting dipoles and leading to weaker diffraction peaks. This behavior is characteristic of thermal exfoliation, where expanded graphite undergoes structural reorganization. A secondary diffraction peak at 55.3°, corresponding to the (004) reflection plane, is observed prior to debonding. This peak shows a decrease in intensity after debonding and shifts slightly to 54.5°, indicating an increase in interlayer spacing and partial exfoliation. Furthermore, this peak appears split into two summits, suggesting the formation of multiple interlayer distances within the exfoliated graphite structure. Another notable feature, particularly visible in Figure 5.9 (b), is the emergence of new peaks at 44° and 44.5° after exposure to T°deb. These peaks are attributed to the restacking of exfoliated graphite layers, which reorganize after the release of intercalants and structural expansion. This stacking behavior, along with the new peaks, may reflect localized structural variations or the formation of distinct crystalline domains, which could be further validated through complementary techniques such as Raman spectroscopy. The thinning of diffraction peaks after debonding indicates structural refinement in expandable graphite. This behavior likely arises from a more uniform distribution of partially restacked layers following exfoliation. The exfoliation process disrupts the stacking order as intercalated agents are released, but some regions reorganize into more ordered layers, resulting in thinner peaks. Despite this refinement, the overall crystallinity decreases due to layer expansion and separation. These structural changes reflected by reduced peak intensity, variations in interlayer spacing, and the emergence of new reflections are consistent with the thermally driven expansion of expandable graphite, a process that is visibly noticeable to the eye. This expansion generates localized stresses within the

resin, weakens adhesive forces, and facilitates mechanical separation, as confirmed by the micro-CT analysis in Section 3.3.1.

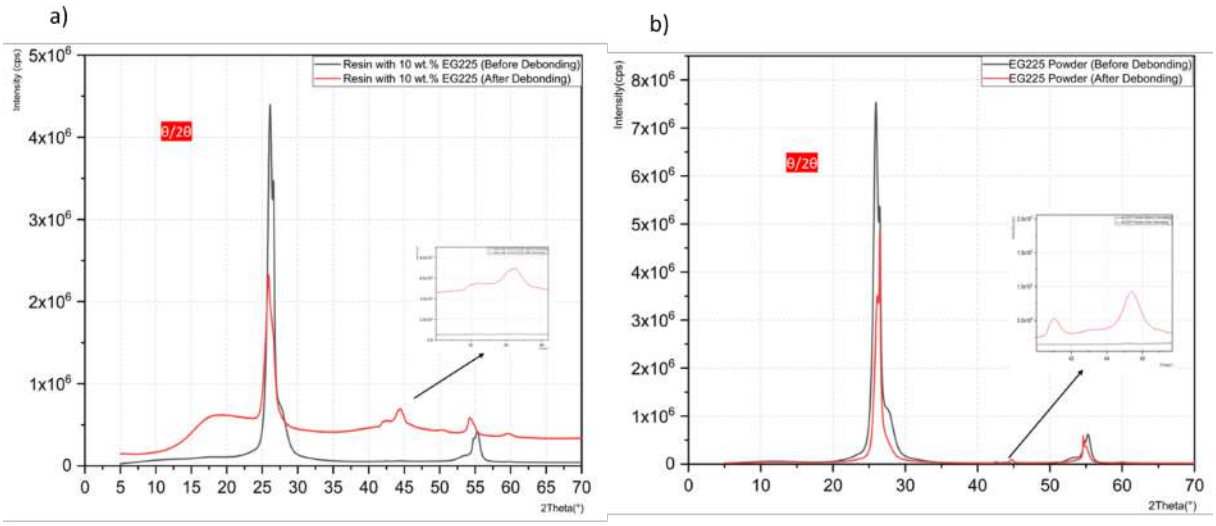

Figure 5.9: X-Ray Diffraction (XRD) Reflection Patterns of EG225: (a) Powder Before and After Debonding, and (b) Resin with 10 wt.% EG225 Before and After Debonding.

3.4.Recycling experiment

The recycling experiment is designed to test the potential of the debonding technology and to which extent it can be used as a recycling technology. For this the results will be segregated in two sections, the first is an SEM analysis and EDS of the substrate surface before the first use, after debonding and activation of the fillers, and after a simple cleaning phase with solvent and a light grinding step before re-use. The second section is a comparison of the joint strength values between a reference formulation, the first bonding, and the re-use with the recycled substrates.

3.4.1.SEM analysis of the surfaces

Figure 5.10 and Table 5.3 summarize the results of the EDS experiment of the different surfaces at the 3 examined states. Comparing the amount of carbon in the zones for different kinds of substrates reveals significant insights into the effectiveness of the debonding and cleaning processes. Before debonding (and applying the adhesive), Zone 1 of the substrate shows a high aluminium content (89.32 wt.%) with no detectable carbon. After debonding, there is an increase in carbon content to 88.87 wt.% in Zone 1, while in Zone 2, after debonding, the aluminium content is 83.57 wt.% with no detectable carbon,

confirming the failure type post deboning as cohesive near the surface. Following the cleaning phase, the EDS results of the recycled surface still show a high surface carbon content value 89.39 wt.% where a residual mark is observed. Even after cleaning, some carbon residue remains, though its volume is significantly diminished when we compare zone 1 from image after debonding and zone 1 from recycled surface. Examination of the SEM images corroborate this, showing that the residue is highly reduced and the abrasion patterns from the mechanical cleaning treatment are clearly visible again.

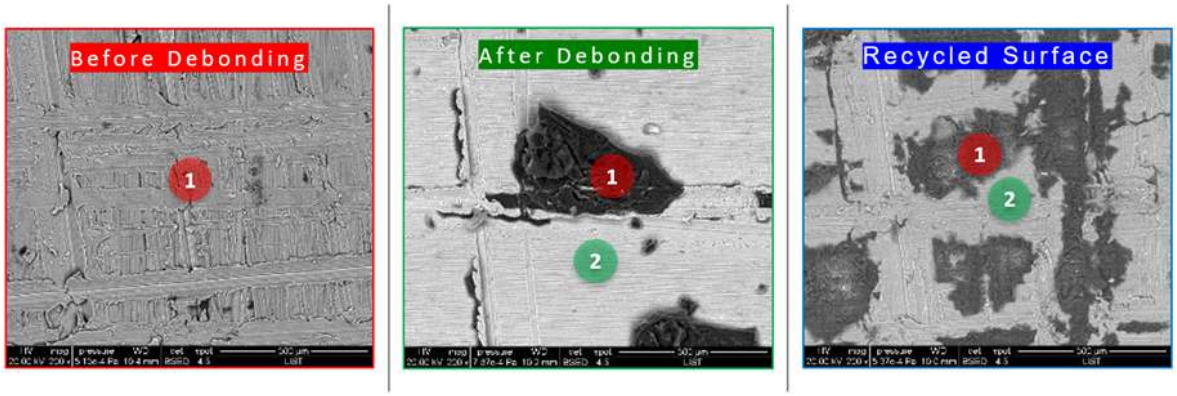

Figure 5.10: SEM observation of the substrate surface at different states, Before Bonding, After debonding and recycled surface.

Table 5.3: EDS results of the substrate surface at different states: Before Bonding, After Debonding, and Recycled Surface

Substrate	Element (wt.%)	Substrate before debonding		Substrate after debonding		Recycled substrate	
		Al	C	Al	C	Al	C
Zone 1		89.32	0	0.44	88.87	0	89.39
Zone 2		—	—	83.57	0	96.95	0

3.4.2.Recycled joint strength

The joint strength results for various formulations demonstrate the effectiveness of the recycling process. As previous joint strength tests, all the values are normalized and compared to the reference formulation (0 wt.% EG) has a joint strength percentage of 100 %. The joint before debonding with 10 wt.% EG shows an increase of strength percentage of 33%, indicating that the addition of EG enhances joint strength. After the recycling process, the recycled joint without EG shows a slightly reduced strength percentage of 97%, which is close to the reference, suggesting that the recycled substrate maintains a comparable level of joint strength. Notably, the recycled joint with 10 wt.%

EG exhibits a strength percentage of 127 %, nearly matching the joint before debonding. This highlights that the recycled substrates, even with some residual carbon detected by EDS, do not degrade the joint strength properties.

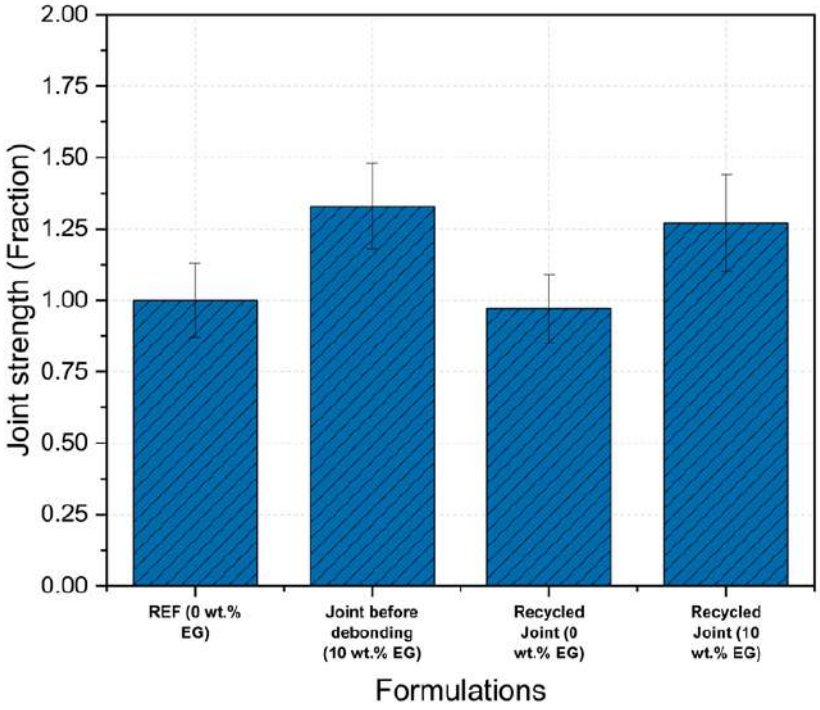

Figure 5.11: Comparison of the joint strength of recycled joints, reference, and modified joint before debonding at RT.

4.Discussion

The use of expandable graphite (EG) as a debonding technology has been previously documented [261], proving effective in preserving joint strength properties and efficient in inducing effective debonding. However, the application of multiple EG with different characteristics to achieve debonding at various temperature windows is relatively novel, demonstrating this technology's versatility. In prior research done by the authors, multiple flame retardants, such as melamine polyphosphate, ammonium polyphosphate, and organo-phosphorus flame retardants like PCO 900, were repurposed for debonding applications successfully in both patented [WO2021219736] and published works [277]. EG was shown in this study to preserve joint strength at room temperature at filler loadings as low as 10 wt.% and even slightly improve it, as observed with EG250 fillers for example where joint strength fraction increased from 100 % to 133 %. Three distinct debonding temperatures 225 °C, 250 °C, and 300 °C were achieved, supporting the premise that EG

can serve as a universal debonding technology. A negative impact on joint strength was noted with increased filler loading, as the joint strength relative values decreased from 112 % at 10 wt.% to 74 % at 40 wt.% of EG225. While expected, examining high filler content samples offered insights into potential behaviors for other resins with varying properties, such as different glass transition temperatures, viscosities, and curing profiles. Unlike previous studies that focused primarily on mechanical aspects, such as adhesive properties and ageing properties, this study provided a comprehensive physicochemical characterization of the modified resins at various loading rates. Thermogravimetric analysis revealed a catalytic effect on the degradation profile, with higher filler concentrations accelerating degradation and reducing residual amounts due to the volatilization of the intercalated acids in EG fillers. A significant delay, ranging from 5 °C to 50 °C, was observed between the debonding temperatures in modified resins and the onset temperature of the fillers, possibly due to the thermoset thermal resistance and the constraining effect of the thermoset. Despite the advantages, EG as a debonding technology has limitations. Fillers were observed settling during curing, creating a resin/resin+EG interface visible through optical microscopy or microtomography. Additionally, an increase in glass transition temperature (Tg) was noted, likely caused by the large specific surface of EG fillers, hindering polymer chains mobility, requiring more thermal energy for the polymer to reach the rubbery state. Another notable limitation of using EG fillers for debonding is related to thermal cycles which are required for curing process. EG fillers may not withstand high temperatures or prolonged curing cycles without partial activation, potentially damaging mechanical properties and debonding effectiveness. In the current study, this disadvantage was mitigated by selecting DGEBA-DETA as the adhesive system, which is a low-temperature curing system. The failure modes observed correlated well with physical trends, as fast-settling fillers impacted the adhesive-substrate interface. Before debonding, failures were adhesive; after debonding and EG filler exfoliation, failures were primarily cohesive/near-interface adhesive, close to the downside interface. This phenomenon can be attributed to the settling behaviour of the fillers observed from the optical microscope images. The EG fillers are inert, and the reaction mechanism involves no interaction with the resin, this observation was confirmed through the XRD experiment where no new peaks appeared before and after debonding temperature for both powder and modified resin samples. Debonding occurred before resin degradation in all three filler types. As elucidated in the literature, upon heating, intercalated acids decompose into gases, such as sulfur dioxide or carbon dioxide, causing rapid expansion and forming expanded graphite [299–301]. This expansion created porosities within the

adhesive joint until mechanical failure occurred, leading to debonding. This physical mechanism was thoroughly observed using micro-CT analysis as the fillers were tracked before and after debonding, showing the difference in volume of porosities in the bulk and the wormhole structure formation of activated EG fillers over the surface of the resin [301]. Moreover, attempts to reduce EG filler sizes to improve homogeneity were unsuccessful, as smaller fillers compromised debonding capabilities by limiting expansion, as discussed in the work of Wang et al. [302]. Larger particles facilitated greater expansion ratios. Factors affecting expansion and activation temperature include the type and concentration of intercalated acids and interlayer spacing, where increasing these variables enhances expansion as well [303, 304]. While reducing filler size positively affects mechanical properties, excessive reduction favors agglomerate formation, negatively impacting joint strength performance. Thus, an optimal filler size exists when working with EG fillers. Although no aging tests were conducted in this study, a similar study [305] showed no significant damage to adhesive joints after water submersion ageing test. Finally, the re-manufacturing experiment involved re-preparing substrates from debonded samples to emphasize the recycling aspect of debonding technology. While most studies stop at substrate separation, this study assessed the feasibility of re-using substrates and re-manufacture an adhesive assembly. Macroscopically, residues were easily removed with light mechanical abrasion and solvent cleaning. Microscopically, however, residues were detectable, with traces of adhesive confirmed by EDS experiments. Despite this, the joint strength values showed a slight decrease from 100% to 97 % which is not significant and 27% increase in the case of the re-manufactured sample with modified resin. EG fillers were shown to be an effective debonding technology, offering various debonding temperatures suitable for multiple applications. However, their inability to distribute homogeneously within adhesive matrices limits their use to adhesive joints, preventing broader application in composites like carbon fiber composites.

5.Conclusion

This study demonstrates that expandable graphite is an effective and versatile debonding technology, capable of achieving distinct debonding temperatures of 225 °C, 250 °C, and 300 °C. At low filler loadings (10 wt.%), EG preserved and slightly enhanced joint strength at room temperature, highlighting its potential for various adhesive applications. EG's inert nature allows for debonding before resin degradation through physical expansion,

and the ability to recycle debonded substrates with no compromise of joint strength was confirmed, supporting sustainable practices and material recycling. To broaden EG's applications, especially in composite materials, further optimization of filler properties and compatibility with different adhesive matrices is needed. This research provides valuable insights into EG's role as a debonding agent and as a ready to use debonding technology.

Acknowledgements

We kindly acknowledge the support of the Luxembourg National Research Fund (FNR C20/MS/14707266).

6

Ammonium polyphosphate as a thermally activated debonding agent: effects of molecular weight and carbon source incorporation

Chapter 6 :

Ammonium polyphosphate as a thermally activated debonding agent: effects of molecular weight and carbon source incorporation

This final study in the dissertation is central to validating the primary hypothesis of this research: that short-chain ammonium polyphosphate (APP I) enables lower debonding temperatures while preserving adhesive joint performance. Expanding on previous investigations into flame-retardant-assisted debonding, this work examines how the molecular characteristics of APP I influence thermal activation and adhesive disassembly. The findings confirm that APP-based formulations enable controlled adhesive failure at reduced temperatures while preserving acceptable mechanical integrity. Furthermore, the addition of pentaerythritol as an external carbon source amplifies the intumescent behavior, promoting more effective thermal expansion and char formation, thereby enhancing the efficiency and reliability of the debonding process in structural adhesive applications. A key contribution of this study is the evaluation of substrate recyclability, an essential consideration for the sustainable reuse of bonded assemblies. While earlier research demonstrated that thermally activated flame retardants enable adhesive disassembly, the feasibility of reusing debonded substrates remained uncertain. This study systematically investigates post-debonding surface conditions, comparing untreated, mechanically cleaned, and solvent-treated substrates. The results indicate that with appropriate cleaning protocols, recycled substrates can recover nearly 100% of their initial adhesion strength.

Another significant aspect of this work is the benchmarking of our lab developed adhesive joint strength evaluation methods. While earlier studies in this dissertation employed custom joint strength tests, this study introduces single-lap shear (SLS) testing, an industry-standard method for adhesion assessment. The strong correlation between the results obtained from these methods reinforces the rigor and reliability of the experimental framework, ensuring that the findings align with established industrial testing standards.

A comprehensive characterization was conducted to achieve a deeper understanding of the mechanical, thermal, and morphological behavior of the modified adhesive formulations. This included physicochemical analyses to elucidate degradation mechanisms

and porosity formation, further correlating the materials performance with its debonding efficiency and debonding mechanism.

These findings support the broader adoption of sustainable adhesive technologies and provide a basis for transitioning this approach from adhesive joints to structural and composite applications.

Ammonium polyphosphate as a thermally activated debonding agent: effects of molecular weight and carbon source incorporation

Oussema Kachouri, Julien Bardon, David Ruch, and Abdelghani Laachachi

Luxembourg Institute of Science and Technology (LIST), Department of Materials Research and Technology (MRT), Bommelscheuer

5, ZAE Robert Steichen, L-4940 Hautcharage, Luxembourg.

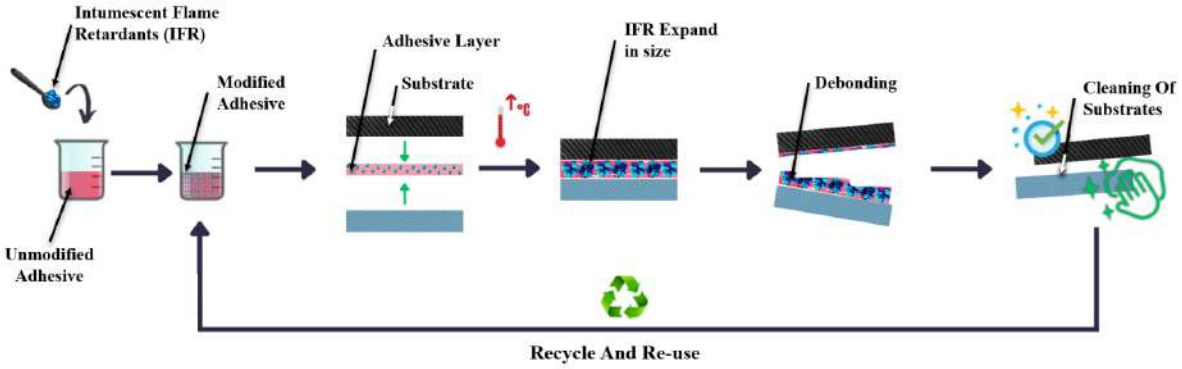

Figure 6.1: Thermally Assisted Debonding and Recycling Process Using intumescent flame retardants

Abstract

This paper exploits the novel approach inspired by the use of intumescent flame-retardant such as melamine polyphosphate (MPP) and ammonium polyphosphate (APP) as additives for disassembling bonded aluminium substrates. Building on our previous work, where we used long-chain APP and MPP, this study investigates lower molecular weight flame retardants to enhance debonding capabilities. Short-chain ammonium polyphosphate (APP) was incorporated into epoxy adhesive joints, acting as both an acid source and a swelling agent to trigger thermal debonding. To enhance this effect, pentaerythritol was added as an external carbon source, promoting a more efficient intumescent reaction and improving debonding performance. Upon exposure to heat, the stimuli-responsive

nature of the system was activated, leading to swelling and foaming of the adhesive layer in the adhesive joint. This created local porosities that facilitated the formation of cracks at the adhesive-substrate interface and enabling efficient disassembling of the bonded aluminium substrates. Comprehensive characterization of the resin with intumescent agents incorporation and its assemblies with aluminium substrates was performed, including structural, morphological, mechanical, and thermal property analyses. Results revealed that incorporating lower molecular weight APP fillers as well as the external carbon source in the intumescent system were crucial for achieving efficient debonding at temperatures as low as 175 °C. In addition, a recycling experiment was conducted at the end to test the feasibility of using recycled adherends and compare their performance to standard adherends. This work demonstrates the potential of utilization of intumescent flame-retardant additives for creating debonding solutions within different temperature windows, making these solutions suitable for a wide range of applications and various material types.

1.Introduction

For thousands of years, adhesive technologies were inspired by nature and mainly extracted from natural sources. They can be derived from plant-based sources such as tree bark or Arabic gum from acacia trees [306, 307] as well as animal based, such as casein glue extracted from milk proteins [307, 308]. In fact, the earliest evidence of mankind's use of bonding technologies can be found in ancient tools, such in stones were bound to sticks with clay or horns attached to handles [309, 310]. It is only within the last century that we have seen the development and widespread use of synthetic adhesives [310]. Thermosetting resins, such as epoxy, polyurethanes, and phenolic resins, have been used as adhesives [311]. These resins offer properties as for example the ability to bond dissimilar and fragile materials, significant weight reduction in structures, and resistance to vibration [312, 313]. Consequently, these adhesives have become industrially produced and have increasingly replaced traditional joining techniques such as welding and riveting [314]. While these adhesive technologies have addressed numerous challenges, they suffer from one major drawback: the permanence of the bond [315] making the recycling of adherends hard and almost impossible. Over the past decade, this need for recycle and repair has led to the development of a new class of adhesives known as reversible or debondable adhesives [141]. These new adhesive technologies are stimuli responsive

and enable easier disassembly and reuse of materials when exposed to specific triggers such as heat, electrical current, and chemical reactions after the components application lifetime [249].

Debonding stimuli are a key factor in adhesive design [315]. To date, six distinct types of stimuli have been documented in literature, each associated with specific technologies. Light stimuli are addressed through photo-debondable adhesive technologies, also known as supramolecular adhesives. These adhesives utilize non-covalent interactions, such as hydrogen bonds and metal coordination, to form reversible bonds that can be dissociated using UV light. While they are effective for temporary adhesion, their mechanical strength is often limited [252, 307]. For heat stimuli, two major technological families exist. The first utilizes additives within the adhesive polymer, such as thermally expanding particles or foaming agents, which facilitate debonding upon heating. However, these additives can reduce joint strength and accelerate material aging, thus rendering them unsuitable for certain epoxy thermosets [256]. The second family involves modifying the adhesive polymer itself; for instance, Diels-Alder-based adhesives employ thermally reversible covalent bonds through the Diels-Alder reaction, enabling both debonding upon heating and re-bonding upon cooling. Additionally, Aromatic ThermoSetting coPolyesters (ATSP), a class of high-performance reactive adhesives designed for structural applications, utilizing dynamic covalent chemistry through interchain transesterification reactions (ITR). These adhesives demonstrate robust mechanical properties however it requires precise tuning and are limited to high-temperature cycles, primarily for space applications [253].

Electrically induced debonding involves the application of an electric current to weaken or sever adhesive bonds, suitable for conductive materials nevertheless requiring the integration of metal patches or conductive substrates [151,152,254]. Magnetic field-responsive adhesives leverage hysteresis heating to achieve debonding, though their effectiveness may be compromised by uneven particle dispersion [254, 263]. Finally, chemical debonding utilizes specific chemical triggers, such as fluoride ions, to initiate bond degradation, offering precise debonding capabilities with the potential downside of leaving chemical residues [149, 307].

Each of the debonding technologies discussed presents distinct advantages and limitations. Despite advances, there remains a pressing need for more streamlined and versatile debonding technologies suitable for diverse assembly scenarios, across different resins and material types, including adhesive joints and composites such as CFRPs in a future step.

In response to this challenge, our team has repurposed intumescent flame retardants [270] traditionally used for fireproofing as fillers to induce a debonding effect [267–269]. Upon exposure to heat, these flame retardants begin to foam and expand within the resin matrix, forming a porous barrier that impedes heat and gas transfer, thereby mechanically weakening the joint and facilitating debonding. Previous studies have demonstrated that ammonium polyphosphates and melamine polyphosphates can effectively lower the debonding temperature to 325 °C [277], suitable for structural adhesives.

To broaden the temperature window suitable for debonding and advance the use of intumescent flame retardants as a debonding technology, we investigated lower molecular weight variants of ammonium polyphosphate (APP). These short-chain APPs exhibit thermal degradation at lower temperatures, potentially enabling debonding to occur below the degradation threshold of the adhesive itself. Traditionally, an intumescent flame retardant system consists of three key components: an acid source, a foaming agent, and a carbon source, which interact synergistically to produce an expanded protective char. In our study, since the primary goal was to initiate debonding at temperatures significantly below the adhesives decomposition point, an external carbon source, specifically pentaerythritol, a well-known intumescent additive, was introduced. This allowed us to examine the influence of pentaerythritol on both the intrinsic properties of the adhesive and the mechanical performance of the resulting adhesive joints. The present work compares the effects of incorporating both short-chain and long-chain ammonium polyphosphates, with and without the carbon source, across a range of structural and thermal properties. To assess the mechanical strength of the modified joints, we fabricated and tested aluminum/modified epoxy joint/aluminum specimens. A specially designed debonding test helped evaluate and determine the debonding temperatures achieved by each system.

The modified resins with different intumescent agents were characterized and analyzed using techniques such as SEM, EDS, pull-off tests, DMA, Micro-CT, flexural tests, and TGA to explore their mechanical and thermal properties and to visualize and identify the debonding mechanism. Further, to complete the cycle of debonding, recycling, and reuse of substrate surfaces, a recycling experiment was specifically designed using single lap shear tests. In this experiment, samples were mechanically tested before debonding. After debonding, the substrates were cleaned and reused in new samples, and the results from the recycled substrates were compared with those from the initial tests.

This study demonstrates that incorporating lower molecular weight APP fillers in the

intumescent system was crucial for achieving efficient debonding at lower temperatures. Moreover, the combination of different forms of APPs with a carbon source resulted in an optimized intumescent system capable of inducing debonding at multiple temperatures, thereby highlighting the versatility of this debonding technology.

2.Materials and methods

See section materials and methods of the thesis.

2.1.Materials

2.1.1.Adhesives

Low viscosity epoxy resin Bisphenol A diglycidyl ether (D.E.R.332, commonly abbreviated as BADGE or DGEBA), was selected for this study. The hardener used is an aliphatic flexible hardener, dithylenetriamine (abbreviated as DETA). All products were supplied by Sigma-Aldrich Germany.

2.1.2.Intumescent flame retardants

Two APP variants, supplied by Shifang (China), were examined: TF-303, a short-chain APP (Phase I), with the general formula $(NH_4)_{n+2}P_nO_{3n+1}$ and a degree of polymerization $n < 20$; and TF-201, a long-chain variant with $n > 1000$. This study aimed to assess the effectiveness of short-chain APP in promoting low-temperature debonding, thereby supporting its suitability for expanding the application range of intumescent flame-retardant systems. In addition, pentaerythritol, supplied by Sigma-Aldrich, was used in this study for its role in forming a char layer during thermal decomposition. For clarity, the characteristics of the three APP variants will be summarized in The following table. In addition, pentaerythritol, supplied by Sigma-Aldrich, was incorporated in this study in powdered form to act as an external carbon source.

Technical details of the used fillers.

Flame Retardant	**Assigned Name**	**Molecule**	**Supplier**	**Nitroge**
APP TF-303	APP I	Ammonium Polyphosphate	Shifang China	17.5%
APP Phase II (TF-201)	APP II	Ammonium Polyphosphate	Clariant	14%

3.Results

This section presents the experimental outcomes related to the influence of different ammonium polyphosphate (APP) fillers on adhesive joint performance. The study investigates enhancements in joint strength, variations in debonding temperatures, and alterations in the physicochemical characteristics of the adhesive system.

3.1.Mechanical analysis

3.1.1.Effect of APP fillers on joint strength

The evaluation of joint strength at room temperature was conducted to assess the effect of APP fillers at varying loadings. A 20 wt.% concentration was selected as the optimal formulation based on previous studies with APP and MPP fillers [125], where this ratio provided the best balance between mechanical integrity, adhesion performance, and controlled debonding. All results were normalized against the reference REF DGEBA-DETA formulation, which was assigned a relative joint strength of 100%. As shown in Figure 6.1, two key trends emerged. First, an increase in joint strength was observed when APP fillers were incorporated at 20 wt.%. Specifically, short-chain APP I increased joint strength from 100% ±7% (reference) to 103% ± 6%, which is not significant , while long-chain APP II exhibited a more pronounced enhancement, increasing from 100% ± 7% to 133% ± 16%. Conversely, the addition of pentaerythritol negatively impacted joint strength. When 10 wt.% pentaerythritol was combined with either APP I or APP II, joint strength decreased relative to both the reference and APP-only formulations. The APP I + PENTA system led to a reduction to 94% ± 7%, while APP II + PENTA lowered joint strength to 105% ±10% from the original 133% ± 16% observed with APP II alone. Despite this reduction, the incorporation of APP fillers did not significantly impair joint strength. Although pentaerythritol slightly weakened adhesion, joint strength values re-

mained within acceptable limits for initial screening at RT. The superior performance of long-chain APP II compared to short-chain APP I is likely attributed to its optimized particle size, powder morphology, and surface treatment of the powders, which enhance dispersion and integration within the adhesive matrix.

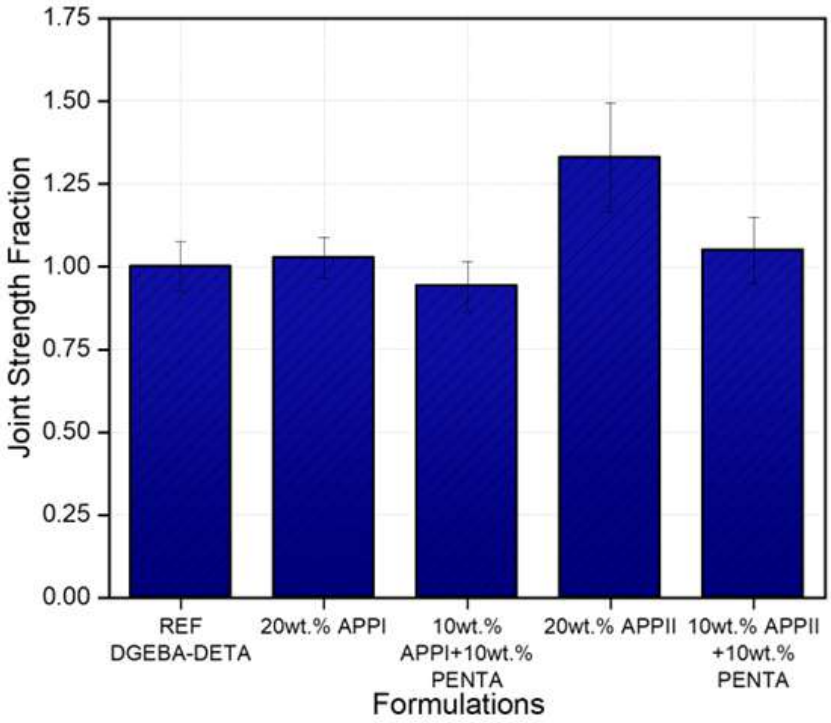

Figure 6.2: Adhesion test at room temperature, joint strength fraction of different formulations.

3.1.2.Debonding performance of APP-modified adhesive joints

The results of the debonding tests are presented in Figure 6.3 , comparing the reference formulation with various modified adhesive systems. These include formulations incorporating 20 wt.% of either short-chain APP I or long-chain APP II, as well as combination formulations containing 10 wt.% APP and 10 wt.% pentaerythritol. The primary focus was to evaluate the thermal degradation behavior of the adhesive matrix using the DETA hardener, with all formulations progressively heated until the non-modified REF DEGBA-DETA (reference) joints underwent complete degradation. The reference formulation exhibited mechanical stability up to 375 °C, beyond which a rapid degradation of adhesive strength was observed. To facilitate interpretation, all results are expressed as joint strength percentages, with the REF DEGBA-DETA formulation set as the 100% baseline. Throughout the heating process, the reference formulation maintained relatively stable joint strength values, fluctuating slightly between 200 °C and 300 °C, with recorded

variations ranging from 94% ± 7% to 115% ±5%. A similar trend was observed across all modified formulations, as each retained mechanical integrity within the operational temperature range of the adhesive joint, with significant strength loss occurring at the respective debonding temperatures. For the 20 wt.% APP II formulation, mechanical integrity was preserved up to 300 °C. However, at 325 °C, debonding was initiated, causing the joint strength to drop from 117% ± 6% to complete failure (0%). In contrast, the 20 wt.% APP I formulation exhibited a much lower debonding temperature, as adhesive failure occurred at 225 °C. Joint strength dropped from 112% ± 7% at 200 °C to 18% ± 10% at 225 °C, reaching complete failure at 250 °C. The incorporation of pentaerythritol, while slightly reducing initial joint strength, facilitated a reduction in the debonding temperature for both combination formulations. For the APP II + PENTA system, the debonding temperature decreased from 325 °C to 250 °C, with joint strength dropping from 106% ± 13% at 200 °C to 80% ± 10% at 225 °C, and further to 4% ± 3% at 250 °C. This effect was even more pronounced in the APP I + PENTA formulation, where the debonding temperature shifted from 225 °C to 175 °C. Joint strength decreased from 111% ± 10% at 175 °C to 11% ±3% before reaching complete failure at 200 °C.

Overall, the findings confirm that the inclusion of APP fillers enhances controlled debonding behavior, with long-chain APP II providing superior thermal resistance. Meanwhile, pentaerythritol accelerates the degradation process, reducing the energy required for joint failure.

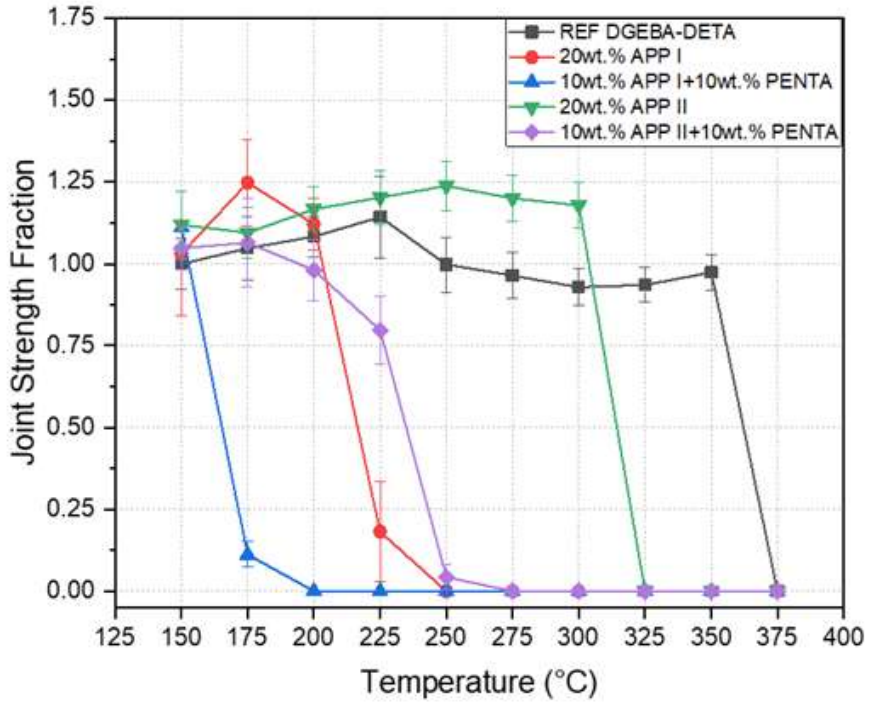

Figure 6.3: Debonding test with temperature gradient for different formulations at 20 wt.%

3.1.3.Analysis of failure modes

The failure mechanisms of the adhesive joints were analyzed to elucidate their mechanical performance and thermal degradation behavior. Figure 6.4 presents representative images of the fracture surfaces at different thermal exposure stages, highlighting the transition from adhesive/mixed failure at room temperature to progressive interfacial degradation before and after debonding temperatures were reached. At room temperature, both the APP I-modified and APP I + PENTA formulations predominantly exhibited adhesive/mixed failure, characterized by cohesive failure within the adhesive layer and partial detachment at the interface. The presence of pentaerythritol did not significantly alter the failure mode at this stage, indicating that the mechanical behaviour of the joint remained comparable between APP-PENTA and APP-only formulations. As temperatures approached the debonding threshold, distinct variations in failure patterns became evident. The APP I formulation maintained strong adhesion, with failure primarily occurring through cohesive mechanisms. However, the APP I + PENTA formulation exhibited an increased tendency toward interfacial failure, suggesting that pentaerythritol influenced the adhesive-substrate interfacial strength, thereby facilitating earlier failure initiation. Upon reaching the debonding temperature, clear distinctions in failure modes emerged.

The APP I formulation retained partial adhesive bonding, while the APP I + PENTA formulation exhibited more pronounced mixed failure, characterized by substantial adhesive breakdown, increased interfacial detachment, and thermal degradation. This observation aligns with the measured reduction in debonding temperature for pentaerythritol-containing formulations, reinforcing its role in promoting bond failure through thermally induced degradation pathways.

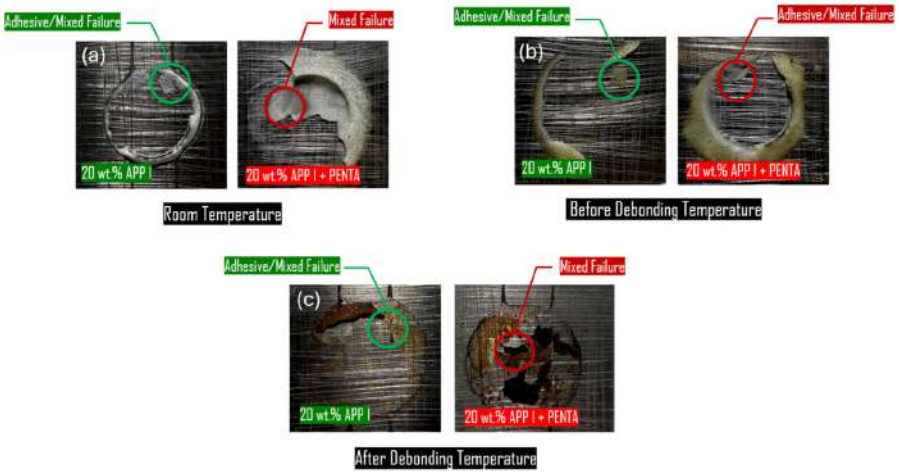

Figure 6.4: Visual Analysis of Failure Modes in APP-Modified Adhesive Joints at Different Thermal Stages.

3.1.4.Flexural analysis

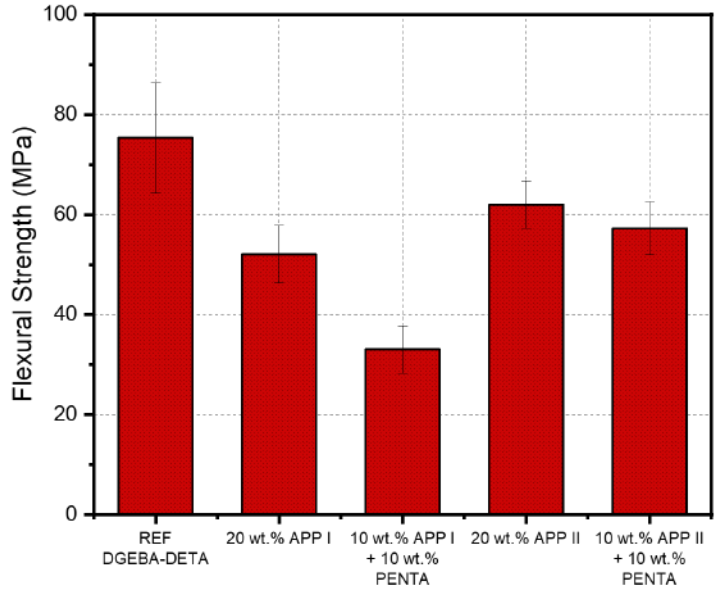

(a) Flexural Strength

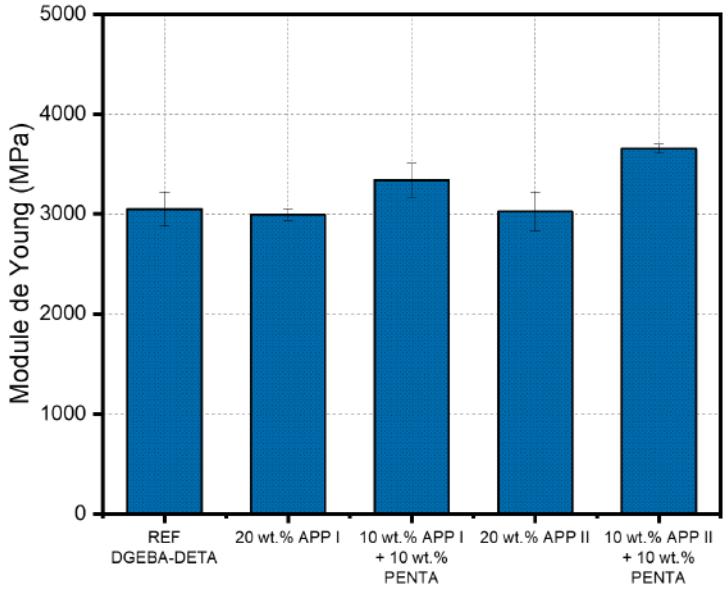

(b) Young's Modulus

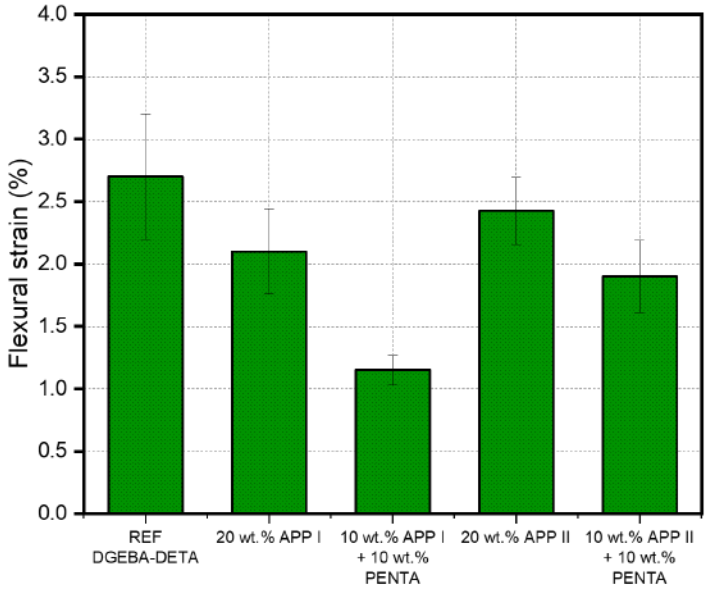

(c) Flexural Strain

Figure 6.5: Flexural Properties of REF DEGBA-DETA and Modified Adhesive Formulations: (a) Flexural Strength, (b) Youngs Modulus, and (c) Flexural Strain.

Following the characterization of adhesive joints through joint strength testing, debonding analysis, and failure mode observations, flexural testing was conducted to examine the mechanical performance of the bulk resin. This approach enables a direct comparison between the unmodified and modified formulations, assessing the impact of APP fillers and pentaerythritol on the resins stiffness, strength, and ductility. The flexural behavior of the modified adhesive formulations was evaluated through flexural strength (Figure 6.5a), Youngs modulus (Figure 6.5b), and flexural strain at break (Figure 6.5c). These mechanical parameters provide insight into the structural integrity and flexibility of the adhesive systems under bending stress. The reference formulation exhibits the highest flexural strength at 75.3 MPa, indicative of its superior mechanical performance. The introduction of APP fillers results in a notable reduction in flexural strength, with the 20 wt.% APP I formulation decreasing to 52 MPa and the 20 wt.% APP II formulation performing slightly better at 62 MPa. The combination formulations display further decreases, with the 10 wt.% APP I + 10 wt.% PENTA formulation presenting the lowest strength at 33 MPa, while the 10 wt.% APP II + 10 wt.% PENTA formulation attains 57.25 MPa. These results indicate that the addition of flame-retardant fillers compromises the overall mechanical performance of the resins relative to the unmodified reference system.

The reference formulation displays the highest flexural strength at 75.3 MPa, whereas APP incorporation reduces this value. The 20 wt.% APP I formulation decreases to 52 MPa, while the 20 wt.% APP II formulation retains slightly better strength at 62 MPa. The addition of pentaerythritol further diminishes flexural strength, with the 10 wt.% APP I + 10 wt.% PENTA formulation reaching the lowest value at 33 MPa, while the 10 wt.% APP II + 10 wt.% PENTA formulation achieves 57.25 MPa. The modulus of elasticity, as shown in Figure 3.36b, provides insight into the stiffness of the formulations. The reference formulation exhibits a modulus of 3051 MPa, with the 20 wt.% APP I formulation showing a slight decrease to 2994 MPa. Meanwhile, the 20 wt.% APP II formulation remains relatively stable at 3024 MPa, indicating that APP II has a lesser impact on stiffness than APP I. Interestingly, the combination formulations show an increase in stiffness, with the 10 wt.% APP I + 10 wt.% PENTA formulation increasing to 3339 MPa and the 10 wt.% APP II + 10 wt.% PENTA formulation reaching the highest value at 3654 MPa. This increase suggests that while flexural strength declines, the synergy between APP and pentaerythritol enhances stiffness, possibly due to modifications in the cross-linking density of the polymer matrix. The reference formulation exhibits a modulus of 3051 MPa, while the 10 wt.% APP I + 10 wt.% PENTA and 10 wt.% APP II + 10 wt.% PENTA formulations achieve the highest stiffness at 3339 MPa and 3654 MPa, respectively. This suggests that while APP decreases strength, it enhances stiffness due to changes in cross-linking density. The flexural strain at break, depicted in Figure 3.36c, illustrates the ductility of the formulations. The reference formulation exhibits the highest strain at 2.7%, signifying its superior flexibility. The addition of APP fillers leads to a reduction in strain, with the 20 wt.% APP I formulation decreasing to 2.1% and the 20 wt.% APP II formulation maintaining slightly greater ductility at 2.425%. The combination formulations further reduce strain at break, particularly in the 10 wt.% APP I + 10 wt.% PENTA formulation, which demonstrates the lowest strain value at 1.15%, while the 10 wt.% APP II + 10 wt.% PENTA formulation shows a strain of 1.9%. These reductions confirm that while pentaerythritol promotes early degradation, it also leads to decreased ductility, as evidenced by the lower strain values. The reference formulation exhibits the highest strain at 2.7%, whereas APP-containing formulations reduce this value. The 20 wt.% APP I and 20 wt.% APP II formulations exhibit strains of 2.1% and 2.425%, respectively. The combination formulations further decrease strain, particularly the 10 wt.% APP I + 10 wt.% PENTA formulation, which reaches the lowest strain at 1.15%. The flexural analysis effectively highlights the complex interplay between flame retardant fillers and mechanical performance. The incorporation of APP fillers, partic-

ularly in combination with pentaerythritol, results in a trade-off between strength and stiffness.

3.2.Influence of the additives on the physicochemical properties

3.2.1.Thermal stability

Figures 6.6 and Table 6.1 summarize the thermogravimetric analysis (TGA) results of APP I, APP II, and pentaerythritol powders, as well as the REF DEGBA-DETA reference system and its modified formulations. These data provide insight into the thermal degradation behavior of the individual components and their influence on the thermal stability of the adhesive matrix. Figure 6.6a presents the TGA curves for APP I and APP II powders, performed in a nitrogen environment at a heating rate of 10°C/min. The thermal degradation profiles of these flame retardants exhibit distinct differences attributed to their molecular weights. APP I, characterized by a lower molecular weight, undergoes earlier degradation, with an onset degradation temperature (T%) of 133°C, compared to 264°C for APP II. This trend is further reflected in the maximum degradation temperature (T), with APP I reaching 202°C, whereas APP II degrades at a significantly higher temperature of 320°C. These results confirm the increased thermal stability of APP II over APP I, which is likely due to differences in chain length and decomposition pathways. In contrast, pentaerythritol follows a distinct degradation pattern, with a T% of 209°C and a T of 245°C, placing it between APP I and APP II in terms of thermal stability. Figure 6.1b compares the degradation profiles of the modified formulations against the REF DEGBA-DETA system. The reference formulation exhibits a T% of 355°C and a T of 374°C, demonstrating its inherent thermal stability. However, the introduction of APP fillers significantly lowers these degradation temperatures, indicating a catalytic effect on decomposition. The 20 wt.% APP I formulation presents a T% of 278°C and a T of 332°C, whereas the 20 wt.% APP II formulation exhibits slightly improved thermal stability with a T% of 303°C and a T of 337°C. As expected, the addition of pentaerythritol further accelerates the degradation process. The 10 wt.% APP I + 10 wt.% PENTA formulation shows a T% of 222°C, while the 10 wt.% APP II + 10 wt.% PENTA formulation degrades at a slightly higher onset temperature of 240°C. Both formulations degrade at lower temperatures than their respective single APP-based formulations, confirming that the presence of pentaerythritol enhances thermal degradation kinetics. Notably, when

APP and pentaerythritol were combined, they exhibited a synergistic effect, further lowering the temperature range for degradation initiation, with significant decomposition occurring between 200°C and 300°C. These findings align closely with the debonding test results, supporting the hypothesis that APP I-modified formulations exhibit debonding at lower temperatures compared to APP II-based systems. Furthermore, the presence of pentaerythritol accelerates early thermal activation, thereby facilitating earlier adhesive bond failure confirming the synergy between APP and pentaerythritol.

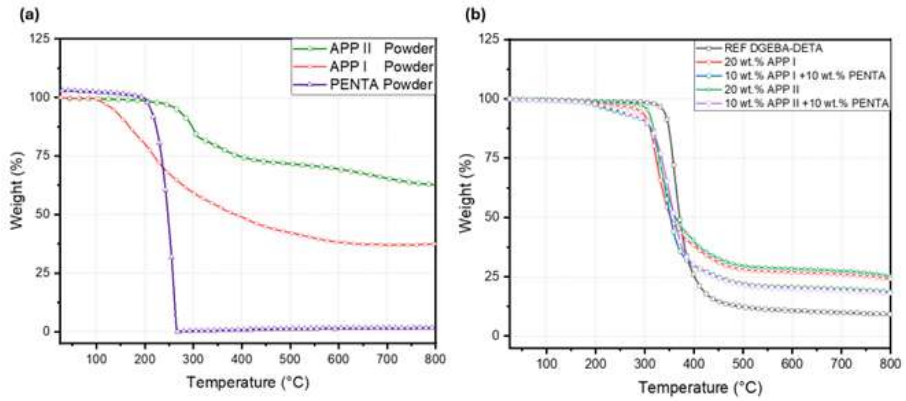

Figure 6.6: Thermogravimetric analysis (TGA) profiles of APP I, APP II, and pentaerythritol (PENTA) powders (a), and REF DEGBA-DETA with modified adhesive formulations (b).

Table 6.1: Onset (T%) and maximum (T) degradation temperatures of REF DEGBA-DETA and modified adhesive.

Formulation	**TOnset 5% (°C)**	**T Max (°C)**
REF DGEBA-DETA	355	374
APP I POWDER	133	202
APP II POWDER	264	320
PENTA POWDER	209	245
20 wt.% APP I	278	332
10 wt.% APP I + 10 wt.% PENTA	222	335
20 wt.% APP II	303	337
10 wt.% APP II+ 10 wt.% PENTA	240	345

3.2.2.Dispersion and morphology

Scanning electron microscopy (SEM) analysis provides further insight into the dispersion and morphology of fillers within the adhesive matrix. The micrographs reveal key differences in filler distribution and agglomeration, directly influencing mechanical performance. For the 20 wt.% APP I formulation, as shown in Figure 6.7a, the SEM images show a uniform distribution of APP I particles within the resin matrix. The presence of relatively large, well-dispersed APP I crystals explains the minimal loss in mechanical properties observed in mechanical testing. Conversely, as shown in Figure 6.7b, the 10 wt.% APP I + 10 wt.% PENTA formulation exhibits a markedly different morphology. While the APP I fillers remain visible and distributed throughout the matrix, the SEM images clearly depict significant agglomeration of pentaerythritol particles. This intense clustering of PENTA is likely responsible for the pronounced loss in mechanical properties observed in this formulation. The agglomeration leads to weak points in the adhesive, disrupting stress distribution and creating localized failure sites, ultimately reducing the overall joint strength. These observations reinforce the hypothesis that the incorporation of APP I contributes to enhanced mechanical stability, while the addition of pentaerythritol, despite promoting thermal degradation, negatively impacts mechanical performance due to filler aggregation.

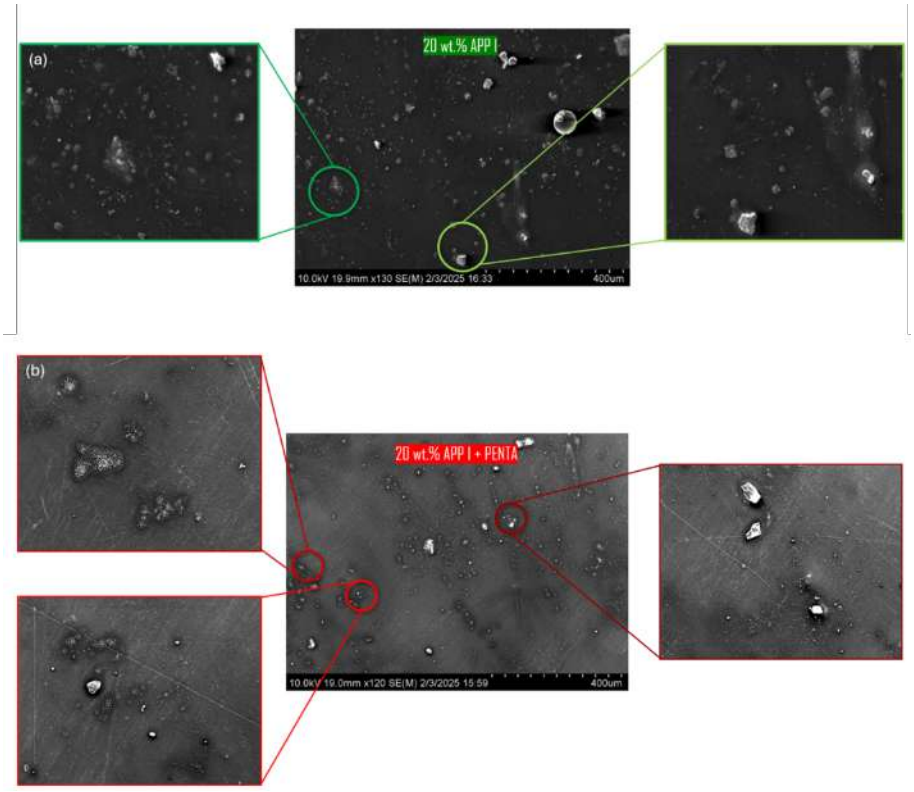

Figure 6.7: SEM Micrographs of Modified Resin Samples: Surface Morphology Comparison of 20 wt.% APP I and 20 wt.% APP I + PENTA Formulations.

3.2.3.Thermomechanical properties

DMA was conducted to assess the viscoelastic properties of the modified formulations, focusing on storage modulus (Figure 6.8a), loss modulus (Figure 6.8b), and tan δ (Figure 6.8c). The results highlight the influence of APP fillers and pentaerythritol on mechanical performance and thermal transitions. The storage modulus results indicate reinforcement effects in formulations containing APP I and APP II, with both exhibiting increased stiffness compared to the REF DEGBA-DETA formulation. The storage modulus results as elucidated in Figure 8a indicate reinforcement effects in formulations containing APP I and APP II, with both exhibiting increased stiffness compared to the REF DEGBA-DETA formulation. The reference formulation has an initial storage modulus of 2000 MPa, while the 20 wt.% APP I and 20 wt.% APP II formulations achieve 2250 MPa and 2300 MPa, respectively. However, the addition of pentaerythritol leads to a reduction in storage modulus, with the 10 wt.% APP I + 10 wt.% PENTA and 10 wt.% APP II + 10 wt.% PENTA formulations showing lower values, though still exceeding the reference. The rate of modulus degradation is notably higher for APP I-based formulations, particularly with pentaerythritol, suggesting faster mechanical softening with temperature. The loss

modulus results, as illustrated in Figure 6.8b, demonstrate a shift in relaxation dynamics. The REF DEGBA-DETA formulation exhibits a peak at 160°C, whereas the APP I and APP II formulations shift to 150°C and 155°C, respectively, indicating modified molecular mobility. The peak intensity is also affected, with the 20 wt.% APP II formulation displaying the highest peak 220 MPa, suggesting increased energy dissipation. In contrast, the addition of pentaerythritol reduces peak intensity, with the 10 wt.% APP I + 10 wt.% PENTA formulation showing the lowest peak at 120 MPa, indicative of reduced damping capacity and potential embrittlement. The tan δ analysis, shown in Figure 6.8c, further elucidates the influence of fillers on the adhesives thermal transition. The REF DEGBA-DETA formulation exhibits a Tg of 153°C. The incorporation of APP fillers alone increases Tg, with 20 wt.% APP I and 20 wt.% APP II formulations reaching 161°C and 163°C. However, the presence of pentaerythritol induces a plasticizing effect, reducing Tg relative to the APP-only formulations. The 10 wt.% APP I + 10 wt.% PENTA formulation exhibits the most pronounced reduction with a tg value of 147°C, while the 10 wt.% APP II + 10 wt.% PENTA formulation shows a slightly higher Tg of 149°C. These findings confirm that APP enhances the structural rigidity of the adhesive, as evidenced by the increased storage modulus, whereas pentaerythritol acts as a plasticizer, promoting polymer chain mobility (lower storage modulus and higher loss modulus at low temperature) and reducing Tg, which facilitates softening of the adhesive matrix.

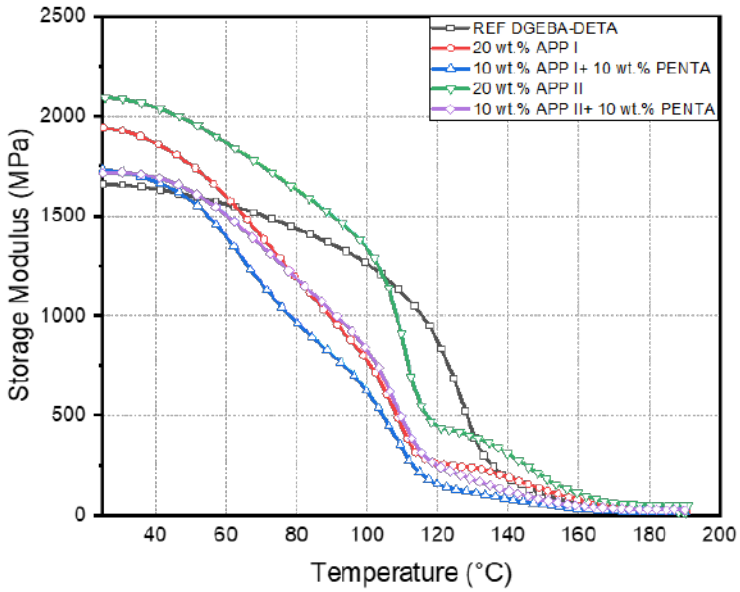

(a) Storage Modulus

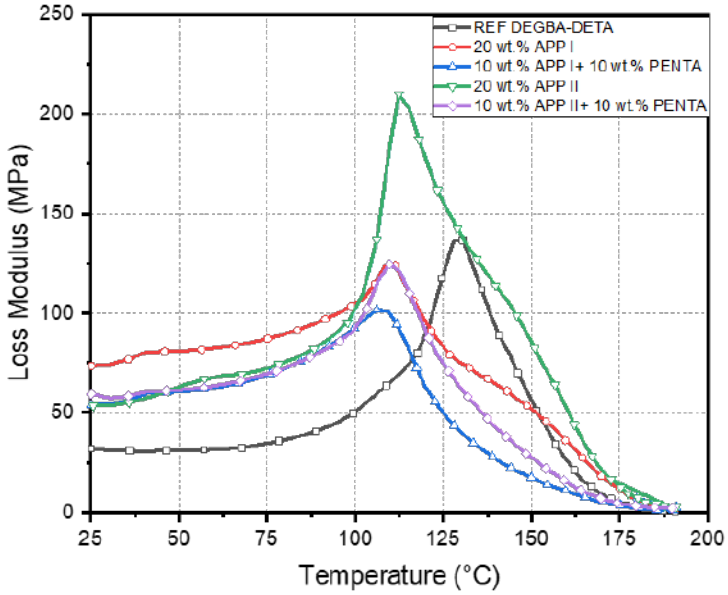

(b) Loss Modulus

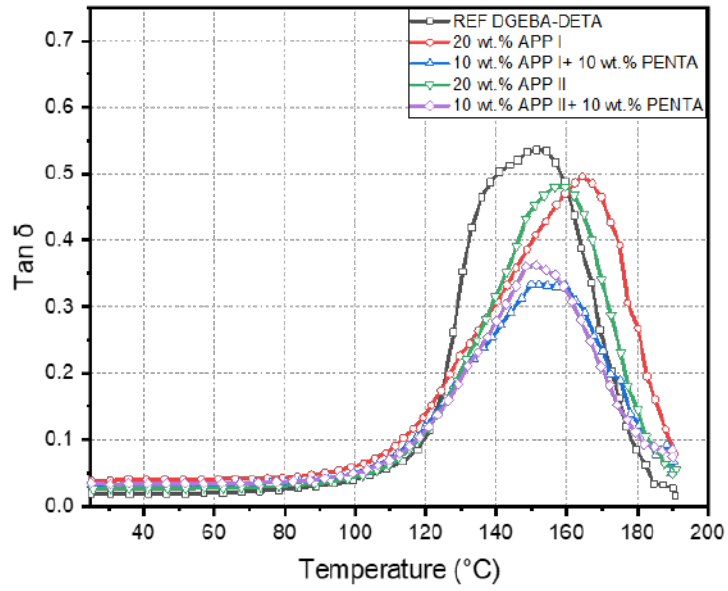

(c) Tan δ

Figure 6.8: Dynamic Mechanical Analysis (DMA) of REF DEGBA-DETA and Modified Formulations: (a) Storage Modulus, (b) Loss Modulus, and (c) Tan as a Function of Temperature.

Table 6.2: Glass transition temperatures of all modified formulations .

Formulation	Tg (°C)
REF DGEBA-DETA	153
20 wt.% APP I	161
10 wt.% APP I + 10 wt.% PENTA	147
20 wt.% APP II	163
10 wt.% APP II+ 10 wt.% PENTA	149

3.3.Micro-CT analysis

High-resolution micro-tomography was employed to investigate the thermally induced evolution of porosity in modified resin samples and its role in adhesive joint failure. All results are summarized in Figure 6.9, providing a comprehensive visualization of porosity distribution before and after thermal exposure. Figure 6.9a illustrates that the 20 wt.% APP I resin initially presents a porosity of 0.89% at room temperature. Following thermal exposure at 250°C for 15 minutes (Figure 6.9b), porosity increases significantly to 11.82%, indicating substantial micropore formation throughout the matrix. This pronounced rise suggests that the thermal activation of APP I promotes void formation both at the bulk and surface levels of the material. Similarly, the 10 wt.% APP I + 10 wt.% PENTA formulation exhibits an initial porosity of 0.55% at room temperature (Figure 6.9c), lower than that of the APP I-only formulation. However, after thermal exposure at 200°C (Figure 6.9d), the porosity sharply increases to 12.56%, surpassing the porosity observed in the APP I system despite the lower temperature threshold. This void formation occurring at lower temperature highlights the synergistic effect of APP I and pentaerythritol, confirming that the addition of pentaerythritol lowers the degradation onset temperature and enhances porosity development. The substantial increase in porosity across both systems directly correlates with the degradation mechanisms observed in debonding tests and thermogravimetric analysis. The APP I formulation undergoes a more gradual thermal activation process, whereas the combination of APP I and pentaerythritol induces a more rapid structural breakdown, as evidenced by the sharp increase in porosity at a lower temperature. Both resin systems displayed porosity increases extending beyond the surface to the internal structure, as visualized in the 3D tomographic reconstructions. In the context of adhesive joints, this pervasive porosity throughout the bulk plays a critical

role in the degradation mechanism.

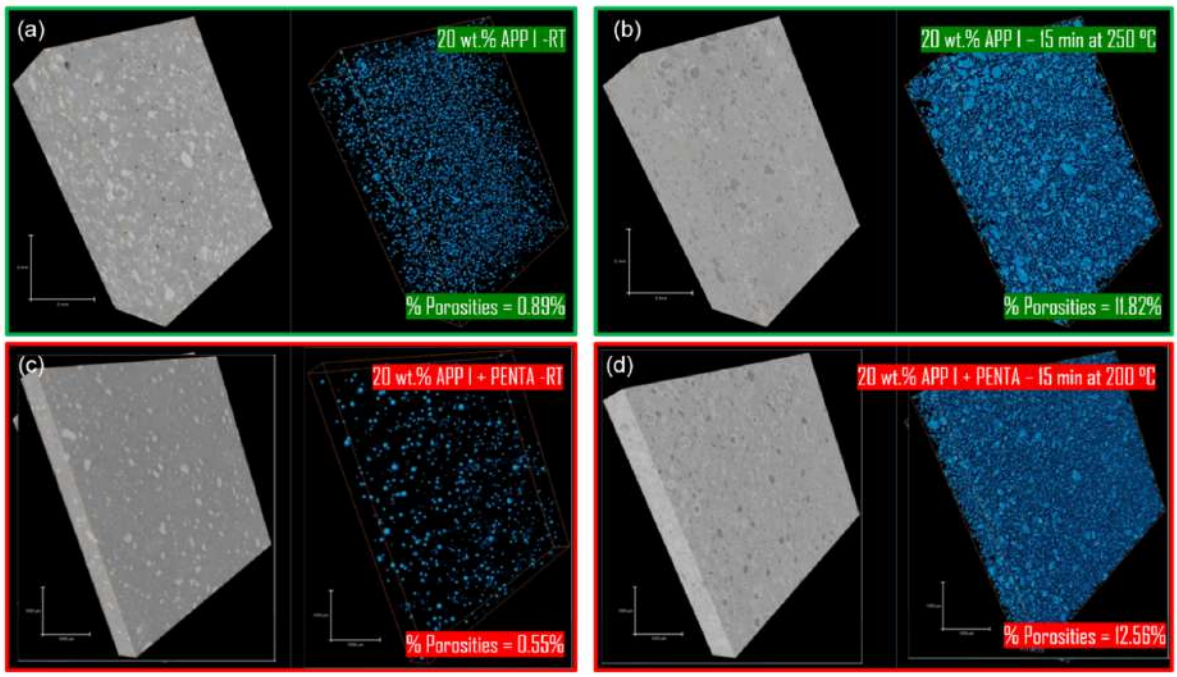

Figure 6.9: Micro-CT Analysis of Porosity in Modified Resin Formulations, (a) 20 wt.% APP I at Room Temperature, (b) 20 wt.% APP I After 15 min at 250°C, (c) 20 wt.% APP I + 10 wt.% PENTA at Room Temperature, (d) 20 wt.% APP I + 10 wt.% PENTA After 15 min at 200°C.

3.4.Recycling experiment

3.4.1.SEM analysis of the surfaces

To evaluate the effectiveness of debonding and substrate reuse, scanning electron microscopy (SEM) and energy-dispersive spectroscopy (EDS) were conducted on the substrate surface at different stages: before bonding, after debonding, and after surface cleaning. The results, summarized in Figure 6.10 and Table 6.3, provide insight into the surface composition, the presence of adhesive residues, and the extent of substrate recovery. Prior to adhesive application, the substrate surface (Figure 6.10a) exhibits a well-defined, clean metallic morphology, with EDS confirming that aluminum (89.32 wt.%) is the sole detected element in Zone 1 (Table 6.3). The absence of carbon or phosphorus suggests that the surface is free of contaminants or pre-existing residues, providing an optimal bonding interface. After debonding (Figure 6.10b), three distinct zones emerge, each characterized by varying degrees of residue accumulation and porosity formation. Zone 1 remains relatively free of adhesive residues, with EDS detecting primarily aluminum (86.85 wt.%)

and a minor phosphorus content (3.04 wt.%). The near-complete absence of carbon suggests minimal adhesive retention in this region. In contrast, Zone 2 exhibits a substantial increase in carbon content (75.15 wt.%), indicating significant adhesive residue accumulation. The presence of phosphorus (4.37 wt.%) further confirms that the residues originate from the flame-retardant-modified adhesive. Structurally, SEM imaging reveals extensive microporosity within this zone, with some pores coalescing into larger cavities, suggesting thermal and mechanical degradation of the adhesive matrix during debonding. Zone 3 shifts toward a phosphorus-rich phase, with phosphorus content reaching 26.63 wt.% and carbon present at 26.6 wt.%, suggesting a localized variation in adhesive degradation behavior or interaction with the substrate. The depth of the residue layer in Zone 2 appears more substantial, whereas Zone 3 presents a thinner, more phosphorus-concentrated residue layer. Following mechanical and solvent-based surface cleaning (Figure 6.10c), significant residue removal is evident, though some adhesive remnants persist. Two distinct zones remain: Zone 1 is nearly identical to the pre-bonding state, with EDS confirming aluminum (96.29 wt.%) as the primary element detected, indicating effective removal of adhesive layers. Zone 2 still contains residual adhesive, with a dominant carbon content of 76.57 wt.% and a significantly reduced phosphorus concentration of 3.34 wt.%. Compared to Zone 2 before cleaning, this indicates that phosphorus-based residues are easier to remove than carbonaceous ones, likely due to differences in adhesion properties or degradation mechanisms. The recycling experiment demonstrates that the cleaning process effectively restores substrate surfaces for potential reuse, though challenges remain in fully eliminating adhesive remnants. While some adhesive remnants persist, particularly in resin-rich areas, phosphorus-containing residues are more readily eliminated than carbonaceous residues. Additionally, SEM observations confirm that the cleaned surface exhibits a more uniform and thinner residual layer compared to the post-debonding state, suggesting improved substrate conditions for potential rebonding applications.

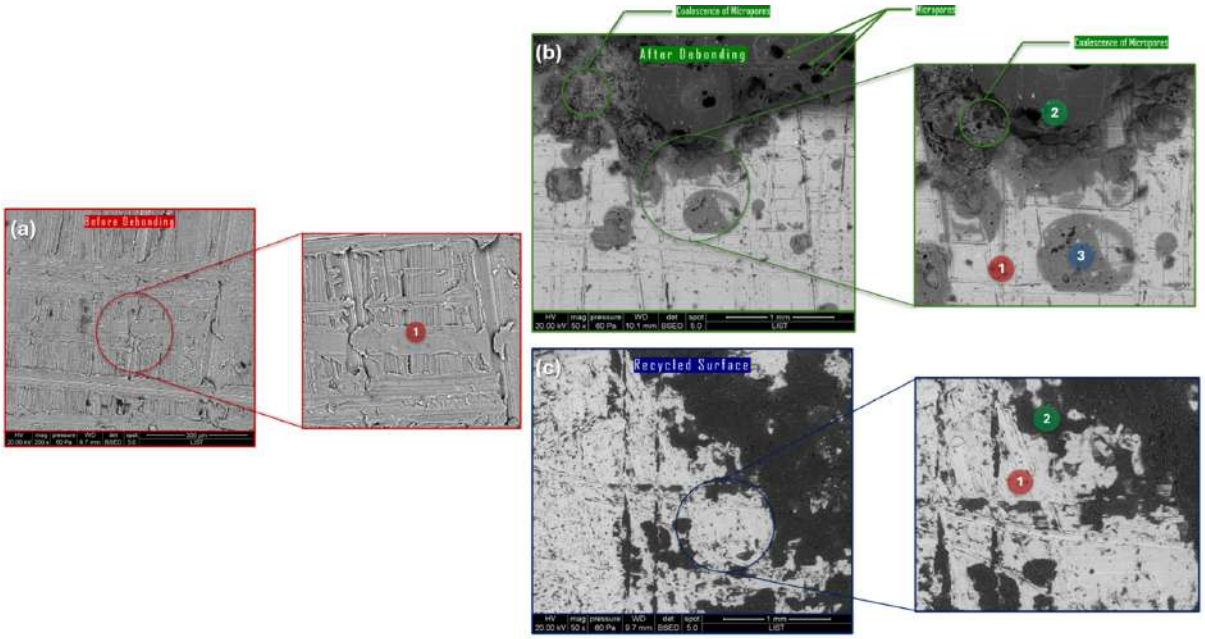

Figure 6.10: SEM observation of the substrate surface at different states, Before Bonding, After debonding and recycled surface.

Table 6.3: Elemental composition (wt.%) in different zones of the substrate before and after debonding, and in the recycled substrate.

Substrate	**Before debonding**			**After debonding**			**Recycled**		
Element (wt.%)	Al	C	P	Al	C	P	Al	C	P
Zone 1	89.32	0	0	86.85	0	3.04	96.29	0	0
Zone 2	-	-	-	2.93	75.15	4.37	8.74	76.57	3.34
Zone 3	-	-	-	9.03	26.6	26.63	-	-	-

3.4.2.Recycled joint strength

The mechanical integrity of the recycled substrates was evaluated using Single Lap Shear (SLS) testing, with results presented in Figure 6.11. To enable direct comparison, all values were normalized to the reference REF DEGBA-DETA formulation. The observed trends in SLS strength not only align with but also validate the findings from joint strength testing, confirming the influence of filler addition and substrate preparation on adhesive performance. The reference DEGBA-DETA formulation serves as the baseline, exhibiting 100% relative SLS strength. The addition of APP fillers alone affects mechanical performance differently: the 20 wt.% APP I formulation reduces SLS strength to 85%, while the 20 wt.% APP II formulation enhances it to approximately 125%, highlight-

ing the reinforcing effect of APP II. However, formulations incorporating pentaerythritol show a substantial decline in adhesive performance. The 10 wt.% APP I + 10 wt.% PENTA formulation results in a 60% SLS strength fraction, whereas the 10 wt.% APP II + 10 wt.% PENTA formulation reaches only 70%, demonstrating the adverse impact of pentaerythritol on joint integrity. The most significant reduction is observed in the non-treated post-debonding substrates, which retain only 25% of their initial SLS strength, demonstrating the detrimental effect of adhesive residues on bonding performance by preventing proper adhesion to the substrate. In contrast, the recycled substrates, following mechanical and solvent-based cleaning, recover approximately 100% of the original SLS strength, confirming their viability for reuse and their potential to restore adhesive performance. The comparison between non-treated and recycled substrates highlights the necessity of surface preparation in ensuring bond performance, reinforcing the need for optimized cleaning methodologies in adhesive recycling applications.

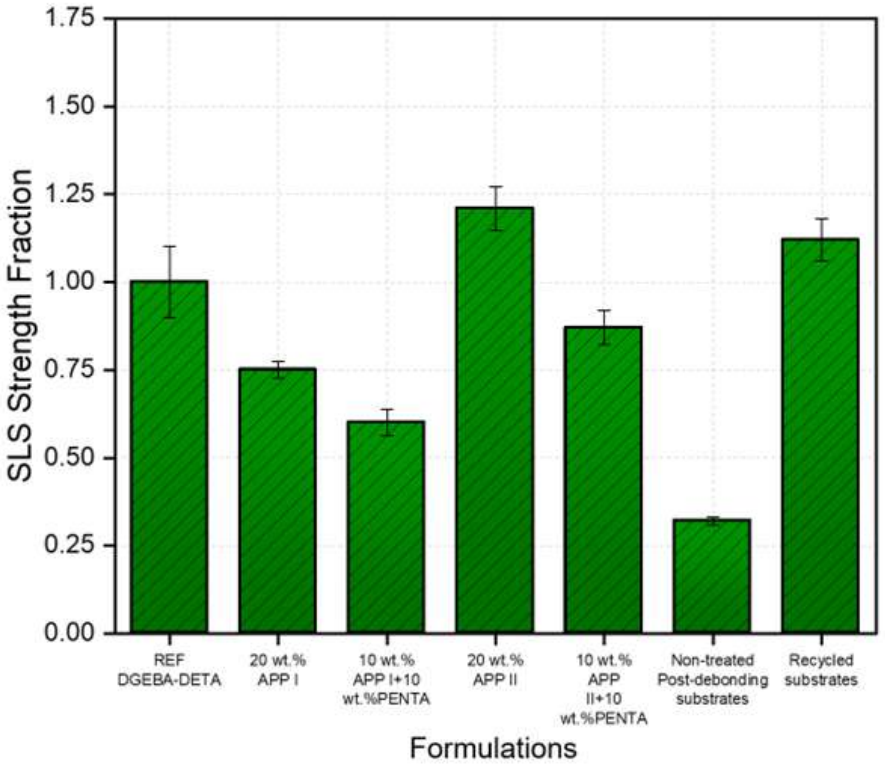

Figure 6.11: Single Lap Shear (SLS) Strength of Reference, Modified, and Recycled Substrates.

4.Discussion

The use of ammonium polyphosphates as a debonding technology has been previously documented, demonstrating that the incorporation of conventional flame retardants into structural adhesives effectively reduces debonding temperatures while maintaining joint strength. This validation highlights their efficiency in preserving mechanical integrity while enabling controlled adhesive failure. Building upon this foundation, the present study advances the research by utilizing short-chain APP I, aiming to further enhance the debonding ability and expand the applicability of this approach. Intumescent flame retardants, particularly APP-based systems, have shown significant promise as debonding agents due to their ability to thermally activate and induce failure at targeted temperatures. This study systematically investigates the role of APP I in lowering debonding temperatures compared to its previously studied counterpart, APP II, by evaluating its effect across multiple characterization techniques. Additionally, the incorporation of pentaerythritol, a secondary carbon source, is explored to assess its synergistic role in modifying degradation behavior and further optimizing the debonding mechanism. To the authors best knowledge, this study represents the first in-depth investigation into how short-chain APP I improves adhesive debonding in structural joints. The methodology employed for determining debonding temperatures follows a consistent approach with previous studies, ensuring comparability across different flame-retardant additives and formulations. The mechanical performance of adhesive joints was evaluated to assess the impact of APP fillers on joint strength. The incorporation of APP I and APP II resulted in distinct mechanical behaviors, demonstrating the influence of molecular weight and chemical structure on adhesion properties. While APP II led to a 25% increase in joint strength relative to the reference, indicating a reinforcing effect, APP I caused a minor reduction in joint strength due to differences in interfacial bonding and filler dispersion. The presence of pentaerythritol, however, introduced a more pronounced weakening effect, with joint strength reductions reaching 40%. This loss in mechanical performance can be attributed to pentaerythritol plasticizing effect, leading to microcomposite softening and a decrease in cohesion. Despite the reduction in joint strength observed in certain formulations, the overall results confirm that APP-based modifications do not compromise mechanical performance beyond acceptable limits for structural adhesives. Second, the evaluation of debonding performance further reinforces these findings, demonstrating that APP-modified formulations enable thermally induced separation at well-defined tempera-

tures. The debonding temperature varied depending on APP type and formulation, with short-chain APP I facilitating earlier failure than APP II. The most efficient formulation, containing 10 wt.% APP I + 10 wt.% PENTA, exhibited the lowest debonding temperature of 175°C, confirming the role of pentaerythritol in accelerating thermal activation. In contrast, APP II-based formulations-maintained adhesion at higher temperatures, with debonding occurring at 250°C, before undergoing failure, suggesting strong filler-filler interactions or a synergistic effect between APP and pentaerythritol. Additionally, failure mode observation provides information into the underlying debonding mechanisms by evaluating how adhesive failure evolves under thermal activation. Prior to debonding, failure in the reference system was predominantly cohesive, indicating strong interfacial bonding between the adhesive and substrate [277]. However, the introduction of APP fillers altered the failure behavior, leading to a transition from adhesive failure to cohesive and near-interface failures. This change is attributed to the thermal activation of APP, which initiates porosity formation within the adhesive matrix, weakening the internal structure and facilitating cohesive failure. Given the notable influence of APP fillers on adhesive joint performance, it was important to examine their impact at the bulk resin level to better understand their interaction with the polymer matrix. Flexural testing provided key insights into the mechanical integrity of the resin, particularly in terms of stiffness, strength, and ductility. The incorporation of APP fillers led to a reduction in flexural strength. For example, the 20 wt.% APP I formulation showed a decrease in flexural strength from 75.3 MPa (REF DGEBA-DETA) to 52 MPa. However, this effect was counterbalanced by an increase in stiffness, especially when pentaerythritol was present. For instance, the 10 wt.% APP I + 10 wt.% PENTA formulation exhibited a flexural modulus of 3339 MPa, compared to 3051 MPa for the reference. Nevertheless, this combination also resulted in increased brittleness, as reflected by the decrease in strain at break. The 10 wt.% APP I + 10 wt.% PENTA formulation showed a reduction in strain at break from 2.7% (REF DGEBA-DETA) to 1.15%, indicating reduced ductility. These results highlight a clear trade-off between reinforcement and material fragility, showing that while flame retardant additives improve stiffness, they simultaneously reduce flexibility and toughness. This trade-off must be considered across different adhesive joint setups and configurations, as the mechanical response of adhesive joints can vary depending on adhesive thickness, filler distribution, and localized stress concentrations. Moreover, physicochemical characterization was performed to investigate the thermal stability, degradation mechanisms, and their direct impact on adhesive performance. Thermogravimetric analysis showed that the reference formulation exhibited an

onset degradation temperature (T 5%) of 355°C, while the 20 wt.% APP I formulation degraded at 278°C and the 20 wt.% APP II formulation at 303°C. The addition of pentaerythritol further reduced the onset degradation temperature, with the 10 wt.% APP I + 10 wt.% PENTA formulation degrading at 222°C and the 10 wt.% APP II + 10 wt.% PENTA formulation at 240°C. Thermogravimetric analysis confirmed that APP I degrades at a lower temperature than APP II, and the addition of pentaerythritol further accelerates degradation, reducing the onset temperature and facilitating a more rapid loss of structural integrity. These results align with the debonding temperatures, confirming that the lower thermal stability of APP I-based formulations correlates with their earlier debonding behavior. To further understand the structural implications of APP incorporation, a morphological analysis was performed to assess the distribution of fillers, the formation of porosities, and the structural changes occurring during thermal activation. SEM imaging confirmed that APP I fillers were well-dispersed within the resin matrix, though their relatively large crystal size contributed to minimal mechanical property loss. In contrast, formulations containing 10 wt.% APP I + 10 wt.% PENTA exhibited significant filler agglomeration, particularly with pentaerythritol, which resulted in a pronounced reduction in mechanical strength. The microstructural evaluation revealed that pentaerythritol-rich areas formed clusters, limiting uniform resin-filler interaction and generating stress concentration zones that contributed to premature failure. Moving forward, dynamic mechanical analysis was conducted to assess the storage modulus, loss modulus, and damping behavior of the modified formulations. The storage modulus results indicated that formulations containing APP I and APP II exhibited an increase in stiffness compared to the reference, with the 20 wt.% APP I formulation increasing by 12% and the 20 wt.% APP II formulation increasing by 15%, reinforcing their structural integrity. However, the addition of pentaerythritol led to a reduction in storage modulus, with the 10 wt.% APP I + 10 wt.% PENTA formulation showing a 9% decrease compared to APP I alone, though the values remained higher than those of the unmodified adhesive. A notable trend was the faster degradation rate observed in APP I-based formulations, particularly when combined with pentaerythritol, suggesting an accelerated loss of mechanical integrity at elevated temperatures. The loss modulus results revealed that all modified formulations peaked at lower temperatures than the reference, with APP I formulations peaking at 110°C, APP II at 114°C, and penta-containing formulations shifting even lower to 107°C, indicating a shift in the materials viscoelastic behavior. While the peak magnitude was generally higher than that of the unmodified system, formulations containing APP I and APP I + PENTA exhibited the lowest values, further emphasizing

the weakening effect of pentaerythritol on mechanical performance. Lastly, the tan delta analysis demonstrated a plasticizing effect with the addition of pentaerythritol, leading to a decrease in the glass transition temperature from 153°C in the reference formulation to 147°C in APP I + PENTA, while APP-modified formulations exhibited an increase, with APP II reaching 163°C due to its reinforcing effect on the polymer network. In contrast, APP-modified formulations exhibited a Tg increase, confirming their stiffening effect on the polymer network. To gain insight into the debonding mechanism, micro-CT analysis was conducted to evaluate the structural evolution of the adhesive matrix during thermal activation. The results demonstrated that as the fillers were activated, significant porosity formation occurred, progressively degrading the mechanical integrity of the resin. Micro-CT analysis quantified this evolution, showing that the 20 wt.% APP I formulation had an initial porosity of 0.89% at room temperature, which increased significantly to 11.82% after exposure to 250°C. A similar trend was observed in the 10 wt.% APP I + 10 wt.% PENTA formulation, where porosity increased from 0.55% at room temperature to 12.56% at the lower activation temperature of 200°C. This difference confirms that the incorporation of pentaerythritol enhances porosity development while reducing the required activation temperature, further facilitating adhesive joint failure under thermal exposure. Complementary to this observation, the chemical mechanism underlying the debonding process is consistent with the well-documented behavior of intumescent flame retardants. Upon thermal degradation, APP undergoes decomposition, releasing phosphoric acid derivatives that catalyze the charring process while simultaneously activating the carbon source, in this case, pentaerythritol. The reaction leads to the release of ammonia (NH_3), which serves as a foaming agent, contributing to the expansion and structural weakening of the adhesive matrix [267–269]. This expansion, coupled with the generation of voids observed in micro-CT analysis, ultimately facilitates adhesive joint failure at controlled temperatures. Finally, to evaluate the potential for substrate reusability, SEM and EDS analyses were conducted to assess the effectiveness of mechanical and solvent-based cleaning methods in restoring adhesive performance. Before debonding, the aluminum substrate exhibited a clean surface with no detectable carbon content. After debonding, distinct zones emerged, indicating variations in residue distribution. Zone 1 showed minimal residue with a slight phosphorus signal, whereas Zone 2 exhibited a high concentration of carbon (76.57%), primarily originating from the adhesive matrix, along with a lower phosphorus content. Zone 3, in contrast, retained a more balanced mix of carbon (26.6%) and phosphorus (26.63%), suggesting an accumulation of phosphorus-rich degradation byproducts. Following mechanical and solvent-based

cleaning, EDS results demonstrated a substantial reduction in surface contamination. Phosphorus-based residues were almost entirely removed, while carbonaceous residues persisted, albeit in a more uniform and thinner layer. The significant reduction in residue thickness suggests that phosphorus-rich degradation products are more easily eliminated than carbon-based residues, which require more aggressive cleaning methods for complete removal. The mechanical evaluation using single-lap shear (SLS) testing confirmed the impact of residual contamination on adhesive performance. Post-debonding, non-treated substrates retained only 25% of their original SLS strength, certainly indicating that a significant part of the residual adhesive creates a weak boundary layer which weakens the adhesive structure after re-manufacturing. In contrast, recycled substrates subjected to cleaning exhibited a complete recovery of SLS strength, reaching nearly 100% of the reference formulation, confirming that the cleaning process successfully restored adhesion properties. The successful restoration of adhesion strength in recycled substrates confirms that APP-based debonding technology enables multiple reuse cycles, making it a viable option for sustainable adhesive applications. Furthermore, the alignment between the standardized SLS testing method and the joint strength evaluation confirms that both approaches follow the same trends, reinforcing the validity of the experimental methodology designed and employed in this study and previous research. To sum up, this study provides a comprehensive evaluation of APP-based debonding systems, demonstrating their effectiveness in lowering debonding temperatures while maintaining an acceptable balance of mechanical properties. The findings confirm that controlled adhesive failure can be achieved through tailored filler selection, with pentaerythritol acting as a key synergist in reducing activation temperatures and enhancing debonding efficiency. Further investigation would be necessary to find another carbon source acting as a synergist, while having a less detrimental effect on the modified adhesive mechanical properties.

5.Conclusion

This study established the effectiveness of short-chain ammonium polyphosphate (APP I) in lowering debonding temperatures, with the 10 wt.% APP I + 10 wt.% PENTA formulation achieving the lowest at 175°C. The addition of pentaerythritol enhanced degradation through increased porosity formation, though at the cost of reduced mechanical strength due to a large plasticization effect. A comprehensive characterization confirmed the relationship between mechanical properties, thermal stability, and debond-

ing efficiency, demonstrating that APP-based formulations maintain an effective balance between structural integrity and controlled failure. The debonding mechanism as well was identified, revealing that thermal activation of APP fillers induces porosity formation, progressively weakening the adhesive matrix and facilitating separation. This behaviour was further enhanced by pentaerythritol, which accelerated degradation and increased void formation. Substrate recyclability assessments further demonstrated the feasibility of reusing debonded substrates, with cleaning protocols successfully restoring nearly 100% of adhesion strength. Our future work will focus on improving cleaning methods, investigating other debonding solution , alternative carbon source synergists, and extending this debonding approach to composite structures to enhance its industrial relevance in sustainable adhesive and structural applications.

Acknowledgements

We kindly acknowledge the support of the Luxembourg National Research Fund (FNR C20/MS/14707266).

7

Summary, conclusions and perspectives

Summary, conclusions and perspectives

1 Benchmarking similar debonding technologies

1.1 Introduction

This section presents a detailed benchmarking framework for thermally responsive technologies used in adhesive debonding. Benchmarking is a critical step in situating the findings of this research within the broader context of existing and emerging debond-on-demand technologies. It facilitates a systematic evaluation of our approach against both commercially available solutions and methods documented in scientific literature, allowing for a clear comparison of performance parameters and identifying the key innovations of this work.

The underlying principle of thermally responsive debonding technologies lies in weakening adhesive cohesion through internal expansion, triggered by heat. Debonding agents are incorporated into the uncured adhesive matrix and remain inert under normal conditions. Upon exposure to a specific thermal stimulus, these agents undergo expansion or release gases, generating porosity and internal stresses that disrupt the adhesive's structural integrity. This process enables the separation of bonded substrates with minimal damage to the adherends. However, for these technologies to be practically viable, the debonding agents must meet stringent performance requirements. These requirements include compatibility with resin systems, stability during the curing process, mechanical performance within operational conditions, and effective debonding activation at controlled temperatures.

Key benchmarking criteria for evaluating thermally responsive debonding technologies include the level of expansion, compatibility with various thermoset resins, and stability under curing and service conditions. It is also essential to assess the impact of debonding agents on the thermal and mechanical properties of the adhesive, particularly at room temperature and within the typical service temperature range, which spans from -55 °C to +200 °C for the aerospace industry for example. Additionally, the activation temperature for debonding must be sufficiently high to prevent unintentional activation during service but low enough to ensure that the debonding process is energy efficient. Another

important factor is the amount of residue left on substrates post-debonding, as excessive residue can hinder the reusability and recyclability of components.

This section will present the results of benchmarking in a summary table, incorporating the aforementioned criteria. The performance of our debonding technologies will be compared to other solutions, with particular emphasis on the two thermoset systems examined in this research: DGEBA/DDS and DGEBA/DETA. This analysis provides a comprehensive evaluation of the thermal and mechanical behavior of our thermally responsive adhesive formulations, thereby supporting future advancements in adhesive bonding technologies and sustainable recycling practices. All the results will be summerized in Table 7.1 and Table 7.2 .

Table 7.1: Benchmarking of Thermally Responsive Debonding Technologies Based on Compatibility, Processing Behavior, Debonding Performance, and Mechanical Properties - Part 1.

Debonding Agent Name	**Commercial Reference**	**Supplier**	**Compatibility**		**Processing Constraints**
			DGEBA/DDS	**DGEBA/DETA**	
Expandable Graphite (EG225)	CXG5B122	ACS Materials	Non-Compatible	Compatible	Not suitable for high-temperature curing. Inhomogeneous mixing, fillers settle fast.
Expandable Graphite (EG250)	CXG00522	ACS Materials	Non-Compatible	Compatible	Not suitable for high-temperature curing. Inhomogeneous mixing, fillers settle fast.
Expandable Graphite (EG300)	CXG00622	ACS Materials	Compatible	Compatible	Not suitable for high-temperature curing. Inhomogeneous mixing, fillers settle fast.
Organo-phosphorus (PCO 900)	AFLAMMIT® PCO 900	Thor Group	Compatible	Compatible	Agglomeration at high loading rates.
Ammonium Polyphosphate (APP)	Exolit AP 422 / AP 740 / TF-201	CIBA Germany / Shifang China	Compatible	Compatible	Agglomeration at high loading rates. Settling of fillers.
Melamine Polyphosphate (MPP)	MELAPUR 200	CIBA Germany	Compatible	Compatible	Agglomeration at high loading rates. Settling of fillers.
Melamine Orthophosphate (MOP)	PMN 185	Thor Group	Compatible	Compatible	Agglomeration at high loading rates. Settling of fillers.
Short-Chain APP	TF-303 / TF-304	Shifang China	Non-Compatible	Compatible	Not suitable for high-temperature curing. Agglomeration and humidity-sensitive fillers.
Short-Chain APP + Pentaerythritol	TF-303 + Pentaerythritol	Shifang China / Sigma-Aldrich	Non-Compatible	Compatible	Not suitable for high-temperature curing. Agglomeration and humidity-sensitive fillers.
Melamine Orthophosphate (MOP) + Pentaerythritol	MOP + Pentaerythritol	Thor Group / Sigma-Aldrich	Compatible	Compatible	Agglomeration at high loading rates.
Ammonium Polyphosphate (APP) + Pentaerythritol	Exolit AP 422 / AP 740 / TF-201	CIBA Germany / Shifang China	Compatible	Compatible	Agglomeration at high loading rates.
Azodicarbon amide Rescoll technology	ADC	Sigma-Aldrich	non-Compatible	Compatible	Not suitable for high temperature extensive curing cycles. Agglomeration at high loading rates. Sensitive to humidity
p-Toluenesulfonyl Semicarbazide	p-TsH	Sigma-Aldrich	non-Compatible	Compatible	Not suitable for high temperature extensive curing cycles. Agglomeration at high loading rates. Settling of the fillers sensitive to humidity
Thermally Expandable Particles (TEP)	TEP	Expancel, Matsumoto	non-Compatible	Compatible	Not suitable for high temperature extensive curing cycles. Agglomeration at high loading rates.

Table 7.2: Benchmarking of Thermally Responsive Debonding Technologies Based on Compatibility, Processing Behavior, Debonding Performance, and Mechanical Properties - Part 2.

Debonding Agent Name	**Temperature of Induced Debonding** ($^{\circ}C$)	**Optimal Loading Rates**	**Effect on Joint Strength at Optimal Loading Rates (% change compared to reference)**	**Visible Intumescence Expansion at** T_{deb}	**Recyclability Potential (Residue left post-debonding and ease of cleaning)**
Expandable Graphite (EG225)	225	10 wt.%	+12%	High	High
Expandable Graphite (EG250)	250	10 wt.%	+33%	Moderate	High
Expandable Graphite (EG300)	300	10 wt.%	+6%	Low	Moderate
Organo-phosphorus (PCO 900)	250-300	20-30 wt.%	+67%	None	Moderate
Ammonium Polyphosphate (APP)	300-350	20 wt.%	+53%	Low	High
Melamine Polyphosphate (MPP)	300-325	20 wt.%	+88%	Low	High
Melamine Orthophosphate (MOP)	275	20 wt.%	+34%	None	Moderate
Short-Chain APP	225-250	20 wt.%	+3%	Low	High
Short-Chain APP + Pentaerythritol	175-200	20 wt.%	-6%	Low	High
APP + Pentaerythritol	250	20 wt.%	+5%	Low	High
MOP + Pentaerythritol	250	20 wt.%	+9%	Moderate	Moderate
Azodicarbonamide (ADC) - Rescoll technology	200–220	10–15 wt.%	-8%	High	High
p-Toluenesulfonyl Semicarbazide	200–220	20 wt.%	-9%	Low	Moderate
Thermally Expandable Particles (TEP)	200–285	10–15 wt.%	N/A	Moderate	Moderate

1.2 Benchmarking and discussion

The benchmarking study provides a comprehensive analysis of thermally responsive debonding technologies by evaluating key parameters, including compatibility, processing behavior, debonding temperature, mechanical reinforcement, expansion behavior, residue removal, and recyclability. These parameters are interrelated, influencing both the performance and application scope of each technology.

Compatibility with adhesive systems such as DGEBA/DDS and DGEBA/DETA depends heavily on the thermal stability of the debonding agents. Technologies such as short-chain APP (TF-303 and TF-304), ADC, and thermally expandable particles (TEP) exhibit limited compatibility with DGEBA/DDS due to their inability to endure the system's high-temperature curing cycles. These agents tend to activate prematurely, causing matrix degradation and weakened mechanical properties. Expandable graphite (EG225 and EG250) faces similar challenges with DGEBA/DDS but performs well in the lower temperature curing environment of DGEBA/DETA. EG300, benefiting from optimized particle size and greater thermal stability, demonstrates compatibility with both systems. By contrast, phosphorus-based flame retardants such as APP, MPP, and MOP maintain high thermal resistance, ensuring strong compatibility across both adhesive systems. This broad adaptability makes phosphorus-based systems suitable for demanding industrial applications.

Processing behavior is influenced by the size and stability of the fillers. Larger particles, such as those in EG225 and EG250, exhibit rapid settling and inhomogeneous mixing during formulation, creating variability in joint properties. Even EG300, with smaller particle size, faces some dispersion challenges. Short-chain APP and ADC suffer from similar issues, particularly under humid conditions that destabilize particle distribution. Phosphorus-based additives such as MPP and APP offer relatively stable dispersion but are prone to agglomeration when loading exceeds 20 wt.%. These constraints highlight the importance of optimized filler dispersion and particle design to ensure stable processing and mechanical performance. Mechanical reinforcement is primarily governed by particle size, distribution, and particle-resin interactions. Well-dispersed additives with strong resin bonding significantly enhance joint strength. For example, MPP at 20 wt.% increases joint strength by 88%, while APP provides a 53% improvement through robust filler-matrix interactions. EG250 achieves moderate reinforcement, improving strength by 33% at 10 wt.% loading, whereas EG225 and EG300 yield smaller gains of 12% and 6%,

respectively. These modest improvements in expandable graphite systems reflect issues related to inconsistent dispersion and aggregation, which reduce the effectiveness of the reinforcement mechanism. Effective mechanical performance requires careful optimization of particle size, uniformity, and resin compatibility.

The debonding temperature influences operational flexibility but does not directly affect mechanical reinforcement. Lower-temperature systems such as ADC (200-220 °C) and short-chain APP with pentaerythritol (175-200 °C) are suitable for applications where rapid debonding and low thermal exposure are necessary. However, these systems tend to exhibit reduced mechanical stability due to weaker structural integration of the filler. Conversely, high-temperature activation systems like MPP and APP (300-350 °C) maintain superior mechanical properties while requiring greater energy input to achieve debonding. Expandable graphite fillers cover a broad temperature range, with EG225 activating at 225 °C, EG250 at 250 °C, and EG300 at 300 °C. This flexibility allows for tailored application-specific performance.

Residue removal and recyclability are crucial parameters for assessing the sustainability of debonding technologies. Systems with high expansion properties, such as ADC, EG225, and short-chain APP, minimize residue by promoting internal matrix disruption during activation. EG225, in particular, demonstrates high recyclability due to its efficient residue reduction at 225 °C. However, rigid thermoset adhesives like DGEBA/DDS, with their high cross-linking density, limit the extent of expansion and thereby retain more residue even with high-expansion agents. In contrast, phosphorus-based systems such as PCO 900, APP, and MPP exhibit moderate expansion and leave manageable residue, which can be mitigated through optimized debonding conditions, such as longer heating durations or higher activation temperatures. These moderate-residue systems strike a balance between structural integrity and recyclability, making them suitable for applications requiring both mechanical performance and manageable cleaning processes.

Recyclability is further enhanced by systems designed to minimize chemical reactions at the interface. High-expansion systems, such as ADC, EG225, and TEP, facilitate straightforward cleaning and reuse by mechanically breaking the adhesive bond without excessive chemical alteration. This results in minimal adhesion residue on the substrate surface, enabling efficient recycling. Systems like MOP and APP II, which interact more strongly with the resin matrix, require additional cleaning but provide enhanced load-bearing properties, which may justify the additional effort in structural applications.

These findings underscore the multifaceted nature of thermally responsive debonding technologies. Expandable graphite systems offer competitive recyclability and residue management, though they face challenges in achieving optimal mechanical reinforcement and dispersion stability. Conversely, phosphorus-based flame retardants provide a well-rounded solution, offering robust mechanical performance, broad compatibility, and adaptable residue control. The ability to optimize these systems through targeted particle engineering and resin formulation enhances their competitiveness across a range of structural and flexible bonding applications. Together, these technologies provide viable pathways for sustainable adhesive bonding and material recycling in industrial settings.

2 Demonstrators and transfer to composites

The transition from adhesive joint studies to practical applications in composite structures is a crucial step in advancing thermally responsive debonding technologies. While the work done through-out this project primarily focused on simple adhesive joint configurations, real-world industrial applications extend also to the need of the implementation of these technologies in complex, multi-material structures. Composite systems, particularly carbon fiber-reinforced polymers (CFRPs) and sandwich panels with honeycomb cores, are extensively used in high-performance sectors such as aerospace, automotive, and renewable energy. Demonstrating successful debonding within these structures is essential to validate the viability of these technologies for large-scale manufacturing, repair, and recycling applications.

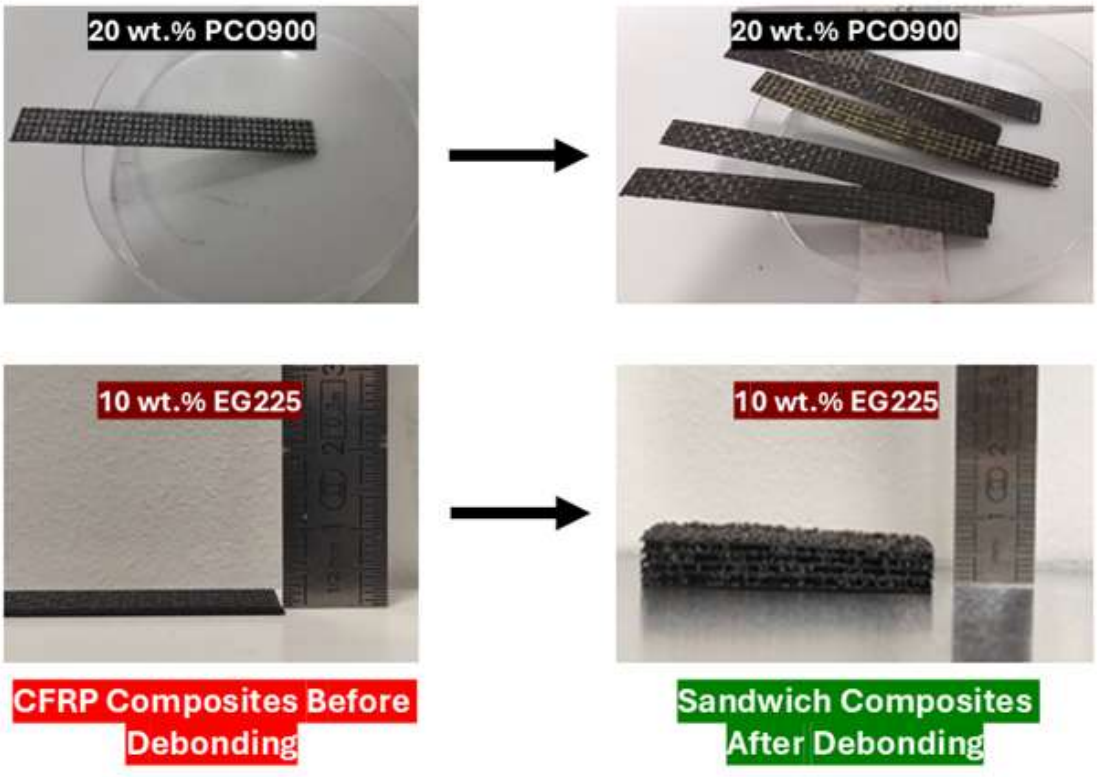

Figure 7.1: Debonding performance of CFRP demonstrators with EG225 and PCO 900 fillers

For this purpose, two debonding technologies PCO 900, a non-intumescent organophosphorus flame retardant, and EG225, an expandable graphite were selected from those discussed in this thesis. These technologies were tested across three demon-

strator configurations: CFRP laminates, sandwich structures with honeycomb cores, and pre-preg-modified CFRP composites designed to induce localized debonding between specific layers. Each configuration aimed to test the effectiveness of these technologies under real structural conditions. Figure 7.1 illustrates the debonding performance in CFRP laminates, Figure 7.2 shows the separation achieved in sandwich structures, and Figure 7.3 highlights the targeted debonding within pre-preg composites. These tests provided critical insights into the success of the debonding process, as well as the influence of heating time and residue accumulation post-activation of the fillers or debonding.

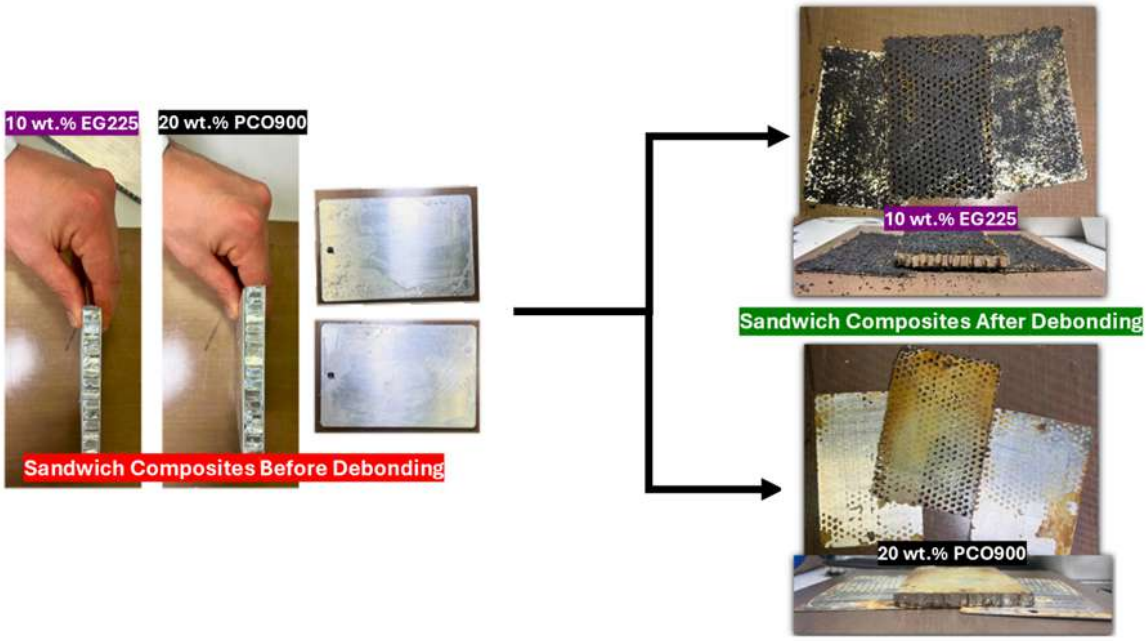

Figure 7.2: Debonding performance of sandwich structures demonstrators with EG225 and PCO 900 fillers

The results confirmed that debonding was successful in all three configurations. In the sandwich structures (Figure 4.1), complete separation of the adhesive skins from the honeycomb core was achieved, demonstrating the potential for effective disassembly in lightweight structural components. The core itself remained structurally intact, supporting the feasibility of reusing both core and skin materials. In the CFRP laminates (Figure 7.2), debonding was localized to specific layers without affecting the surrounding laminate, an essential requirement for selective disassembly in high-performance applications. Similarly, in the pre-preg-modified CFRP composite (Figure 7.3), localized debonding was successfully induced at the sacrificial layer, proving that thermally responsive layers can be integrated within composite structures to facilitate controlled separation between

chosen layers.

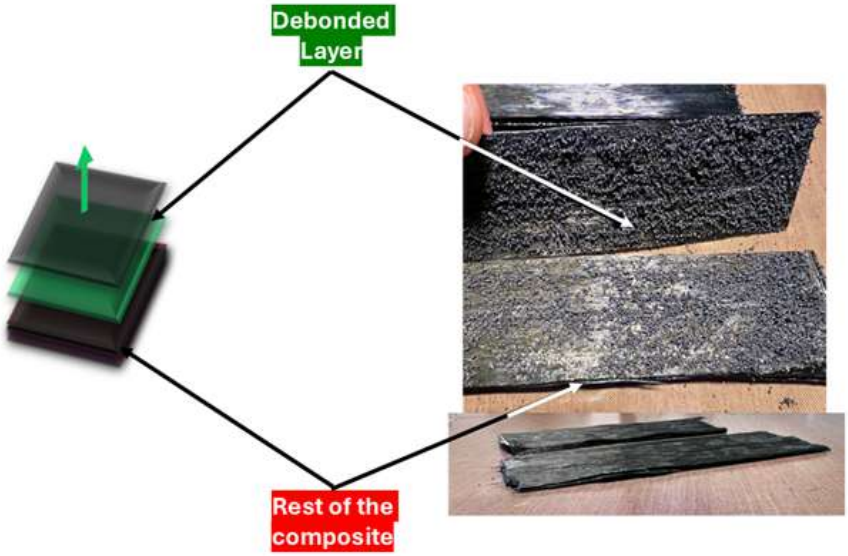

Figure 7.3: Pre-preg targeted debonding demonstrator.

Two critical observations were made during these tests. The first relates to the heating time required for complete debonding. As detailed in the second article, extending the heating duration at the debonding temperature (T°deb) can significantly improve separation by fully activating the debonding agents. In the case of CFRP laminates using expandable graphite (EG), 10 minutes of heating was insufficient, with full debonding occurring only after 15 minutes. For the CFRP laminate incorporating PCO 900, a non-intumescent flame retardant, 25 minutes of heating was necessary to achieve complete separation. This longer heating period reflects the slower activation of non-intumescent systems. By contrast, the sandwich structures required less heating time, with successful separation achieved within 10 minutes, likely due to more efficient heat transfer through the thin adhesive layers and honeycomb core.

The second key observation concerns residue accumulation. Across all configurations, significant residue was found on the debonded surfaces, though the extent varied depending on the structure. In the sandwich structures, residue was more concentrated on the adhesive skins compared to the honeycomb core. In CFRP laminates, residue primarily accumulated on the surface of the carbon fiber textile, consisting of both adhesive remnants and inactive filler particles. This residue was observed in both EG- and PCO 900-based systems, indicating that while mechanical debonding was effective, chemical degradation of the adhesive was incomplete. The residue presents a challenge for re-

manufacturing purposes where clean surfaces are needed for substrate reuse, emphasizing the need for optimization in both formulation and thermal processing. Strategies such as modifying heat cycles or introducing post-debonding cleaning steps may help reduce residue and improve substrate recyclability.

Overall, the demonstrators effectively validated the integration of thermally responsive debonding technologies within complex composite architectures. The successful induction of localized separation in CFRP laminates, sandwich panels, and pre-preg-modified systems highlights the practical feasibility of these approaches for advanced composite disassembly and reuse. This work also culminated in a collaborative research article, currently under review in *Composites Part B*, with Samet Ozygit as first author and myself as second author. In this study, CFRP composites were processed through the entire debonding cycle, achieving complete fiber recovery post-debonding. Nevertheless, further developments are required to refine thermal activation protocols and reduce surface contamination, in order to meet industrial benchmarks for recyclability, process repeatability, and structural integrity.

3 Conclusions

This PhD research investigated the potential use of flame-retardant systems, particularly intumescent and non-intumescent types, as debonding agents in adhesive joints and composite structures. The work spanned multiple studies, each contributing to the validation and development of thermally responsive debonding technologies. The initial study served as a proof of concept, demonstrating that intumescent flame retardants could be successfully integrated into adhesive layers to induce debonding. This research explored and optimized the conditions required for effective debonding, including the appropriate filler loading rates and thermal activation characteristics. In the first publication, intumescent systems such as melamine polyphosphate (MPP) and ammonium polyphosphate (APP) were tested, proving that these materials could facilitate debonding at temperatures around 300-325 °C, depending on the formulation. This work confirmed that intumescent flame retardants not only provided the necessary expansion but also maintained mechanical properties in the adhesive until activation. The second paper expanded the research to PCO 900, a non-intumescent organophosphorus flame retardant, which achieved debonding at a temperature range of 250-300 °C. This study explored an alter-

native mechanism of debonding, driven not by expansion but by the thermal degradation of the resin matrix. The third paper examined the use of EG225, an expandable graphite, which provided flexibility in debonding temperatures, ranging from 225-300 °C, depending on particle size and formulation. Finally, the fourth study pushed the boundaries of the proof of concept by evaluating short-chain APP forms, demonstrating that under optimized conditions, debonding could be achieved at significantly lower temperatures, around 175-225 °C. Across these studies, we successfully validated the original hypothesis that flame retardants could be incorporated into adhesive layers and resin matrices to create effective debonding solutions. Traditionally, flame retardants are used in high concentrations to reduce flammability and, at times, production costs. However, in this work, we identified optimal filling rates that balanced debonding performance, mechanical properties, and processability. These findings revealed critical trade-offs and the need for careful formulation to ensure both structural integrity and reliable debonding performance. Another major contribution of this research was the development of an in-house debonding evaluation method a modified version of the pull-off test. This method provided a practical and reproducible alternative to conventional mechanical testing methods, such as single lap shear tests. As demonstrated in the fourth article, the pull-off test yielded consistent results with greater ease of sample preparation, reduced equipment requirements, and improved flexibility for monitoring debonding behavior. The test also allowed the correlation of mechanical performance and temperature data, enabling the characterization of debonding temperatures, resin degradation, and activation behavior of the debonding agents. Each study included detailed characterization of the modified resins, tailored to the technology under investigation. These characterizations supplemented by existing literature provided the necessary parameters for evaluating mechanical properties, thermal stability, and the mechanisms underlying debonding. Together, these studies equipped this research with a complete framework of knowledge, making the technologies discussed ready for application in industrial adhesive systems. Additionally, this work extended beyond adhesive joints by demonstrating the application of these technologies to more complex composite structures, such as CFRP laminates and sandwich panels. One of the final contributions of this PhD research was the investigation of recycling. This study explored the possibility of substrate reuse after debonding by recycling debonded materials and re-testing their mechanical performance. The results showed that with mild abrasion and solvent cleaning (ethanol), the recycled substrates retained comparable mechanical properties. However, this also highlighted that further research is needed to develop more efficient residue-cleaning technologies, particularly in composite structures.

Such solutions should align with sustainable practices, possibly involving environmentally friendly cleaning agents such as acetic acid. Despite the successes of this research, certain limitations were noted. While the two epoxy adhesive systems chosen DGEBA/DDS and DGEBA/DETA are among the most challenging in terms of curing and debonding, additional testing on other thermosets, such as polyurethanes, would have broadened the applicability of the technology. As discussed in the benchmarking section, systems compatible with rigid thermosets are likely to perform well in more flexible thermosets. Another area for further exploration is the method of delivering these fillers in industrial applications, such as coating or spraying directly onto composites or primers, which could offer additional versatility. In terms of aging performance, although extensive long-term studies were not conducted, this was justified by the existing body of knowledge on the long-term stability of the selected flame-retardant fillers. These materials, including APP, MPP, and EG225, have been widely used and documented in both academic literature and industrial applications for their durability under thermal and environmental conditions. Furthermore, the research priorities of this PhD focused on advancing new debonding technologies rather than dedicating time to extended aging tests. The dissemination of this work was carried out through both traditional methods, such as publications and conferences, and creative approaches, including promotional videos to showcase the technology. Through the guidance of my supervisors and collaboration with my research team, I gained valuable expertise in materials chemistry and scientific research methodologies. Coming from an engineering background focused on practical problem-solving, this experience enabled me to develop a deeper scientific understanding of material behavior, bridging both theoretical and application-oriented perspectives.

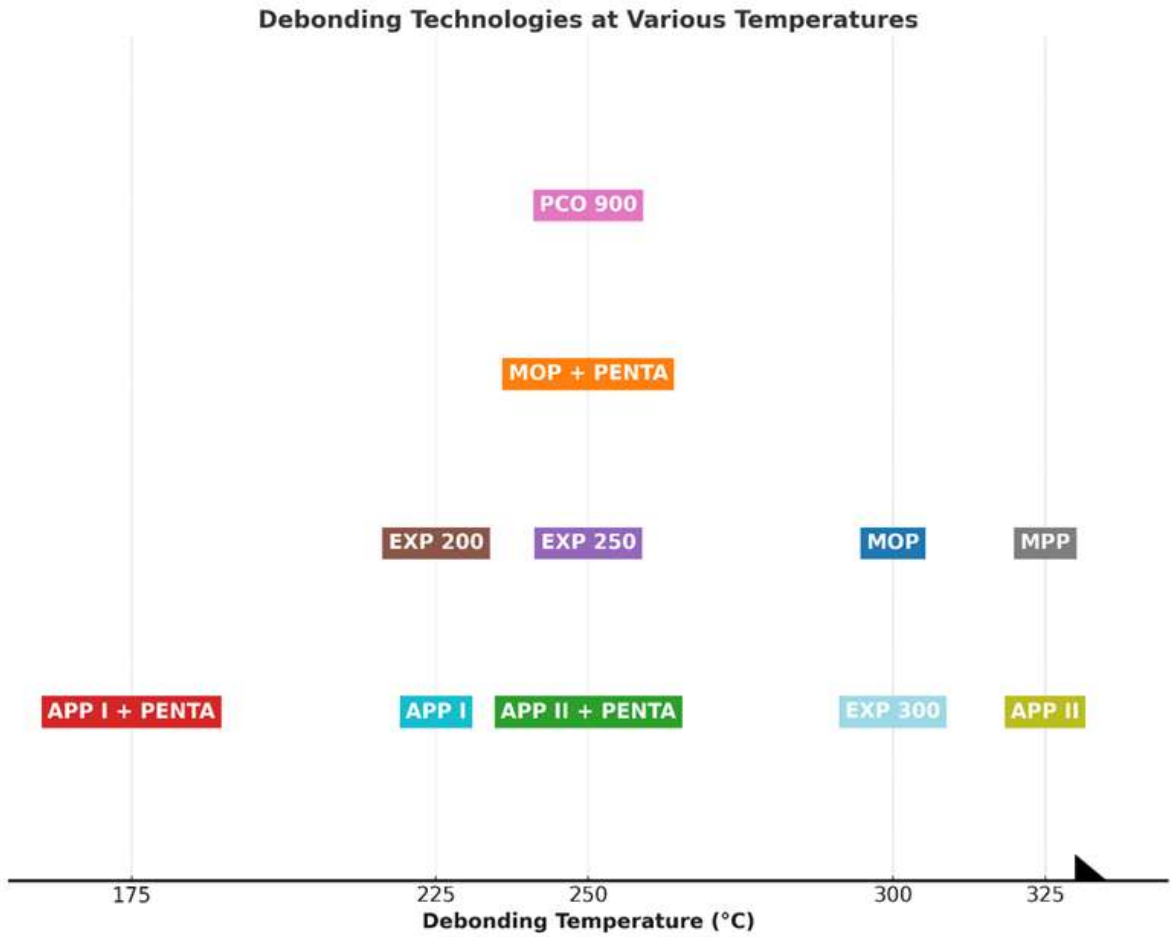

Figure 7.4: Summary of the debonding technologies studied in this thesis and their activation temperatures.

Acronym	Description
APP-I	Short-Chain Ammonium Polyphosphate
APP-II	Ammonium Polyphosphate Phase-II
PENTA	Pentaerythritol
EXP	Expandable Graphite
MPP	Melamine Polyphosphate
MOP	Melamine Orthophosphate
PCO-900	Organo-Phosphorus Compound

Table 7.3: Acronyms and Their Descriptions

4 Perspectives

This PhD research aimed to develop debond-on-demand technologies inspired by flame-retardant systems. Throughout this work, we explored a variety of flame-retardant fillers

and systems to create multi-window debonding technologies. We systematically screened both established and novel possibilities, building on existing literature and previous scientific advancements. The studies conducted within this thesis demonstrated the potential for flame retardants traditionally used to improve flammability resistance in resins and polymers to serve as effective debonding agents when optimized for adhesive joints and composite structures. A key realization I gained during this research is that while conducting innovative experiments and exploring new perspectives is essential, the long-term value of scientific work relies on continuity and the ability to integrate findings into broader research efforts and industrial applications. Ensuring that our technologies can be applied to composite structures and closing the recycling loop without compromising material performance are critical components of this continuity. These efforts are currently being carried forward by my colleague, Samet Ozygit, who is focusing on optimizing composite debonding processes and developing advanced fiber-cleaning methods for post-debonding reuse. Looking forward, several pathways have been identified to expand the scope and applications of the debonding technologies developed in this work. The first pathway involves aligning with current trends in flame-retardant technology, particularly in response to sustainability and health concerns. There is growing demand for environmentally friendly alternatives to conventional flame retardants, as some materials, such as melamine-based compounds, have raised health and safety concerns. To address these challenges, our research has initiated testing of bio-based intumescent flame retardant systems. These systems involve replacing conventional components acid sources, foaming agents, and carbon sources with sustainable, naturally derived alternatives. Examples include cellulose and starch for carbon sources, urea as a foaming agent, and natural acid extracts to activate the system under thermal conditions. The first phase of this research focuses on evaluating the thermal interactions among these components to confirm their compatibility and performance. Once validated, the next step will be to integrate these bio-based systems into adhesive joints and assess their impact on both mechanical properties and debonding efficiency. A second pathway involves enhancing the versatility of debonding technologies through deeper integration into composite structures. One particularly promising approach is to embed debonding agents directly into the sizing of carbon fibers. This strategy could address one of the major challenges identified in this work residue accumulation after debonding. By incorporating debonding agents into the fiber sizing, we could minimize residue on the fiber surfaces, allowing for more efficient recovery and reuse of fibers with reduced cleaning requirements. This method would also enable greater flexibility in resin compatibility, streamline composite fabrication pro-

cesses, and reduce the energy and resources needed for post-debonding recycling. Such advancements would strengthen the position of these technologies as practical, scalable solutions for composite manufacturing. The third pathway focuses on expanding the application of debonding technologies to non-structural bonding markets, which are gaining increasing attention due to the rise in adhesive use in electronic devices. Electronics are typically produced using expensive and rare materials, making their recycling a critical component of the circular economy. Incorporating debond-on-demand technologies into electronic components could enhance recyclability by enabling the efficient separation of bonded parts, thereby facilitating material recovery and improving sustainability. A fourth pathway leverages the advancements in artificial intelligence (AI) and machine learning (ML) to optimize material design and testing. The past few years have seen significant progress in AI-driven technologies, including neural networks, large language models, and data analysis frameworks. During the course of this research, correlations between input parameters such as filler concentration, processing conditions, and curing cycles and performance metrics, including fracture toughness, adhesive strength, and debonding behavior, became evident after extensive data analysis. These relationships were not immediately obvious through conventional experimental methods, highlighting the potential value of a data-driven approach to material optimization. By training ML models on experimental data, it would be possible to predict key material properties, streamline the design process, and reduce the need for time-consuming iterative testing. Such models could provide rapid predictions for new formulations, identify critical performance variables, and ultimately enhance the efficiency of both material development and industrial implementation. These pathways bio-based flame retardant systems, fiber sizing integration, non-structural bonding applications, and AI-driven material optimization represent promising directions for future research. They address the need to continually improve and diversify the technology's capabilities while responding to evolving market demands and sustainability goals. Additionally, they offer opportunities to refine the performance of these technologies in a range of contexts, from large-scale composite manufacturing to precision applications in electronics. While these pathways form the core of our current research focus, many other ideas remain in the conceptual stage, awaiting further development and refinement. These ideas will be explored and materialized in future research efforts within our team. All in all, these were the main ideas that we began exploring, which is why they were discussed in this perspectives section. While many more possible pathways remain at the stage of ideas, these ideas will be developed, worked on, and concretized in the next stages of research by our team.

Bibliography

[1] S. Yamada, A. Kurotani, E. Chikayama, and J. Kikuchi. Signal deconvolution and noise factor analysis based on a combination of timefrequency analysis and probabilistic sparse matrix factorization. *International Journal of Molecular Sciences*, 21, 2020.

[2] A. K. Nizampatnam. Bird strike simulations on composite aircraft structures. In *Proceedings of the SIMULIA Customer Conference*, 2007.

[3] Composites market worth $152.98 billion by 2027. https://www.marketsandmarkets.com/PressReleases/composite.asp, 2019. Accessed: 2019-10-08.

[4] Jürgen Fleischer, Roberto Teti, Gisela Lanza, Paul Mativenga, Hans-Christian Möhring, and Alessandra Caggiano. Composite materials parts manufacturing. *CIRP Annals*, 67:603–626, 2018.

[5] Suschem. Polymer composites circularity, 2018. White Paper.

[6] S. Gharde and B. Kandasubramanian. Mechanothermal and chemical recycling methodologies for the fibre reinforced plastic (frp). *Environmental Technology Innovation*, 14:100311, 2019.

[7] S. Job. Recycling glass fibre reinforced composites - history and progress. *Reinforced Plastics*, 57:19–23, 2013.

[8] S. Pimenta and S. T. Pinho. Recycling carbon fibre reinforced polymers for structural applications: Technology review and market outlook. *Waste Management*, 31:378–392, 2011.

[9] W. Dang, M. Kubouchi, S. Yamamoto, H. Sembokuya, and K. Tsuda. An approach to chemical recycling of epoxy resin cured with amine using nitric acid. *Polymer*, 43:2953–2958, 2002.

[10] *Green Chemistry*, 24:36–61, 2022.

[11] S. Li, H. Tian, J. Shao, H. Liu, D. Wang, and W. Zhang. Switchable adhesion for nonflat surfaces mimicking geckos' adhesive structures and toe muscles. *ACS Applied Materials Interfaces*, 12(35):39745–39755, 2020. PMID: 32666785.

[12] J. Zhou, H. Zhang, D. Liu, and J. Sun. Electrically debondable adhesives based on dynamic covalent chemistry. *ACS Applied Materials Interfaces*, 6(10):7742–7747, 2014.

[13] Paul Robert Steiner. The forests as a source of natural adhesives, 1981.

[14] J. Cognard. *Science et technologie du collage*. Presses Polytechniques et Universitaires Romandes, 2003.

[15] Zahidah binti Hamdi and A. Ghafar Ahmad. Sick building syndrome: The effects of animal and plant-based adhesive in wood furniture. *ARTEKS: Jurnal Teknik Arsitektur*, 2023.

[16] E. Dinte and B.S. Sylvester. Adhesives: Applications and recent advances. In *Chapter 7*. 2018.

[17] D.T. Anders. Polyurethanes with components made of renewable resources and recyclates, 2015.

[18] E.M. Pearce, J.R. Schaefgen, W.J. Bailey, , E.J. Vandenberg, and M.C. Shen. *Contemporary Topics in Polymer Science*. 1984.

[19] Fatipec Congress and Hans-Juergen P. Adler. *Quo vadis - coatings? Lectures presented at the XXVI FATIPEC congress*. European Organization of Paint Scientists and Engineers, Dresden University of Technology, Dresden, Germany, 2002.

[20] R. A. Pike. Adhesive. Encyclopedia Britannica. Access date unknown.

[21] Sina Ebnesajjad. Introduction and adhesion theories. In *Handbook of Adhesives and Surface Preparation*, pages 3–13. 2011.

[22] S. Wu. *Polymer Interface and Adhesion*. Marcel Dekker, New York, 1st edition, 1982.

[23] Shicun Jin, Jieping Xing, Tao Liu, Kuang Li, Fudong Zhang, Jinfeng Cao, Sheldon Q. Shi, and Jianzhang Li. Organic-inorganic building block of phytic acid intercalated graphene oxide for performance enhancement of plant-derived adhesives. *Industrial Crops and Products*, 2023.

[24] Johannes Urstöger, Günther Kain, Felix Prändl, Marius Ctlin Barbu, and ubo Kriák. Physical-mechanical properties of light bark boards bound with casein adhesives. *Sustainability*, 2023.

[25] C.T. Lo, F.C. Laabs, and B. Narasimhan. Interfacial adhesion mechanisms in incompatible semicrystalline polymer systems. *Journal of Polymer Science Part B*, 42:2667–2679, 2004.

[26] E.J. Kramer. Polymer-polymer interdiffusion. *MRS Proceedings*, 40:227, 1984.

[27] F. Ruch, M. David, and M.F. Vallat. Adhesion in epdm joints: Role of the interdiffusion mechanism on interfacial cocrosslinking. *Journal of Polymer Science Part B*, 38:3189–3199, 2000.

[28] V.D. Maria and A. Ianakiev. Adhesive connections in timber: A comparison between rough and smooth wood bonding surfaces. *International Journal of Chemical, Molecular, Nuclear, Materials and Metallurgical Engineering*, 9:395–401, 2015.

[29] Y. Rahmawan, S.M. Kang, S.Y. Lee, K.Y. Suh, and S. Yang. Enhanced shear adhesion by mechanical interlocking of dual-scaled elastomeric micropillars with embedded silica particles. *Macromolecular Reaction Engineering*, 7:616–623, 2013.

[30] E.M. Petrie. Plastics and adhesives as adhesives. In C.A. Harper, editor, *Handbook of Plastics and Elastomers*. McGraw-Hill, New York, 4th edition, 2002.

[31] B.V. Deraguin and V.P. Smilga. *Journal of Applied Physics*, 38:4609, 1967.

[32] P.S. Ho, R.A. Haight, R.C. White, and B.D. Silverman. Chemistry and microstructure at metal-polymer interfaces. *Le Journal De Physique Colloques*, 49, 1988.

[33] B.V. Deraguin and Y.P. Toporov. Physiochem aspects of polymer processing. In *International Symposium*, volume 2, page 605, 1983.

[34] D. Hays. Role of electrostatics in adhesion. pages 249–278. 1991.

[35] Y. Uetsuji, N. Fukui, T. Yagi, and Y. Nakamura. The effect of number of chemical bonds on intrinsic adhesive strength of a silane coupling agent with metals: A first-principles study. *Journal of Materials Research*, 37:923–932, 2022.

[36] X. Zhang, S. Li, J. Kang, J. Su, and K. Deng. Hydrogen bonds determine the nonbonding adhesion at hmx-based pbx interface. *Physica Scripta*, 98, 2023.

[37] V. Gutmann. *Donor-Acceptor Approach to Molecular Interaction*. Plenum Press, New York, 1978.

[38] K.L. Mittal. *Adhesion Measurement of Films and Coatings, Vol. 2*. Brill Academic Publishers, Netherlands, 2001.

[39] J.J. Bikerman. Causes of poor adhesion: Boundary layers. 1967.

[40] R.E. Robertson. The strength of an adhesive weak boundary layer. *Journal of Adhesion*, 7:121–136, 1975.

[41] S. Bharti. Adhesives and adhesion technologies: A critical review. 2018.

[42] T.B. Grimley. Adhesionfundamentals and practice: The ministry of technology (u.k.); maclaren: London, 1969. *Polymer*, 10:706, 1969.

[43] G. Juhász, M. Berczeli, and Z. Weltsch. Surface activation of high impact polystyrene substrate using dynamic atmospheric pressure plasma. *International Journal of Engineering and Management Sciences*, 2019.

[44] B. Bateup. Surface chemistry and adhesion. *International Journal of Adhesion and Adhesives*, 1:233–239, 1981.

[45] P. Geiss and M. Schumann. Time-, temperature- and frequency-dependent viscoelastic properties of a curing epoxy adhesive. *Materials Science Forum*, 1016:119–124, 2021.

[46] J. Gillham. Cure and properties of thermosetting polymers, 1987.

[47] G. Mays and A. Hutchinson. Adhesives in civil engineering: Adhesive classification and properties. 1992.

[48] B. George, F. Touyeras, Y. Grohens, and J. Vebrel. Analysis of curing mode and mechanical properties of an anaerobic adhesive. *European Polymer Journal*, 34:399–404, 1998.

[49] C. Chen, B. Li, M. Kanari, and D. Lu. Epoxy adhesives. In *Adhesives and Adhesive Joints in Industry Applications*. 2019.

[50] C. Fan, C. Pang, X. Liu, J. Ma, and H. Gao. Self-curing furan-based elastic thermosets derived from citric acid. *Green Chemistry*, 18:6320–6328, 2016.

[51] B. Milosheva, K. Jansen, J. Janssen, H. Bressers, and L. Ernst. Viscoelastic characterization of fast curing moulding compounds. In *EuroSimE 2005. Proceedings of the 6th International Conference on Thermal, Mechanical and Multi-Physics Simulation and Experiments in Micro-Electronics and Micro-Systems*, pages 462–466, 2005.

[52] N. Schellmann. Animal glues: a review of their key properties relevant to conservation. *Studies in Conservation*, 52:55–66, 2007.

[53] H. Kennedy. Starch- and dextrin-based adhesives. pages 326–336. 1989.

[54] S. Omura, Y. Kawazoe, and D. Uemura. Development of a novel adhesive composed of all-natural components. *International Journal of Adhesion and Adhesives*, 74:35–39, 2017.

[55] Q. Yang, L. Tang, C. Guo, F. Deng, H. Wu, L. Chen, L. Huang, P. Lu, C. Ding, Y. Ni, and M. Zhang. A bioinspired gallol-functionalized collagen as wet-tissue adhesive for biomedical applications. *Chemical Engineering Journal*, page 127962, 2020.

[56] J. Jansen. Comparing thermoplastic elastomers and thermoset rubber: Each class of material is well suited for its range of applications, but there are key differences. *Plastics Engineering*, 72:36–38, 2016.

[57] S. Ebnesajjad. Chapter 5 characteristics of adhesive materials. pages 84–159. 2015.

[58] C. Creton. Pressure-sensitive adhesives: An introductory course. *MRS Bulletin*, 28:434–439, 2003.

[59] M. Niaounakis. Chapter 15 adhesive compositions. pages 459–480. 2015.

[60] J. Licari and D. Swanson. Chemistry, formulation, and properties of adhesives. pages 75–141. 2011.

[61] Ali Fazli and D. Rodrigue. Waste rubber recycling: A review on the evolution and properties of thermoplastic elastomers. *Materials*, 13:782, 2020.

[62] C. Boeder. Anaerobic and structural acrylic adhesives. pages 217–247. 1986.

[63] P. Briggs and G. Jialanella. Advances in acrylic structural adhesives. pages 132–150. 2010.

[64] A. Pizzi. Phenolic resin adhesives. pages 223–261. 2017.

[65] U. Vaidya and K. Chawla. Processing of fibre reinforced thermoplastic composites. *International Materials Reviews*, 53:185–218, 2008.

[66] I. Gofman, V. Yudin, O. Orell, J. Vuorinen, A. Grigoriev, and V. Svetlichnyi. Influence of the degree of crystallinity on the mechanical and tribological properties of high-performance thermoplastics over a wide range of temperatures: From room temperature up to 250řc. *Journal of Macromolecular Science, Part B*, 52:1848–1860, 2013.

[67] L. Picard, P. Phalip, E. Fleury, and F. Ganachaud. Bonding of silicone rubbers on metal: (1) chemistry of adhesion. *Progress in Organic Coatings*, 87:250–257, 2015.

[68] S. Ebnesajjad. Characteristics of adhesive materials. pages 137–183. 2011.

[69] X. Deng. Progress on rubber-based pressure-sensitive adhesives. *The Journal of Adhesion*, 94:77–96, 2018.

[70] S. Gharde, G. Sharma, and B. Kandasubramanian. Hot-melt adhesives: Fundamentals, formulations, and applications: A critical review. *Reviews of Adhesion and Adhesives*, 2020.

[71] W. Hong, M. Meng, J. Xie, D. Gao, M. Xian, S. Wen, S. Huang, and C. Kang. Properties and thermal analysis study of modified polyvinyl acetate (pva) adhesive. *Journal of Adhesion Science and Technology*, 32:2180–2194, 2018.

[72] A. Kaboorani and B. Riedl. Effects of adding nano-clay on performance of polyvinyl acetate (pva) as a wood adhesive. *Composites Part A: Applied Science and Manufacturing*, 42:1031–1039, 2011.

[73] M. Tripathi, R. Dwivedi, D. Kumar, and P. Roy. Thermal activation of mendable epoxy through inclusion of microcapsules and imidazole complexes. *Polymer-Plastics Technology and Engineering*, 55:150827134358001, 2015.

[74] N. Allen and M. Edge. Perspectives on additives for polymers. part 2. aspects of photostabilization and role of fillers and pigments. *Journal of Vinyl and Additive Technology*, 27:211–239, 2020.

[75] L. Jing-ying. Determination of antioxidant d in pressure-sensitive adhesive and its products by high performance liquid chromatography. *Journal of Instrumental Analysis*, 2011.

[76] A. Baldan. Adhesively-bonded joints in metallic alloys, polymers and composite materials: Mechanical and environmental durability performance. *Journal of Materials Science*, 39:4729–4797, 2004.

[77] G. Jeevi, S. Nayak, and M. Kader. Review on adhesive joints and their application in hybrid composite structures. *Journal of Adhesion Science and Technology*, 33:1497–1520, 2019.

[78] N. Encinas, B. Oakley, M. Belcher, K. Blohowiak, R. Dillingham, J. Abenojar, and M. Martínez. Surface modification of aircraft used composites for adhesive bonding. *International Journal of Adhesion and Adhesives*, 50:157–163, 2014.

[79] J. Wingfield. Treatment of composite surfaces for adhesive bonding. *International Journal of Adhesion and Adhesives*, 13:151–156, 1993.

[80] Edward M. Petrie. *Handbook of Adhesives and Sealants*. McGraw-Hill, New York, 2nd edition, 2007.

[81] S. Abrahami, J. Kok, V. Gudla, R. Ambat, H. Terryn, and J. Mol. Interface strength and degradation of adhesively bonded porous aluminum oxides. *npj Materials Degradation*, 1:1–8, 2017.

[82] A. Vasconcellos, J. Oliveira, and R. Baumhardt-Neto. Adhesion of polypropylene treated with nitric and sulfuric acid. *European Polymer Journal*, 33:1731–1734, 1997.

[83] F. Vautard, P. Fioux, L. Vidal, J. Dentzer, J. Schultz, M. Nardin, and B. Defoort. Influence of an oxidation of the carbon fiber surface by boiling nitric acid on the ad-

hesion strength in carbon fiberacrylate composites cured by electron beam. *Surface and Interface Analysis*, 45, 2013.

[84] N. Gonzalez-Canche, E. Flores-Johnson, P. Cortes, and J. Carrillo. Evaluation of surface treatments on 5052-h32 aluminum alloy for enhancing the interfacial adhesion of thermoplastic-based fiber metal laminates. *International Journal of Adhesion and Adhesives*, 82:90–99, 2018.

[85] D. Myers. *Surfactant Science and Technology*. John Wiley Sons, 3rd edition, 2005.

[86] A. Harris and A. Beevers. The effects of grit-blasting on surface properties for adhesion. *International Journal of Adhesion and Adhesives*, 19:445–452, 1999.

[87] D. Varacalle, D. Guillen, D. Deason, W. Rhodaberger, and E. Sampson. Effect of grit-blasting on substrate roughness and coating adhesion. *Journal of Thermal Spray Technology*, 15:348–355, 2006.

[88] E. M. Petrie. Chapter 6: Surface preparation for adhesive bonding. In *Handbook of Adhesives and Sealants*, pages 167–214. McGraw-Hill, 2006.

[89] F. F. Chen. *Introduction to Plasma Physics and Controlled Fusion*, volume 54. 2012.

[90] N. Encinas, B. Oakley, M. Belcher, K. Blohowiak, R. Dillingham, J. Abenojar, and M. Martínez. Surface modification of aircraft used composites for adhesive bonding. *International Journal of Adhesion and Adhesives*, 50:157–163, 2014.

[91] R. Wolf and A. Sparavigna. Role of plasma surface treatments on wetting and adhesion. *Engineering*, 2:397–402, 2010.

[92] C. Chan, T. Ko, and H. Hiraoka. Polymer surface modification by plasmas and photons. *Surface Science Reports*, 24:1–54, 1996.

[93] J. Park and T. Lee. Surface activation beneath the flip chip by plasma treatments. *IEEE Transactions on Components, Packaging and Manufacturing Technology*, 12:1712–1718, 2022.

[94] I. Arellano and A. Zapanta. Evolution of the topographical and chemical signatures of plasma-treated surfaces along the staging time pathway. In *2016 IEEE 18th Electronics Packaging Technology Conference (EPTC)*, pages 679–683, 2016.

[95] J. C. Ion. *Laser Processing of Engineering Materials: Principles, Procedure and Industrial Application*. Elsevier, 2005.

[96] J. Lawrence, J. Pou, D.K.Y. Low, and E. Toyserkani. *Advances in Laser Materials Processing: Technology, Research and Application*. 2010.

[97] Z. Zhou, W. Sun, J. Wu, H. Chen, F. Zhang, and S. Wang. The fundamental mechanisms of laser cleaning technology and its typical applications in industry. *Processes*, 11:1445, 2023.

[98] D. Tod, R. Atkins, and S. Shaw. Use of primers to enhance adhesive bonds. *International Journal of Adhesion and Adhesives*, 12:159–163, 1992.

[99] B. Liang, H. Fan, Y. Chen, J. Yan, T. Yang, and G. Yuliang. Effect of surface free energy and wettability on the adhesion property of waterborne polyurethane adhesive. *RSC Advances*, 6:99346–99352, 2016.

[100] J. Custódio, J.G. Broughton, H. Cruz, and A. Hutchinson. A review of adhesion promotion techniques for solid timber substrates. *The Journal of Adhesion*, 84:502–529, 2008.

[101] J. Bajat and O. Dedic. Adhesion and corrosion resistance of epoxy primers used in the automotive industry. *Journal of Adhesion Science and Technology*, 21:819–831, 2007.

[102] A. Prabu and M. Alagar. The right mix: Interpenetrating silicone-polyurethane-epoxy networks for improved solventless anticorrosive primers. *European Coatings Journal*, pages 59–62, 2004.

[103] E. M. Petrie. Chapter 5: Primers and adhesion promoters. In *Handbook of Adhesives and Sealants*. McGraw-Hill, 2nd edition, 2007.

[104] M. Shishesaz and M. Hosseini. Effects of joint geometry and material on stress distribution, strength and failure of bonded composite joints: an overview. *The Journal of Adhesion*, 96:1053–1121, 2018.

[105] N. Barbosa, R. Campilho, F. Silva, and R. Moreira. Comparison of different adhesively-bonded joint configurations for mechanical structures. *Procedia Manufacturing*, 17:721–728, 2018.

[106] J. Silva, R. Campilho, R. Rocha, and F. Silva. Comparative evaluation of adhesively-bonded single-lap and stepped-lap joints. *Procedia Manufacturing*, 2019.

[107] D. Alves, R. Campilho, R. Moreira, F. Silva, and L. Silva. Experimental and numerical analysis of hybrid adhesively-bonded scarf joints. *International Journal of Adhesion and Adhesives*, 2018.

[108] A. Kanani, X. Hou, R. Laidlaw, and J. Ye. The effect of joint configuration on the strength and stress distributions of dissimilar adhesively bonded joints. *Engineering Structures*, 226:111322, 2021.

[109] E. M. Petrie. Chapter 6: Adhesive mixing and application techniques. In *Handbook of Adhesives and Sealants*. McGraw-Hill, 2nd edition, 2007.

[110] K. Katnam, J. Stevenson, W. Stanley, M. Buggy, and T. Young. Tensile strength of two-part epoxy paste adhesives: Influence of mixing technique and micro-void formation. *International Journal of Adhesion and Adhesives*, 31:666–673, 2011.

[111] I. Skeist. Chapter 9: Adhesive application and processing techniques. In *Handbook of Adhesives*. Van Nostrand Reinhold, 3rd edition, 1990.

[112] K. Go, Y. Kim, A. Lee, K. Staricha, P. Messersmith, and M. Glucksberg. Design of novel mixer and applicator for two-component surgical adhesives. *Journal of Medical Devices*, 9(4):0450011–0450016, 2015.

[113] G. Meschut, O. Hahn, D. Teutenberg, and L. Ernstberger. Influence of the dosing and mixing technology on the property profile of two-component adhesives. *Welding in the World*, 59:91–96, 2014.

[114] M. Bhuvaneswari, R. ArunChakravarthy, M. Arun, T. Naveenkumar, T. Premchand, M. Rajkumar, and R. Vijay. Low cost design automated adhesive dispenser for industry. *Journal of Critical Reviews*, 2020.

[115] T. Melbye and R. Dimmock. Modern advances and applications of sprayed concrete. In *Shotcrete: Engineering Developments*. 2020.

[116] G. Marx. Evolution of fibrin glue applicators. *Transfusion Medicine Reviews*, 17(4):287–298, 2003.

[117] R. Jain and S. Wairkar. Recent developments and clinical applications of surgical glues: An overview. *International Journal of Biological Macromolecules*, 2019.

[118] R. Inoue. Studies on the adhesive strength improvement between resins and ag-pd-cu-au surface-treated alloy by the flame spraying methodan investigation of spraying materials. *Nihon Hotetsu Shika Gakkai Zasshi*, 38:821–834, 1994.

[119] S. Chokka, B. Ben, and K. Srinadh. Vacuum infusion processed adhesive bonding of ss plates. *Materials Today: Proceedings*, 2020.

[120] F. Flaig, T. Fräger, M. Kaufmann, T. Vallée, H. Fricke, and M. Müller. A practical strategy to identify appropriate application patterns for adhesively bonded joints. *PAMM*, 23, 2023.

[121] B. Watson, M. Worswick, and D. Cronin. Quantification of mixed mode loading and bond line thickness on adhesive joint strength using novel test specimen geometry. *International Journal of Adhesion and Adhesives*, 102:102682, 2020.

[122] D. Zhang and Y. Huang. Influence of surface roughness and bondline thickness on the bonding performance of epoxy adhesive joints on mild steel substrates. *Progress in Organic Coatings*, 153:106135, 2021.

[123] Y. Sekiguchi and C. Sato. Effect of bond-line thickness on fatigue crack growth of structural acrylic adhesive joints. *Materials*, 14, 2021.

[124] R. Fernandes, S. Freitas, M. Budzik, J. Poulis, and R. Benedictus. From thin to extra-thick adhesive layer thicknesses: Fracture of bonded joints under mode i loading conditions. *Engineering Fracture Mechanics*, 2019.

[125] Y. Liu, C. Carnegie, H. Ascroft, W. Li, X. Han, H. Guo, and D. Hughes. Investigation of adhesive joining strategies for the application of a multi-material light rail vehicle. *Materials*, 14, 2021.

[126] A. Ajdani, M. Ayatollahi, A. AkhavanSafar, and L. Silva. Mixed mode fracture characterization of brittle and semi-brittle adhesives using the scb specimen. *International Journal of Adhesion and Adhesives*, 101:102629, 2020.

[127] J. Cardoso, P. Gamboa, and A. Silva. Effect of surface pre-treatment on the behaviour of adhesively-bonded cfrp t-joints. *Engineering Failure Analysis*, 2019.

[128] A. Akhavan-Safar, M.R. Ayatollahi, S.A. Bahreinian, and L.F.M. Silva. Application of adhesively bonded single lap joints for fracture assessment of adhesive materials. *The Journal of Adhesion*, 95, 2017.

[129] M. Santos and R. Campilho. Experimental and numerical analysis of the fracture envelope of composite adhesive joints. *Science and Technology of Materials*, 2018.

[130] F. Loureiro, R. Campilho, and R. Rocha. Mixed-mode fracture toughness of a structural adhesive by the single-leg bending test. *Procedia Structural Integrity*, 25:63–70, 2020.

[131] A. Proia and S. Matthys. Influence of environmental conditions on the glass transition temperature of epoxy used for strengthening applications. *Polymer Testing*, 2019.

[132] R. Verker, E. Wallach, Y. Vidavsky, A. Bolker, and I. Gouzman. Novel axial dynamic mechanical analysis setup for thermo-analytical study and curing kinetics optimization of thermoset adhesives. *The Review of Scientific Instruments*, 93(3):034104, 2022.

[133] T. Srivastava, N. Katari, B. Ravuri, J. Kushwaha, S. Mohan, and S. Jonnalagadda. Studies on thermal stability and life estimation of epoxy adhesive by thermogravimetric analysis for high-temperature applications. *Bulletin of Materials Science*, 43:1–6, 2020.

[134] H. Obeid, S. Marguet, B. Hassoune-Rhabbour, T. Mérian, A. Léonardi, J. Ferrero, and H. Welemane. Evolution of physico-chemical and mechanical properties of bonded epoxy assemblies during hygrothermal cyclic aging. *Mechanics Industry*, 2023.

[135] K. Machalická, M. Voká, P. Pokorný, and M. Pavlíková. Effect of various artificial ageing procedures on adhesive joints for civil engineering applications. *International Journal of Adhesion and Adhesives*, 97:102476, 2019.

[136] T. Babra, M. Wood, J. Godleman, S. Salimi, C. Warriner, N. Bazin, C. Siviour, I. Hamley, W. Hayes, and B. Greenland. Fluoride-responsive debond on demand adhesives: Manipulating polymer crystallinity and hydrogen bonding to optimise adhesion strength at low bonding temperatures. *European Polymer Journal*, 2019.

[137] S. Salimi, T. Babra, G. Dines, S. Baskerville, W. Hayes, and B. Greenland. Composite polyurethane adhesives that debond-on-demand by hysteresis heating in an oscillating magnetic field. *European Polymer Journal*, 2019.

[138] D. Hohl and C. Weder. (de)bonding on demand with optically switchable adhesives. *Advanced Optical Materials*, 7, 2019.

[139] N. Blelloch, H. Yarbrough, and K. Mirica. Stimuli-responsive temporary adhesives: enabling debonding on demand through strategic molecular design. *Chemical Science*, 12:15183–15205, 2021.

[140] A. Schenzel, C. Klein, K. Rist, N. Moszner, and C. BarnerKowollik. Reversing adhesion: A triggered release selfreporting adhesive. *Advanced Science*, 3, 2016.

[141] C. Bandl, W. Kern, and S. Schlögl. Adhesives for debonding-on-demand: Triggered release mechanisms and typical applications. *International Journal of Adhesion and Adhesives*, 2020.

[142] M. Banea, L. Silva, and R. Carbas. Debonding on command of adhesive joints for the automotive industry. *International Journal of Adhesion and Adhesives*, 59:14–20, 2015.

[143] M. Banea. Debonding on demand of adhesively bonded joints: A critical review. *Reviews of Adhesion and Adhesives*, 7:33–50, 2019.

[144] L. Gan. Effect of foaming agent on performance of foaming structural adhesive. *Heilongjiang Science*, 2013.

[145] Y. Wang, Z. Hu, H. Li, W. Xu, and J. Liu. Expansive deformation and mechanical properties of cementitious materials with azodicarbonamide expansive agent: influencing factors and mechanisms. *Journal of Sustainable Cement-Based Materials*, 12:1141–1155, 2023.

[146] S. Salimi, T. Babra, G. Dines, S. Baskerville, W. Hayes, and B. Greenland. Composite polyurethane adhesives that debond-on-demand by hysteresis heating in an oscillating magnetic field. *European Polymer Journal*, 2019.

[147] M. Kanidi, N. Loura, A. Frengkou, T. Milickovic, A. Trompeta, and C. Charitidis. Inductive thermal effect on thermoplastic nanocomposites with magnetic nanoparticles for induced-healing, bonding and debonding on-demand applications. *Journal of Composites Science*, 2023.

[148] X. Cheng, Y. Zhou, A. Charles, Y. Yu, M. Islam, S. Peng, J. Wang, A. Rider, M. Lim, V. Timchenko, and C. Wang. Enabling contactless rapid on-demand

debonding and rebonding using hysteresis heating of ferrimagnetic nanoparticles. *Materials Design*, 2021.

[149] M. Wu, S. Chen, Y. Mei, L. Liu, and Y. Wei. Interfacial electrochemistry-induced detachable adhesives with ultra-high bonding strength and detaching efficiency. *ACS Applied Materials Interfaces*, 2022.

[150] S. Leijonmarck, A. Cornell, C. Danielsson, and G. Lindbergh. Electrochemical characterization of electrically induced adhesive debonding. *Journal of The Electrochemical Society*, 158:109, 2011.

[151] S. Leijonmarck, A. Cornell, C. Danielsson, T. Åkermark, B. Brandner, and G. Lindbergh. Electrolytically assisted debonding of adhesives: An experimental investigation. *International Journal of Adhesion and Adhesives*, 32:39–45, 2012.

[152] Green chem., 2022, 24, 36. *Green Chemistry*, 24:36, 2022.

[153] H. Li, C. Jiang, Z. Yu, Y. Wan, Y. Ma, and Z. Yang. Numerical study on the progressive damage behavior of the interfacial debonding between shape memory alloy and polymer matrix. *Materials*, 16, 2022.

[154] J. Kang, E. Siochi, R. Penner, and T. Turner. Enhanced adhesive strength between shape memory polymer nanocomposite and titanium alloy. *Composites Science and Technology*, 96:23–30, 2014.

[155] W. Li, J. Liu, W. Wei, and K. Qian. Harnessing reversible dry adhesion using shape memory polymer microparticles. *RSC Advances*, 11:19616–19622, 2021.

[156] C. Heinzmann, S. Coulibaly, A. Roulin, G. Fiore, and C. Weder. Light-induced bonding and debonding with supramolecular adhesives. *ACS Applied Materials Interfaces*, 6(7):4713–4719, 2014.

[157] C. Heinzmann, U. Salz, N. Moszner, G. Fiore, and C. Weder. Supramolecular cross-links in poly(alkyl methacrylate) copolymers and their impact on the mechanical and reversible adhesive properties. *ACS Applied Materials Interfaces*, 7(24):13395–13404, 2015.

[158] X. Li, Y. Wen, Y. Wang, H. Peng, X. Zhou, and X. Xie. Co2-based biodegradable supramolecular polymers with well-tunable adhesive properties. *Chinese Journal of Polymer Science*, 40:47–55, 2021.

[159] E. Platonova, I. Chechenov, A. Pavlov, V. Solodilov, E. Afanasyev, A. Shapagin, and A. Polezhaev. Thermally remendable polyurethane network cross-linked via reversible dielsalder reaction. *Polymers*, 13, 2021.

[160] S. Das, S. Samitsu, Y. Nakamura, Y. Yamauchi, D. Payra, K. Kato, and M. Naito. Thermo-resettable cross-linked polymers for reusable/removable adhesives. *Polymer Chemistry*, 9:5559–5565, 2018.

[161] J. Li, Q. Liu, G. Zhang, B. Zhao, R. Sun, and C. Wong. Thermally reversible and crosslinked polyurethane based on diels-alder chemistry for ultrathin wafer temporary bonding at low-temperature. In *2017 IEEE 67th Electronic Components and Technology Conference (ECTC)*, pages 746–751, 2017.

[162] M. Carbonell-Blasco, M. Moyano, C. Hernández-Fernández, F. Sierra-Molero, I. Pastor, D. Alonso, F. Arán-Aís, and E. Orgilés-Calpena. Polyurethane adhesives with chemically debondable properties via dielsalder bonds. *Polymers*, 2023.

[163] B. Vaezian, J. Meyer, and J. Economy. Processing of aromatic thermosetting copolyesters into foams and bulk parts: characterization and mechanical properties. *Polymers for Advanced Technologies*, 27:1006–1013, 2016.

[164] M. Bakir, J. Meyer, J. Economy, and I. Jasiuk. Aromatic thermosetting copolyester nanocomposite foams: High thermal and mechanical performance lightweight structural materials. *Polymer*, 123:311–320, 2017.

[165] Z. Parkar, C. Mangun, D. King, T. Field, G. Sutton, and J. Economy. Ablation characteristics of an aromatic thermosetting copolyester/carbon fiber composite. *Journal of Composite Materials*, 46:1819–1830, 2012.

[166] T. Yeingst, J. Arrizabalaga, F. Rawnaque, L. Stone, A. Yeware, A. Helton, A. Dhawan, J. Simon, and D. Hayes. Controlled degradation of polycaprolactone polymers through ultrasound stimulation. *ACS Applied Materials Interfaces*, 2023.

[167] T. Babra, A. Trivedi, C. Warriner, N. Bazin, D. Castiglione, C. Sivour, W. Hayes, and B. Greenland. Fluoride degradable and thermally debondable polyurethane based adhesive. *Polymer Chemistry*, 8:7207–7216, 2017.

[168] T. Babra, C. Warriner, N. Bazin, W. Hayes, and B. Greenland. A fluoride degradable crosslinker for debond-on-demand polyurethane based crosslinked adhesives. *Materials Today Communications*, 2020.

[169] S. Giraud, F. Rault, A. Cayla, and F. Salaün. History and evolution of fire retardants for textiles. 2016. Conference or review article.

[170] B. Schartel and T. R. Hull. Development of fire-retarded materialsinterpretation of cone calorimeter data. *Fire and Materials*, 31(5):327–354, 2007.

[171] A. Al-Mosawi. Flame retardants, their beginning, types, and environmental impact: A review. *Epitoanyag-Journal of Silicate Based and Composite Materials*, 74:2–8, 2022.

[172] Ceresana presents a new study on the world market for flame retardants. *Additives for Polymers*, 2022.

[173] S. Brown. Flame retardants: inorganic oxide and hydroxide systems. In *Inorganic and Organometallic Polymers*, pages 287–296. 1998.

[174] L. Morf, J. Tremp, R. Gloor, Y. Huber, M. Stengele, and M. Zennegg. Brominated flame retardants in waste electrical and electronic equipment: substance flows in a recycling plant. *Environmental Science Technology*, 39(22):8691–8699, 2005.

[175] G. Wei, D. Li, M. Zhuo, Y. Liao, Z. Xie, T. Guo, J. Li, S. Zhang, and Z. Liang. Organophosphorus flame retardants and plasticizers: sources, occurrence, toxicity and human exposure. *Environmental Pollution*, 196:29–46, 2015.

[176] Flame-retardant. https://www.merriam-webster.com/dictionary/flame-retardant, 2024. Accessed: 2024-06-05.

[177] H. Kruger, W. Focke, W. Mhike, A. Taute, and A. Roberson. Thermal properties of polyethylene flame retarded with expandable graphite and intumescent fire retardant additives. *Fire and Materials*, 41:573–586, 2017.

[178] M. Lewin and E. Weil. Mechanisms and modes of action in flame retardancy of polymers. In *Flame Retardant Polymer Nanocomposites*. 2001.

[179] X. Shi, S. Luo, X. Du, Q. Li, and S. Cheng. Improvement the flame retardancy and thermal conductivity of epoxy composites via melamine polyphosphate-modified carbon nanotubes. *Polymers*, 14, 2022.

[180] Y. Feng, J. Hu, Y. Xue, C. He, X. Zhou, X. Xie, Y. Ye, and Y. Mai. Simultaneous improvement in the flame resistance and thermal conductivity of epoxy/al2o3 com-

posites by incorporating polymeric flame retardant-functionalized graphene. *Journal of Materials Chemistry A*, 5:13544–13556, 2017.

[181] S. Lazar, T. Kolibaba, and J. Grunlan. Flame-retardant surface treatments. *Nature Reviews Materials*, 5, 2020.

[182] W. Wattanatanom, S. Churuchinda, and P. Potiyaraj. Intumescent flame retardant finishing of polyester fabrics via the layer-by-layer assembly technique. *International Journal of Clothing Science and Technology*, 29:96–105, 2017.

[183] X. Qiu, Z. Li, X. Li, and Z. Zhang. Flame retardant coatings prepared using layer by layer assembly: A review. *Chemical Engineering Journal*, 334:108–122, 2018.

[184] K. Wazarkar, M. Kathalewar, and A. Sabnis. Reactive modification of thermoplastic and thermoset polymers using flame retardants: An overview. *Polymer-Plastics Technology and Engineering*, 55:71–91, 2016.

[185] Z. X. Zhang, J. Zhang, B.-X. Lu, Z. X. Xin, C. K. Kang, and J. K. Kim. Effect of flame retardants on mechanical properties, flammability and foamability of pp/woodfiber composites. *Composites Part B: Engineering*, 43(2):150–158, 2012.

[186] P. Parcheta-Szwindowska, J. Habaj, I. Krzemiska, and J. Datta. A comprehensive review of reactive flame retardants for polyurethane materials: Current development and future opportunities in an environmentally friendly direction. *International Journal of Molecular Sciences*, 25(10):5512, 2024.

[187] A. Toldy. Chemically modified flame retardant polymers. *Express Polymer Letters*, 3:267–267, 2009.

[188] T. R. Hull, R. J. Law, and Å. Bergman. Environmental drivers for replacement of halogenated flame retardants. In C. D. Papaspyrides and P. Kiliaris, editors, *Polymer Green Flame Retardants*, pages 119–179. Elsevier, 2014.

[189] G. Camino and L. Costa. Performance and mechanisms of fire retardants in polymersa review. *Polymer Degradation and Stability*, 20(3–4):271–294, 1988.

[190] H. Atay and E. Çelik. Flame retardant properties of boric acid and antimony oxide accompanying with huntite and hydromagnesite in the polymer composites. *Polymers and Polymer Composites*, 24:419–428, 2016.

[191] Z. Wang, E. Han, and W. Ke. Effect of nanoparticles on the improvement in fire-resistant and anti-ageing properties of flame-retardant coating. *Surface Coatings Technology*, 200:5706–5716, 2006.

[192] M. Martins, B. Schartel, F. Magalhães, and C. Pereira. The effect of traditional flame retardants, nanoclays and carbon nanotubes in the fire performance of epoxy resin composites. *Fire and Materials*, 41:111–130, 2017.

[193] H. Vahabi, F. Laoutid, M. Mehrpouya, M. R. Saeb, and P. Dubois. Flame retardant polymer materials: An update and the future for 3d printing developments. *Materials Science and Engineering: R: Reports*, 144:100604, 2021.

[194] B. Schartel, B. Perret, B. Dittrich, M. Ciesielski, J. Krämer, P. Müller, V. Altstädt, L. Zang, and M. Döring. Flame retardancy of polymers: The role of specific reactions in the condensed phase. *Macromolecular Materials and Engineering*, 301:9–35, 2016.

[195] B. Schartel, C. Wilkie, and G. Camino. Recommendations on the scientific approach to polymer flame retardancy: Part 2–concepts. *Journal of Fire Sciences*, 35, 2016.

[196] M. Zhang, W. Zhang, Y. Chen, and B. Yang. Preparation of efficiently intumescent-flame-retarded polypropylene composite: synergistic effect of novel phosphorus-containing polyhedral oligomeric silsesquioxane. *Plastics, Rubber and Composites*, 50:464–476, 2021.

[197] H. Horacek and R. Grabner. Advantages of flame retardants based on nitrogen compounds. *Polymer Degradation and Stability*, 54:205–215, 1996.

[198] K. A. Salmeia, J. Fage, S. Liang, and S. Gaan. An overview of mode of action and analytical methods for evaluation of gas phase activities of flame retardants. *Polymers*, 7(3):504–526, 2015.

[199] R. Myers and E. Licursi. Inorganic glass forming systems as intumescent flame retardants for organic polymers. *Journal of Fire Sciences*, 3:415–431, 1985.

[200] L. Li, Z. Chen, J. Lu, M. Wei, Y. Huang, and P. Jiang. Combustion behavior and thermal degradation properties of wood impregnated with intumescent biomass flame retardants: Phytic acid, hydrolyzed collagen, and glycerol. *ACS Omega*, 6:3921–3930, 2021.

[201] B. Howell. Thermal degradation of organophosphorus flame retardants. *Polymers*, 14, 2022.

[202] S. Zhou, L. Song, Z. Wang, Y. Hu, and W. Xing. Flame retardation and char formation mechanism of intumescent flame retarded polypropylene composites containing melamine phosphate and pentaerythritol phosphate. *Polymer Degradation and Stability*, 93:1799–1806, 2008.

[203] X. Sun, C. Huang, Z. Chen, R. Zhou, and J. Jiang. Multi-element synergistic effects to improve the flame retardancy of high impact polystyrene. *Polymer Testing*, 115:107766, 2022.

[204] E. Peuvrel-Disdier. Dispersion of agglomerated fillers in a polymer matrix: Input of a rheo-optical approach and rheology. *Polymer Testing*, 2015.

[205] P. Dey, K. Naskar, B. Dash, S. S. Nair, G. Unnikrishnan, and G. Nando. Selective dispersion of carbon fillers into dynamically vulcanized rubber/plastic blends: a thermodynamic approach to evaluate polymer reinforcement and conductivity enhancement. *RSC Advances*, 5:31886–31900, 2015.

[206] C. Chevigny, N. Jouault, F. Dalmas, F. Boué, and J. Jestin. Tuning the mechanical properties in model nanocomposites: Influence of the polymerfiller interfacial interactions. *Journal of Polymer Science Part B: Polymer Physics*, 49:781–791, 2011.

[207] T. Nguyen and T. Bui. Study the effects of carbon nanotubes and graphene oxide combinations on the mechanical properties and flame retardance of epoxy nanocomposites. *Journal of Nanomaterials*, 2021:1437929, 2021.

[208] W. Wang, Y. Peng, M. Zammarano, W. Zhang, and J. Li. Effect of ammonium polyphosphate to aluminum hydroxide mass ratio on the properties of woodflour/polypropylene composites. *Polymers*, 9, 2017.

[209] K. M. Holder, R. J. Smith, and J. C. Grunlan. A review of flame retardant nanocoatings prepared using layer-by-layer assembly of polyelectrolytes. *Journal of Materials Science*, 52:12923–12959, 2017.

[210] Rsc adv., 2023, 13, 22639–22662. *RSC Advances*, 13:22639–22662, 2023.

[211] Charles Anderson Jr, Jerome Dziuk, William Mallow, and John Buckmaster. Intumescent reaction mechanisms. *Journal of Fire Sciences*, 3:161–194, 1985.

[212] G. Camino and S. Lomakin. Intumescent materials. In A. R. Horrocks and D. Price, editors, *Fire Retardant Materials*, pages 318–336. Woodhead Publishing, 2001.

[213] F. Tomiak, K. Rathberger, A. Schöffel, and D. Drummer. Expandable graphite for flame retardant pa6 applications. *Polymers (Basel)*, 13(16):2733, 2021.

[214] M. Modesti, A. Lorenzetti, F. Simioni, and G. Camino. Expandable graphite as an intumescent flame retardant in polyisocyanurate-polyurethane foams. *Polymer Degradation and Stability*, 77:195–202, 2002.

[215] Sebastien Depaifve, Carlos Eloy Federico, David Ruch, Sophie Hermans, and Abdelghani Laachachi. Nitrene functionalization as a new approach for reducing the interfacial thermal resistance in graphene nanoplatelets/epoxy nanocomposites. *Carbon*, 167:646–657, 2020.

[216] Sebastien Depaifve, Sophie Hermans, David Ruch, and Abdelghani Laachachi. Combination of micro-computed x-ray tomography and electronic microscopy to understand the influence of graphene nanoplatelets on the thermal conductivity of epoxy composites. *Thermochimica Acta*, 691:178712, 07 2020.

[217] Abdelghani Laachachi, Nicolas Burger, Kadir Apaydin, Rodolphe Sonnier, and Michel Ferriol. Is expanded graphite acting as flame retardant in epoxy resin? *Polymer Degradation and Stability*, 117, 04 2015.

[218] Nicolas Burger, A. Laachachi, Bohayra Mortazavi, M. Ferriol, M. Lutz, V. Toniazzo, and David Ruch. Alignments and network of graphite fillers to improve thermal conductivity of epoxy-based composites. *International Journal of Heat and Mass Transfer*, 89, 10 2015.

[219] E. Peuvrel-Disdier. Dispersion of agglomerated fillers in a polymer matrix: Input of a rheo-optical approach and rheology. *Polymer Testing*, 2015.

[220] J. Kim, J. Yeom, K. Ha, J. Kim, and M. Kim. Ultrasonic streaming and cavitation for nano particle dispersion. In *2016 IEEE International Ultrasonics Symposium (IUS)*, pages 1–4, 2016.

[221] Y. Miyazaki, T. Uchino, and Y. Kagawa. Compounding of low-dose pharmaceutical powders using a planetary centrifugal mixer. *Journal of Drug Delivery Science and Technology*, 2019.

[222] R. Kottala, B. Chigilipalli, S. Mukuloth, R. Shanmugam, V. Kantumuchu, S. Ainapurapu, and M. Cheepu. Thermal degradation studies and machine learning modelling of nano-enhanced sugar alcohol-based phase change materials for medium temperature applications. *Energies*, 2023.

[223] X. Sun, K. Lee, M. Medina, Y. Chu, and C. Li. Melting temperature and enthalpy variations of phase change materials (pcms): a differential scanning calorimetry (dsc) analysis. *Phase Transitions*, 91:667–680, 2018.

[224] M. Arulmurugan, K. Prabu, G. Rajamurugan, and A. Selvakumar. Viscoelastic behavior of aloevera/hemp/flax sandwich laminate composite reinforced with baso4: Dynamic mechanical analysis. *Journal of Industrial Textiles*, 50:1040–1064, 2019.

[225] J. Blazy, . Drobiec, and P. Wolka. Mechanical properties of polymer fibre reinforced concrete in the light of various standards. *Archives of Civil Engineering*, 2024.

[226] Y. Lestyowati, H. Herawati, and B. Panandita. Experimental flexural strength of glass fiber reinforced polymer (gfrp) hybrid reinforced concrete beams. *Jurnal Teknik Sipil*, 2023.

[227] A. Redmann, V. Damodaran, F. Tischer, P. Prabhakar, and T. Osswald. Evaluation of single-lap and block shear test methods in adhesively bonded composite joints. *Journal of Composites Science*, 2021.

[228] M. Demiral, F. Abbassi, A. Zahedi, and S. Akpinar. Critical assessment of the bonded single lap joint exposed to cyclic tensile loading. *Aerospace*, 2023.

[229] M. Banea, L. Silva, R. Campilho, and A. Jesus. Characterization of aluminium single-lap joints for high temperature applications. *Materials Science Forum*, 721–726, 2012.

[230] H. Hosseini and S. Jafari. Fourier transform infrared (ft-ir) spectroscopy of nanoencapsulated food ingredients. In *Characterization of Nanoencapsulated Food Ingredients*. Elsevier, 2020.

[231] Marc S. Sabatine, Ern Liu, and David A. Morrow. The emergence of proton nuclear magnetic resonance metabolomics in the cardiovascular arena as viewed from a clinical perspective. *Metabolomics*, 6:501–503, 2010.

[232] K. Cujia, J. Boss, K. Herb, J. Zopes, and C. Degen. Tracking the precession of single nuclear spins by weak measurements. *Nature*, 571:230–233, 2018.

[233] K. Hirakawa, K. Koike, Y. Kanawaku, T. Moriyama, N. Sato, T. Suzuki, K. Furihata, and Y. Ohno. Short-time fourier transform of free induction decays for the analysis of serum using proton nuclear magnetic resonance. *Journal of Oleo Science*, 68(4):369–378, 2019.

[234] Y. Ma, D. Liu, J. Hua, and W. Lu. Dual-energy micro-focus computed tomography based on the energy-angle correlation of inverse compton scattering source. *Journal of X-ray Science and Technology*, 2023.

[235] X. Lu and L. Chan. Micro-voids quantification for damage prediction in warm forging of biocompatible alloys using 3d x-ray ct and rve approach. *Journal of Materials Processing Technology*, 2018.

[236] K. Akhtar, S. Khan, S. Khan, and A. Asiri. Scanning electron microscopy: Principle and applications in nanomaterials characterization. In *Nanomaterials Characterization*, pages 113–145. 2018.

[237] T. Hyams, K. Mam, and M. Killingsworth. Scanning electron microscopy as a new tool for diagnostic pathology and cell biology. *Micron*, 130:102797, 2019.

[238] H. Liang, Q. Lin, X. Xie, Q. Sun, Y. Wang, L. Zhou, L. Liu, X. Yu, J. Zhou, T. Krauss, and J. Li. Ultrahigh numerical aperture metalens at visible wavelengths. *Nano Letters*, 18(7):4460–4466, 2018.

[239] P. Soni and S. Vyas. Studies on x-ray diffraction (xrd) patterns of soya-hulls for interpretation of crystallinity index. *Asian Journal of Research in Chemistry*, 2022.

[240] G. Mandal. *X-ray Diffraction for Characterization of Nanomaterials*. Not specified, 2019. Details of publisher not available.

[241] S. Chowdhury. X-ray diffraction: principles and its application to structural analysis. *Not specified*, 1999. Journal name and volume not specified.

[242] A. Marques, A. Mocanu, N. Tomi, S. Balos, E. Stammen, A. Lundevall, S. Abrahami, R. Günther, J. De Kok, and S. Teixeira De Freitas. Review on adhesives and surface treatments for structural applications: Recent developments on sustainability and implementation for metal and composite substrates. *Materials*, 13:5590, 2020.

[243] N. Anaç. Assessment of adhesively bonded joints of similar and dissimilar materials: Industrial case study. *Processes*, 11:1312, 2023.

[244] C.S.P. Borges, A. Akhavan-Safar, P. Tsokanas, R.J.C. Carbas, E.A.S. Marques, and L.F.M. Da Silva. From fundamental concepts to recent developments in the adhesive bonding technology: a general view. *Discover Mechanical Engineering*, 2:8, 2023.

[245] A. Akhavan-Safar, G. Eisaabadi Bozchaloei, S. Jalali, R. Beygi, M.R. Ayatollahi, and L.F.M. Da Silva. Impact fatigue life of adhesively bonded composite-steel joints enhanced with the bi-adhesive technique. *Materials*, 16:419, 2023.

[246] F.M.G. Ramírez, M.F.S.F. De Moura, R.D.F. Moreira, and F.G.A. Silva. A review on the environmental degradation effects on fatigue behaviour of adhesively bonded joints. *Fatigue Fracture of Engineering Materials Structures*, 43:1307–1326, 2020.

[247] M. Gonçalves, H. Monteiro, and M. Iten. Life cycle assessment studies on lightweight materials for automotive applications - an overview. *Energy Reports*, 8:338–345, 2022.

[248] Y. Lu, J. Broughton, and P. Winfield. A review of innovations in disbonding techniques for repair and recycling of automotive vehicles. *International Journal of Adhesion and Adhesives*, 50:119–127, 2014.

[249] K.R. Mulcahy, A.F.R. Kilpatrick, G.D.J. Harper, A. Walton, and A.P. Abbott. Debondable adhesives and their use in recycling. *Green Chemistry*, 24:36–61, 2022.

[250] A. Hutchinson, Y. Liu, and Y. Lu. Overview of disbonding technologies for adhesive bonded joints. *The Journal of Adhesion*, 93:737–755, 2017.

[251] M. Vauthier, L. Jierry, J.C. Oliveira, L. Hassouna, V. Roucoules, and F. BallyLe Gall. Interfacial thermoreversible chemistry on functional coatings: A focus on the dielsalder reaction. *Advanced Functional Materials*, 29:1806765, 2019.

[252] C. Heinzmann, C. Weder, and L.M. De Espinosa. Supramolecular polymer adhesives: advanced materials inspired by nature. *Chemical Society Reviews*, 45:342–358, 2016.

[253] J.L. Meyer, M. Bakir, P. Lan, J. Economy, I. Jasiuk, G. Bonhomme, and A.A. Polycarpou. Reversible bonding of aromatic thermosetting copolyesters for inspace assembly. *Macromolecular Materials and Engineering*, 304:1800647, 2019.

[254] D. Haydon. Electrelease electrically disbonding epoxy adhesive. *Assembly Automation*, 22:326–329, 2002.

[255] Y. Nishiyama, N. Uto, C. Sato, and H. Sakurai. Dismantlement behavior and strength of dismantlable adhesive including thermally expansive particles. *International Journal of Adhesion and Adhesives*, 23:377–382, 2003.

[256] M.D. Banea, L.F.M. Da Silva, R.J.C. Carbas, and S. De Barros. Debonding on command of multi-material adhesive joints. *The Journal of Adhesion*, 93:756–770, 2017.

[257] R.H. McCurdy, A.R. Hutchinson, and P.H. Winfield. The mechanical performance of adhesive joints containing active disbonding agents. *International Journal of Adhesion and Adhesives*, 46:100–113, 2013.

[258] M.D. Banea, L.F.M. Da Silva, and R.J.C. Carbas. Debonding on command of adhesive joints for the automotive industry. *International Journal of Adhesion and Adhesives*, 59:14–20, 2015.

[259] H. Ishikawa, K. Seto, S. Shimotuma, N. Kishi, and C. Sato. Bond strength and disbonding behavior of elastomer and emulsion-type dismantlable adhesives used for building materials. *International Journal of Adhesion and Adhesives*, 25:193–199, 2005.

[260] V. Dumont, C. Badulescu, J. Adrien, N. Carrere, D. Thévenet, and E. Maire. Experimental investigation of porosities evolution in a bonded assembly by means of x-ray tomography. *The Journal of Adhesion*, 97:528–552, 2021.

[261] N. Pausan, Y. Liu, Y. Lu, and A.R. Hutchinson. The use of expandable graphite as a disbonding agent in structural adhesive joints. *The Journal of Adhesion*, 93:791–810, 2017.

[262] M.D. Banea, L.F.M. Da Silva, R.J.C. Carbas, D.K.K. Cavalcanti, and L.F.G. De Souza. The effect of environment and fatigue loading on the behaviour of teps-modified adhesives. *The Journal of Adhesion*, 96:423–436, 2020.

[263] Monika Shankarrao Satpute and Rajeshkumar U. Sambhe. The fundamentals of epoxy composites with filler for different applications: A review. *International Journal of Scientific Research in Science and Technology (IJSRST)*, pages 88–100, 2022.

[264] A. Szewczak. Impact of epoxy resin modification on their strength parameters. *Budownictwo i Architektura*, 18:041–050, 2020.

[265] A. Szewczak and M. Szelag. Modifications of epoxy resins and their influence on their viscosity. In *IOP Conference Series: Materials Science and Engineering*, volume 471, page 022038, 2019.

[266] K. Apaydin, A. Laachachi, V. Ball, M. Jimenez, S. Bourbigot, and D. Ruch. Layer-by-layer deposition of a tio2-filled intumescent coating and its effect on the flame retardancy of polyamide and polyester fabrics. *Colloids and Surfaces A: Physicochemical and Engineering Aspects*, 469:1–10, 2015.

[267] E.D. Weil. Fire-protective and flame-retardant coatings - a state-of-the-art review. *Journal of Fire Sciences*, 29:259–296, 2011.

[268] B. Schartel. Phosphorus-based flame retardancy mechanismsold hat or a starting point for future development? *Materials*, 3:4710–4745, 2010.

[269] R.G. Puri and A.S. Khanna. Intumescent coatings: A review on recent progress. *Journal of Coatings Technology and Research*, 14:1–20, 2017.

[270] A. Laachachi, N. Burger, G. Mertz, and D. Ruch. Multi-material disassembly. WO Patent WO2021219736, 2021. November 4, 2021.

[271] P. Verge, V. Toniazzo, D. Ruch, and J.A.S. Bomfim. Unconventional plasticization threshold for a biobased bisphenol-a epoxy substitution candidate displaying improved adhesion and water-resistance. *Industrial Crops and Products*, 55:180–186, 2014.

[272] R. Riahipour, A. Alizadeh Sahraei, N. Van De Werken, M. Tehrani, K. Abrinia, and M. Baniassadi. Improving flame-retardant, thermal, and mechanical properties of

an epoxy using halogen-free fillers. *Science and Engineering of Composite Materials*, 25:939–946, 2018.

[273] P. Gradziuk and B. Gradziuk. Prospects for the development of the heat pumps market in poland in the context of the new eu strategy a clean planet for all. *Annals PAAAE*, XX:77–82, 2018.

[274] K. Machalická and M. Eliáová. Adhesive joints in glass structures: effects of various materials in the connection, thickness of the adhesive layer, and ageing. *International Journal of Adhesion and Adhesives*, 72:10–22, 2017.

[275] W. Dang, M. Kubouchi, S. Yamamoto, H. Sembokuya, and K. Tsuda. An approach to chemical recycling of epoxy resin cured with amine using nitric acid. *Polymer*, 43:2953–2958, 2002.

[276] N. Blelloch, H. Yarbrough, and K. Mirica. Stimuli-responsive temporary adhesives: enabling debonding on demand through strategic molecular design. *Chemical Science*, 12:15183–15205, 2021.

[277] Oussema Kachouri, Julien Bardon, David Ruch, and Abdelghani Laachachi. Use of intumescent flame-retardant systems in epoxy adhesives for debonding purpose. *Heliyon*, 10(3):e25240, 2024.

[278] D. Hoang, J. Kim, and B.N. Jang. Synthesis and performance of cyclic phosphorus-containing flame retardants. *Polymer Degradation and Stability*, 93:2042–2047, 2008.

[279] D. Hoang and J. Kim. Synthesis and applications of biscyclic phosphorus flame retardants. *Polymer Degradation and Stability*, 93:36–42, 2008.

[280] M.E. Üreyen, E. Kaynak, and G. Yüksel. Flameretardant effects of cyclic phosphonate with hals and fumed silica in polypropylene. *Journal of Applied Polymer Science*, 137:48308, 2020.

[281] K.P. Venkitaraj, S. Suresh, B. Praveen, Arjun Venugopal, and Sreeju C. Nair. Pentaerythritol with alumina nano additives for thermal energy storage applications. *Journal of Energy Storage*, 13:359–377, 2017.

[282] H. Xiang, C. Sun, D. Jiang, Q. Zhang, C. Dong, and L. Liu. A novel halogen-free intumescent flame retardant containing phosphorus and nitrogen and its application

in polypropylene systems. *Journal of Vinyl and Additive Technology*, 16:261–271, 2010.

[283] S. Alessi, E. Caponetti, O. Güven, M. Akbulut, G. Spadaro, and A. Spinella. Study of the curing process of dgeba epoxy resin through structural investigation. *Macromolecular Chemistry and Physics*, 216, 2015.

[284] K. Song, Y. Wang, F. Ruan, W. Yang, and J. Liu. Synthesis of a novel spirocyclic inflatable flame retardant and its application in epoxy composites. *Polymers*, 12:2534, 2020.

[285] C. Geschwindner, D. Goedderz, T. Li, et al. Investigation of flame retarded polypropylene by high-speed planar laser-induced fluorescence of oh radicals combined with a thermal decomposition analysis. *Experiments in Fluids*, 61:30, 2020.

[286] M.D. Banea. Debonding on demand of adhesively bonded joints. In K.L. Mittal, editor, *Progress in Adhesion and Adhesives*. Wiley, 2020.

[287] D. Hohl and C. Weder. (de)bonding on demand with optically switchable adhesives. *Advanced Optical Materials*, 7, 2019.

[288] M. Banea, L. Da Silva, R. Carbas, A. Barbosa, S. De Barros, and G. Viana. Effect of water on the behaviour of adhesives modified with thermally expandable particles. *International Journal of Adhesion and Adhesives*, 84:250–256, 2018.

[289] J. Bonaldo, M. Banea, R. Carbas, L. Da Silva, and S. De Barros. Functionally graded adhesive joints by using thermally expandable particles. *The Journal of Adhesion*, 95:1014–995, 2019.

[290] X. Pang, D. Ming-Wei, Z. Zhi-Xiao, and T. Yu. An intumescent flame retardant - expandable graphite: Preparation, characteristics and flame retardance for polyethylene. *Kuwait Journal of Science*, 42, 2015.

[291] F. Tomiak, K. Rathberger, A. Schöffel, and D. Drummer. Expandable graphite for flame retardant pa6 applications. *Polymers*, 13:2733, 2021.

[292] Toshiaki Enoki, Morinobu Endo, and Masatsugu Suzuki. Structures and phase transitions. In *Graphite Intercalation Compounds and Applications*. Oxford University Press, New York, 2003. Accessed 9 June 2024.

[293] M. Salvatore, G. Carotenuto, S. De Nicola, C. Camerlingo, V. Ambrogi, and C. Carfagna. Synthesis and characterization of highly intercalated graphite bisulfate. *Nanoscale Research Letters*, 12(1):167, 2017.

[294] P. Murugan, R.D. Nagarajan, B.H. Shetty, M. Govindasamy, and A.K. Sundramoorthy. Recent trends in the applications of thermally expanded graphite for energy storage and sensors - a review. *Nanoscale Advances*, 3(22):6294–6309, 2021.

[295] G. Lin. Review on porous structure and relevant applications of expanded graphite. *Journal of Yangtze University*, 2008.

[296] P. Gong-pei. Progress on the application of expandable graphite. *Jiangsu Chemical Industry*, 2005.

[297] W. Focke, H. Badenhorst, W. Mhike, H. Kruger, and D. Lombaard. Characterization of commercial expandable graphite fire retardants. *Thermochimica Acta*, 584:8–16, 2014.

[298] M. Inagaki, Y. Kaburagi, and Y. Hishiyama. Thermal management material: Graphite. *Advanced Engineering Materials*, 16, 2014.

[299] J. Gu, N. Li, L. Tian, Z. Lv, and Q. Zhang. High thermal conductivity graphite nanoplatelet/uhmwpe nanocomposites. *RSC Advances*, 5:36334–36339, 2015.

[300] T. Peng, B. Liu, X. Gao, L. Luo, and H. Sun. Preparation, quantitative surface analysis, intercalation characteristics and industrial implications of low temperature expandable graphite. *Applied Surface Science*, 2018.

[301] Z. Xian-you. Preparation and affecting factors of expandable graphite. *Journal of Harbin University of Science and Technology*, 2007.

[302] H. Hong-ya. Preparation and characterization of expanded graphite with high expansion ratio. *Journal of Materials Science Engineering*, 2014.

[303] M. Wang and L. Ji. Expansion mechanism of expandable graphite formed by natural graphite with different particle size. *Advanced Materials Research*, 499:16–19, 2012.

[304] Z. Guo-jian. Preparation of expandable graphite by using fine flake graphite. *The Chemical Engineer*, 2015.

[305] X. Wei. Preparation and characterization of high rate of expandable graphite. *Guangzhou Chemical Industry*, 2014.

[306] Y. Hoong, M. Paridah, Y. Loh, H. Jalaluddin, and L. Chuah. A new source of natural adhesive: Acacia mangium bark extracts co-polymerized with phenol-formaldehyde (pf) for bonding mempisang (annonaceae spp.) veneers. *International Journal of Adhesion and Adhesives*, 31:164–167, 2011.

[307] Z. Liu and F. Yan. Switchable adhesion: On-demand bonding and debonding. *Advanced Science*, 9:2200264, 2022.

[308] M. Guo and G. Wang. Milk protein polymer and its application in environmentally safe adhesives. *Polymers*, 8, 2016.

[309] M. Rodrigo, J. Serrallonga, J. Juan-Tresserras, L. Alcalá, and L. Luque. Woodworking activities by early humans: a plant residue analysis on acheulian stone tools from peninj (tanzania). *Journal of Human Evolution*, 40(4):289–299, 2001.

[310] M. Wilson, A. Perrone, H. Smith, D. Norris, J. Pargeter, and M. Eren. Modern thermoplastic (hot glue) versus organic-based adhesives and haft bond failure rate in experimental prehistoric ballistics. *International Journal of Adhesion and Adhesives*, 104:102717, 2021.

[311] T. Engels. Thermoset adhesives: epoxy resins, acrylates and polyurethanes. In *Handbook of Adhesion Technology*, pages 228–253. 2012.

[312] S. Cao, L. Shouhai, M. Li, X. Lina, H. Ding, J. Xia, M. Zhang, and K. Huang. A thermal self-healing polyurethane thermoset based on phenolic urethane. *Polymer Journal*, 49:775–781, 2017.

[313] S. Panchireddy, J. Thomassin, B. Grignard, C. Damblon, A. Tatton, C. Jérôme, and C. Detrembleur. Reinforced poly(hydroxyurethane) thermosets as high performance adhesives for aluminum substrates. *Polymer Chemistry*, 8:5897–5909, 2017.

[314] H. Tsai, Y. Nakamura, T. Fujita, and M. Naito. Strengthening epoxy adhesives at elevated temperatures based on dynamic disulfide bonds. *Materials Advances*, 2020.

[315] Z. Wang, B. Liu, F. Zeng, X. Lin, J. Zhang, X. Wang, Y. Wang, and H. Zhao. Fully recyclable multifunctional adhesive with high durability, transparency, flame retardancy, and harsh-environment resistance. *Science Advances*, 8, 2022.